Chemoenzymatic Synthesis of Chiral Alcohols Relevant to Pharmaceutical Industry

TECHNISCHE UNIVERSITÄT DARMSTADT

Vom Fachbereich Chemie
der Technischen Universität Darmstadt

zur Erlangung des Grades
Doctor rerum naturalium
(Dr. rer. nat.)
genehmigte

Dissertation

M. Sc. Nguyen Yen Chi Thai
geboren in Frankfurt a/M

Erstgutachter: Prof. Dr. Wolf-Dieter Fessner
Zweitgutachter: Prof. Dr. Harald Kolmar

Darmstadt, 2021

Thai, Nguyen Yen Chi: Chemoenzymatic Synthesis of Chiral Alcohols Relevant to Pharmaceutical Industry
Darmstadt, Technische Universität Darmstadt,
Jahr der Veröffentlichung der Dissertation auf TUprints: 2022
URN: urn:nbn:de:tuda-tuprints-206199

Tag der mündlichen Prüfung: 31.01.22

Tag der Einreichung: 14. Dezember 2021

Die experimentellen Arbeiten für die vorliegende Dissertation wurden unter der Leitung von Prof. Dr. Wolf-Dieter Fessner am Clemens-Schöpf-Institut für Organische Chemie und Biochemie der TU-Darmstadt im Zeitraum von Mai 2015 bis Februar 2021 durchgeführt.

Eidesstattliche Erklärung

Ich erkläre hiermit, dass ich meine Dissertation selbstständig und nur mit den angegebenen Hilfsmitteln angefertigt habe. Die vorgelegte Dissertation wurde in der vorliegenden oder einer ähnlichen Fassung zu keinem früheren Zeitpunkt an einer in- oder ausländischen Hochschule zum Promotionsversuch eingereicht.

Darmstadt, 14.12.21 

Nguyen Yen Chi Thai

Erklärung der Übereinstimmung

Ich versichere hiermit, dass die elektronische Version meiner Dissertation mit der schriftlichen Version übereinstimmt und für die Durchführung des Promotionsverfahrens vorliegt.

Darmstadt, 14.12.21 

Nguyen Yen Chi Thai

Teile dieser Arbeit sind bereits publiziert.

Zeitschriftenartikel:

Yen Chi Thai, Anna Szekrenyi, Yuyin Qi, Gary W. Black, Simon J. Charnock, Wolf-Dieter Fessner, ***"Fluorogenic kinetic assay for high-throughput discovery of stereoselective ketoreductases relevant to pharmaceutical synthesis"*** Bioorganic & Medicinal Chemistry, **2017**, *26 (7)*, 1320-1326, DOI: 10.1016/j.bmc.2017.05.024

Konferenzbeiträge:

Titel:

- Poster: Biotrans 2019, Groningen, Niederlande.
- Poster und Kurzvortrag: Doktorandentag, FB Chemie TU Darmstadt 2019, Darmstadt, Deutschland.
- Poster: Dechema-Tag 2019, Frankfurt, Deutschland.
- Poster: Novel Enzymes 2018, Darmstadt, Deutschland.
- Poster: Biotrans 2017, Budapest, Ungarn.
- Poster und Kurzvortrag: Summer School „Biocatalysis as a Key Enabling Technology" 2017, Siena, Italien.
- Poster und Kurzvortrag: Training School „Systems Biocatalysis: New Enzymes, New Pathways, New Products" 2016, Siena, Italien.

Acknowledgements

First of all, I would like to express my sincere gratitude and appreciation to my supervisor Prof. Dr. Wolf-Dieter Fessner for his continuous guidance that led me through this research and brought me here. Without his motivation and encouragement this work would never have reached such a fulfilment.

I would also like to thank the other members of the examination board: Prof. Kolmar, Prof. Schmitz, and Prof. Buntkowsky.

I greatly appreciate all the help and solidarity I received during the past years from my colleagues:

I am very grateful to Dr. Anna Szekrenyi, who acted as a mentor during the first episode of my work. With kindness and patience, she gave me an insight into the discipline of biocatalysis. Furthermore, she helped to create a joyful and productive working atmosphere and always brought encouragement to me when needed.

I would like to thank Dr. Alexander Mertsch for his company and friendship through the years, which brought me trust and comprehension.

I very much appreciate Ines Fuster-Fernandez, whose open and cheerful character brought a lot more fun into the hardships of long working days. I thank her for sharing that joyful spirit.

Furthermore, I thank Hans-Michael Orfgen for his continuous and great helpfulness within all issues – no matter if laboratory and technical or personal concerns, I was always able to count on him.

I sincerely thank all my fellow lab mates for forming this special group - especially, Michael Hofmeister, who is the greatest team-player of all time.

I would like to thank Serbet Pinar-Safi, Bettina Harnischfeger and Michael Kickstein for their great and meaningful work regarding administrative, organizational and laboratorial aspects this project relied on.

Besides, I would like to acknowledge Dr. Yuriy Sheludko for taking wonderful care of my plants throughout my absence from the lab during the last episode of this work.

Furthermore, I am very grateful to the scientific members of the NMR and mass department. Prof. Meusinger and Mrs. Rudolph, whose work was a great contribution to this thesis.

Special thanks go to Marko Fischer, who has taught me to always keep an open mindset and gain different perspectives in life.

I thank all my friends and family for the relaxing moments that helped me disconnect from work and gain new motivation.

Last but not least, I would like to express special gratitude to my parents for their continuous support and patience.

Table of contents

Zusammenfassung in deutscher Sprache

Eine große Anzahl an Verbindungen der lebendigen Natur sind chiral (z. B. DNS, Aminosäuren).[1] Dies bedeutet, dass deren Bild und Spiegelbild sich nicht zur Deckung bringen lassen. Sie bilden somit ein Enantiomerenpaar gleicher Konstitution aber unterschiedlicher Konfiguration. Diese inhärente Eigenschaft der Verbindungen führt zu einer außergewöhnlichen Spezifität bei der Erkennung **chiraler Wirkstoffe** in Organismen. Daher ist die optische Reinheit vieler Arzneimittel häufig ein Schlüsselfaktor für deren Wirksamkeit und oft erforderlich für eine sichere Anwendung.[2]
Das Erschließen effizienter Synthesewege zur Erzeugung enantiomerenreiner Verbindungen ist daher stets von hoher Relevanz. In den letzten Jahren ist hierfür die Verwendung **biokatalytischer Systeme** immer weiter in den Vordergrund gerückt, denn der Einsatz stereoselektiv arbeitender Enzyme bietet vielerlei Vorteile: Zum einen operieren Enzyme meist unter milden Bedingungen (Raumtemperatur, physiologische pH-Werte) und in wässrigen Medien.[3] Dies ist sowohl ökologisch als auch ökonomisch vorteilhaft, da auf toxische, metallkatalysierte Prozesse verzichtet werden kann.[4] Besonders im Hinblick auf medikamentöse Anwendungen, fällt dieser Faktor vermehrt ins Gewicht.[5] Des Weiteren agieren Enzyme oft mit hoher **Stereo-, Regio- und Chemoselektivität**, sodass auch bei multifunktionalen Verbindungen und Eintopfsynthesen auf eine aufwendige Schutzgruppenchemie verzichtet werden kann.[3]
Der universelle Einsatz in der synthetischen organischen Chemie war jedoch aufgrund der mäßigen Zugänglichkeit der Enzyme und deren oft sehr spezifischen Substratspektrum und/oder unzureichenden Stabilität lange Zeit begrenzt. Diese Situation änderte sich Ende der 1970er Jahre dramatisch, als die Implementierung der **rekombinanten DNA-Technologie** die Überexpression von Enzymen in Wirtsorganismen ermöglichte, um auch größere, für praktische Anwendungen ausreichende Katalysatormengen bereit zu stellen.[6] Darüber hinaus öffnete der Fortschritt in den Bereichen **rationales Design** (1970er Jahre) und **gerichtete Evolution** (1990er Jahre) die Bühne für das weite Gebiet des Proteinengineerings, welches schließlich das Entwickeln reaktionsspezifischer, maßgeschneiderter Enzyme ermöglichte.[7]

Der erste Teil dieser Arbeit behandelt die biokatalytische Synthese von **Statinen** und Statinbausteinen. Statine, darunter vor allem Atorvastatin, sind die am häufigsten eingesetzten Arzneimittel zur Verringerung des Risikos für kardiovaskuläre Erkrankungen und wirken effektiv durch Senkung des Cholesterinspiegels.[8] Die sogenannte Statin-Seitenkette, das Strukturmerkmal aller Statine, besteht aus einem 3,5-Diol-Baustein mit **zwei stereogenen Zentren** und gleicht dem natürlichen Substrat der HMG-CoA Reduktase, dem Schlüsselenzym in der Cholesterinbiosynthese. Hierdurch erhalten Statine ihre inhibierende Wirkung.[9]
Da Statine noch immer eine große Marktmacht besitzen und jüngste Studien zusätzlich vielfältige, pleiotropische Effekte enthüllten, ist das Erschließen und Optimieren neuer Prozesssysteme zur Synthese neuer Statine oder von Statinbausteinen weiterhin äußerst gefragt und lukrativ.
Innerhalb dieser Forschungsarbeit wurde das komplexe Statinmotiv durch **stereoselektive, sequenzielle Aldoladdition** mit Hilfe einer 2-Deoxy-D-ribose-5-phosphat-Aldolase (**DERA**) aufgebaut. Diese ist in der Lage, Aldehyde durch **C-C Bindungsknüpfung** zu addieren und ist damit weitestgehend, mit Ausnahmen mutierter Varianten der Fructose-6-phosphat Aldolase

(FSA), einzigartig.[10] Zur Identifizierung geeigneter DERA-Enzyme mit vergrößerter Akzeptorsubstrat-Bandbreite und erhöhter Stabilität wurde ein **Enzymassay** zum Hochdurchsatz-Screenen von DERA-Bibliotheken mitentwickelt.
Schema 0.1 zeigt die sequenzielle, DERA-katalysierte Aldolreaktion zweier Moleküle Acetaldehyd (**2**) an ausgewählte Akzeptoraldehyde sowie die spontane Ringschließung zur Laktolvorstufe **3**. Eine anschließende, **regioselektive Oxidation** zu den korrespondierenden Laktonen führt schließlich zur Bildung des jeweiligen Statins. Für diesen Schritt wurde eine entsprechende, durch Hochdurchsatz-Screening identifizierte **Alkoholdehydrogenase** (ADH)eingesetzt.
Eine gelungene **Reaktionsoptimierung zur Eintopfsynthese** durch das Implementieren einer **Enzymkaskade** mit integrierter **Cofaktor-Regeneration** machen die verfolgte Strategie besonders attraktiv. Hierdurch konnten sowohl die Produktion eines wertvollen Amin-funktionalisierten Statin-Bausteins **4a** als auch die Synthese des natürlich vorkommenden Solistatins (**4b**) und fünf einfacheren Derivaten (**4c-g**) auf simple, aber effektive Art realisiert werden. Sämtliche, hierbei eingesetzte DERA-Akzeptorsubstrate wurden über klassische chemische Synthesewege hergestellt.
Die hergestellten Statine wurden anschließend in *in vitro*-Experimenten erfolgreich auf ihre **biologische Aktivität** getestet.

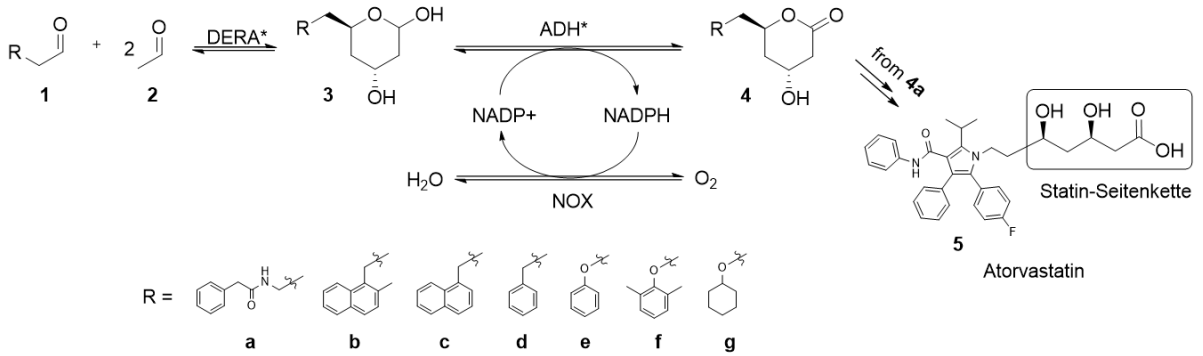

Schema 0.1 Enzymatische Kaskade zur Darstellung von Solistatin (**4b**) und einfacheren Derivaten **4c-g** sowie eines Amin-funktionalisierten Synthesebausteins **4a** für die Produktion von Atorvastatin (**5**). Der erste Schritt erfolgt durch DERA-katalysierte, sequenzielle Aldoladdition von Acetaldehyd (**2**) an das entsprechende Akzeptoraldehyd **1**. Eine anschließende Oxidation durch eine ADH mit integriertem Cofaktor-Regenerierungssystem durch eine Nikotinamidoxidase (NOX) führt zur Bildung der Statine in laktonisierter Form.

Ein weiterer Hauptfokus dieser Arbeit lag in der **Entwicklung neuer Enzymvarianten** der ***(R)*-selektiven Ketoreduktase** aus *Lactobacillus brevis* (*Lb*KRED) in Hinblick auf deren Anwendung zur Produktion des **chiralen Medikaments Ticagrelor (8)**. Dieses ist ein Thrombozytenaggregationshemmer, d. h. es wirkt reduzierend auf die Bildung von Blutgerinnseln und kann daher zur Verbeugung von Herzinfarkten eingesetzt werden.[11] Ticagrelor‘s strukturelles Schlüsselmotiv besteht aus einer ***trans*-konfigurierten Aryl-Cyclopropylamin**-Einheit, welche unter anderem ausgehend von der **chiralen Alkoholvorstufe 7** hergestellt werden kann.[12] Für die Synthese dieses wichtigen Alkoholbausteins wurde innerhalb dieser Forschungsarbeit ein optimierter Darstellungsweg mittels KRED-katalysierter **stereoselektiver Oxidation** behandelt (Schema 0.2).

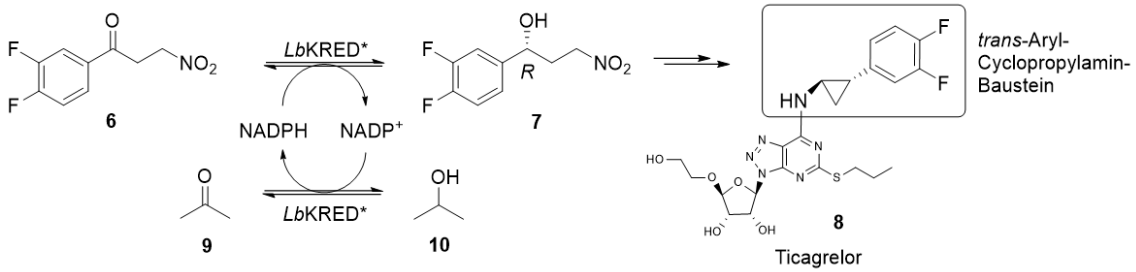

Schema 0.2 Stereoselektive Oxidation des prochiralen Ketons **6** zum Alkohol-Precursor **7** für die Produktion von Ticagrelor (**8**). Der Katalyseschritt erfolgt unter Verwendung der durch gerichteter Evolution und rationalem Design entwickelten *Lb*KRED Variante E144A/L152R. Der NADPH-Cofaktor wird hierbei durch Umsetzung von *iso*-Propanol (**10**) durch dasselbe Enzym regeneriert.

Hierzu wurden ausgehend vom Wildtyp der *Lb*KRED über eine Kombination aus rationalem Design und gerichteter Evolution innerhalb **zweier Mutationszyklen Enzymbibliotheken** konstruiert, die mittels eines eigens entwickelten, **fluoreszensbasierten Hochdurchsatz-Assays**[13] auf aktive Varianten geprüft wurden. Durch den strategisch schrittweisen Einsatz fluorogener, leicht detektierbarer Substrate, welche sich strukturell immer weiter dem eigentlichen, **pharmazeutisch-relevanten** Zielmolekül annäherten, konnten die umfangreichen Proteinbiobliotheken in kurzer Zeit und mit einfacher Handhabung evaluiert werden. Eine **modulare Synthesemethode** ermöglichte die einfache Herstellung des benötigten Substratsets.

Es wurden schließlich drei Enzymvarianten identifiziert, die in der Lage waren, das pharmazeutisch relevante Substrat erfolgreich umzusetzen. Die Doppelmutante E144A/L152R, welche die höchste Aktivität aufwies, wurde erfolgreich in einem optimierten, hoch skalierten Reaktionsansatz mit integriertem Cofaktor-Recycling eingesetzt und lieferte das chirale Zielmolekül in guter Ausbeute (79%) und **exzellenter Enantiomerenreinheit** (100% *ee*).

Durch den Einsatz der neu entwickelten *(R)*-selektiven Ketoreduktase konnte somit eine **stark vereinfachte, neue Strategie** zur Synthese des komplexen Ticagrelor-Bausteins **7** realisiert werden. Bisher veröffentlichte chemische und biokatalytische Syntheserouten verlangen dagegen weit aufwendigere Reaktionsabfolgen.[12, 14] Des Weiteren besteht die Möglichkeit, die entwickelte Mutante auch für die Synthese ähnlicher Cyclopropylaminbausteine, die sich in vielerlei Wirkstoffen wiederfinden,[15] einzusetzen.

Enzyme Catalysis in Organic Synthesis

"By far, nature is the best chemist of all time."

- Dr. FRANCES H. ARNOLD
(Nobel Prize in Chemistry 2018 for 'Directed Evolution')

Although science seems to be advanced, nature has had billions of years over which patterns and processes evolved into a highly optimized state with elaborate cooperation and interplay. Based on this fact, the term "*biomimicry*" arose from the idea that nature has already developed many solutions to challenging problems that humans are seizing today[16] and even without understanding all of its secrets, the list of innovations inspired by nature is long and ongoing (e. g. new material coating technologies that mimic nature's lotus effect,[17] solar technologies originating from the plant's and bacteria's ability to use and convert solar energy,[18] adhesives capable of supporting human weight mimic the biomechanics of gecko feet,[19] etc.).
Likewise is the list of biological tools that are exploited by (bio)chemists - to mention are applications employing bacteria, viruses, or yeasts in biotechnology or proteins and enzymes as catalysts in bio- and pharmaceutical synthesis.
As abundant as enzymes are in nature and being highly diverse catalysts, they offer a wide scope of reaction varieties comprising redox reactions, transfer reactions, hydrolysis, isomerization, and breaking or forming of chemical bonds.[20] In this context, the application of enzymes in synthesis strategies for purposes they were not evolved for is referred to as "***biocatalysis***".[20] With microorganisms being used for the production of prominent goods like wine, beer, cheese, vinegar, bread etc., 6.000 – 8.000 years ago, biocatalysis represents one of oldest chemical transformations known to humans.[21] Since the pioneering work of EDUARD BUCHNER in 1897 (Nobel prize 1907), who presented the fermentation of sugar by cell-free yeast extracts, proof was brought that biological transformations do not necessarily require living cells.[7] Thus, from the mid-20th century on, biocatalysis was also employed for chemical transformations of non-natural organic compounds and was increasingly regarded as an attractive approach for the production of fine chemicals as an alternative to the traditional routes of classical synthesis, metal catalysis, or organocatalysis.[22]
However, the generalization of biocatalysis in synthetic organic chemistry was long limited due to the moderate accessibility of enzymes and their often very specific substrate scope or insufficient stability. This situation changed dramatically in the late 1970s, when the implementation of **recombinant DNA technology** allowed for overexpression of enzymes in host organisms to provide larger quantities required for practical applications.[6] In addition, the advances of **rational design** (1970s) and **directed evolution** (1990s) opened the door for the vast field of **protein engineering** (chapter 5.4), offering reaction tailored enzymes[7] and leading to the 2018 chemistry Nobel prize awarded to FRANCIS H. ARNOLD.
One of the greater attraction of enzyme technology lies in the enzymes' ability to act under **mild and benign conditions**, such as water as reaction medium, ambient temperatures between 20 – 40 °C, and physiological pH, constituting ecologically and economically beneficial practices.[3c]

Their preference for similar reaction parameters makes the application of enzymes perfectly suited for catalyzing sequential transformations known as **cascade reactions**. Multi-enzymatic one-pot cascade reactions offer cost and waste reduction by preventing tedious isolation and purification processes of (unstable) product intermediates, which are otherwise required in classical step-by-step synthesis. Higher yields can be achieved through control and shifting of unfavorable reaction equilibria.[23] To further meet the demands of biotechnological industry for higher enzyme productivity and increased shelf life, **enzyme immobilization** on natural and synthetic solid supports enabled facile recovery of active catalysts and addressed the disadvantage of unstable enzymes or high production and separation costs.[24]

However, one of the key advantages is brought by the fact that enzymes exhibit high selectivity towards their substrates, including **chemoselectivity** (acting on a single type of functional group), **regioselectivity** (differentiating between functional groups located in different parts of the substrate molecule), and **stereoselectivity** (recognition of chirality present in the substrate molecule or transforming prochiral substrates into an optically active product).[20] These properties make enzymes highly advantageous catalysts for the synthesis of **polyfunctional and/or chiral compounds.**[3c]

In pharmaceutical industry, the enantiomeric excess of chiral compounds often plays an important role, as different enantiomers can exhibit varying pharmacokinetic behavior, have no activity, or are even toxic. Indeed, due to this reason, above 50% of our current pharmaceuticals are used as single enantiomers.[4]

Hence, although being no more a white spot, biocatalysis provides a wide and future oriented research field, as the term of "**green chemistry"** becomes more and more meaningful.[20] In fact, in the last two decades, many pathways for the synthesis of complex drugs have been reconsidered in the favor of enzyme application.[25] This turn is especially found for the generation of **chiral alcohols**, which constitute one of the most utilized synthons in the production of pharmaceuticals.[26] Herein, five main enzyme families can be employed:[27]

1. Hydrolases - act by resolving racemic mixtures of chiral alcohols by transforming only one of the enantiomers.
2. Mono- and dioxygenases - generate hydroxyls by introducing molecular oxygen into the substrate upon one or two electron reduction.
3. Hydratases - form alcohols by addition of water to unsaturated C=C double bonds.
4. Hydroxynitrile lyases and aldolases - generate alcohols by nucleophilic addition of small molecules such as HCN or acetaldehyde at carbonyl groups resulting in a new C–C bond.
5. Dehydrogenases or reductases - reduce ketones to enantiopure secondary alcohols.

This work is focused on the biocatalyzed synthesis of chiral alcohols used as precursors and building blocks for the production of biologically active compounds comprising cholesterol lowering statin drugs (Part I) and the anti-thrombotic agent ticagrelor (Part II).

PART I

Development of a One-Pot Three-Enzyme Cascade for the Synthesis of Statin Drugs

1. Theoretical background

1.1. The discovery of statin drugs

Cholesterol was first isolated from gallstones in 1784.[28] Since then it has awakened the fascination of many scientists due to its multifaceted emergence and functionality in our body: It is not only an integral part of our cell membranes but also essentially needed as a precursor for certain steroid hormones, vitamin D3, and for the production of bile acid, which aids in fat digestion.[29] From 1928 to 1975, thirteen scientists, who dedicated essential parts of their scientific work to cholesterol research, have been awarded with the Nobel Prize in the domains of chemistry and physiology or medicine.[30] Amongst these were KONRAD BLOCH and FEODOR LYNEN (Nobel Prize 1964), whose landmark studies on the cholesterol biosynthetic pathway laid significant foundations for today's cardiovascular and cholesterol-lowering therapies.[31]
In the 1950s, after evidence was found that elevated levels of cholesterol-rich low-density lipoprotein (LDL) in plasma correlated to atherosclerotic plaques and **cardiovascular disease**,[32] lipid-lowering agents like clofibrate[33] (e.g. *Atromid-S*®), nicotinic acid[34] (e.g. *Niaspan*®), and cholestyramine[35] (*Lipocol*®, *Vasosan*®) entered the market. But given the fact that neither of them was considered safe or very effective against illnesses related to atherosclerosis, in the 1970s, AKIRA ENDO, a scientist from *Sankyo Company* in Tokyo, realized the need for the development of an improved, better applicable cholesterol-lowering drug.[8] Based on the knowledge provided by BLOCH and LYNEN, it was proven that 3-hydroxy-3-methylglutaryl (HMG)-CoA reductase was the rate-limiting enzyme in one of the first steps of cholesterol biosynthesis.[36] This led ENDO to seek for compounds that would inhibit this catalyst. He reasoned that certain microbes must exist that would produce such metabolites as a defense mechanism against others in need of cholesterol-derived sterols for living. Thus, ENDO *et al.* screened through 6.000 strains of **microbial organisms** and finally succeeded after a period of two years when the first so-called ***statin* drug** was born in 1973, isolated from *P. citrinum*, a blue-green mold that was collected from a rice sample in Kyoto (Figure 1.1).[8] In independently conducted studies by a British group in 1976, the very same compound was also isolated from *Penicillium brevicompactum* and therefore given the name "***compactin***" (**26**).[37] Although being an extremely potent **HMG-CoA reductase inhibitor**, compactin never entered the pharmaceutical market due to various adverse effects but opened the stage for a variety of its descendants.

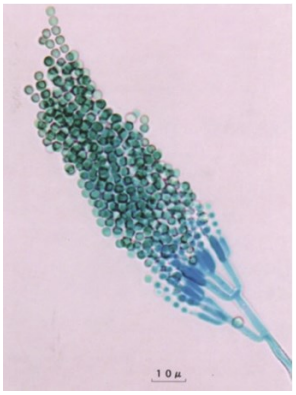

Figure 1.1 Micrograph of *Penicillium citrinum*.[18]

The first statin that made its way through medical approval was lovastatin (mevinolin), sold under the names *Mevacor*® (*Merck*) or *Altoprev*® (generic). Lovastatin (**11**) is a natural fermentation product isolated from *Aspergillus terreus* or *Monsascus ruber* and is also utilized as a precursor for its semisynthetic derivatives simvastatin (**12**) and pravastatin (**13**), which were commercially available shortly after. Fluvastatin (**14**), the first non-natural statin, entered the market in 1994 and was exclusively followed by fully synthetic drugs, comprising atorvastatin (**5**), cerivastatin (**15**), rosuvastatin (**16**), and pitavastatin (**17**) (Figure 1.2). Until today, eight pharmaceuticals from the statin drug family have been available on the market, although cerivastatin (*Baycol*®*, Lipobay*®), promoted by *Bayer* was withdrawn

in 2001 due to reported side effects of rhabdomyolysis, a condition in which damaged skeletal muscle is destroyed.[38]

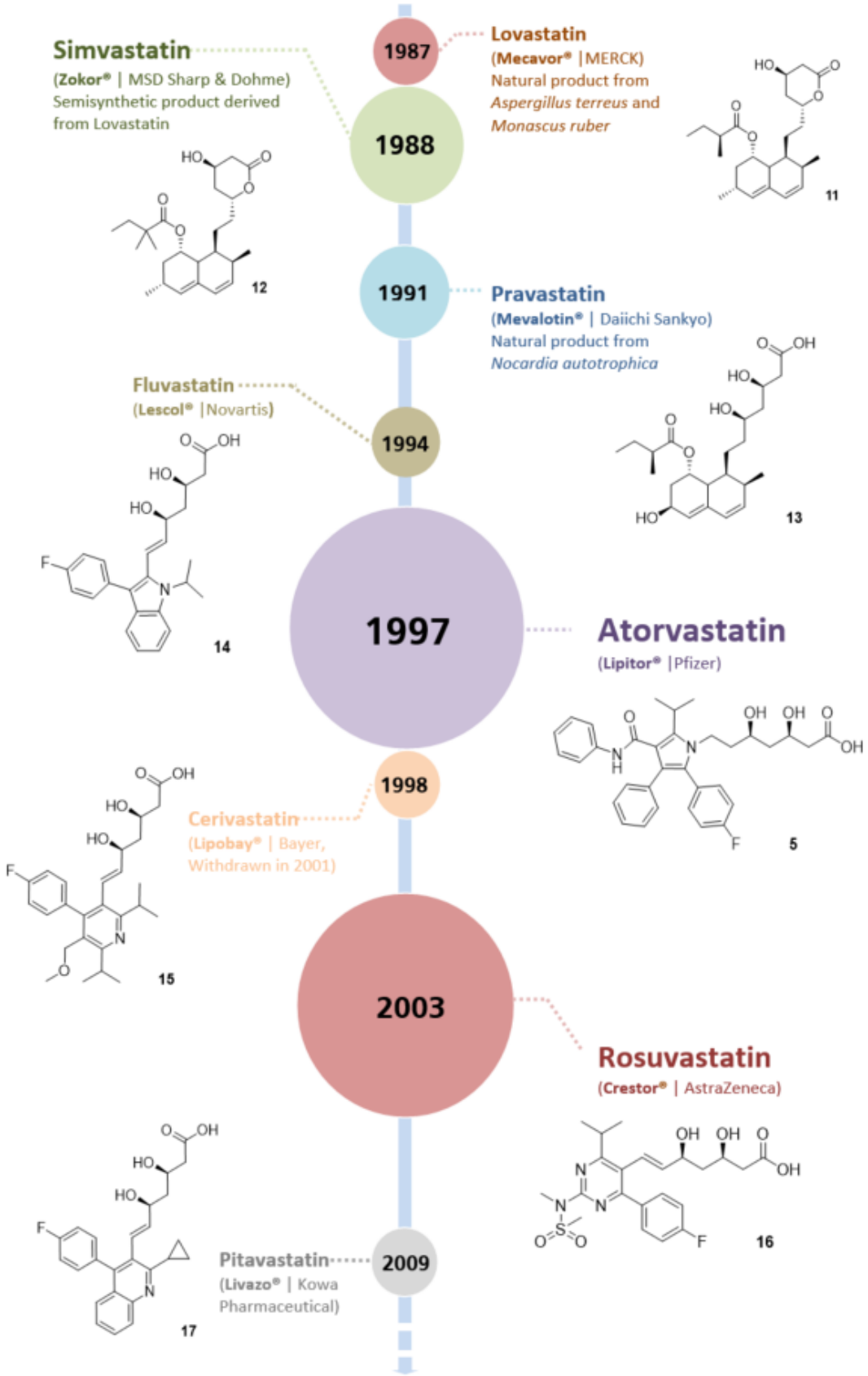

Figure 1.2 Overview of commercial statins according to their market proportion from 1987 – 2009.

Today, statins completely dominate the market of cholesterol lowering agents. Their use led to a 50% decrease in deaths from heart attacks and strokes over the past 30 years in the developed world.[39] Atorvastatin (Lipitor™) (**5**), designed by *Pfizer*, was the commercially most profitable therapeutic until 2012 - with more than US$125 billion in sales.[40] Even though most of their patents are expired, the revenue for statins is expected to continuously rise,[41] as cardiovascular diseases are still the number one cause of death globally, with almost 18 million cases in 2016 (World Health Organization).

1.2. The operating principle of statins

In order to understand the cholesterol lowering mechanism of statins, it is necessary to understand how and where cholesterol is produced in our bodies: The **cholesterol biosynthesis pathway** predominantly takes place in the liver and is divided into three major stages, starting with the mevalonic pathway. Here, the active isoprenoids isopentenyl pyrophosphate (IPP) (**22**) and dimethylalkyl pyrophosphate (DMAPP) (**23**) are formed from acetyl-CoA (**18**) and are precursors to around 30.000 terpenes essentially needed in our bodies. The next two stages include the condensation of three molecules of IPP and three molecules of DMAPP to generate squalene (**24**). Further cyclization leads to the tetracyclic intermediate lanosterin, which is transformed into cholesterol (**25**) within 19 additional steps. All 27 carbon atoms present in cholesterol have their origin in acetyl-CoA (**18**) (Scheme 1.1).[29]

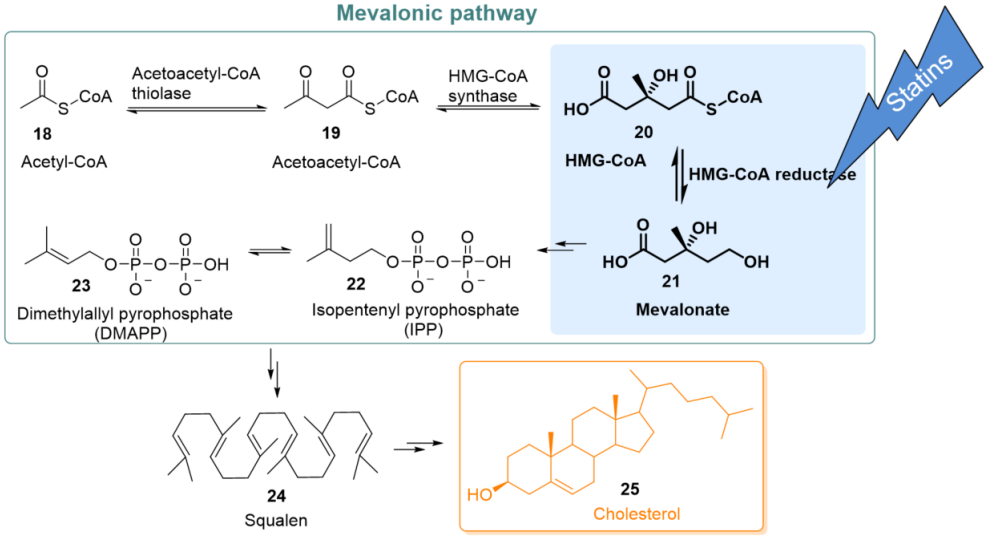

Scheme 1.1 Cholesterol biosynthesis via mevalonate pathway. The rate limiting step is catalyzed by HMG-CoA reductase and is highlighted in blue. Inhibition of the enzyme leads to a decreased production of cholesterol (**25**).[29]

The **rate limiting step** during the whole process is found at a very early episode of the mevalonic pathway and is controlled by **HMG-CoA reductase (HMGR)**. HMGR is an NADPH-dependent enzyme that utilizes *(S)*-HMG-CoA (**20**) to produce *(R)*-mevalonic acid (**21**) by reductive deacylation.[36]

With the discovery of the first statin, scientists recognized the **structural similarity** between its dihydroxy heptanoic acid side chain and HMG-CoA (**20**) or mevalonic acid (**21**), which is why today, compactin (**26**) is also known under the name "*meva*statin", indicating its resemblance.[42] Herein, the key motif, also referred to as the ***statin side chain***, is shared by all

statin drugs and occurs as the biologically active open chained carboxylic acid or as an inactive cyclic hydroxylactone prodrug, which is then *in vivo* hydrolyzed to the corresponding active acid
Scheme 1.2).[43] Therefore, it is no surprise that the statin side chain allows the drug to mimic HMG-CoA as the natural substrate of HMG-CoA reductase, thus, being able to act as **competitive antagonists** and block cholesterol biosynthesis.[42]

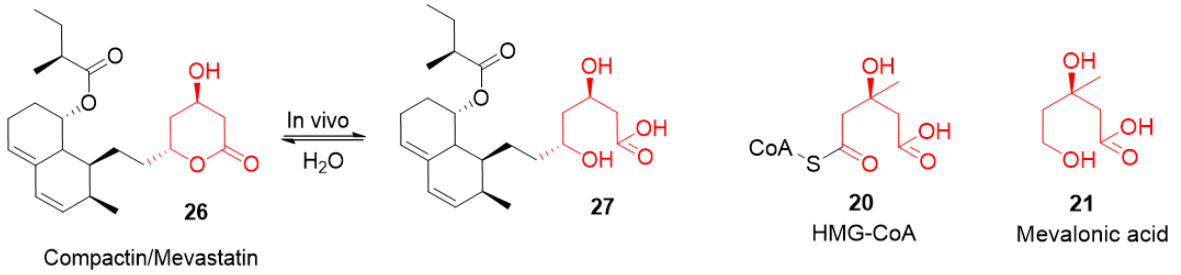

Scheme 1.2 Comparison between the chemical structures of compactin/mevastatin (**26**) and the native substrates of HMG-CoA reductase (HMG-CoA (**20**) and mevalonic acid (**21**)). The statin side chains and their related structures are highlighted in red.

Fascination arose, when it was discovered that inhibiting HMGR does not only lead to a reduced release of cholesterol from the liver to the blood stream but also induced a promoted transport of blood cholesterol back into the liver. This effect happens as low levels of intracellular (hepatic) cholesterol stimulates the over-expression of low-density lipoprotein receptors (LDLR), which enable an increased transport of LDL from the bloodstream to the liver (Figure 1.3).[44] LDL is a conglomerate of various proteins that packs cholesterol and other lipids into minuscule protein-covered particles, which can therefore easily mix with blood and transport fat molecules throughout the body to the cells, where they are needed for vital purposes. However, elevated LDL levels plus inflammations or metabolic changes to the arterial wall can lead to LDL depositions and plaque formation.[45]

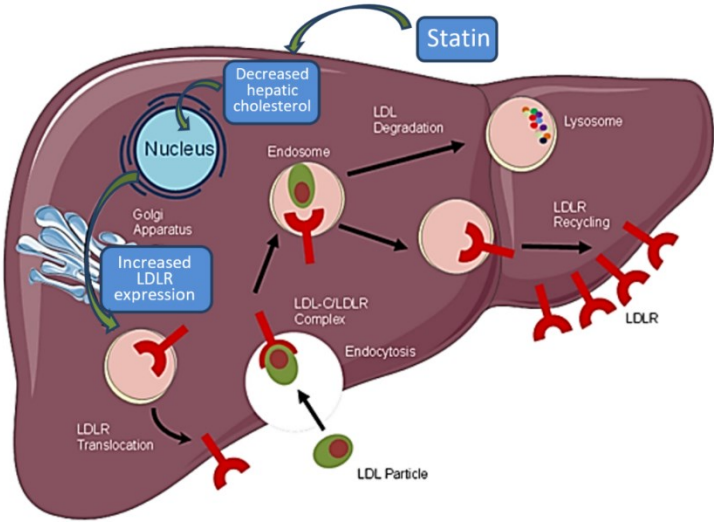

Figure 1.3 Physiological reception and converting of blood cholesterol in liver. LDL(R) = low density lipoprotein (receptor).[27]

The described principle of reverse cholesterol transport, however, benefits the potency of statins treatment dramatically, as cholesterol that is accumulated in the liver can be degraded by lysosomal proteases.[46]

In order to perform effectively, statins need to exhibit **optimal binding** to the **catalytic domain of HMGR**. X-ray crystallographic studies have given insight into the catalytic portions of the enzyme in complex with statin drugs and verified the assumption that the statin side chain occupies the HMG binding site.[9] Located here, the enzyme features an amino acid motif appearing as a "*cis-loop*". This sequence contains the residues S684, D690, K691, and K692, which are in direct proximity to the HMG-like moiety and interact via **hydrogen bonding**. The residue E559, located at the opposite side, is known to bind to the CoA-moiety of the native substrate. In case of the statin drugs, it stabilizes the molecule by **polar interaction** with the statins' hydroxyl group (Figure 1.4).[9]

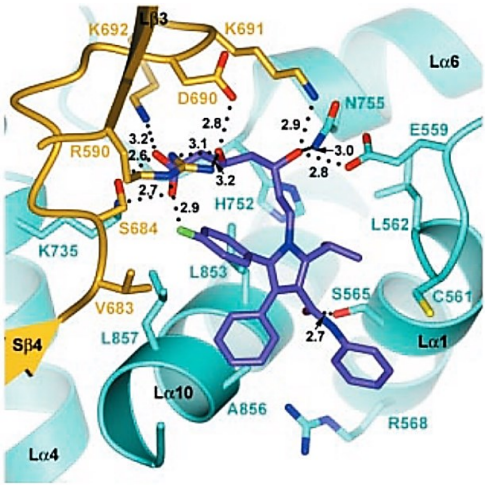

Figure 1.4 3D-modeled view of atorvastatin (purple) bound to human HMG-CoA reductase. The statin side chain is interacting with the amino acid residues of S684, D690, K691, and K692 present in the "cis-loop". The drug's hydrophobic part is placed in a gap between helices Lα1 and Lα10 (petrol).[9]

Variable additional binding characteristics are controlled by each of the statins' individual core molecule and can strongly influence the potency of pharmacological effects.[9] In this context, the first generation statins, such as lovastatin and compactin, are classified as **type I statins**. This group possesses a decalin based core structure, which is typically substituted with a **butyryl group**. Further statins considered as type I are simvastatin and pravastatin, which are semi-synthetic drugs derived from the first.[9] Fully synthetic drugs, on the other hand, belong to **type II statins**. These are second and third generation drugs, which were designed to possess larger, **fluorinated groups,** as in fluvastatin, atorvastatin, cerivastatin, rosuvastatin, or pitavastatin.[9] Figure 1.5 shows the molecular structures of the first generation natural lovastatin (**11**) and the fully synthetic fluvastatin (**14**).

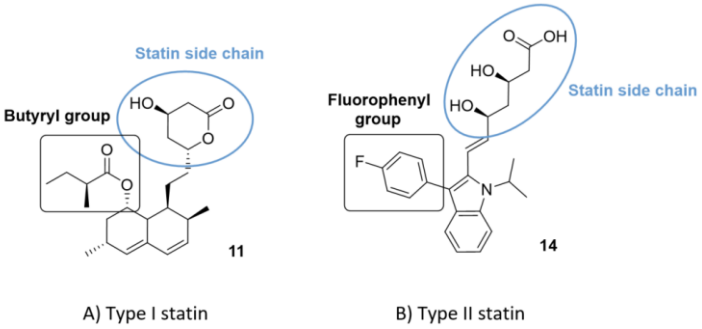

Figure 1.5 Comparison between type I and type II statins. A) Lovastatin (**11**) bearing a butyryl group B) Fluvastatin (**14**) featuring a fluorophenyl group. The statin side chains are highlighted in blue circles.

While the orientation of type I statins in the enzyme pocket is mainly directed by the decalin ring structure, for type II statins it has been reported that the fluorophenyl unit plays a major role in polar interactions with the R590 residue in the cis-loop. Rosuvastatin and atorvastatin, for example, exhibit hydrogen bonding with S565.[17]

Despite the fact that the enzyme-substrate-binding is in principle reversible, the inhibition outcome is extremely effective, because it is amplified by the drug's ability to alter the enzyme's

conformation upon binding at such an extent that the enzyme is prevented from remaining a functional structure.[47]

1.3. The future of statins: New use for an old drug?

Recent studies have enlightened the **pleiotropic biological and pharmacological response** that statins exhibit beyond their lipid-lowering properties.[40a, 48] Certainly, it is no surprise that the downstream event caused by interference into the mevanolate pathway compellingly goes far beyond simply blocking the generation of cholesterol in the liver.[49] Inhibiting a key enzyme at such an early stage of a complex circuit will forcefully exhibit rather multilateral effects: Isoprenoid metabolites like farnesyl pyrophosphate (FPP) or geranylgeranyl pyrophosphate (GGPP), which are known for prenylation of various cell signaling proteins, are transformed from early mevalonate-derived intermediates. They are also used for the synthesis of ubichinon-10 (Co-enzyme Q_{10}), which is a derivative of vitamin K and vitamin E.[50] Possible effects caused by their deficit include minor **side effects** commonly observed, such as headaches, insomnia, tenderness, nausea or vomiting, abdominal cramping, or pain. However, more severe outcomes can be hepatotoxicity, hemorrhagic stroke, cognitive decline, peripheral neuropathy, type II diabetes, muscle pain, digestive problems, or liver damage.[51] In very few cases, statins have been responsible for **life-threatening muscle damage** called rhabdomyolysis, causing severe muscle pain/muscle break down and potentially leading to kidney failure and even death.[38] The reasons behind most of these adverse effects have not been fully elucidated yet. However, the mainly occurring syndromes with up to 72% of all adverse events are muscle related and play the biggest role in **statin restriction** (cerivastatin, 2001).[38]
On the contrary, scientists are also studying on the statins' **emerging beneficial effects**, including anti-inflammatory[52] and immunosuppressive properties,[53] potential to treat neurological disorders,[49] sepsis,[49, 54] osteoporosis,[55] kidney disorders,[49] or even cancer.[40b] In fact, it is speculated that beside the cholesterol-lowering effects, the anti-inflammatory properties actually play a major role in lowering the risk for cardiovascular disease, as also inflammations in blood vessels are suppressed.[52b] These circumstances result into the manifold possibilities in statin treatment, making them remaining drugs with unresolved potential and holding a promising future. Needless to say that further intensified research is mandatory and represents a fascinating and multifaceted challenge.

1.4. The synthesis of statins

Since statins entered the market as blockbuster drugs over three decades ago, many scientists have been working on feasible routes to obtain large und pure quantities in order to adequately serve the needs of pharmaceutical industry. While the first generation statins were based on natural products and could be gained from **microbial fermentation processes**,[56] the second and third generation statins were initially obtained by **classical chemical synthesis**.[57] Nowadays, industry has also uncovered the potential of **semi-enzymatic routes**, navigating towards higher efficiency and a greener chemistry.[58] The following chapters will give an insight into the three mentioned strategies.

1.4.1. Microbial fermentation

Thousands of years ago, mankind started to use yeasts in winemaking, brewing beer, or baking bread.[59] Today, the exploitation of microorganisms for food processing or for the production of antibiotics and other drugs has become substantial. This is due to the fact that they can generate a diversity of natural products while often keeping the production costs very low in comparison to chemical synthesis.

In this context, commercially available **lovastatin** is isolated from microbial fermentation broths as a **secondary metabolite** produced by various fungal strains such as *Penicillium citrinum*, *Aspergillus terreus*, *Paecilomyces viridis*, and different *Monascus species* (*M. ruber, M. purpureus, M. pilosus, M. vitreus, M. pubigerus* and *M. anka*).[56] In batch fermentations of large scale processes, the employment of Aspergillus terreus has been mostly reported in literature. Investigations on the metabolic route showed that it resembles the pathway of fatty acid synthesis, which starts from acetate units that are repetitively condensed to each other in a head-to-tail manner. This process is catalyzed by a multi-domain enzyme complex called "polyketide megasynthase".[56]

Regarding reaction engineering processes, parameters such as temperature, pH, cell homogeneity, carbon source, time, and oxygen level were studied and adjusted towards maximal product yield.[56] Production by *A. terreus* was also brought to a higher level by **altering its gene**. An eightfold higher yield compared to the wildtype was reported by MUKHTAR *et. al.* after random mutagenesis by UV irradiation. This finally lead to increased product concentrations in the range of 1 g/L.[60]

1.4.2. Chemical synthesis

Due to the challenging structure of the chiral polyhydroxylated side chains numerous strategies have been suggested and continuously devised for the chemical production of synthetic statins.[61] This chapter focuses on the mostly applied routed with the possible carbonyl synthons shown in Scheme 1.3.[61]

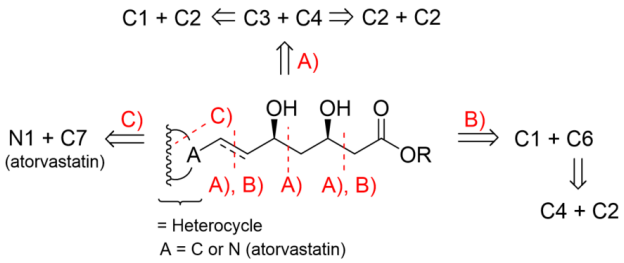

Scheme 1.3 Main retrosynthesis strategies A), B), and C) for the assembling of the statin side chain starting from basic carbon synthons.[61]

A) Many approaches typically start by first introducing a C1 synthon to the drug's heterocyclic core via formylation reaction followed by an elongation with a C2 unit. In some cases, this step is skipped by rather directly embedding a C3 unit via vinylogous formylation. The resulting aldehyde precursor is then elongated with a C4-acetoacetate derivative through **stereoselective aldol addition**. A **NARASAKA–PRASAD**[62] **type stereoselective reduction of the β-hydroxy ketone** finally gives the desired syn-diol (Scheme 1.4).[61] For this purpose, sodium borohydride is typically utilized in combination with a stereo-directing boron agent

such as di/trialkylborane, which directs in a stereoselective manner via formation of six-membered boron chelates with the reactant. Subsequent hydrolysis gives the target molecule.[61, 63]

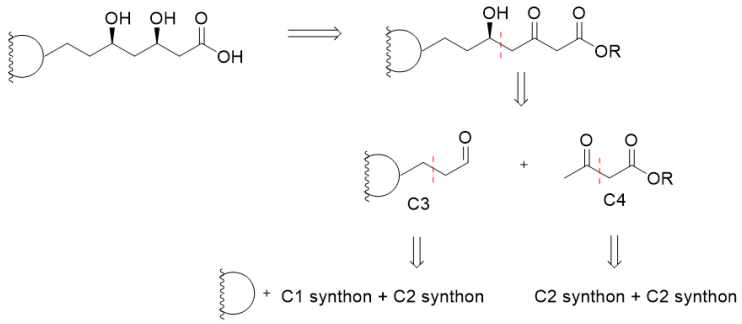

Scheme 1.4 Synthesis of statin building block starting from simple C1 and C2 synthons.[61]

However, the main disadvantage of this route is the rather late asymmetric reduction step after a long and tedious multi-step linear reaction sequence, which can lead to insufficient enantiomeric excess. Purification then tends to be problematic and leads to reduced yields, making this synthesis process very costly. Nevertheless, in the case of fluvastatin, this strategy still pays off as this drug is prescribed as a racemic mixture comprising equimolar amounts of the (*3R,5S*)- and (*3S,5R*)-enantiomer.[64]

B) Other methodologies are based on directly using larger **chiral C6 or C4 + C2 synthons** that are connected to the heterocyclic core via **WITTIG coupling**. For this purpose, either a phosphorous functionalized statin side chain is reacted with an aldehyde derivatized core molecule or the functionalities are used *vice versa* (Scheme 1.5).[61]

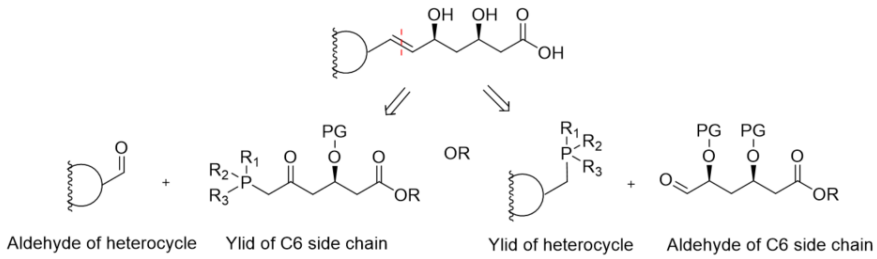

Scheme 1.5 Synthesis of statin building block via WITTIG coupling starting from C6 synthons.[61]

The chiral C6 synthons are mainly obtained via chiral pool synthesis in combination with a stereoselective borohydride reduction:

- One of the first approaches was reported by *Hoechst AG* and starts from the protected *(S)*-malic acid derivative **29**. Elongation by reacting with *tert*-butylacetate gives the ester intermediate **30**. The stereoselective key step to furnish the syn-diol **33** is performed by using triethylborane and sodium borohydrate as reduction agent (Scheme 1.6).[65]

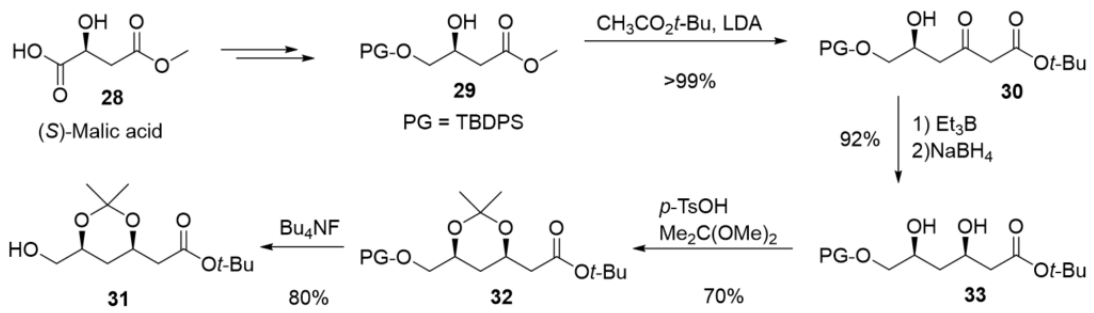

Scheme 1.6 Synthesis of C6 statin building block starting from chiral diol **29** obtained from *(S)*-malic acid (**28**). The stereoselective key step is performed by reduction with triethylborane and sodium borohydrate.[65]

- Another similar route was reported by SHIN *et al.* and starts with the ring-opening sequential transformation of *(S)*-epichlorohydrin (**34**). The asymmetric key reduction step is again carried out by treatment with triethylborane and sodium borohydride (Scheme 1.7).[66]

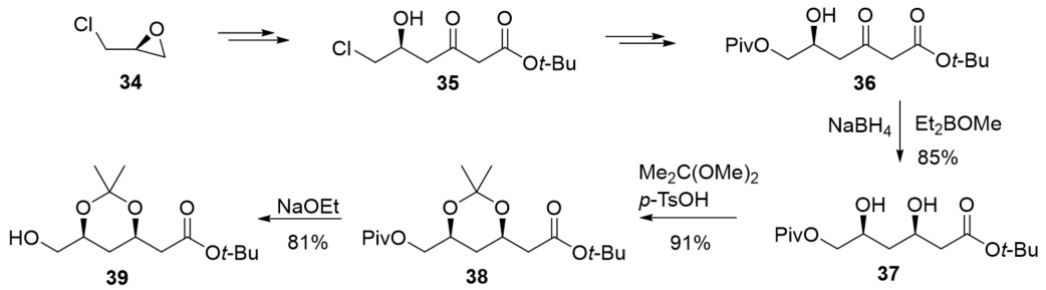

Scheme 1.7 Synthesis of C6 statin block **39** starting from a ring-opening sequential transformation of *(S)*-epichlorohydrin (**34**). The stereoselective key step is performed by reduction with sodium borohydride.[66]

The (protected) alcohols obtained in both approaches can be transformed into the corresponding aldehydes by simple oxidation reaction, e.g. SWERN oxidation.

C) Most strategies used for the assembly of atorvastatin (**5**) benefit from its very unique feature: The statin side chain is attached to the nitrogen atom of the heterocyclic core. This gives the opportunity to build the molecule from a complete C7 + N1 unit that will form the future pyrrol ring (Scheme 1.8).[61]

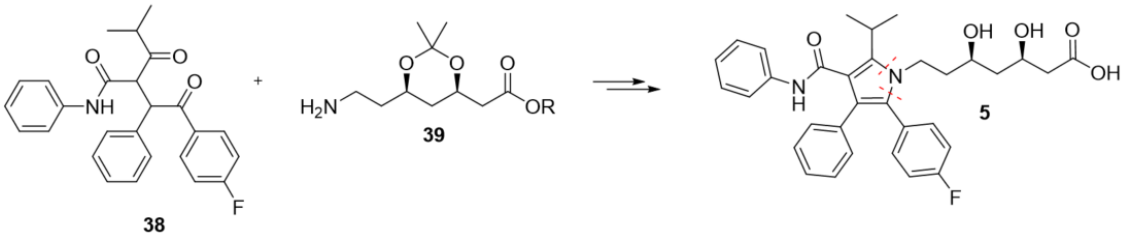

Scheme 1.8 Synthesis of atorvastatin (**5**) from C7 + N1 synthon.[61]

For the synthesis of the C7+N1 building block, following routes are possible:

- A very efficient way was reported by RADL and coworkers and is carried out starting from symmetric homoallylic alcohol **40.** A six-membered cyclic iodocarbonate **41** is formed by addition reaction with CO_2 as C1-carbon source. This **asymmetric synthesis** step directly furnishes the required syn-configuration of the protected diol **41.** Further chemical transformation yields the nitrile-functionalized building block **46** (Scheme 1.9).[61, 67]

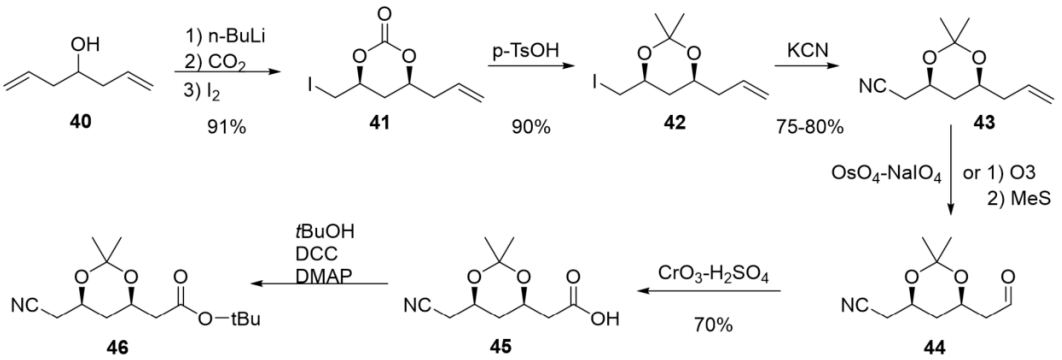

Scheme 1.9 Synthesis of C7 + N1 statin building block starting from homoallylic alcohol **40**.[61, 67]

- Other approaches are based on the assembly of a lactonized statin side chain instead of the open chain configuration. In this context, a strategy reported by JENDRALLA and co-workers starts with chiral cyclic ether **47** obtained from **chiral D-glucose** (Scheme 1.10).[68]

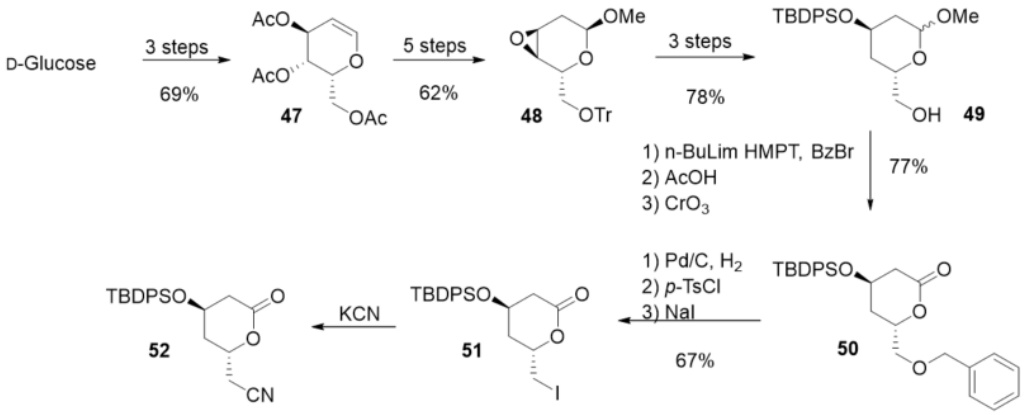

Scheme 1.10 Synthesis of C7 + N1 statin building block starting from chiral D-glucose.[56]

To sum it up, many different pathways have been investigated and reported for the chemical synthesis of statins. Although many advances have been accomplished, most pathways require tedious multistep synthesis and involve toxic catalysts and organic solvents.

1.4.3. Biocatalytic synthesis: An overview of enzymatic strategies

The requirement for extremely high chemical and stereochemical purity of statin drugs in multi-ton quantities has driven scientists into the field of enzyme catalysis, directing to a **greener** and more **environmentally friendly production**.[58]

For the formation of the chiral key fragments, various routes that include biocatalytic transformations have been reported in the literature. Scheme 1.11 summarizes the most promising approaches from the last years.[69] Details on the different routes (A – F) are discussed within the next chapters.

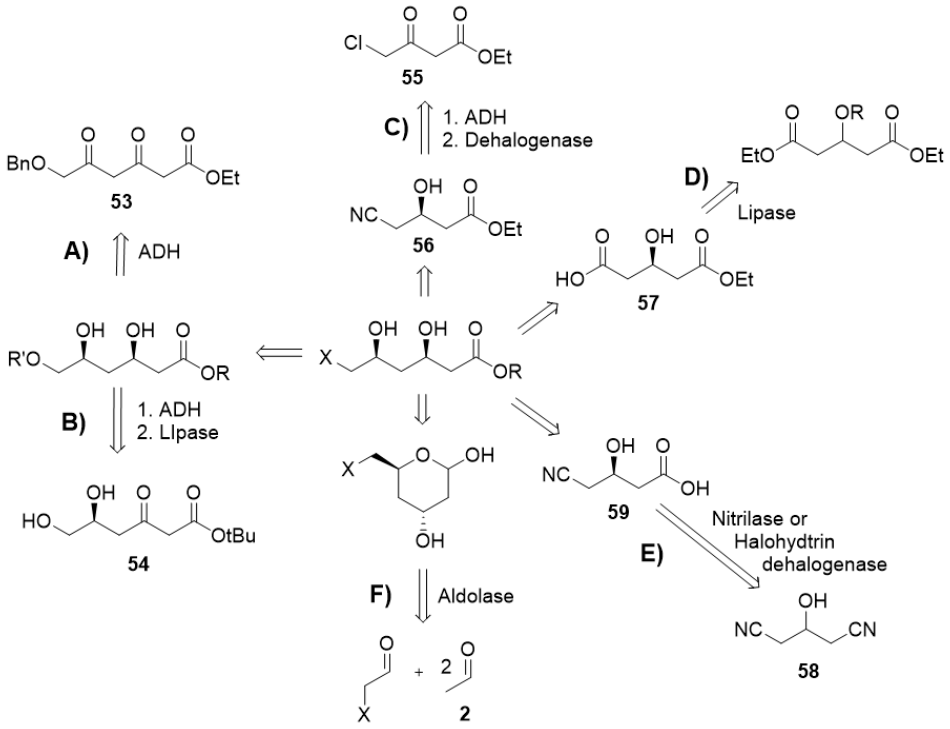

Scheme 1.11 Retrosynthetic routes for the production of statin side chains via biocatalytic transformations.[69]

A) A strategy based on the utilization of a **ketoreductase** (KRED) for **stereoselective** reduction of diketone **53** was introduced by scientists from *Bristol Myers Squibb* in 1993. Here, living cell suspensions of *Acinetobacter calcoaceticus* were applied in the presence of a glucose dehydrogenase (GDH) for NADPH-cofactor recycling (Scheme 1.12). At a substrate concentration of 10 g/L, yields of 72% and 99% *ee* were reached for a 1 L batch reaction.[70]

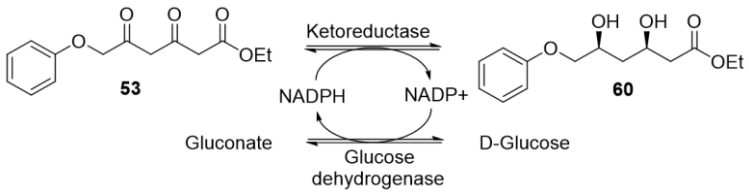

Scheme 1.12 KRED-catalyzed reduction of prochiral diketone **53**.[70]

B) A similar approach was presented by *Avecia Pharmaceuticals*. Starting from chiral 3-hydroxyketone **51** obtained from *(S)*-malic acid (**28**), **diastereoselective reduction** was performed by the KRED from *Pichia angusta*. Application of resting cells at a substrate concentration of 25 g/L gave the syn-diol with 80% yield. This intermediate was additionally regio- and stereoselectively acetylated by immobilized lipase from *Candida antarctica* to furnish statin precursor **62** with >99% *de* (Scheme 1.13).[71]

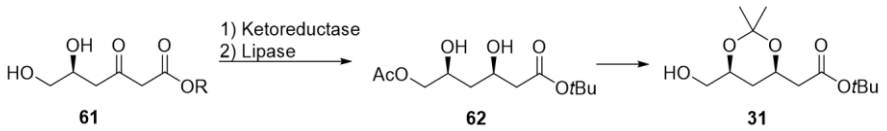

Scheme 1.13 KRED-catalyzed diastereoselective reduction of hydroxy ketone **61** and subsequent lipase-catalyzed regioselective acetylation to furnish building block **62**.[71]

C) Recently, *Codexis* introduced a **three-enzyme two-step** pathway starting from 4-chloroacetoacetate (**55**). The first stereoselective reduction step was previously reported by SHIMIZU and coworkers, who applied a **stereoselective KRED** from *Candida magnoliae* to yield the chiral precursor **63** with >99% *ee*. NADPH-cofactor recycling was accomplished by utilizing a glucose dehydrogenase from *Bacillus megaterium*. Application of a recombinant *E. coli* strain for overexpression of both enzymes elegantly simplified process handling. A yield of 95% was reached with >99% *ee* at a substrate concentration of 10 g/L.[72]

A subsequent enzymatic step involved a **halohydrin dehalogenase** (HHDH), which is known to catalyze the elimination of halides from vicinal halo alcohols, to furnish the desired nitrile-functionalized building block **56** upon treatment with NaCN. This step is performed by generating epoxides as intermediates by intramolecular nucleophilic displacement of the halogen group by the adjacent alcohol group (Scheme 1.14).[40b, 73]

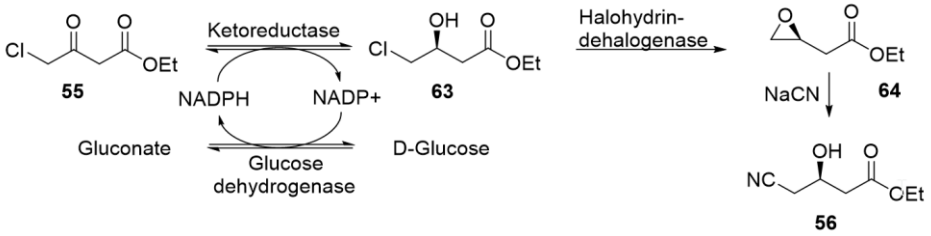

Scheme 1.14 KRED-catalyzed reduction of 4-chloroacetoacetate (**55**) and subsequent HHDH-catalyzed transformation to nitrile-functionalized **56**.[40b]

However, a major disadvantage that all of these systems bear lies in the formation of high amounts of gluconate due to the cofactor-recycling by GDH.

D) Another method is based on **desymmetrization** of symmetrical building blocks. Scientist at *Ciba Speciality Chemicals* applied **α-chymotrypsin** (α-CHY) for hydrolysis of the prochiral glutaric acid diethyl ester (**66**) obtained by acylation of readily available and low-priced glutaric acid ester (**65**). The resulting chiral monoacid **67** was produced in almost quantitative yield and high optical purity (94%, 98% *ee*). **67** can be easily converted to the corresponding acid chloride **68** for further coupling (Scheme 1.15).[74]

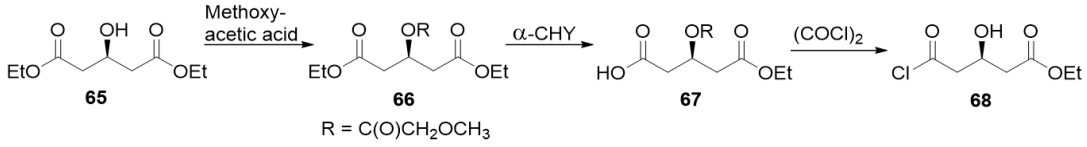

Scheme 1.15 α-Chymotrypsin-catalyzed desymmetrization of prochiral triester **66** to glutaric acid ester **67**.[74]

E) RUECROFT *et al.* followed a process that involved a **nitrilase-catalyzed desymmetrization** of 3-hydroxyglutaronitrile (**69**) obtained from epichlorohydrine (**34**) (Scheme 1.16). The resulting chiral monoacid **70** was achieved with 100% conversion and 99% *ee* after the reaction was optimized to work at 3 M (330 g/L) substrate concentration.[75]

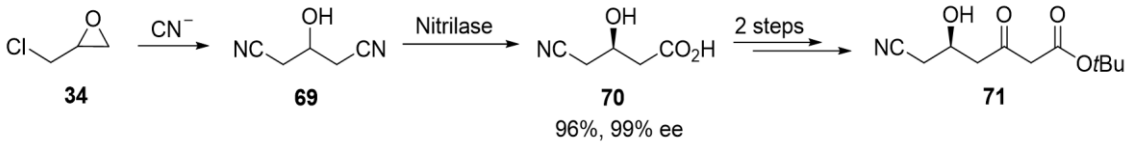

Scheme 1.16 Nitrilase-catalyzed desymmetrization of prochiral 3-hydroxyglutaronitrile starting from readily available epichlorohydrin (**34**).[62]

F) Recently, many scientists have gained great interested in approaches relying on **aldolases**.[76] This method appears to be very unique, as all previously mentioned enzymatic strategies sooner or later rely on the utilization of ketoreductases for enantioselective reduction of ketones, whereas the application of aldolases directly furnishes the desired stereocenters during a sequential assembling of the statin side chain.[76]
Aldolase catalysis will be discussed in detail within the next chapters.

1.5. Aldolase catalysis

1.5.1. Introduction to aldol additions

One of the main and fundamental focuses of organic synthesis has always been the **stereo-controlled** formation of new **carbon-carbon bonds**. Since aldol additions have been independently discovered by the French chemist ALEXANDER BORODIN[77] in 1869 and the Russian chemist CHARLES WURTZ[78] in 1872, they are highlighted as a cornerstone in a chemist's toolbox. Traditional aldol additions are **base- or acid-mediated** and connect a **nucleophile** (enolate/enol of aldehyde or ketone) to an **electrophile** (aldehyde or ketone) to form a β-hydroxy aldehyde or ketone. Herein, the greatest attraction lies in the formation of up to two **new stereogenic centers**, ultimately, turning two relatively simple molecules into a more complex chiral one (Scheme 1.17).[79]

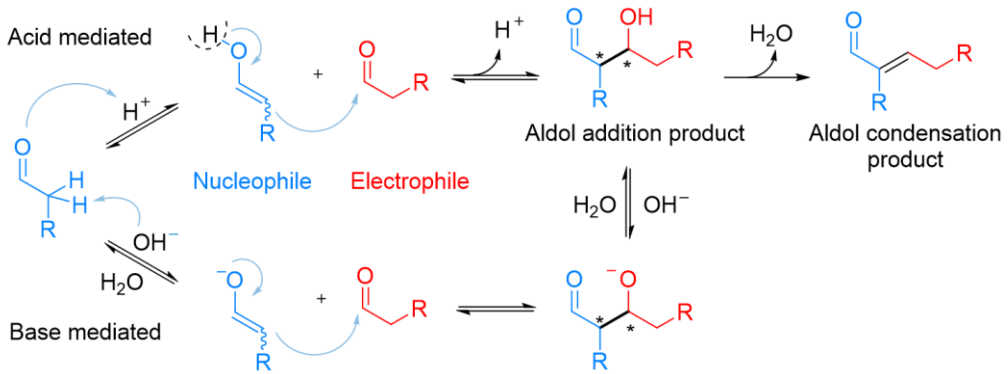

Scheme 1.17 Mechanism of acid and base-mediated aldol addition reaction. Subsequent elimination of water leads to the unsaturated condensation product.[79]

However, classical aldol additions are often accompanied with greater limitations for the practical use. The reactions are usually reversible or are prone to proceed to dehydration (aldol condensation) to form β-unsaturated carbonyl compounds (Scheme 1.17). In addition, the lack of stereoselectivity and, in the case of cross aldol reactions, chemoselectivity constitutes a major drawback. When reacting an aldehyde with a ketone, the aldehyde will typically take the role of the electrophilic component due to higher carbonyl reactivity, whereas the ketone serves as the CH-acidic counterpart. If both substrates are aldehydes, the reaction can yield a mix of different cross-aldol reaction products or homo-aldol products.[79]

To address these issues, various strategies have been applied, including the application of **pre-formed *(Z)*- or *(E)*-enolates**, which predetermine the substrate's role and also directs the electrophile into a certain orientation, predominantly giving the *syn*- or *anti*-aldol product, respectively.[79] Other methods rely on the use of **Lewis acid chiral metal complexes** as catalysts,[80] **chiral organo catalysts** (e.g. *L*-proline),[81] or **catalytic antibodies** (abzymes).[82]

A highly attractive alternative is offered by applying aldolases, which belong to the enzyme class of lyases, known for the reversible addition of a ketone or aldehyde (nucleophile) to an aldehyde (electrophile) in a typically stereocontrolled manner.[76]

In vivo, aldolases are responsible for the formation or cleavage of C-C bonds present in amino acids, hydroxy acids, or carbohydrates.[83] Regarding their catalytic mechanism, aldolases follow two different methods for the generation of the carbanion donor (nucleophile) and can therefore be classified into two distinct groups:[84] **Type I aldolases** are predominantly found in higher eukaryotes (animals and plants). They function without the need of metal cofactors and perform aldol reactions via formation of a **Schiff-base intermediate** that later transforms into an activated **enamine**. This requires a highly conserved **lysine as catalytic residue** in the active site, whose ε-amine group executes a nucleophilic attack on the carbonyl group of the donor substrate. Abstraction of the α-proton forces tautomerization to the corresponding enamine, which again, attacks the acceptor aldehyde upon C-C-bond formation. This step is performed strictly from the suited site, which explains control over the stereocenter. During this course, the imine is restored and subsequent hydrolysis finally releases the aldol addition product with up to two new chiral centers (Scheme 1.18).[85]

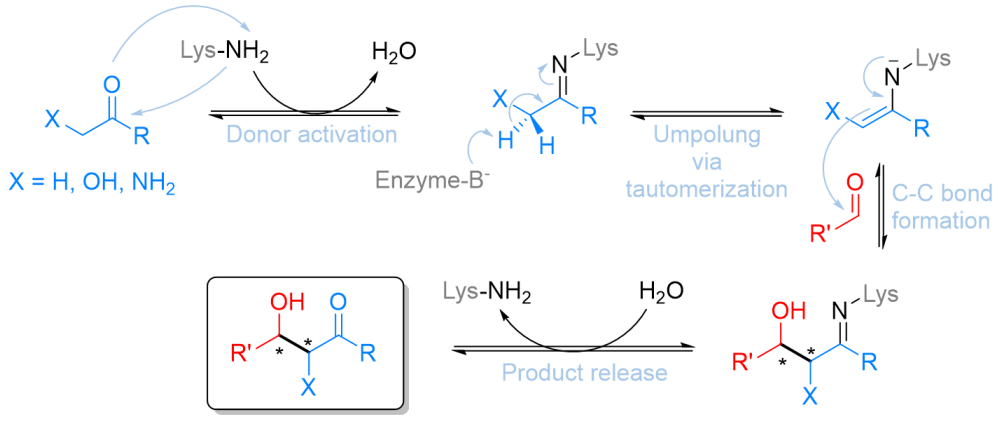

Scheme 1.18 Mechanism of aldolase-catalyzed aldol addition found in type I aldolases.[85]

Type II aldolases only exist in prokaryotes or lower eukaryotes: bacteria and fungi. They are typically **zinc (Zn^{2+})-dependent** enzymes and form activated **metal-enolates** with the donor

substrates. The metal cofactor is coordinated by the nitrogen atoms of three histidine active site residues and acts as a **Lewis acid**, enabling the deprotonation of the donor substrate by a glutamic acid side chain. The activated enol launches the nucleophilic attack onto the acceptor aldehyde, which is activated by the OH-group of a nearby tyrosine residue. In conclusion, type II aldolases activate both, donor and acceptor substrate (Scheme 1.19).[3c, 86]
Evidently, due to the metal-dependency, enzyme inhibition can be effectively induced by treatment with strong complexing agents such as EDTA.[87]

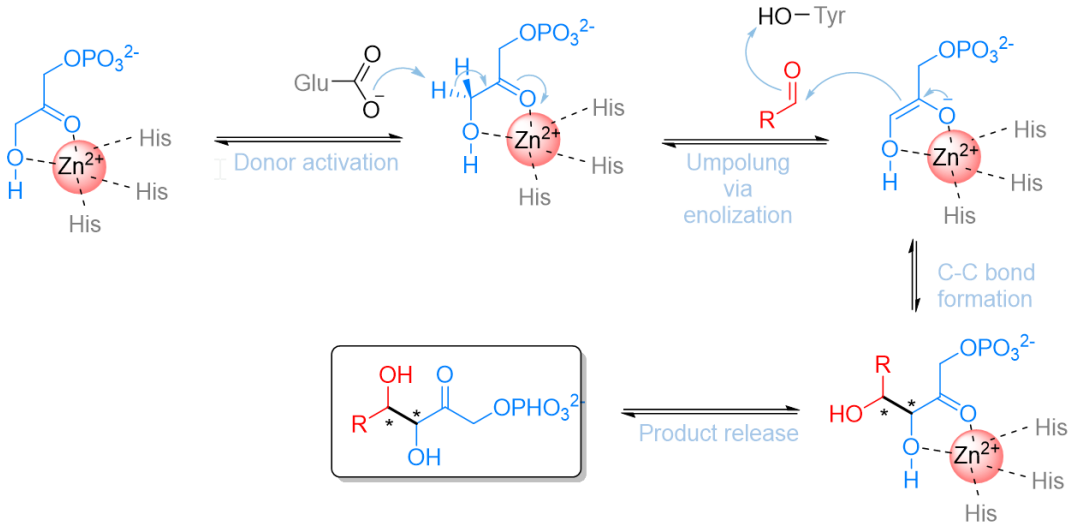

Scheme 1.19 Mechanism of aldolase-catalyzed aldol addition found in type II aldolases.[3c]

Mechanistic pathways for both, class I and II aldolases, have been elucidated by several crystal structure studies, giving insights into the stereo controlling events.[88] The stereochemical outcome of aldolase-catalyzed reactions is typically predetermined by the enzyme employed and does not depend on the utilized substrates. The obtained configuration is therefore mostly predictable for known enzymes.[3c]
Regarding the substrate scope, aldolases are usually highly restrictive when it comes to the nucleophiles and generally accept only minor isosteric modifications.[84, 89] Hence, apart from their catalytic mechanism, aldolases can be classified according to the donor substrates they transform in nature, comprising typically 2-carbon or 3-carbon fragments (Figure 1.6).[83]

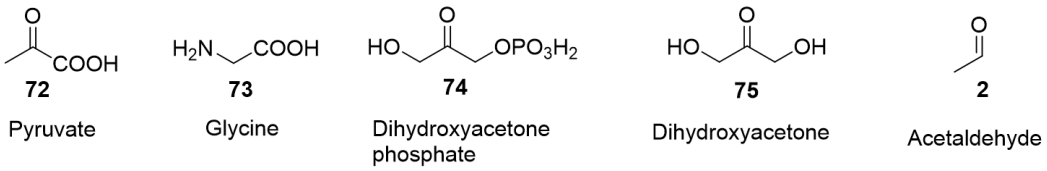

Figure 1.6 Natural donor substrate of different aldolase families.[83]

Group (i): Pyruvate-dependent aldolases

Pyruvate-dependent aldolases belong to a large family of enzymes, which, *in vivo,* have catabolic functions and are responsible for degrading keto acids such as sialic acids[3c, 90] and 2-

keto-3-deoxy-manno-octosonate (KDOs).[84] *In vitro*, they can be used for the synthesis of α-keto-γ-hydroxy acids. With pyruvate (**72**) as their native substrate, they utilize an inexpensive bulk chemical that is stable under most conditions.[91] This advantage becomes important when regarding the fact that reaction equilibrium is typically not favoring product formation but shifted towards the retro-aldol direction. Applying an excess of pyruvate, however, will lead to reasonable conversions.[3c] Decomposition of left-over pyruvate by generation of CO_2 and volatile acetaldehyde facilitates product isolation and can be realized by employing pyruvate decarboxylases.[92]

Interestingly, the α-keto-γ-hydroxybutyrate aldol products achieved from pyruvate addition to aldehydes offer all four commonly found oxidation states of the carbon atom, which enables selective transformations in consecutive steps yielding versatile building blocks (Scheme 1.20).[91]

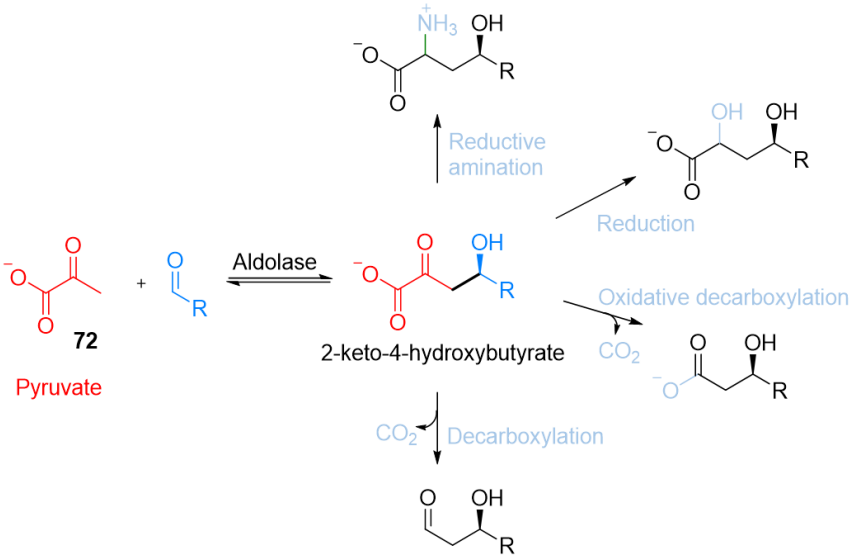

Scheme 1.20 Pyruvate aldolase-catalyzed stereospecific synthesis of 2-keto-4-hydroxy-butyrate and subsequent transformations to various building blocks.[92][74]

Group (ii): Glycine dependent aldolases

Glycine dependent aldolases catalyze the reversible aldol addition between the amino acid glycine (**73**) and different aldehydes to form *β*-hydroxy-*α*-amino acids upon utilizing pyridoxal-5'-phosphate (PLP) as cofactor. There are two members of this class of enzyme: Serine hydroxymethyl transferase (SHMT) and threonine aldolases. *In vivo*, SHMT produces serine (**77**) from addition of glycine (**73**) to formaldehyde (**76**) in a highly selective favor for the L-configuration (Scheme 1.21).[93]

Scheme 1.21 SHMT-catalyzed production of *L*-serine (**77**) by aldol addition of glycine (**73**) to formaldehyde (**76**).[93]

Similar *in vivo* activity is found in the group of threonine aldolases, which utilize acetaldehyde instead of formaldehyde as acceptor substrate. Therefore, unlike in the case of SHMT, these aldolases create two new stereocenters upon addition of glycine. Thus, formally, the reaction outcome delivers four different stereoisomers, depending on the enzyme used (D or L specific aldolases). While threonine aldolases act highly selective, regarding the configuration of the α-amino group, they typically show low to moderate control over the specificities of the *β*-hydroxy group, leading to diastereomeric mixtures of *threo*- and *erythro*-compounds.[3c]

Group iii): Dihydroxyacetone phosphate (DHAP) dependent aldolases

In the case of DHAP-dependent aldolases, nature has developed four stereocomplementary enzymes needed for the selective formation of all four possible stereoisomers that can be obtained from addition of DHAP (**75**) to an acceptor aldehyde (Scheme 1.22).[3c, 94]

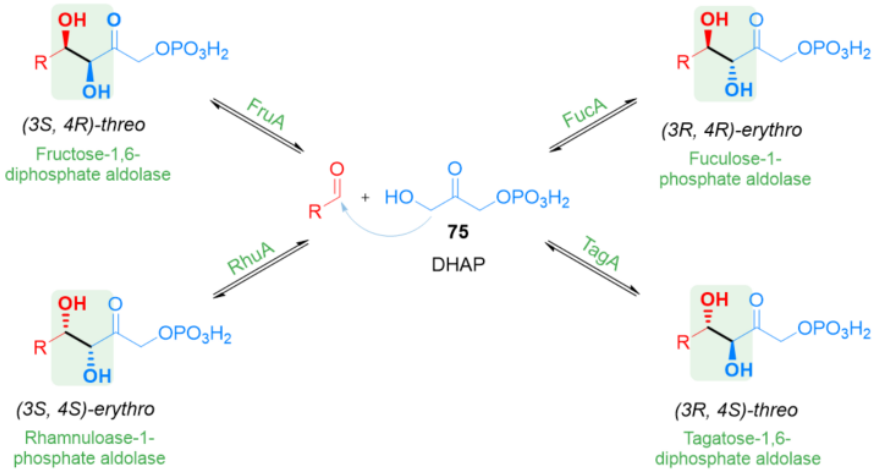

Scheme 1.22 Stereoisomeric products of aldol addition reaction between DHAP (**75**) and acceptor aldehyde depending on the aldolase applied.[3c]

To date, many of the DHAP-dependent aldolases have emerged into broad synthetic applications. D-Fructose-1,6-bisphosphate aldolase (FruA) from rabbit muscle, also referred to as "rabbit muscle aldolase" (RAMA), *in vivo* produces D-fructose 1,6-bisphosphate by reversible addition of DHAP to D-glyceraldehyde 3-phosphate.[95] Advantageously, *in vitro*, DHAP dependent enzymes have been found to tolerate a broad range of electrophiles, enabling the formation of unnatural carbohydrates[96] including nitrogen- and sulfur containing sugars,[97] fluorinated sugars,[98] and deoxy sugars.[98] Therefore, RAMA is most likely the best studied aldolase and has been widely applied in the synthesis of biologically active sugar analogs.
Anyhow, limitations are given by the restrict requirement of the phosphorylated donor substrate, which has limited chemical stability and easily decomposes into inorganic phosphate and methyl glyoxal.[84]

Group (vi): Dihydroxyacetone dependent aldolases

With the discovery of dihydroxyacetone dependent aldolases, a helpful solution for avoiding the need of phosphorylated substrates required for the group of DHAP-dependent aldolases was

found. D-Fructose-6-phosphate aldolase (FSA) from *E. coli.,* a class I aldolase, consumes dihydroxyacetone (DHA) (**75**) as its natural substrate but exhibits identical stereospecificity compared to D-fructose-1,6-aldolase and accepts a broad range of acceptor aldehydes as well. Therefore, these aldolases offer a valid alternative to the application of RAMA.[3c, 89, 99]
Many studies were performed to investigate on the nucleophile promiscuity of FSA, which shows rather relaxed specificities by also accepting non-natural donors such as hydroxyacetone (HA), hydroxybutanone (HB), and glycolaldehyde (GO) with full stereo- and regiospecificity (Scheme 1.23).[100]

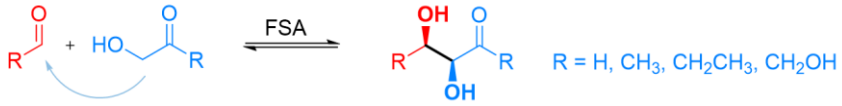

Scheme 1.23 FSA-catalyzed stereoselective aldol addition reaction.[100a]

Group (v): Acetaldehyde dependent aldolases

This group comprises only one member, which is the 2-deoxy-D-ribose-5-phosphate aldolase (DERA). As this enzyme will play an important role in this work, it will be described in greater detail within the next chapter.

1.5.2. 2-Deoxy-D-ribose-5-phosphate aldolase (DERA)

Physiologically, DERA plays a role in the pentose phosphate pathway and, therefore, belongs to the core metabolism of living organisms. In humans, DERA is mainly expressed in lung, liver, and colon and is responsible for the **stereoselective synthesis of 2-deoxy-D-ribose 5-phosphate** (D-R5P) (**80**) from D-glyceraldehyde 3-phosphate (D-G3P) (**78**) and acetaldehyde (**2**).[101] It is therewith one of the rare aldolases that utilizes acetaldehyde (**2**) as natural donor substrate and catalyzes aldol additions between two aldehydes in a cross-aldol manner instead of typically consuming an aldehyde and a ketone (Scheme 1.24).[102] With this feature, DERA is unique and unprecedented among aldolases, except for a few recently discovered variants of D-fructose-6-phosphate aldolase.[103]

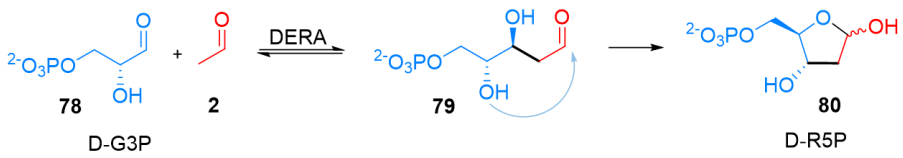

Scheme 1.24 DERA-catalyzed aldol addition reaction between glyceraldehyde 3-phosphate (D-G3P) (**78**) and acetaldehyde to form 2-deoxy- D-ribose 5-phosphate (D-R5P) (**80**) via spontaneous intramolecular cyclization.[102]

Crystal structure determination of DERA from *Escherichia coli* (*E. c.*)[88f, 104] as well as of its orthologs in *Thermus thermophilus,*[105] and in the archae *Aeropyrum pernix*[106] allowed for determination of the enzyme's reaction mechanism. Identification of **highly condensed lysine residues** (Lys167 and Lys201) implicated a typical **SCHIFF base**-mediated mechanism of **class I aldolases**. It was found that, while the active Lys167 forms an enamine with the donor molecule, Lys201 is responsible for decreasing the pK_a of Lys167 and together with Asp102 functions as a proton-relay system (Scheme 1.25).[101]

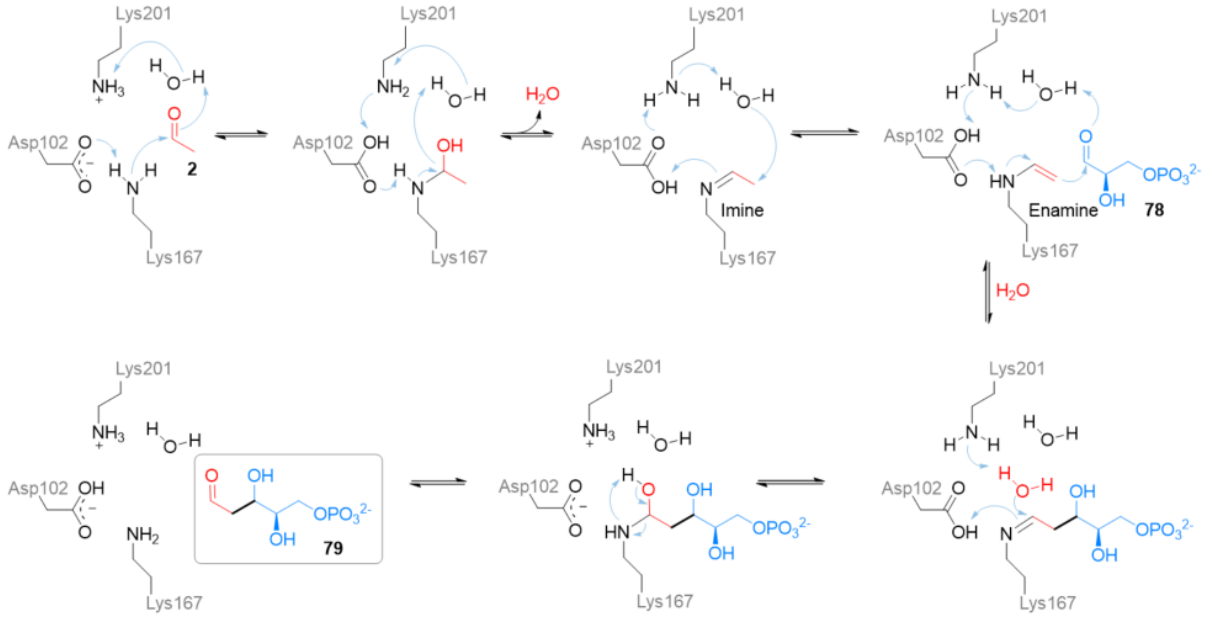

Scheme 1.25 Mechanism of DERA-catalyzed stereoselective aldol addition reaction between acetaldehyde (**2**) and glyceraldehyde-3-phosphate (D-G3P) (**78**) via enamine formation.[101]

Regarding DERA's tolerance for unnatural substrates, it was found that a broad variety of aldehydes can be utilized. Herein, DERA exhibits **relaxed substrate specificity** not only on the acceptor side but also on the donor side, displaying complementarity to applications using FSA, which was initially known as the only aldolase with a large nucleophile promiscuity.[103] Besides acetaldehyde (**2**), nucleophiles such as propanal (**81**), acetone (**9**), and fluoroacetone (**82**) are consumed, albeit at much lower rates.[103] Recent studies also revealed enzyme activity towards various cyclic or hydroxylated nucleophiles such as cyclobutanone (**83**), cyclopentanone (**84**), hydroxy acetone (**85**), and dihydroxyacetone (**75**) when applying the natural substrate G3P as acceptor. Figure 1.7 summarizes the nucleophiles that are known to be accepted by DERA to date.[103]

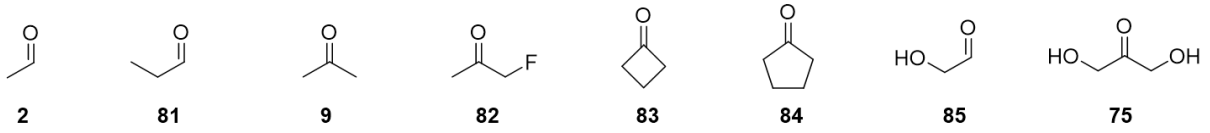

Figure 1.7 Nucleophiles accepted by DERA reported in literature.[103]

It is therefore no wonder that, since the start in 1990 with the initial work of BARBAS and WONG, the application of DERA has gained interest as an interesting tool for the synthesis of carbohydrates.[102a] Especially, when four years later, in 1994, GIJSEN and WONG took the application of DERA to the next level by utilizing three achiral aldehydes in a **sequential aldol addition** manner to generate highly desirable polyfunctional chiral (*3R,5R*)-2,4,6-trideoxy hexoses.[107] Herein, the aldol product of the first addition reaction is again consumed as an acceptor substrate in a second aldol addition. This reaction is thermodynamically controlled and shifted towards product formation due to a spontaneous, **intramolecular cyclization** and hereby generating a **stable half-acetal/lactol** (Scheme 1.26 and Scheme 1.27).[102b]

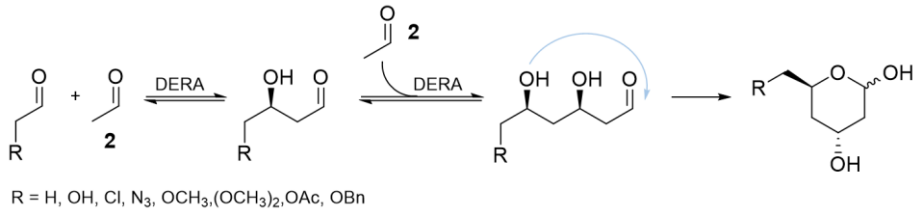

Scheme 1.26 DERA-catalyzed two sequential aldol addition reactions of acetaldehyde to various acceptor aldehydes reported in literature.[102b, 108]

Sequential aldol addition reactions of even up to four molecules of acetaldehyde in a self-aldol manner have been reported by GIJSEN and WONG in 1995[102b] and were later also confirmed by HELAINE.[109] In her works, addition of up to three molecules of acetaldehyde to hydroxypyruvaldehyde phosphate (HPP) in a cross-aldol reaction has been observed as well.[109]

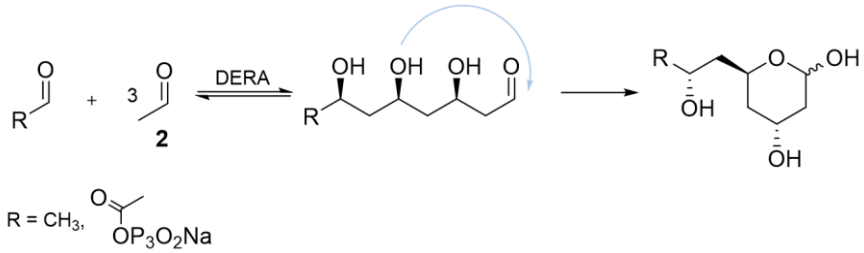

Scheme 1.27 DERA-catalyzed three sequential aldol addition reactions.[109]

As each addition is typically performed in a **highly stereoselective** fashion, the furnished deoxy-sugars are often used as chiral building blocks for the pharmaceutical industry. Deoxy-sugars feature notable biological and physiological activities and are for example used in anti-cancer drugs or cholesterol lowering agents.[110] Therefore, DERA has attracted great attention in both, academic and industrial fields and is considered an extremely powerful and useful catalyst for the synthesis of highly functionalized products with stereochemical fidelity.
However, initially, DERA was not adapted in many large-scale commercial applications due to the bottleneck of rapid enzyme inactivation caused by high substrate concentrations relevant to industry.[111] Especially, greater amounts of acetaldehyde, even though being the natural substrate, could not be utilized. Incubation in 200 to 300 mM acetaldehyde for 2 to 3 hours typically led to a loss of activity, which could not be restored upon washing.[88e] Therefore, various technological strategies have been researched and employed to address these difficulties. Some of these strategies will be further addressed in the next chapter.

1.6. DERA-catalyzed statin synthesis: State of the art

The pioneering work of GIJSEN and WONG in 1994[107] provided the pharmaceutical industry with a novel, elegant and efficient way for the production of statin side chain building blocks. Thus, today's block buster drugs like atorvastatin, rosuvastatin, and pitavastatin are produced based on DERA's capability to build up the entire carbon skeleton of the statin side chains via sequential stereoselective aldol additions. This strategy has been implemented on lab scale as well as on industrial scale (e. g. *DSM Sinochem Pharmaceuticals*).[76]
This chapter gives an overview of the recent research, strategies, and new perceptions towards the application of DERA in statin synthesis.

1.6.1. DERA acceptor substrates for the synthesis of statins

Since DERA can discriminate very well between acetaldehyde as acceptor and as donor substrate, it is only consumed as the acceptor as long as no better electrophile is available. This creates the opportunity to build the side chain starting from electrophiles that are well accepted by the enzyme and bear **customized functionalities** that will later allow for simple coupling of the statin building block to the drug's molecular core.

In order to evaluate the enzyme's preference for the possible electrophiles, scientists have measured the relative reaction rates for various acceptor substrates when utilizing acetaldehyde as nucleophile. In these experiments the native DERA from *E. coli* was employed, as this catalyst is regarded as the most prominent due to its status as the first discovered DERA.[112] The substrates applied and corresponding results are shown in Figure 1.8. Here, the relative rate for the natural substrate D-glyceraldehyde-3-phosphate (***(R)*-78**) is set to 100. As can be seen, *Ec*DERA$_{WT}$'s tolerance is typically limited to very **small or negatively charged acceptor substrates** with strong preference for phosphorylated ones.[112]

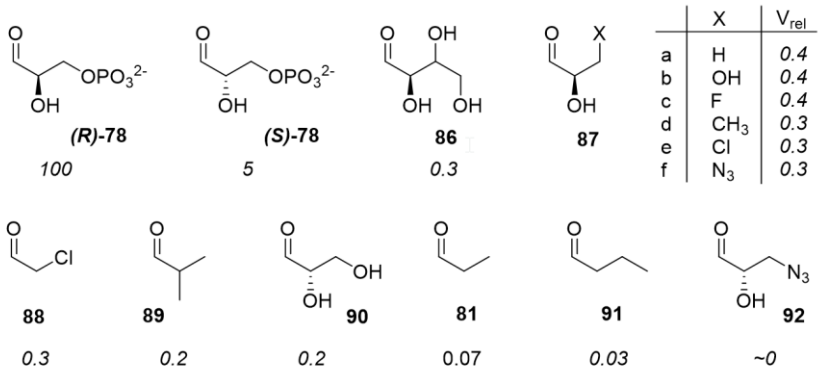

Figure 1.8 Relative rates of *Ec*DERA$_{WT}$-catalyzed aldol additions between different acceptor aldehydes and acetaldehyde. The relative rate of the natural substrate D-glyceraldehyde-3-phosphate (***(R)*-78**) is set to 100.[112]

The activity measured for functionally interesting substrates like chloroacetaldehyde (**88**) or azide **92** are rather low in comparison to D-glyceraldehyde 3-phosphate (***(R)*-78**) (V_{rel}=0.3%). However, their values are still amongst the higher ones reported for alternative (non-phosphorylated) acceptor substrates, offering potential for further development and application. Hence, today, many approaches utilize substrates with functional groups such as **azide**, **chlorine**, or **protected alcohols/esters**, which are tolerated by the enzyme, don't interfere within the actual reaction, and can later be easily transformed into amines or aldehydes via chemical synthesis for further coupling to the statin core molecule (Scheme 1.28).[113] Employing 3-azidopropionaldehyde (**93a**) as substrate offers a straight-forward route to yield the amine functionality of **98** for atorvastatin synthesis via hydrogenation or STAUDINGER reaction. Starting from chloroacetaldehyde (**96b**) the same amine **98** can be generated after C1-elongation of the chain by treatment with cyanide via nucleophilic substitution of the chloride functionality. Subsequent reduction of the nitrile intermediate **96** yields the desired building block. Alternatively, an aldehyde can be obtained from the chlorine functionality via generating an alcohol intermediate **31** and subsequent oxidation. The same counts for approaches utilizing masked alcohols and esters (**96c-f**).

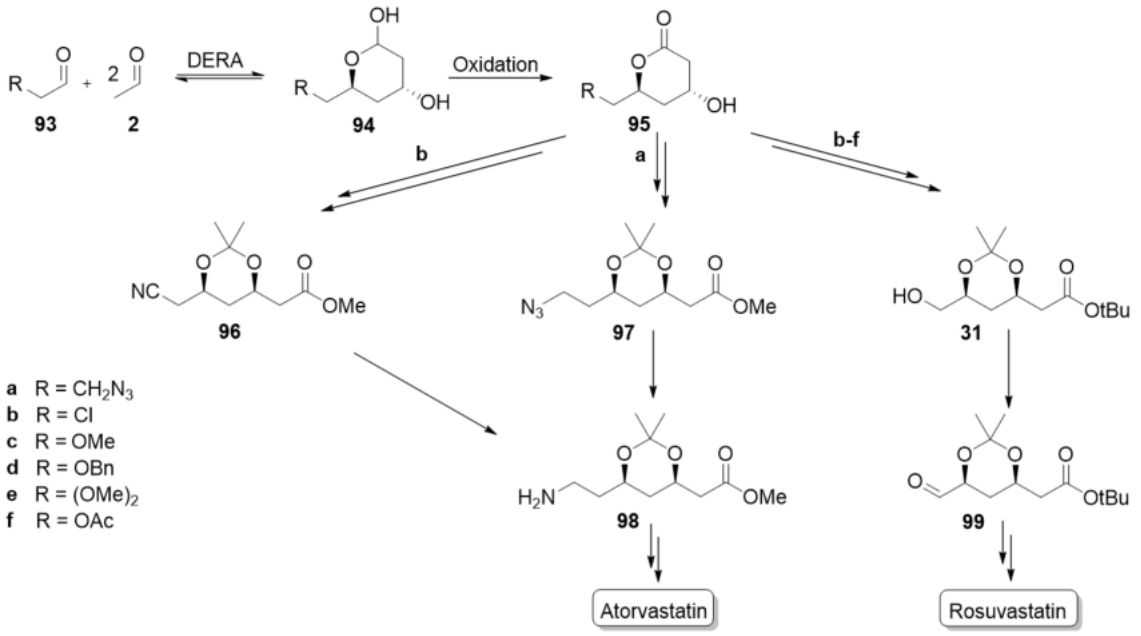

Scheme 1.28 Synthesis scheme of blockbuster statins atorvastatin and rosuvastatin starting from diversely functionalized aldehydes **93a-f**.[113]

All mentioned strategies share the benefits of starting from cheap bulk chemicals and following easy standard reaction processes to reach the final target molecule and are therefore all viable. In the case of chloroacetaldehyde (**93b**), early works of GIJSEN and WONG in 1994 have shown that *Ec*DERA$_{WT}$ already prioritizes the chlorinated substrate over acetaldehyde. When both were applied as electrophiles in a competitive manner, higher conversions were reached for the cross-aldol reaction.[102b, 107, 108b] This finding was later also confirmed by SHEN and co-workers in 2013 after measuring a lower docking energy, thus higher preference in the electrophile's binding site for chloroacetaldehyde compared to acetaldehyde (-1.95 and -2.16 kJ/mol, respectively).[114]

Anyhow, following the quest to explicitly find more DERAs with higher affinity for chloroacetaldehyde (**93b**), in 2006, JENNEWEIN *et al.* created a novel *Ec*DERA library of 10.000 clones via random point mutagenesis (error-prone PCR). The screening was performed by direct GC-MS quantification of the aldol addition product **94b** between chloroacetaldehyde (**93b**) and acetaldehyde (**2**) and revealed seven candidates with improved activity compared to the wildtype. Two of the seven hits were double mutants (T19I/I166L, S93G/A174V) while the other five showed single amino acid alterations (K13C, F200I, T19S, M185T, S239C). Among these, the most **remarkable variant** was the **F200I**, which showed an almost 14-fold increase in productivity with a significantly lower K_m value of 24 ± 4 mM compared to the wildtype (K_m = 55 ± 5 mM).[111a]

Transformation of azide **93a** was achieved by applying an engineered *Ec*DERA variant reported by DESANTIS and WONG in 2003.[115] This novel catalyst was identified within the process of creating variants with higher affinity for non-phosphorylated substrates by altering specific amino acid residues that are responsible for binding of the phosphate group. It was reasoned that changing the active site residue S238 for an aspartate will remain the hydrophilic nature of the binding pocket but enhance preference for neutral or positively charged groups. In fact, for the **S238D** variant a 2.5-fold improvement in the K_{cat}/K_m value compared to the wildtype

was measured. 3D-modeling enlightened that the substrate's hydroxyl group at the C-3 position forms a hydrogen bond with the carboxylate of D238 resulting in an increase of reactivity.[115] The *Ec*DERA$_{S238D}$-catalyzed process, starting from azide **93a**, was finally performed by LIU and WONG in 2004. Subsequent chemical synthesis to achieve the target amine functionalized building block **98** (according to Scheme 1.28) was conducted with a satisfactory total yield of 14%.[116]

1.6.2. DERA's intolerance for high substrate concentrations

One of the greatest limitations in DERA application lies in the enzyme's low tolerance for high amounts of aldehydes. For instance, within 1 minute of incubation in 200 mM chloroacetaldehyde or acetaldehyde, the wildtype enzyme of *Ec*DERA already loses a large part of 84.9 ± 0.5% of its catalytic activity.[113] Therefore, the next chapters will summarize advances in the discovery of DERAs with increased stability (I) and also recapture the so far elucidated mechanisms of enzyme inhibition (II).

I) The search for DERA variants with improved stability

In order to match commercial feasibility of DERA-catalyzed processes, in 2004, GREENBERG *et al.* (*Diversa*) screened for DERA variants with improved parameters like tolerance for higher chloroacetaldehyde concentrations and reduced catalyst load. Among their **large genomic libraries** collected from samples around the world, they identified over 15 DERAs that showed activity in the relevant reaction and one variant (unknown source) with superior characteristics over the wildtype DERA from *E. coli* (30% sequence identity).[113] Additional reaction engineering approaches (e. g. embedding a fed batch process) led to a 7-fold higher product concentration (>0.5 M) upon reducing the reaction time dramatically (3 h) and utilizing a much smaller catalyst load of only 2.0% (wt/wt) instead of 20% (wt/wt) compared to the application of *Ec*DERA$_{WT}$ reported in WONG's work.[108b, 113] The process was optimized for an industrial scale at low temperatures (2 – 4 °C), leading to a final product concentration of >100 g/L.[117]

In 2006, the *Ec*DERA mutant library, created by JENNEWEIN *et al.* for chloroacetaldehyde activity screening, was also scanned for variants with increased tolerance for higher substrate concentrations.[111a] Herein, the screening was performed by measuring the enzyme's residual activity for DRP cleavage after treatment with up to 300 mM chloroacetaldehyde. The group was able to identify various candidates with increased stability, among which several variants differed only in the protein's C-terminal amino acids. Here, the terminal Y259 was either swapped for a threonine or was completely deleted from the sequence. In some cases, a sequence of nine additional amino acids was added. As observed in the protein's crystal structure, the C-terminal amino acids occurred to fold back towards the active site and therefore might play a certain role in substrate binding. Surprisingly, it was found that the described changes actually lead to a decrease of DRP cleavage activity, but incubation in chloroacetaldehyde caused a permanent activation, which was explained through eventual covalent modification. Combination of the most beneficial mutations led to three superior variants (N80S/E127G/M185V/S158T/Y159T+9 additional amino acids, Y49F/M185T and D84/ΔY159), which were able to retain up to 31% of their activity after being incubated in 400 mM chloroacetaldehyde for 5 min.

LI and coworkers later combined the results provided by JENNEWEIN and DESANTIS, whose most promising variants were reported as the *Ec*DERA variants F200I/ΔY259 and S238D, respectively. In his study, DERA from *Klebsiella pneumoniae* (KDERA) was altered to yield the triple mutant **S238D/F200I/ΔY259** that, in comparison to the wildtype, showed a 3.15-fold increase in activity and a 1.54-fold improvement in substrate tolerance towards D-glyceraldehyde. It is speculated that the mutations are also beneficial in regard to tolerance for non-phosphorylated aldehydes.[118]

In 2007, SAKURABA *et al.* published results of their studies on DERAs from the **hyperthermophiles** *Pyrobaculum aerophilum* (*Pa*) and *Thermotoga maritima (Tm)*. It was reported that these enzymes exhibited much greater catalytic activity in the sequential aldol condensation of three molecules of acetaldehyde than *Ec*DERA$_{WT}$, and were able to retain 50% of their activity even after incubation in 300 mM acetaldehyde for 20 h. This extremely high stability was explained due to the **quaternary structure** given in *Pa*DERA and *Tm*DERA. It was reasoned that compared to *Ec*DERA the subunit interfaces between the dimeric structures present in the thermophilic enzymes are much larger and thus feature stronger hydrophobic subunit interactions.[119]

In 2011, KULLARTZ and PIETRUSZKA introduced a novel DERA from the bacterium *Rhodococcus erythropolis (Re)*. This organism was chosen due to its widespread occurrence in extremely different habitats. *Re*DERA preferably operates in the alkaline pH range of 9.0 and showed a 2.5-fold longer half-life upon exposure to 300 mM acetaldehyde than *Ec*DERA.[120]

In 2015, JIAO *et al.* identified a novel thermostable DERA from *Lactobacillus brevis (Lb)*, which offered a 2-fold larger half-life in high concentrations of acetaldehyde compared to *Ec*DERA$_{WT}$. The enhanced thermostability presumably results from the enzyme's quaternary build, which was visualized via crystal structure resolution. Starting from the wildtype gene, a single mutation was introduced by exchanging the glutamate residue at position 78 to a lysine. This swap allowed for the formation of two additional hydrogen bonds between the side chain of K78 and G71, and V96, as well as one salt bridge connecting to D113 (Figure 1.9 A). These changes finally added to an enhanced thermostability and aldehyde tolerance, allowing for concentrations of up to 700 mM of chloroacetaldehyde and 1.4 M acetaldehyde. Thus, an unprecedented space time yield of 792 g/L/d while still utilizing a very low catalyst load of 2.5 g/L was reached with *Lb*DERA$_{N78L}$.[121]

In 2016, the same group (JIAO *et al.*) created a novel error-prone PCR *Lb*DERA library of 2000 clones that, via high-throughput screening, furnished two new, improved *Lb*DERA variants (T29L with 3-fold and F163Y with 4.5-fold higher activity than the wildtype). Combination of these hits gave the double mutant T29L/F163Y with a 7-fold higher activity compared to the native enzyme. In order to understand the mechanism responsible for activity improvement, the structural changes were elucidated by resolution of the crystal structure as depicted in Figure 1.9.[122] Even though T29 does not appear to exhibit close contact to the substrate, substitution with a leucine residue erases the hydrogen bond with N16, which is present in the loop between the enzyme's subunits. This makes enzyme movement more flexible and thus facilitates access of substrates. Introducing a phenylalanine instead of the tyrosine at position 163 also enlarges the active site entrance for easier entry. In addition to that, tyrosine, being a hydrophilic residue, while phenylalanine is a hydrophobic one, also levers the binding of hydrophilic substrates (Figure 1.9 B).[122]

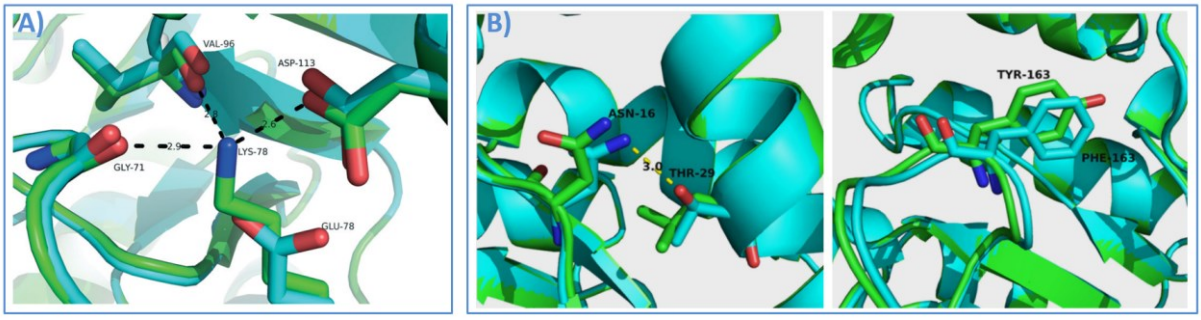

Figure 1.9 Superimposition of the crystal structures of *Lb*DERA wildtype (blue) and variants (green). A) The introduced K78 forms hydrogen bonds with G71 and V96 as well as a salt bridge with D113. B) Substitution of the residue T29 for L29 erased the hydrogen bond connecting to N16. Substitution of F163 with Y163 enhances the hydrophilic character of the active site.[122]

II) Mechanism of enzyme inhibition

In 2015, YANG and co-workers tried to shed more light on the matter of substrate-based enzyme inhibition by conducting structure-dependent substrate tolerance studies on the DERA from *Staphylococcus epidermidis (S. ep.)*.[111b] This strain was chosen, because earlier studies revealed that its DERA showed higher activity towards DRP-synthesis than *Ec*DERA but, at the same time, showed low tolerance towards acetaldehyde. Based on their earlier works, which indicated a positive correspondence between solvent tolerance and protein rigidity, molecular simulations predicted a variant with three amino acid alterations (T120C, G174I and G213C) that promised much higher structure stability compared to the wildtype. In fact, the predicted variant retained 70% residual catalytic activity after exposure to 300 mM acetaldehyde for 2 h, whilst the wildtype was left with only 11% activity.[111b] Since enhancing the **rigidity of the protein structure** seemed to also **enhance substrate tolerance**, these results suggested that inactivation of DERA by exposure to high amounts of aldehyde may result from protein structural damage. However, the clear mechanism was still not understood.

In very early works of HABEEB (1968), the effect of **enzyme inactivation** was reported to be due to **formation of SCHIFF bases with surface-accessible lysine residues**.[123] Hence, in 2006, JENNEWEIN substituted all of the surface lysine residues of *Ec*DERA by site-directed mutagenesis. Still, none of the resulting active candidates showed an enhanced acetaldehyde tolerance, presuming that SCHIFF base formation was not the only reason for enzyme inactivation.[111a]

It was until 2016, when the working group of PIETRUSZKA dedicated very detailed investigations on the mechanism of aldehyde deactivation in order to identify a way to prevent or withdraw this effect.[88e] PIETRUSZKA found that a reason for inactivation was caused by **crotonaldehyde (101)**, which readily forms from the acetaldehyde dimer by elimination reaction and proved to block the enzyme's catalytic center by acting as a **covalent linker**, connecting the **catalytic lysine 167** to the adjacent **cysteine 47 residue** in an **irreversible** fashion. The mechanism starts from crotonaldehyde (**101**) generating an imine (**102**) with the amino group of K167 upon elimination of water. Subsequent MICHAEL addition of the thiol group of C47 to the β-C and hydration of the imine double bond leads to the stable final compound **104** (Scheme 1.29).[88e]

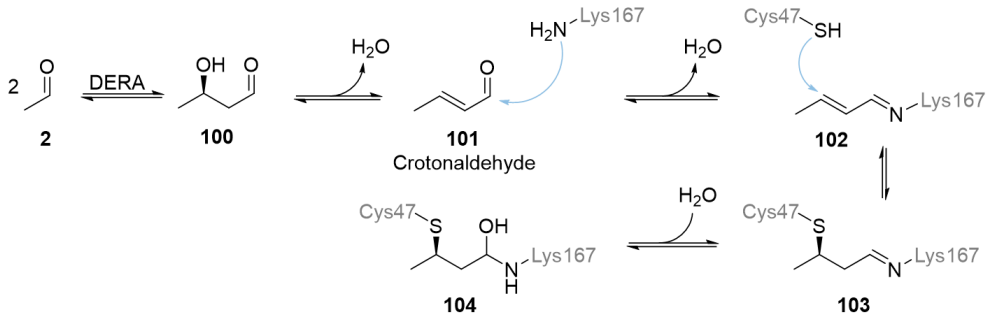

Scheme 1.29 Mechanism of crotonaldehyde-induced inactivation of DERA via covalent linker formation between catalytic lysine and cysteine residue.[71e]

Figure 1.10 illustratively shows the enzyme's active site before and after incubation with acetaldehyde, with the free catalytic lysine and the cysteine coupled residue, respectively.[88e]

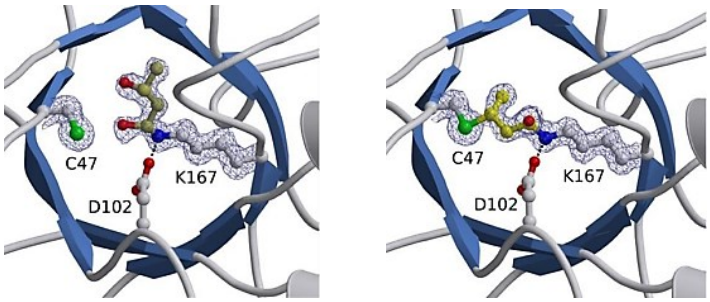

Figure 1.10 Illustration of DERA active site before (left) and after (right) incubation with acetaldehyde.[88e]

In conclusion, two different strategies were followed to overcome this deactivation mechanism, including temperature control and active site mutation:[88e]

1) Temperature control

As *Ec*DERA exhibits a rather thermostable dimeric structure, it is able to sustain activity upon several hours of heat treatment at 55 °C. Interestingly, it was observed that **incubation at 55 °C** even regains enzyme activity of up to 70% (wildtype) after acetaldehyde treatment. In order to understand this **partial reactivation**, the protein structures before and after heat treatment were examined by NMR. Data revealed distinct changes in the chemical shifts after acetaldehyde incubation, which however partially reverted back to their original frequency after heating. Therefore, developing reaction processes at higher temperature might be beneficial.[88e]

2) Active site mutation

In order to prevent irreversible coupling and thus blocking the catalytic K167 residue, a viable strategy was realized by **exchanging** the responsible **C47 coupling partner** by site-directed mutagenesis. Sequence alignment of *Ec*DERA with its orthologs revealed a frequency of 91% of cysteine in the 47 position, which indicates that C47 is not essential for the enzyme's catalytic activity.[104b] Thus, methionine, being a similar but non-nucleophilic amino acid, was chosen as replacement. This strategy turned out to be very fruitful, as no loss of enzyme functionality was observed after 16 h of incubation in 1 M acetaldehyde.

Hence, the **C47M variant** appeared to be **fully crotonaldehyde and acetaldehyde resistant**. Interestingly, in follow-up studies, conducted by the same group, C47 was also replaced by other non-nucleophilic amino acids, such as serine, threonine, leucine, isoleucine, alanine, and glycine, but not all mutations resulted into acetaldehyde resistance, although providing tolerance for crotonaldehyde.[88e] It was speculated that there must be an additional inactivation mechanism, which is independent from bridging C47 to L167. This mystery is unfortunately not fully resolved until today. Evidence had been found that resistance to both, acetaldehyde and crotonaldehyde, might correlate with the space available in the active site cavity. While replacing cysteine with the rather bulky lysine created a fully resistant variant, C47A and C47G appeared to be highly sensitive.[124]

1.6.3. The application of DERA resting cells

In order to continue making DERA more applicable for industrial use, in 2013, OSLAJ *et al.* introduced the first whole-cell approach by developing a **fed-batch process**, starting directly from the **fermentation broth** containing native *Ec*DERA. Avoiding larger expensive and tedious enzyme purification steps, the aldol reaction was performed at **very low cost** (0.2 € per kg of the whole-cell catalyst), while allowing for a **high yield** (80%) and productive bioconversion (50 g/L/h) starting from readily accessible acetyloxyacetaldehyde (400 mM) and acetaldehyde (800 mM) as substrates.[108a]

1.6.4. Summary of DERA advances in statin synthesis

In summary, various organisms express DERA orthologs with different substrate tolerance and affinity. Additional genetic modifications can be useful for improving the desired characteristics. However, since the mechanism of inactivation has not been fully elucidated, scientists are often left with the approach of trial and error.
Process engineering towards fed-batch and whole cell approaches has improved the industrial applicability and made DERA a viable catalyst for the synthesis of statin precursors.
Table 1.1 recapitulates the up-to-date reported DERA variants with improved activity/aldehyde tolerance and synthesis strategies.

Table 1.2 Recapitulation of advances in DERA-catalysis towards statin synthesis.

Year	Reference	DERA variant	Advances
1993	GIJSEN/WONG[107]	*E. c.* WT	First reported sequential aldol addition
2003	DESANTIS/WONG[115]	*E. c.* S238D	Tolerance for 3-azidopropionaldehyde as acceptor substrate
2004	GREENBERG[113]	Unknown source	Enhanced product concentration of 500 mM after 3 h and 2 % catalyst load with chloroacetaldehyde as substrate
2006	JENNEWEIN[111A]	*E. c.* M185V	3-fold higher activity than wildtype
		E. c. ΔY159	5-fold higher activity than wildtype
		E. c. F200I	14-fold higher activity than wildtype

2007	SAKURABA[119]	P. a. WT *T. m.* WT	Enhanced residual activity of 50% after incubation in 400 mM acetaldehyde for 20h
2011	KULLARTZ/PIETRUSZKA[120]	*R. e.* WT	2.5-fold higher half-life than *E. c.* WT
2013	OSLAJ[108A]	*E. c.* WT	Whole-cell approach starting from acetyl-oxyacetaldehyde as acceptor
2015	JIAO[121]	*L. b.* E78K	Enhanced tolerance for 700 mM chloro-acetaldehyde and 1.4 mM acetaldehyde
2016		*L. b.* T29L	3-fold higher activity than wildtype
		L. b. F163Y	4.5-fold higher activity than wildtype
2015	YANG[111B]	*S. ep.* T120C/G174I/G213C	70% residual activity after exposure to 300 mM chloroacetaldehyde for 2 h
2015	LI[118]	*K. p.* S238D/F200I/ΔY159	3.15-fold higher activity and 1.54-fold higher tolerance for non-phosphorylated substrate than wildtype
2016	PIETRUSZKA[88E]	*E. c.* C47M	No activity loss after exposure to 1 M acetaldehyde for 16 h

2. Objective

2.1. Main objective

Although statin drugs have been on the market since the 1980s, their pharmacological activity is yet not fully understood, especially when regarding the complexity of *in vivo* bioprocesses.[125] Also their structure related binding properties are not completely elucidated. It is therefore quite meaningful to continue the development of novel statins with structural diversity for further investigations. Concomitantly, there is a high demand for improved synthesis strategies towards easier access to their highly challenging chiral key motif.
Hence, this work focuses on the development of a **green** and simple route for the production of **novel simple statins**, as well as valuable **statin building blocks**. Following trending biocatalytic approaches, it is intended to construct the drug's chiral motif by **DERA-catalyzed aldol addition** reactions of acetaldehyde to various non-natural acceptor substrates. Due to the drawbacks and the complexity of DERA-application including inhibitory/inactivation effects or potential formation of various side-products, it is intended to employ DERAs with improved activity/stability and substrate selectivity. A broader substrate tolerance is demanded in order to apply new, simplified synthesis strategies starting from respective aldehydes. Herein, also **reaction engineering processes towards industrial application** including high efficiency, scalability, and economical feasibility are part of the goal.

2.2. Specific objectives

2.2.1. Substrate synthesis

DERA acceptor substrates, which are not commercially available, will be synthesized by **starting from readily available chemicals** and following **standard laboratory procedures**. These substrates include various aldehydes for the production of simple analogs to the naturally occurring solistatin, as well as a protected amine functionalized aldehyde that can be applied as a direct building block for atorvastatin synthesis.

2.2.2. Identification of suitable DERA variants

In order to identify suitable DERAs from larger protein panels, an assay method is required that allows for fast and reproducible screenings. As DERA reactions mostly don't exhibit typical characteristics that can be exploited for enzyme assays like colorimetric effects, changes in pH, or consumption of cofactors, monitoring of the reactions have often been performed by analysis via HPLC. This method unfortunately is hardly applicable for larger libraries as it is very time consuming. Hence, this work aims for the development and optimization of a **medium-throughput screening** method based on **thin layer chromatography**.

2.2.3. ADH-screening method

Since all DERA-catalyzed pathways to statins require a subsequent oxidation of the DERA products, it is intended to utilize an alcohol dehydrogenase (ADH) for this purpose. Therefore, a suitable catalyst shall be systematically identified from a commercial library via **high-throughput screening**. Herein, the colorimetric **INT-assay** method can be applied.

2.2.4. Reaction engineering towards industrial application

In order to improve efficiency, reaction handling, and economic factors, a **one-pot reaction cascade** for the enzyme catalyzed steps of aldol addition and lactol oxidation is aimed for. This includes the introduction of an efficient **cofactor regeneration** system as well as reaction engineering towards **optimized parameters** like substrate/enzyme concentrations and pH.

2.2.5. Testing for biological activity

The synthesized novel statins will be tested for their **inhibitory activity** towards HMG-CoA via a standard commercial **NADPH-assay**.

3. Results and Discussion

3.1. Design and synthesis of DERA substrates

The majority of the DERA substrates utilized in this work were synthesized starting from simple commercially available compounds. Their structural designs as well as synthesis pathways are explained in detail in the following chapters.

3.1.1. Phenylacetyl (PhAc)-protected substrate

Within functional group chemistry, **amines** offer manifold possibilities for **cross linking**. As nucleophiles they can form products with a variety of electrophiles like alkyl halides, alkyl sulfonates, aldehydes or ketones, acid halides or anhydrides, sulfonyl chlorides, and nitrous acids.[126] Hence, incorporating a free amino group into a statin building block widens the scope for **easy coupling methods**. For example, amino-functionalized precursors are directly reacted with aldehyde functionalities during the synthesis of atorvastatin to build the pyrrol core of the drug molecule.[127] However, due to the reactivity of free amines, the use of protecting groups is often mandatory. In this context, the phenylacetyl (PhAc)-group effectively masks amine functionalities and has been widely applied in peptide synthesis.[128] It can be chemically or enzymatically introduced and selectively cleaved under mild conditions.[129] For enzymatic introduction and cleavage, a **penicillin G acylase** (PGA) can be applied as catalyst. These enzymes are known to catalyze the hydrolysis of penicillin G.[130]
In this work, the PhAc-protected amine functionalized DERA substrate **1a** was synthesized following two different approaches, comprising a chemical pathway **(A)** and an enzymatic route **(B)** (Scheme 3.1).

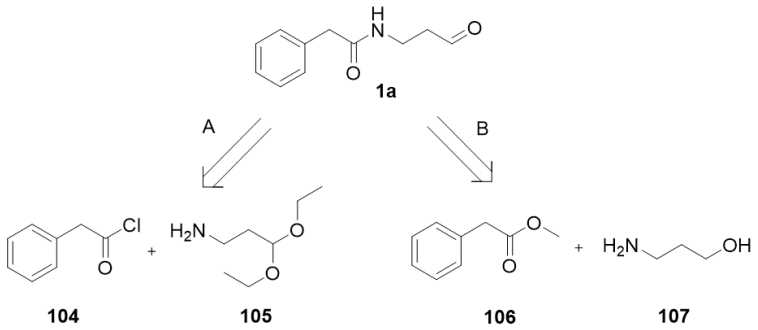

Scheme 3.1 Retrosynthesis pathways to aldehyde **1a**.

A) Conducting the **chemical approach,** the target aldehyde substrate **1a** was furnished after two steps by proceeding through a **nucleophilic addition** of the protected amino propionaldehyde **105** to phenylacetyl chloride (**104**) followed by an acetal cleavage. As the first reaction step generates amide **108** upon release of hydrochloric acid, the process was performed in a biphasic system containing THF as organic solvent and an aqueous sodium carbonate solution for neutralization of the formed acid. Herein, the removal of HCl from the system does not only retain an ambient pH but also helps to shift reaction equilibrium to the product side (Scheme 3.2).
During the reaction process, the reactants as well as the product constituted the organic layer, which later facilitated product isolation by simple separation from the aqueous phase. This facile and time efficient procedure lead to a very successful outcome with **yields ranging**

between 85-90%. Analysis via NMR revealed **high product purity** after standard washing steps and removal of the organic solvent. Acetal **108** could therefore be used within the next step without additional purification.

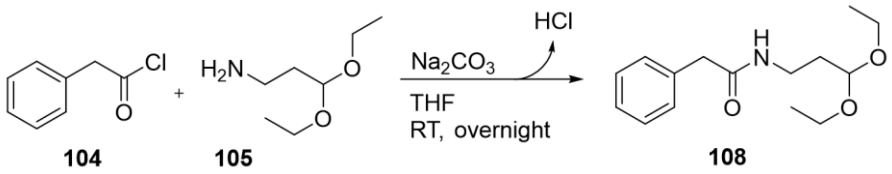

Scheme 3.2 Synthesis of diacetal-protected aldehyde **108**.

For the **acetal deprotection**, three different methods were considered:

- Incubation in 1 M **HCl**/THF (1:1)
- Treatment with **Dowex (H^+)** ion exchange resin in H_2O/THF (1:1)
- Heat treatment at **80 °C** in H_2O/THF (1:1)

Employing HCl for the deprotection constitutes a cheap and efficient way but requires a subsequent neutralization step before product isolation. Alternatively, Dowex (H^+) follows the same principle but offers a simplified reaction workup, as the resin can be easily removed from the mixture by filtration. On the other hand, applying Dowex (H^+) is linked with higher material costs. Heat treatment avoids the necessity of additional agents but demands higher energy costs.

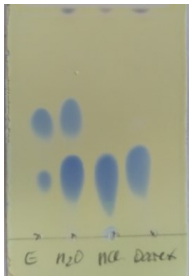

Figure 3.1 TLC of cleavage reaction.

Anyhow, each strategy was principally regarded as **industrially viable** and was tested on analytical scale. Analysis by TLC showed that after a period of two hours the heat treated sample still contained a good amount of starting material, while **full conversions** were observed when applying HCl or Dowex (H^+) (Figure 3.1). In both cases, products were isolated from scale-up reactions and furnished a **yield of 82%** after recrystallization.

B) A **fully enzymatic pathway** towards **1a** was followed by employing a lipase for the coupling of methyl 2-phenylacetate (**106**) to 3-aminopropan-1-ol (**107**) and an alcohol dehydrogenase for the subsequent oxidation of the alcohol intermediate **109** to the corresponding aldehyde **1a**.

Lipase B from the *Candida Antarctica* strain (CAL B) technically belongs to the enzyme family of hydrolases and is mostly known for its capability to perform kinetic resolutions of racemic alcohols.[131] Nevertheless, this versatile enzyme is also able to catalyze **amidation reactions** between amines and carboxylic esters or acids.[132] Thus, being the most widely studied enzyme and well established in industrial processes,[133] it was assumed that CAL B constituted a reliable and effective catalyst for our purpose (Scheme 3.3).

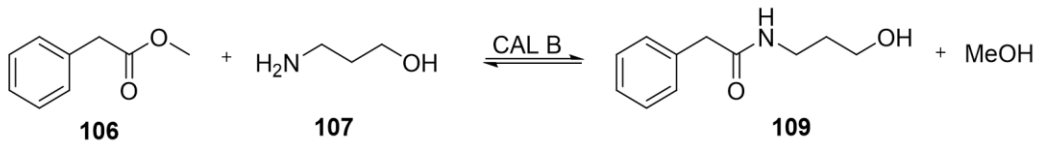

Scheme 3.3 Cal B-mediated amidation reaction for the generation of PhAc-protected **109**.

A small drawback, however, was brought by the nucleophilic nature of alcoholic groups, allowing for potentially formation of **ester byproducts 110** and **111** via attack from the OH-group instead of from the NH_2-group. Indeed, HPLC-analysis of a test reaction ran with 1 M substrates and 3 mg immobilized enzyme/mL for 24 h verified the formation of both (Figure 3.2). Even though the percentage was low, when compared to product quantity, these undesired reactions makes product purification fairly more difficult and hence lowers the yield.

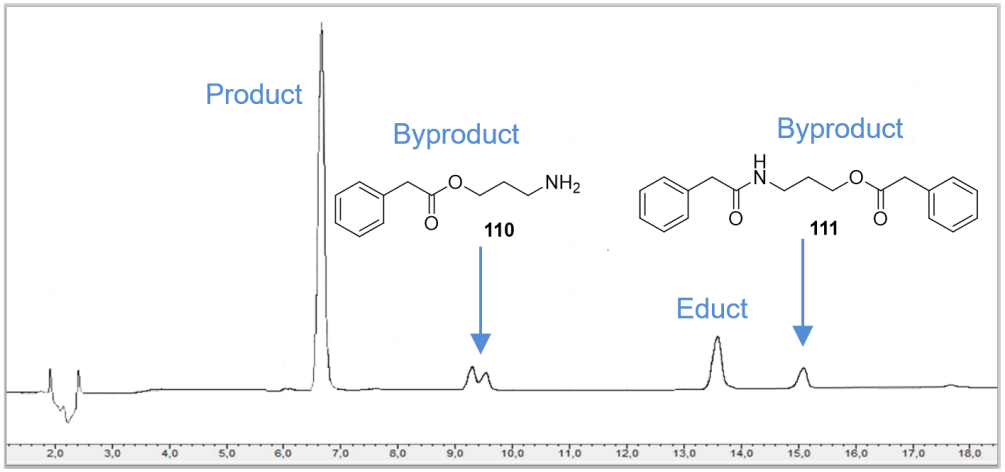

Figure 3.2 HPLC of Cal B-catalyzed amidation reaction after 24 h.

In order to further investigate on that matter, analytical scale reactions were conducted with changing parameters including **temperature** and enzyme amount. Herein, the commercial catalyst was employed as immobilized enzyme on resin beads and varied from 20 – 124 mg/mmol substrate. The reactions were conducted at 25 °C, 40 °C, and 70 °C with a substrate concentration of 1 M and the outcome was evaluated by HPLC analysis. Table 3.1 summarizes the results. As can be seen, amide **109** was even produced in absence of the enzyme. Herein, **spontaneous amidation reaction** was most likely promoted due to the utilization of an activated carboxy compound as reactant. Therefore, conducting the reaction at 25 °C already gave a conversion of 36% after 24 h without catalyst. Increasing the temperature to 70 °C even lead to almost full conversion to the target product with little occurrence of byproducts (~7%). Anyhow, in order to reach high conversions of around 85% at ambient temperature (25 °C), 125 mg enzyme/mmol substrate were required. Adversely, in this case, both byproducts **110** and **111** were observed at a little higher extend (3% and 10%, respectively).

Table 3.1 Conversion to amide **109** at different temperatures and enzyme amounts after 24 h.

Enzyme amount [mg/mmol substrate]	**Conversion** [%]		
	25 °C	**40 °C**	**70 °C**
125	85	89	95
64	79	85	94
32	75	80	94
20	65	75	94
0	36	70	92

From industrial point of view, energy costs for heating and costs for the catalyst need to be calculated and assessed - but most of all, the generation of side products, which demands costly purification processes, assumingly makes the application of CALB less attractive.
Anyhow, for academic reasons, a CALB-catalyzed reaction was conducted on preparative scale and successful product formation was verified by NMR analysis. Here, a yield of 50% was achieved after product purification by flash column chromatography.
Conversion of alcohol **109** to the corresponding aldehyde **1a** can be either achieved by chemical **oxidation** or by an oxidoreductase-catalyzed path. For the latter, the NAD^+-dependent **alcohol dehydrogenase from horse liver** (HLADH) was tested on analytical scale (Scheme 3.4). This ADH is known for its broad specificity, allowing the conversion of a wide range of both, primary and secondary alcohols, to their corresponding aldehydes and ketones.[134]
Successful oxidation to the corresponding aldehyde was verified by performing the colorimetric INT-assay (see chapter 3.4.1). A large scale reaction was not conducted in this case. Anyhow, a simple oxidation step of non-complex alcohols can be regarded as basic chemistry. Therefore, this fully-enzymatic or semi-enzymatic pathway for the generation of the aldehyde substrate **104** was considered to be highly viable.

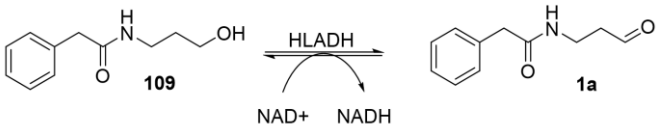

Scheme 3.4 HLADH-catalyzed oxidation to aldehyde **1a**.

When comparing strategies **A)** and **B)**, it is speculated that both routes will lead to comparable product yields, even though route **B)** was not conducted on larger scale for product isolation. However, the latter is clearly more advantageous regarding costs and atom economy. The amino alcohol **107**, utilized as starting material, comes with a price of 26.60 €/100 g and is, thereby, much more affordable than the acetal protected aldehyde (676 €/100 g) required for pathway **A)**. Besides, when applying heat treatment to assist on the spontaneous amidation step, it is not even necessary to provide an additional catalyst. In case CALB is employed, this route is still attractive, as CALB represents an established catalyst in industry and its application has been already optimized for cost efficiency. Immobilization on resin has made this catalyst more stable and also allows for easy regeneration.[135]

3.1.2. Substrates towards solistatin and its analogs

Solistatin is a **naturally occurring statin** found in *Penicillum solitum* and is an aromatic analog of compactin.[136] Solistatin (**4b**) and its **simpler derivatives 4c-g** are, compared to pharmaceutically relevant statins, rather **small in size** and exhibit **non-complex structures**. Thus, there is great potential for a simple, direct synthesis by sequential aldol addition of acetaldehyde to the respective acceptor aldehydes – presupposed the latter is tolerated by DERA. The resulting statin products are interesting compounds for experimental studies regarding biological activity of statin class drugs. Therefore, the set of following precursor-aldehydes, apart from **1d**, which is commercially available, were chemically synthesized (Figure 3.3).

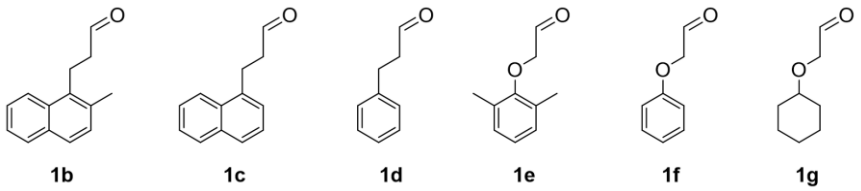

Figure 3.3 Aldehyde precursors for the DERA-catalyzed synthesis of solistatin (**4b**) and its simplified analogs (**4c-g**).

Aldehyde **1b** is the direct precursor to solistatin (**4b**). **1c** is its analog without a methyl substitution in 2-position and will be referred to as 'norsolistatin'. It was considered for the set, as it represents the most similar derivative and can be synthesized following the same route. The resulting statin is an interesting alternate substrate to HMG-CoA for assessment of the role of alkyl group functionalization. Phenylpropionaldehyde (**1d**), which was commercially available, represents the closest single aromatic derivative. The oxy acetaldehyde **1f** and the double-methylated analog **1e** were synthesized to generate potentially better soluble substrates, while oxy aldehyde **1g** was an interesting non-aromatic alternative.

A) Synthesis of solistatin and norsolistatin precursors

Synthesis of the aldehydes **1b** and **1c** will be jointly discussed here, as their synthetic routes are very similar: The first step starts from the commercially available naphthaldehydes **112** and is based on a **KNOEVENAGEL-DOEBNER type** reaction for **C2-chain elongation** to furnish the cinnamic acid derivatives **113**. Subsequent reduction by treatment with $LiAlH_4$ gives the saturated alcohols **114**, which can be simply oxidized to the target aldehydes **1b** and **1c** by a mild agent like PCC (Scheme 3.5).

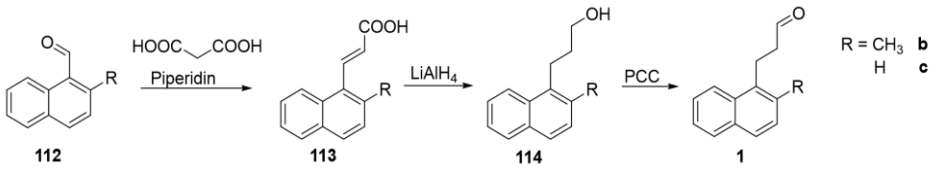

Scheme 3.5 Synthesis of solistatin and norsolistatin precursors **1b** and **1c**.

However, the methylated starting material **112b** was at a price of 115 €/g rather costly. Therefore, it was not directly used from a commercial source but synthesized from the less expensive ether **115** via a **chromium-catalyzed chemoselective KUMADA-TAMAO-CORRIU reaction** (Scheme 3.6).[137]

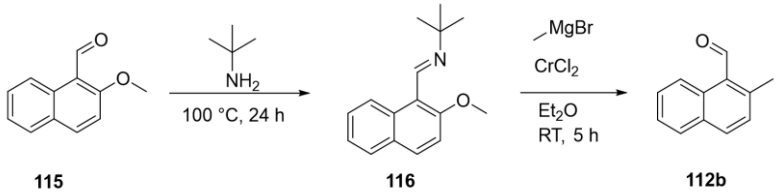

Scheme 3.6 Synthesis of aldehyde starting material **112b** via chromium-catalyzed chemoselective KUMADA-TAMAO-CORRIU reaction.[137]

Herein, intermediate **116** was first generated from **115** by reaction with *tert*-butylamine. This process masks the aldehyde functionality and activates the molecule for a subsequent reaction with methyl magnesium bromide. During this selective cross coupling step, $CrCl_2$ is utilized as a mild and inexpensive pre-catalyst for the cleavage of the rather inert C-O bond. Herein, the chromium(II) species is coordinated and assisted by the imino auxiliary positioned in direct proximity. This intermediate **116** readily reacts with the GRIGNARD reagent (methylmagnesium bromide) to furnish the desired product **112b** after hydrolysis.

Synthesis was conducted following a protocol reported by ZENG *et al.*[137] The first step, which constituted the generation of the imine intermediate **116**, was successfully performed with a very high yield of 93%. No additional purification process was necessary, since full conversion was reached after 24 h and residual *tert*-butylamine was removed by simple evaporation under reduced pressure. The second step was performed under inert atmosphere, as $CrCl_2$ rapidly oxidizes in moist air, and aldehyde **112b** was achieved with a good yield of 80%. Both of the isolated products were analyzed and verified by NMR measurements. As the reactions worked very well and demanded basic laboratory skills, it was legitimate to synthesize the desired starting material instead of purchasing it from a commercial source.

The C-C prolongation step by **aldol condensation of malonic acid** (**117**) to the aldehyde functionality and subsequent spontaneous decarboxylation is a commonly established type of reaction in chemical synthesis and typically yields the unsaturated mono acid. The standard work-up procedure comprises a crystallization step from aqueous hydrochloric acid solution. Isolation by simple filtration usually gives the product in high purity.

In this work, synthesis was performed following standard protocols reported in literature.[138] Starting from aldehyde **112c**, acid **113c** was obtained in high purity and a high yield of 87%. However, in the case of the methylated derivative **112b**, full conversion was not even reached after overnight reaction. Besides, the target product **113b** was not furnished, as spontaneous decarboxylation and crystallization by treatment with hydrochloric acid did not occur. Instead, analysis by NMR revealed an intermediate product, obtained by extraction, which was the **unsaturated diacid 118** (Scheme 3.7). Therefore, the standard protocol had to be adjusted and the decarboxylation step was finally achieved by a harsher treatment of **119** with **15% dimethylamino pyridine** (DMAP) as nucleophilic catalyst upon heating to 150 °C in pyridine overnight. Anyhow, product isolation still had to be performed by extraction of the aqueous hydrochloric acid solution, as the product did not crystallize in a complete manner. Analysis by NMR verified the successful formation of mono acid **113b** with very high purity and a yield of 85%.

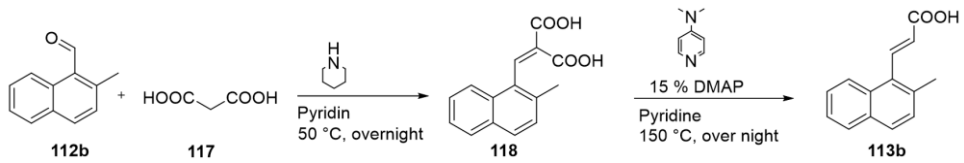

Scheme 3.7 Synthesis of unsaturated acid **113b**. The reaction proceeds through the formation of intermediate diacid **118**.

The corresponding alcohols **114** were achieved by treatment with $LiAlH_4$, which is a strong reducing agent not only capable of completely reducing the carboxylic acid functionality to the alcohol but also acting on the conjugated double bond to generate the saturated product.

Following standard reaction protocols, both products were achieved with moderate yields of around 60%.
For the subsequent oxidative step, a mild agent was required, which would not over-oxidize the alcohol to the carboxylic acid but will stop at the aldehyde state. For this purpose, pyridinium chlorochromate (PCC) was applied. This so-called **COREY-SUGGS-oxidation** generates aldehydes from primary alcohols or ketones from secondary alcohols as long as water is not present in the reaction mixture.[139] A typical PCC-catalyzed oxidation is therefore carried out in dry solvents under inert atmosphere and often involves addition of drying agents such as molecular sieves or $MgSO_4$. These additives also help to bind and absorb viscous reagent-derived byproducts that will otherwise form slurry precipitations that are difficult to remove. Addition of NaOAc as buffer helps to compensate the slightly acidic character of PCC in case acid-labile groups need to be protected. Alternatively, pyridinium dichromate (PDC) is often used as a milder catalyst.
In this case, the reactions to form the aldehydes **1b** and **1c** were performed according to standard procedures, utilizing PCC, dry DCM as solvent, and molecular sieves as well as $MgSO_4$ as drying agents. Simple work-up by removing the precipitates by filtering through a short silica column and evaporation of the organic solvent gave the products in good yields of around 80% and high purity, which was verified by NMR analysis.

B) Synthesis of oxyacetaldehydes 1e-g

The oxy-functionalized aldehydes **1e-g** were synthesized starting from simple alcohol building blocks **119e-g** by **WILLIAMSON ether synthesis** (Scheme 3.8). In all cases, the protected alkyl halide **120** was used as the electrophile in the nucleophilic substitution reaction. Subsequent treatment with hypochloric acid released the target aldehydes.

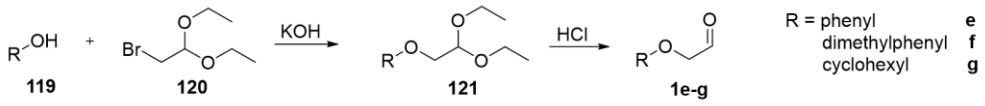

Scheme 3.8 Synthesis of oxyaldehydes **1e-g**.

The S_N-reactions were performed based on a protocol by XINQUAN,[140] which relies on the ***in situ* generation** of **highly reactive alkoxides** from the alcohols **119** by adding KOH to the reaction mixture. The reactions furnished the protected aldehydes **121** with yields ranging from 60 - 80%. The higher yields of 80% and 75% were achieved for the aromatic compounds **1e** and **1f**, respectively, which was due to the beneficial electronic effects provided from the aromatic system as well as the methyl substituents, which enhanced the molecule's nucleophilicity. The deprotection reactions were carried out using HCl as catalyst and furnished typical yields around 80%.

3.2. Development and application of a screening method for DERA libraries

There are not many possibilities to monitor DERA reactions in an efficient way, since product formation typically does not exhibit colorimetric or pH changes or rely on measurable cofactor consumption. Thus, many strategies depend on linear methods like analysis via HPLC by UV-

detection, which is tedious, time-consuming and cost-intensive as it often requires additional sample derivatization of substrates that are not intrinsically UV-active and expend large solvent amounts.

In this work, an approach of **medium-throughput screening** was realized via **high-performance TLC (HPTLC)**. This method offers reliable **qualitative and quantitative detection** of compounds and can be conducted in a **semi-automated manner** by utilizing an HPTLC auto-sampler in combination with the associated plate scanner (**Figure 3.4**). Herein, the instrument applies extremely accurate bands of exact, programmable sample amounts onto HPTLC silica plates via a precise spray-on technique. This typically allows for very distinct and well separated bands upon manual standard development of the plates. The compound bands are then visualized by treatment with a suitable staining agent, or in case of colored, UV-active, or fluorescent compounds, the plates are directly submitted to the HPTLC scanner for color/UV-density measurement. Reliable quantification of products/educts can be achieved by applying the respective internal standards on the same plate.

Figure 3.4 HPTLC auto-sampler and scanner from CAMAG.

As many of the DERA products are not necessarily UV-active, a reliable method was required to stain the product bands very evenly while also retaining a uniform background throughout the whole plate area. Quantification will otherwise be highly error prone and not reproducible. For this purpose, **anisaldehyde** was utilized as **staining agent**, as it typically gives colorful bands upon heating while generating only little background discoloration. In order to distribute the heat in a steady manner for equal staining, the plates were placed in an oven with their edges arranged on two glass rods to reduce direct surface contact with the oven tray as best as possible. The staining procedures were typically conducted at 120 °C and timed for 90 s.

This medium-throughput screening method was successfully tested on a commercial DERA panel provided by *Prozomix Ltd.* containing a mixed set of literature known, engineered, and novel DERAs. This library was screened against the **propanal homoaldol addition**. This reaction typically furnishes a mixture of the single and double addition products **122** and **123** (Scheme 3.9) and was examined as propanal offers interesting sterical hindrance and electrophilicity similar to the acceptor substrates that were considered for statin synthesis.

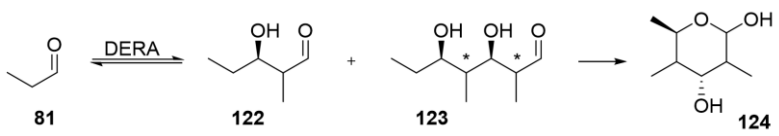

Scheme 3.9 DERA-catalyzed homoaldol reaction of propanal (**81**). The reaction typically furnishes a mix of single and double addition products.

The reactions were performed as described in the Experimental part. Internal standards for the double and triple addition products were applied to each plate. Linearity between product quantity and color density was assessed by measuring a dilution series for the relevant detection range.

Figure 3.5 shows an exemplary HPTLC plate containing twelve 6 h samples after development of the plate. The staining process can be rated successful, as colorization of the bands is well distributed and the background exhibits an even taint. The last two rows (13 and 14) comprised the standards for the propionaldehyde dimer and trimer, respectively (obtained via chemical synthesis). On this plate, it appeared that none of the DERAs tested (row 1 - 12) were able to generate the double addition product after 6 h, while more than half of them catalyzed the formation of the single addition product. This outcome was rated as quite conclusive, as propionaldehyde is known to be rather poorly accepted by most DERA variants.[10] In earlier works of WONG *et al.* the same reaction was investigated with *Ec*DERA$_{WT}$ as catalyst. Formation of the propionaldehyde trimer was in fact reported with a yield of 13% but only by utilizing very large amounts of catalyst and running the reaction for a very long period of 14 days.[102b]

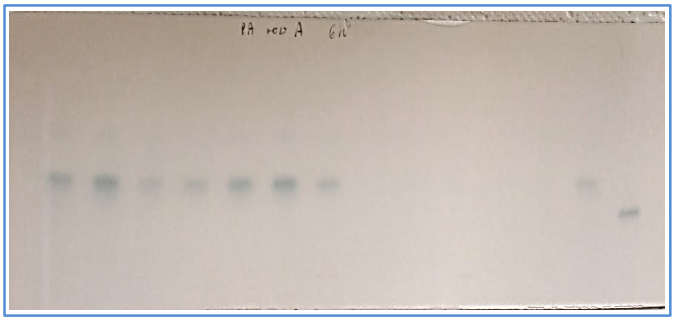

Figure 3.5 HPTLC of propionaldehyde homoaldol additions catalyzed by 12 different DERA variants (lane 1-12). Samples were collected after 6 h and sprayed on the plate via an HPTLC auto sampler. The plate was developed in chloroform/MeOH 10 : 1 and stained with anisaldehyde reagent by heating in an oven. Lane 13 and 14 contained samples of the propionaldehyde dimer and trimer as internal standards for quantification.

Figure 3.6 summarizes the color density scanning results for the complete enzyme panel. Samples were taken after 48 h and assessed via HPTLC.

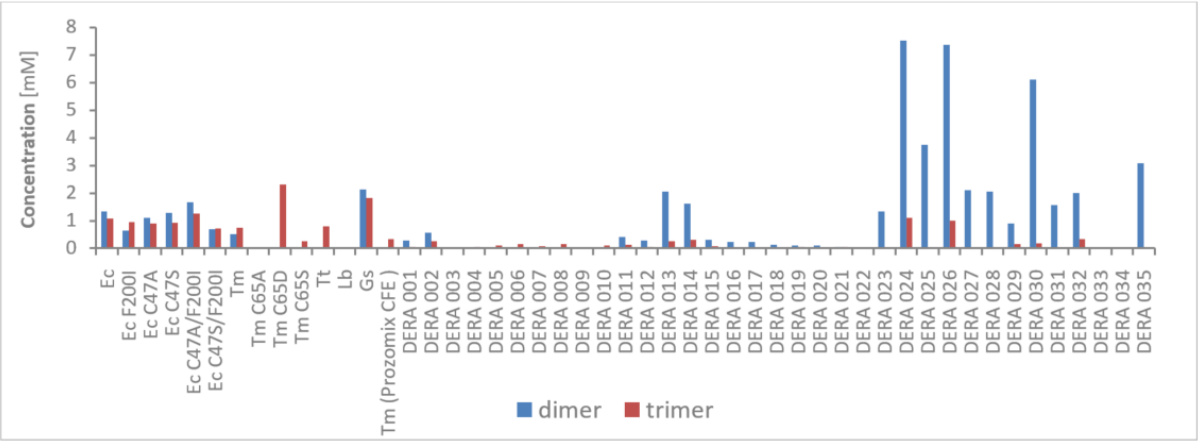

Figure 3.6 Screening results of DERA-panel towards homo-aldol additions of propionaldehyde.

The assay method was also utilized by Dr. ANNA SZEKRENYI (FESSNER group) for the screening of a larger DERA panel towards **acetaldehyde trimerization**. In this vein, the variant **DERA062** was identified as particularly efficient and was therefore mainly utilized for the aldol reactions described within the next chapters. Other DERAs that were utilized are the wildtype DERAs

from *E. coli* and the one from *Thermatoga maritima* (*Tm*DERA$_{WT}$). This hyperthermophilic organism was exploited in speculation for a DERA with higher stability and aldehyde tolerance.[141]

3.3. DERA-catalyzed aldol additions

3.3.1. Acetone as donor

In order to evaluate DERA's tolerance towards non-natural acceptor substrates, preliminary test reactions were usually conducted with **acetone as nucleophile**, instead of directly performing sequential aldol additions with acetaldehyde. This brought the advantage that, when applying acetone, **no additional side products** were expected, as ketones can neither undergo self-aldol reactions nor lead to sequential aldol additions. Scheme 3.10 compares the simple reaction with acetone as donor to the much more complex potential reaction outcome when applying acetaldehyde.

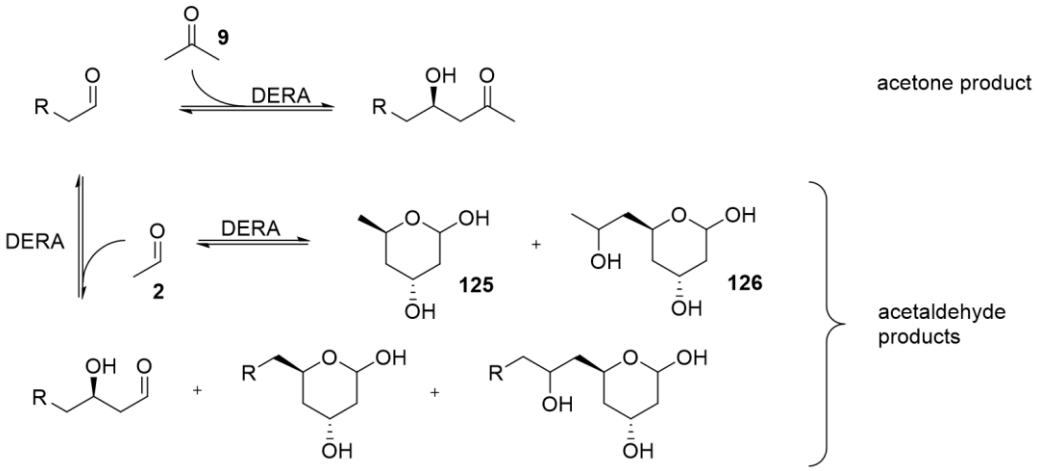

Scheme 3.10 Reaction scheme of DERA-catalyzed addition of acetone (**9**) and acetaldehyde (**2**) to an acceptor aldehyde.

Another advantage lies in the fact that acetone is well tolerated by DERA at up to 10% concentration and can be used in great excess or as **cosolvent**, driving the **reaction equilibrium towards product formation**. All these factors helped to facilitate reaction analysis and most likely lead to conclusive results. Therefore, acetone reactions offered a quick validation if the acceptor was tolerated by the enzyme and were often conducted as positive controls. Typically, these analytical reactions were performed at 500 μL total volume. The reaction vessels were kept at room temperature on a shaker and the reaction process was monitored by TLC or HPLC analysis over a period of 24 h. Acetone was usually applied at 10% concentration while the acceptor substrate concentrations varied between 10 – 100 mM, depending on the solubility (see chapter 3.3.5). In addition to the substrates mentioned in the previous chapter, *Tm*DERA$_{WT}$ was also challenged with several other non-natural acceptor substrates with acetone as donor, in order to assess the enzyme's spectrum. These substrates included alkyl aldehydes such as propanal (**81**), butanal (**91**), and *iso*-propanal (**127**), as well as aromatic aldehydes like benzaldehyde (**128**) and cinnamaldehyde (**129**), which are extremely challenging substrates due to their higher electron density. Table 3.2 lists the substrates that were reacted with acetone on preparative scale with the corresponding yields. Even though the application of

cinnamaldehyde (**129**) and benzaldehyde (**128**) was problematic due to extremely low solubility and very low tolerance by the enzyme, it was possible to isolate the corresponding products. The fact that even these highly challenging substrates lead to a positive outcome, showed that it is often a question of reaction engineering in order to make a reaction work.

Table 3.2 Acceptor substrates with applied concentrations and isolated yields for *Tm*DERA$_{WT}$–catalyzed addition of acetone.

Acceptor	Conc.	Yield	Acceptor	Conc.	Yield
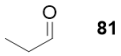 **81**	100 mM	35%	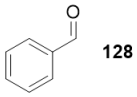 **128**	10 mM	4%
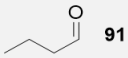 **91**	100 mM	56%	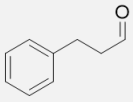 **1d**	50 mM	42%
 **127**	100 mM	52%	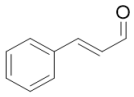 **129**	10 mM	2%
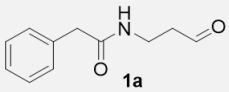 **1a**	100 mM	88%			

3.3.2. Homo aldol addition of acetaldehyde

As discussed above, cross aldol reactions with acetaldehyde as nucleophile will typically involve acetaldehyde homo additions as byproducts. Therefore, it is useful to produce the related materials as references. Thus, from a larger scale reaction (100 mL) with 100 mM substrate concentration and purified *Tm*DERA$_{WT}$ as catalyst, **trimer 125** was isolated as the main product with a yield of 85%. The **triple addition product 126** was obtained with a 5% yield.
Although DERA is known to typically catalyze aldol additions in a stereoselective manner, a **second diastereomer** of the trimerization product (**125**) was also isolated (8%). As diastereomers are not chemically equivalent and show different properties, they can be separated via different approaches such as recrystallization or chromatographic methods. In this work, separation was performed by flash column chromatography.

3.3.3. Analysis of stereoselectivity

On paper, the sequential double addition of acetaldehyde can lead to the formation of **four possible configurations** shown in Figure 3.7.
The major isomer of **125** is *(R,R)*-configured, as this orientation is naturally most favored by the enzyme. Although analysis by NMR or non-chiral HPLC gives no information about the presence of the *(S,S)*-configured enantiomer, the likelihood for an unfavorable stereochemistry at both centers of the same molecule is vanishingly small. Hence, the second diastereomer observed must bear improper setting of the first or second stereocenter only, thus, exhibiting either *(R,S)* or *(S,R)*-configuration, respectively.

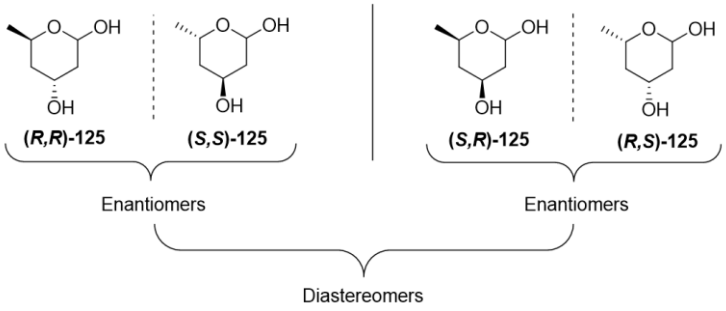

Figure 3.7 Set of four different stereoisomers of lactol **125**.

When visualizing the molecules in their chair conformation, an equatorial or axial arrangement of vicinal protons can be visualized (Figure 3.9). Explained by the **KARPLUS relationship**, this relative position of the protons causes different **coupling effects** in ^{1}H-NMR spectroscopy, as coupling phenomena are a result of the overlap between the C−H bonds involved. When the H−C−C−H dihedral angle is ~90°, the overlap of the two vicinal C−H bonds is minimized, which results in very low coupling constants. A maximized magnitude is reached, when vicinal C−H bonds are aligned in an eclipsed conformation (dihedral angle =0°) or axial conformation (dihedral angle =180°), leading to large coupling constants (Figure 3.8). Therefore, determination of the ^{3}J-coupling constants reveals distinct information about a molecule's stereochemistry.[142]

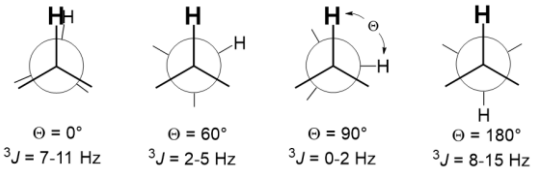

Figure 3.8 Newman projection for different molecular conformations and resulting coupling constants according to KARPLUS relation.[142]

Figure 3.9 shows the ^{1}H-NMR spectra measured from each of the trimerization products **125** with the resulting different coupling motifs as well as varying shifts in ppm. Peak assignment was conducted with the help of two-dimensional methods including COSY and HSQC (both spectra show a second set of peaks due to the presence of α- and β-anomeric structures at the C1-position).

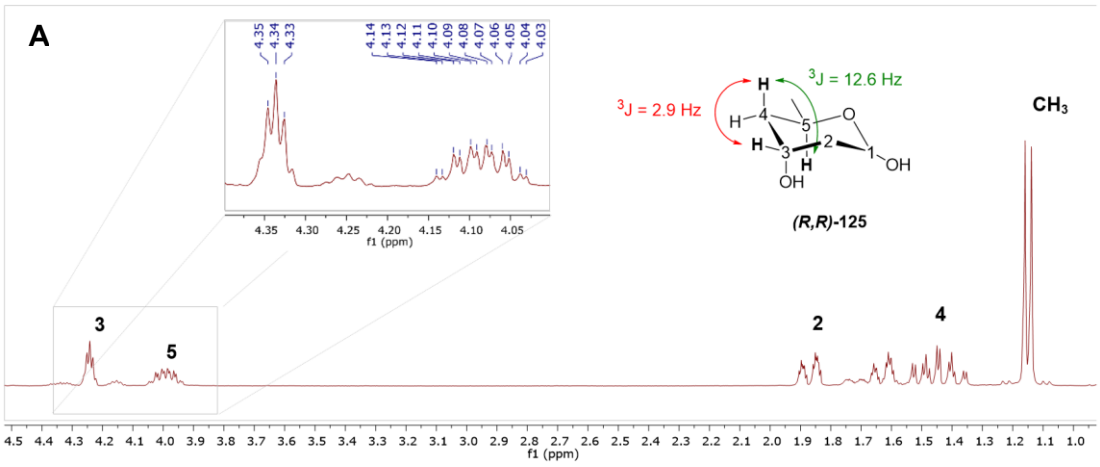

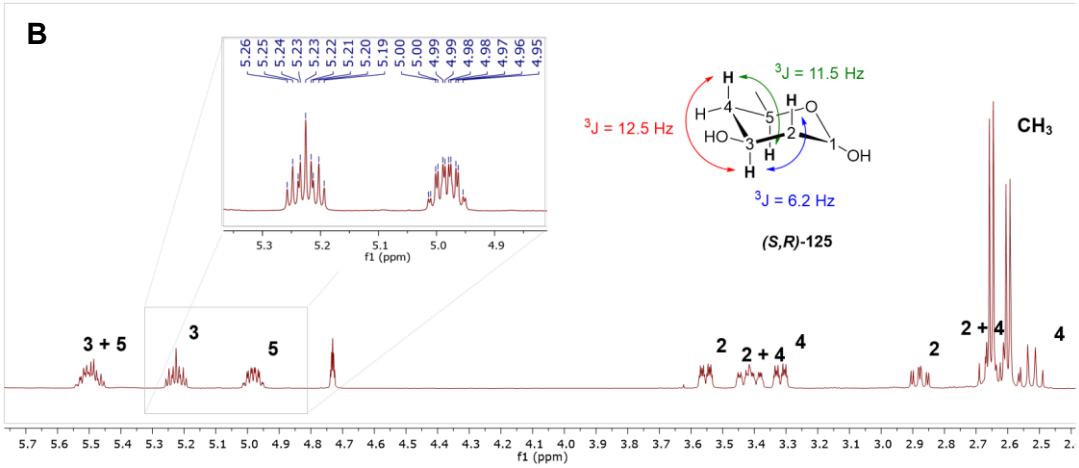

Figure 3.9 NMR-spectra of acetaldehyde trimers ***(R,R)***- (A) and ***(S,R)*-125** (B) measured in D_2O at 300 MHz. Relevant coupling constants were examined in order to determine the molecules' stereo configuration.

As expected, the spectrum measured for the *(R,R)*-enantiomer revealed a small coupling constant between the protons at position 3 and 4, indicating an equatorial arrangement of 3-H and an *(R)*-configuration. In contrast, a very high $^3J = 12.5$ Hz was measured for the respective protons in the second diastereomer, resulting from an axial placement of 3-H and *(S)*-configuration. The coupling constants between the protons at positions 4 and 5 showed very high values (12.6 Hz and 11.5 Hz) for both enantiomers, speaking for axial orientations of 5-H and *(R)*-configuration in both cases. The second diastereomer was therefore found to exhibit *(S,R)*-configuration.

In order to also investigate on *Tm*DERA$_{WT}$'s **stereochemistry in cleavage direction**, both enantiomers of the acetaldehyde dimerization product, 3-hydroxybutanal (3-HB) (**130**), were offered as the only substrate in individual reactions. The enantiomers were obtained by lipase resolution of the racemic alcohol and were kindly provided by SARAVANAN THANGAVELU. The reactions were monitored by HPLC and the chromatograms measured from samples taken after 24 h. In both cases, peaks that corresponded with the diastereomers of **125** were observed, proving that the catalyst was able to accept and cleave both substrates to reassemble the trimerization products from the obtained monomers. Interestingly, when utilizing *(S)*-3HB (**130**) as starting material, a different peak ratio between the two diastereomers was reached than when applying the *(R)*-enantiomer or the racemic mixture (Figure 3.10).

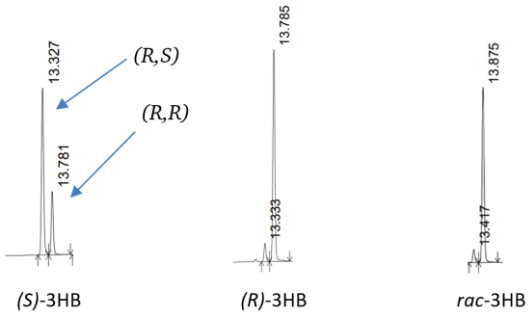

Figure 3.10 HPLCs of DERA-cleavage reactions of a) (*S*)-3HB, b) (*R*)-3HB, and c) *rac*-3HB after 24 h.

This showed that the enzyme was also able to utilize *(S)*-3HB as acceptor substrate if offered in excess, hence, generating the *(R,S)*-diastereomer, predominantly (**Scheme** 3.11).

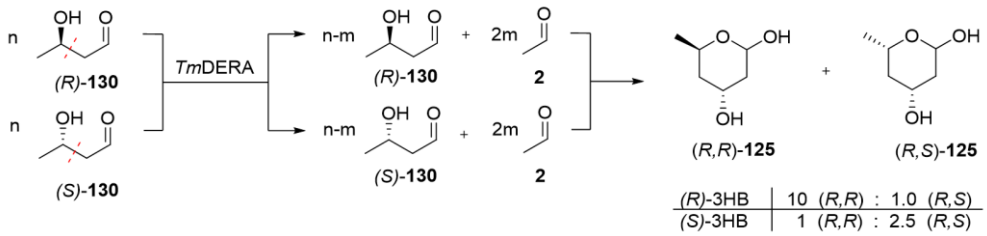

Scheme 3.11 DERA-catalyzed cleavage of (R/S)-3HB (**130**) and reassembling of trimerization products **125**.

In conclusion, these findings verified that DERA does not act completely stereoselectively but also accepts substrates of both configurations in synthesis and cleavage direction.

3.3.4. Optimization of reaction conditions

The PhAc-protected statin precursor **3a** constitutes an important and highly versatile building block. Therefore, its synthesis process was chosen as the main model system for the optimization of reaction conditions towards industrial application.

DERA's tolerance for acceptor aldehyde **1a** was first tested for aldol addition of acetone as nucleophile. The substrate concentration was set to 100 mM with 10% acetone and purified *Tm*DERA$_{WT}$ was utilized as catalyst (1.5 mg/500μL). After TLC analysis gave clear evidence that the substrate was tolerated, a larger scale reaction was performed. Herein, successful reaction was verified by NMR analysis of the aldol product isolated after a reaction time of 24 h and a yield of 85%. This positive outcome allowed for quickly proceeding to the sequential aldol addition of acetaldehyde (Scheme 3.12). The reaction was first carried out on 500 μL scale with 100 mM acceptor substrate concentration, 2 equivalents of donor substrate, and 1.5 mg purified enzyme and analyzed by TLC. Herein, reference material of the product was kindly provided by partners from the group of P. CLAPÉS.

Scheme 3.12 DERA-catalyzed sequential addition of two molecules of acetaldehyde (**2**) to PhAc-protected aldehyde **1a**.

The chromatogram prepared after a reaction time of 3 h clearly showed formation of the target lactol **3a**, but in addition to the known educt and product signals, also prominent spots that assumingly corresponded to the single addition product and the second diastereomer were present. Also, weaker traces of the non-UV-active acetaldehyde trimer **125** were visualized by treatment with Hanessian's staining reagent. This finding confirmed the necessity for further reaction engineering processes in order to increase product yield while minimizing byproducts and the need for tedious purification steps. Thus, optimal reaction conditions were rendered by stepwise changing each of the following parameters:

1. Variation of donor substrate concentration

As acetaldehyde is not only consumed through cross-aldol addition but also via homo-aldol reaction, the available donor amount plays a major role for the reaction outcome. Therefore, first test reactions were carried out at different acetaldehyde concentrations ranging from 200 – 400 mM, corresponding to 2 – 4 equivalents, while no other changes were made to the original protocol. Analysis by HPTLC revealed the relative conversions shown in Figure 3.11. Applying more than the minimum amount of two equivalents of acetaldehyde lead to significantly higher product concentrations with the highest indeed observed at 400 mM. However, with a relative conversion of 95% for when applying 300 mM substrate, the gap between three and four equivalents was rather small and did not justify applying the larger amount, as this would also increase formation of undesired homo aldol products. An optimized acetaldehyde concentration was therefore chosen at 300 mM and this concentration was applied in the following reactions.

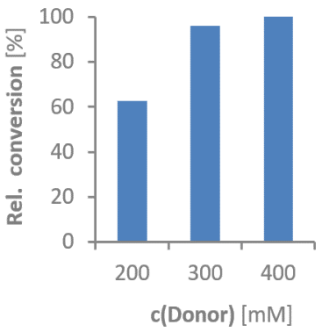

Figure 3.11 Relative conversion to **3a** at different substrate concentrations.

2. Variation of enzyme preparation

In the previous test reactions, purified *Tm*DERA$_{WT}$ was used as catalyst. However, application of purified enzyme is not economically viable from an industrial point of view. Thus, other enzyme preparations were compared on analytical scale including cell free extract (CFE), crude extract (CE), and resting cells (RC). In order to apply catalyst concentrations in an equivalent manner, the amounts were adapted from the quantities obtained from the same volume of bacterial culture according to Table 3.3.

Table 3.3 Enzyme quantities obtained from 1 L culture and amounts used in reactions.

	PE	CFE	CE	RC
Amount obtained from 1 L culture [mg]	150	732	54000	9200
Amount used in reaction [mg]	1.5	7.32	540	92

The different conversions obtained after 6 h were again measured by HPTLC analysis via UV-detection. Figure 3.12 depicts the corresponding TLC (A) and the measured conversions (B).

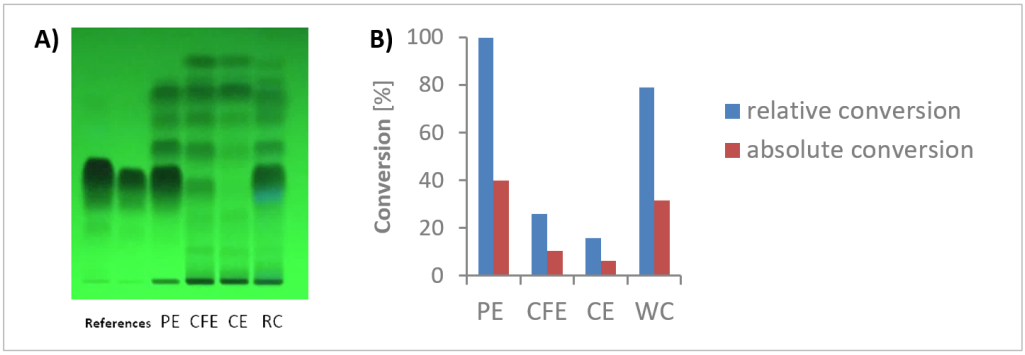

Figure 3.12 Analysis of DERA-catalyzed reactions carried out with PE, CFE, CE, and RC via HPTLC.

As expected, the reaction carried out with purified enzyme furnished the highest conversion with a total value of around 40%. Approximately 32% total conversion was reached when applying resting cells, which corresponds to 80% conversion relative to the purified enzyme. Utilizing CFE gave a much lower value of around 25% relative conversion, while the crude extracts seemed hardly viable with only about 16% relative conversion. It was therefore decided to proceed to the next experiments using resting cells.

3. Variation of enzyme amounts

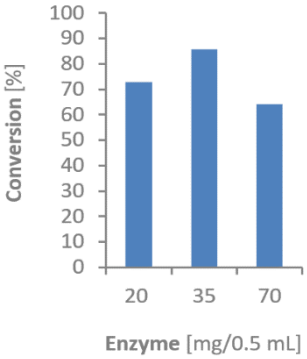

Figure 3.13 Absolute conversion to **3a** at different enzyme amounts.

Reactions with varying amounts of resting cells ranging from 20 – 70 mg/500μL reaction mixture were conducted to determine the best suitable enzyme quantity. The acceptor and donor substrate concentrations were kept at 100 mM and 300 mM, respectively. The reactions were analyzed by HPTLC measurements and according to the results (Figure 3.13) a moderate cell amount of 35 mg led to the highest product concentration. This showed that increasing the cell quantity does not ultimately lead to higher product formation. This finding can be most likely explained through reduced molecular movements in cell suspensions of higher thickness/viscosity. The optimized quantity of 35 mg cells/500 μL reaction mixture led to a conversion of around 88% and was employed in further experiments.

3.3.5. Substrate solubility

Low solubility of hydrophobic substrates in aqueous media is typically a limiting factor in preparative enzymatic reactions, especially at concentrations required for cost-effective industrial implementation. This issue is usually addressed by adding **cosolvents** or surfactants such as polyoxyethylene sorbitan monooleate (Tween 80) or ***β*-cyclodextrins** (β-CD), applying lower substrate concentrations, or running reactions in **suspensions/emulsions**. Anyhow, these solutions sometimes come with disadvantages like reduced enzyme stability, aggravated product isolation or low space-time yield.

Many of the DERA substrates applied in this work were, due to their rather hydrophobic groups, very little soluble in water. Even when applying 10-20% DMSO as cosolvent, it was usually not possible to create solutions at industrially relevant concentrations of >100 mM.

The PhAc-protected aldehyde **1a** with its polar amide group was one of the most soluble molecules among the applied acceptor substrates. Anyhow, this compound was not soluble above 50 mM concentration, either. Attempts by applying (2-Hydroxypropyl)-β-cyclodextrin as complexing agent allowed solutions with higher educt concentrations but made product isolation and purification extremely tedious, as stringy, sugary residuals were formed. Thus, reactions were successfully carried out as suspensions, instead.

Reactions involving the more hydrophobic solistatin-derived aldehydes were typically prepared from concentrated DMSO solutions. In these cases, addition of aqueous buffer mostly led to oily precipitations instead of homogenous suspensions or emulsions. Therefore, a strategy of forming ‘macroemulsions’ was followed for this substrate type. **Macroemulsions** are homogenous, thermo-dynamically unstable but kinetically stable systems of milky appearance, as their droplets are of greater size than a wavelength of light. They can be formed through

different strategies, including spontaneous assembly at correct compound ratios, stirring/shaking, or by **ultrasonic treatment** of water/oil mixtures.[143] In this work, the latter method was implemented as a very efficient and rapid procedure. Utilization of a sonotrode with 20 kHz beams over a period of 5 minutes lead to macroemulsions that remained stable over several days. However, they were usually freshly prepared right before application in the enzyme reactions. Figure 3.14 depicts a sample of commercial phenylpropanal (**1d**) in buffer at a concentration of 100 mM before and after sonication.

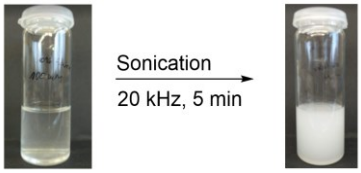

Figure 3.14 Sample of 100 mM phenylpropanal (**1d**) in buffer before and after sonication.

3.3.6. DERA-catalyzed synthesis of building block 3a

In order to test industrial feasibility of the parameters and conditions obtained, a larger scale reaction (10 g scale) was conducted with the PhAc-protected aldehyde **1a** as substrate (100 mM suspension) and resting cells of *Tm*DERA as catalyst. Acetaldehyde (**2**) (3 eq) was added to the reaction in a continuous feed over the period of 8 h via a syringe pump in order to keep the donor concentration at a constant low. Although HPLC analysis after 24 h showed a similarly high conversion of 85% compared to the analytical scale reaction, the isolated yield was with 44% rather low due to the demanding handling of huge amounts of cell material, which hindered efficient and neat product isolation. Removal of cell parts by filtration through silica or celite was always accompanied with larger product losses. Besides, even purification by column chromatography always left the product with a darker coloration. It is assumed that this staining was caused by extracted cell compositions. Therefore, utilization of resting cells did not seem applicable, as neither an adequate yield nor purity was achieved in our case.
The reaction was instead repeated with cell free extract of *Tm*DERA, as the utilization of purified enzyme was beyond questions due to economic reasons, and applying crude extract hardly furnished the product. The CFE used here was produced by *Prozomix Ltd* and was applied at an amount of 10 mg/mL reaction mixture. This finally led a much higher isolated yield of 72%.
As mentioned in chapter 3.2, the screening of a large DERA panel revealed a DERA (DERA062) that showed higher activity in the sequential aldol additions of acetaldehyde than *Tm*DERA. Hence, this catalyst was also tested for the conversion of aldehyde **1a**. Besides repeating the experiments under the same conditions, a higher acceptor concentration of 1 M was also applied with very good results. Table 3.4 summarizes the reaction outcomes depending on the different conditions.

Table 3.4 Isolated yields of DERA lactol product **3a** depending on the used catalyst and the substrate concentration.

Catalyst	c(Acceptor) [M]	Isol. Yield [%]
*Tm*DERA resting cells	0.1	34
*Tm*DERA CFE	0.1	72
DERA062 CFE	0.1	86
DERA062 CFE	1.0	84

3.3.7. DERA-catalyzed synthesis of statin precursors 3b-g

For the conversion of the aldehydes **1b-g**, CFE of DERA062 was applied as catalyst. Depending on the solubility, different acceptor-substrate concentrations were applied within macroemulsions. 10% DMSO was used as cosolvent in all cases and acetaldehyde (3 eq) was slowly added via syringe pump over a period of 8 h. Table 3.5 summarizes the concentrations used in each reaction with the corresponding isolated yields.

Table 3.5 Isolated yields for conversions of substrates **1b-g** by DERA062-catalysis.

Substrate	**C(Acceptor)** [mM]	**Isol. yield** [%]
Solistatin aldehyde **1b**	10	14
Norsolistatin aldehyde **1c**	25	17
Phenylpropanal **1d**	100	23
Phenoxy aldehyde **1e**	100	32
Dimethylphenoxy aldehyde **1f**	100	34
Cyclohexyloxy aldehyde **1g**	100	14

To our satisfaction, all targeted DERA lactol products were formed and successfully isolated after purification by column chromatography. However, the conversion of solistatin aldehyde **1b** was most problematic, as the molecule's hydrophobic nature allowed for a very low substrate concentration only and the substrate did not seem to be well accepted by DERA. Even after a long reaction time of 24 h, a large portion of starting material was still visible on TLC leading to a very low isolated yield of 14%. Similar outcomes were observed for the unmethylated analog **1c** as well as the non-aromatic substrate **1g**. The best results were furnished with the oxy-functionalized aromatic aldehydes **1e** and **1f**. It is assumed that the additional oxygen atom distinctively changes the molecule's electrophilicity and solubility, which benefitted appropriate substrate binding.

3.4. Lactol oxidation by ADH-catalysis

All DERA-catalyzed reaction pathways to synthetic statins require the conversion of the 6-membered lactol intermediate **3** to the corresponding lactone. For this purpose, many chemical oxidation methods have been reported, e. g. utilizing NaOCl/HOAc,[113] $Br_2/BaCO_3$,[144] N-iodo-succinimide,[145] Ag_2CO_3,[146] Pt/CO_2,[147] $RuCl_2(PPh_3)_3$/ cyclohexanone,[148] or MnO_2.[149]
Alternatively, the employment of enzyme catalysis offers a greener and non-toxic route. Herein, two main classes of enzymes are able to catalyze alcohol oxidations: Alcohol oxidases (EC 1.1.3) and **alcohol dehydrogenases** (ADHs, EC 1.1.1.1). Oxidases, being only dependent on molecular oxygen as electron acceptor, are very attractive biocatalysts. Anyhow, until today there are not many representatives of this group known.[150] In contrast, dehydrogenases are present in a plethora of organisms and offer **broad substrate specificities**.[151]
For the oxidation of statin precursor **94f**, VAJDIC *et al.* have reported a regiospecific PQQ-dependent glucose dehydrogenase (GDH). Here, a whole-cell system from an *E. coli* culture with overexpressed membrane-bound protein that provided cofactor recycling through the cell's respiratory chain was applied (Scheme 3.13).[152]

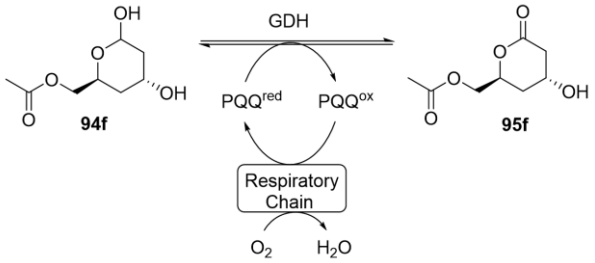

Scheme 3.13 Biocatalytic oxidation of hydroxy-lactol **94f** by GDH including PCC cofactor recycling.[148]

In 2019, the group of SCHÜRMANN engineered an ADH to efficiently catalyze the oxidation of chloro-functionalized lactol **94b**. Cofactor recycling was, in this case, provided by employing a water-forming nicotinamide oxidase (NOX) (Scheme 3.14).[76]

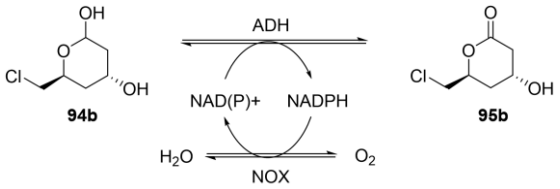

Scheme 3.14 Biocatalytic oxidation of lactol **94b** by an ADH including a $NADP^+$ cofactor recycling by a NOX.[76]

3.4.1. Screening of ADH panel

In this work, a novel ADH was identified for the regioselective oxidation of the DERA products from a larger protein panel provided by our industrial partner *Prozomix Ltd*. The company's **commercial enzyme library kit** ("kREDy-to-go plate") offered a simple **high-throughput colorimetric screening** method in a ready to use 96-well format. The assay is performed by pipetting 100 μL of a combined solution of the alcohol of interest (5 mg/mL) and iodonitrotetrazolium (**INT**) (**132**) (0.25 mg/mL) to each of the 96 wells containing lyophilized cell free extracts. Upon alcohol oxidation, $NAD(P)^+$ is converted to NADPH. The reduced cofactor readily reacts with the INT molecules to form the **red formazan dye 131**, which is visible to the naked eye. Alternatively, conversion can also be monitored by measuring the absorption on a plate reader at a wavelength of 492 nm for higher accuracy. The assay principle is visualized in Scheme 3.15.[153]

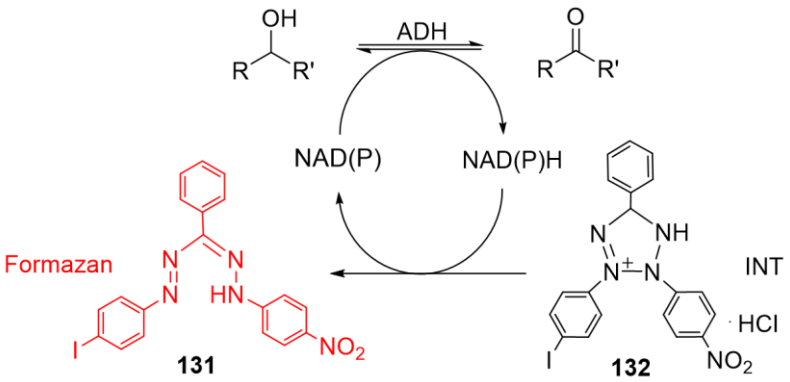

Scheme 3.15 INT assay principle. The red formazan dye (**131**) is produced from INT (**132**) upon oxidation to NAD(P)H.[153]

The beauty of this assay lies in the fact that INT/formazan additionally acts as a **cofactor recycling** system that helps to shift the equilibrium towards product formation while the formazan dye is continuously further accumulated, leading to an **amplified color response**. Therefore, positive candidates can be identified with high sensitivity while requiring very low substrate amounts (<50 mg/96-well plate).
In our case, the assay was used for identification of a catalyst that acted in a **regiospecific** manner by exclusively attacking the lactol functionalities, while leaving the hydroxyl-groups in C3-position untouched (Scheme 3.16).

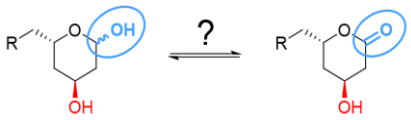

Scheme 3.16 Conversion of C1-alcohol group (blue) to corresponding ketone. The OH-group at C3 position (red) is not reacted.

In order to find suitable enzymes, **systematic screening rounds** with the four substrates shown in Figure 3.15 were performed.

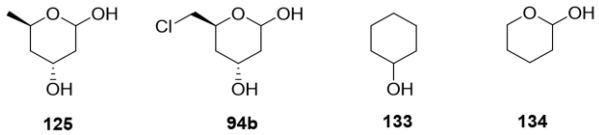

Figure 3.15 Substrates for systematic screening of ADH library towards regioselective candidates.

In the initial screening (A), the ADHs were assessed for tolerance towards the acetaldehyde trimer (**125**). As this molecule bears the most basic structure present in the DERA products, the minimal premise for a suitable candidate is tolerance for **125**. In the following round (B) the panel was screened for conversion of the chlorine-functionalized derivative **94b**. Here, the Cl-group is supposed to represent bulkier substituents and it was speculated that positive hits will exhibit higher probabilities for acceptance of diversely functionalized substrates. However, in both first screening rounds, it remained unclear which of the two alcohol functionality was actually oxidized by the hit enzymes. In order to exclude catalysts that would transform the alcohol group in position 3, cyclohexanol (**133**) was next applied as substrate (C). In this case, all positive hits were sorted out and were not further considered. In the last screening round (D), tetrahydro-2H-pyran-2-ol (**134**) served as substrate to identify enzymes that explicitly target the lactol functionality.
Figure 3.16 shows the screening plates and the corresponding absorbance measurements at 492 nm. The assay furnished four candidates that met the requirements of converting the DERA products **125** and **94b,** and also lactol **134**, while not consuming cyclohexanol (**133**) as substrate and were identified as:

A3 = ADH298
C6 = ADH318
F5 = ADH353
F6 = ADH354

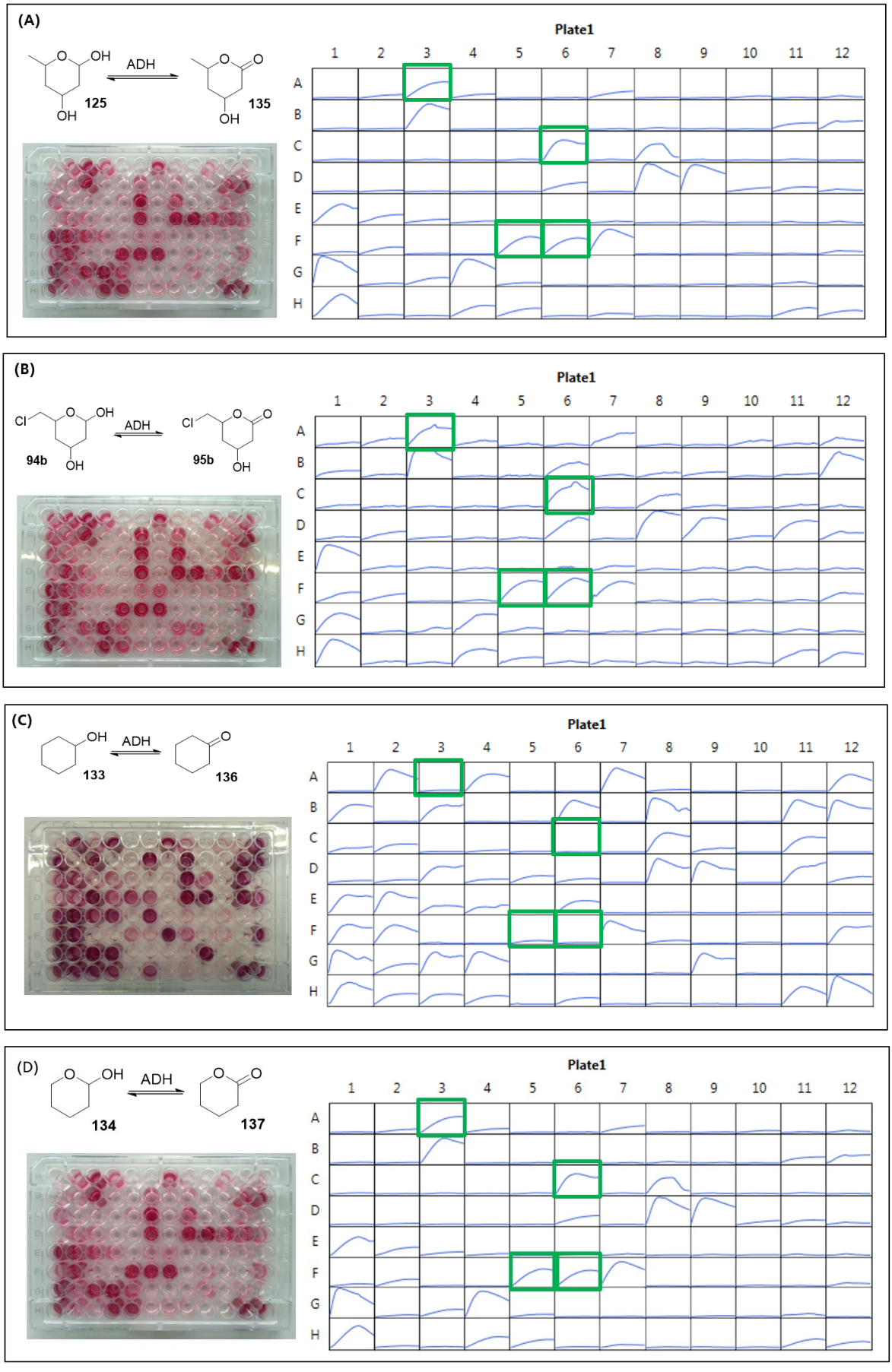

Figure 3.16 Screening of commercial ADH library towards substrates **125**, **94b**, **133**, and **134**. Suitable candidates are highlighted in green boxes.

The hit enzymes were rescreened in a separate experiment utilizing the PhAc-protected statin building block **3a** as substrate. Among these candidates, ADH354 showed the best results by generating the highest color density (Figure 3.17). The catalyst was therefore employed in a larger scale of 10 mL reaction volume in order to isolate the corresponding lactone **4a** in sufficient amount for verification by NMR-analysis. As a cofactor regeneration method was not implemented yet, NAD(P)$^+$ was applied in a stoichiometric amount to allow full conversion. Analysis was conducted by TLC with reference material obtained from a chemical oxidation reaction carried out with NaOCl. PhAc-protected lactone **4a** was produced in a quantitative manner after a reaction time of 20 h. Product isolation by simple extraction with EtOAc finally gave the desired lactone in high purity.

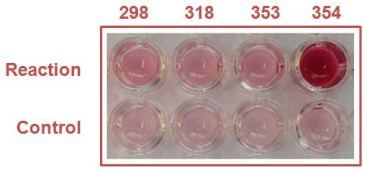

Figure 3.17 Rescreening of hit enzymes against lactol **3a** via INT assay. The highest color density was observed for ADH354.

3.4.2. Towards NAD(P)$^+$ cofactor recycling

Since the costs for NAD(P)$^+$ average out at around 500 €/g, utilization of equimolar amounts of cofactor is financially and economically unfavorable. This issue has been long regarded as the major challenge for industrially applied oxidoreductase reactions. Therefore, a range of *in situ* regeneration systems involving co-substrates have been developed in order to use NAD(P)$^+$ in smaller catalytic amounts.[150, 154]
The strategies that have been followed within this work are:

1. NADP$^+$-regeneration by a glutamate dehydrogenase
2. NADP$^+$-regeneration by a (second) ketoreductase
3. NADP$^+$-regeneration by a nicotinamide oxidase

1. NADP$^+$-regeneration by a glutamate dehydrogenase

Glutamate dehydrogenases (GDHs) are enzymes that are present in all living organisms. They catalyze the reversible conversion of glutamate (**138**) and water to α-ketoglutarate (**139**) and ammonia upon reducing NAD(P)$^+$ to NAD(P)H (Scheme 3.17).[155]

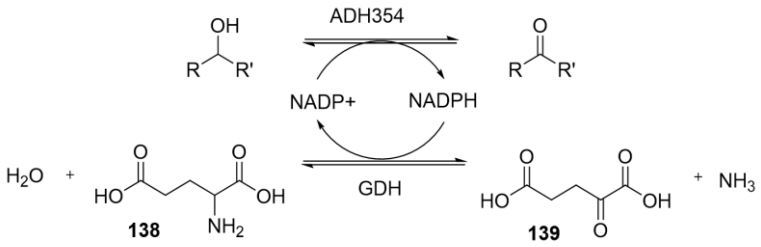

Scheme 3.17 Cofactor recycling by GDH-catalyzed conversion of α-ketoglutarate (**138**) to glutamate (**137**).[155]

As can be seen, stoichiometric amounts of ammonia are required, which inevitably leads to a **dramatic increase in pH**. Since it was questionable, if ADH354 would tolerate such basic conditions (pH = 11), its oxidation activity was tested upon incubation in 100 mM NH_4Cl. The

acetaldehyde trimer **125** was applied as model substrate in an equimolar concentration. The reaction was performed in a 96-well plate format and monitored by INT-assay. A positive control was conducted without addition of ammonia and kept at a pH of 7.5. As can be seen in Figure 3.18, color formation correlating to successful alcohol oxidation is at much lower extent in the reaction performed in 100 mM NH_4Cl compared to the positive control. These results indicated that higher amounts of ammonia/higher pH can lead to enzyme deactivation and make this cofactor regeneration method not viable in our case.

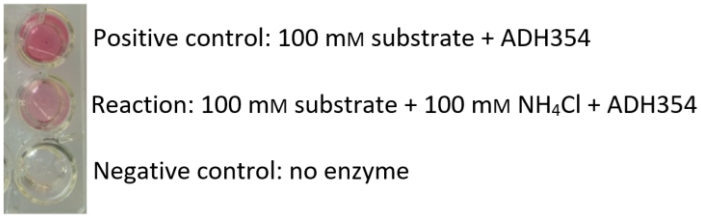

Figure 3.18 INT assay for assessment of applicability of GDH.

2. $NADP^+$-regeneration by a second ketoreductase (KRED)

Alcohol dehydrogenase/ketoreductase from *Lactobacillus brevis* (*Lb*ADH/*Lb*KRED) is a versatile catalyst known for **consumption of simple aldehydes or ketones** to generate primary or secondary alcohols upon conversion of NADPH to $NADP^+$.[156] In this work, acetone, being a cheap and easily removable compound, was chosen as the sacrificial ketone (Scheme 3.18).

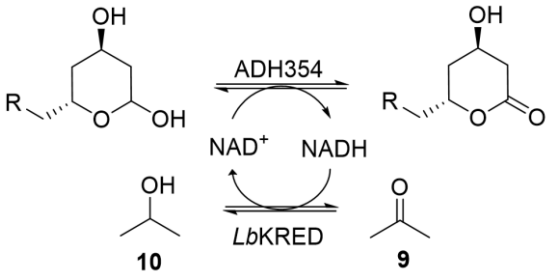

Scheme 3.18 Cofactor recycling by *Lb*KRED-catalyzed conversion of acetone (**9**) to *iso*-propanol (**10**).

Conversion to *iso*-propanol (**10**) does not induce changes in pH, which otherwise can be observed for many enzyme-coupled recycling approaches. An additional benefit is that acetone acts as a cosolvent and assists in solubilizing apolar substrates. Concentrations of 10% or even higher are usually well tolerated by enzymes.[157]

The reaction was therefore tested on the acetaldehyde trimer **125** (100 mM) as model substrate in 10% acetone. ADH354 and *Lb*KRED were added in a 1 : 1 ratio with a concentration of 10 mg/mL reaction volume. In order to monitor the conversion, analytical HPLC samples were taken after 1, 3, 6, and 24 h and treated with a UV-active derivatization reagent (O-benzylhydroxylamine hydrochloride), which reacts with the open form of lactol **125** upon oxime formation. The corresponding lactone **135**, on the other hand, remains untouched and invisible for UV-detection at 215 nm. Analysis showed a decrease of the lactol peak over time and an almost complete disappearance after 24 h, proving nearly full conversion through successful cofactor regeneration.

In order to prove that *Lb*KRED does not also convert the DERA products as substrate, an additional experiment utilizing the INT assay principle was performed: The acetaldehyde trimerization product **125**, cyclohexanol (**133**), tetrahydro-2H-pyran-2-ol (**134**), and the PhAc-protected lactol **3a** were incubated with *Lb*KRED for 6 h at 100 mM concentration. A positive control utilizing ADH354 in the case of lactol **3a** and a negative control without substrate were run in parallel (Figure 3.19).

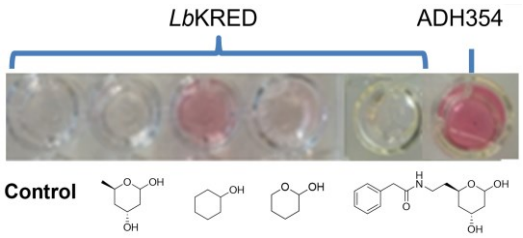

Figure 3.19 Assessment of *Lb*KRED's tolerance towards lactol substrates via INT assay.

The results showed that, with very minor and neglectable effects on tetrahydro-2H-pyran-2-ol (**134**), *Lb*KRED only converted cyclohexanol (**133**) as substrate, fulfilling our hopes that the OH-groups present in the statin precursors will remain untouched. Hence, the employment of *Lb*KRED for cofactor recycling seemed highly feasible. Further reaction engineering was performed, in order to optimize conditions such as acetone concentration, buffer, and enzyme amounts:

Experiment A: Variation of acetone concentration

It is of great importance to identify the most appropriate amount of acetone in the reaction mixture, as acetone acts as both, substrate for *Lb*KRED and a cosolvent, but can also lead to enzyme inactivation at higher concentrations. Therefore, analytical reactions of 300 μL total volume were performed for the conversion of the acetaldehyde trimer **125** as model substrate (100 mM) at different concentrations of acetone ranging from 150 – 500 mM. The amount of enzyme was kept at 1 mg/100 μL reaction volume containing 50 mM phosphate buffer at pH 7.5. Figure 3.20 depicts the results gathered from RP-HPLC analysis. Conversion was measured for each concentration after 1, 3, 6, and 24 h. Figure 3.20 shows that with only minor difference, the highest conversion was already observed for the lowest concentration of 150 mM acetone. Experiments with 100 mM only were not conducted due to acetone's high volatility and evaporation can result in insufficient quantity. Hence, the acetone amount was kept at 150 mM in all further experiments.

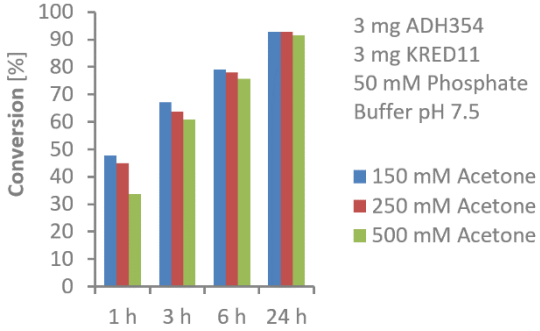

Figure 3.20 Measured conversion to lactone **135** at different acetone concentrations.

Experiment B: Variation of buffer

The reaction was also tested in two different kinds of buffers, namely TEA and phosphate buffer, both utilized at a pH of 7.5 and a concentration of 50 mM. The reactions were run with an enzyme amount of 3 mg/300 μL reaction volume in 150 mM acetone. Monitoring by RP-HPLC showed no significant difference between phosphate and TEA buffer (Figure 3.21) and since phosphate buffer is inexpensive and easier to remove, it was applied in further experiments.

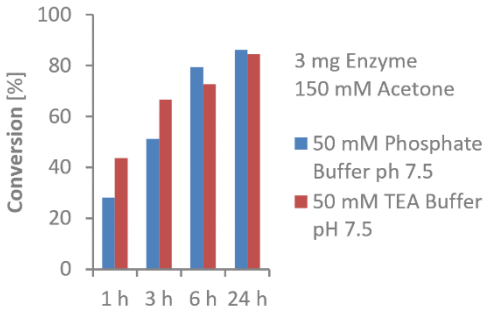

Figure 3.21 Measured conversions to lactone **135** in different buffers.

Experiment C: Variation of enzyme concentration

The most crucial part within reaction engineering is defining the required enzyme amounts and ratios, as the enzymes are often the most cost-intensive components. Therefore, in the following experiments, the enzyme amounts were varied between 1 – 3 mg CFE/300 μL reaction volume of each enzyme. Analysis by RP-HPLC revealed a much higher conversion rate when utilizing 3 mg catalysts by reaching around 94% after 24 h, while 1 mg or 2 mg only furnished 70% and 80%, respectively (Figure 3.22). This lead to the conclusion that at least one of the enzymes applied was required at this higher amount.

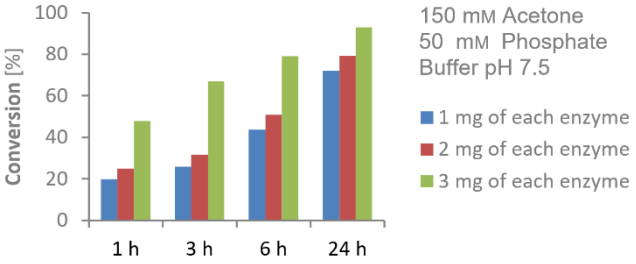

Figure 3.22 Measured conversion to lactone **135** at different enzyme amounts.

In a subsequent experiment, it was determined which of the enzymes was the limiting one. The enzyme ratio was therefore changed to 1 : 3 and the conversion was again measured by RP-HPLC over a period of 1, 3, 6, and 24 h. Figure 3.23 shows that after 24 h a conversion of almost 90% was reached when utilizing 3 mg of ADH354 and 1 mg of *Lb*KRED, while the opposite ratio resulted in a conversion of only around 70%. Thus, it was concluded that the limiting enzyme was ADH354. Its amount was therefore kept at 3 mg/300 μL reaction volume in further experiments.

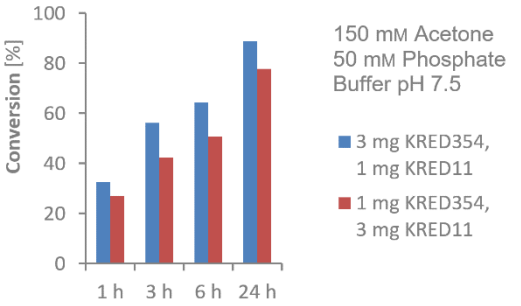

Figure 3.23 Measured conversion to lactone **135** at different enzyme ratios.

In order to further investigate on the most suitable enzyme proportion required for highest possible conversion, ratios between 3:1, 3:2, and 3:3 were directly compared. The results of the RP-HPLC analysis indicated that a ratio of 3:1, meaning 3 mg of ADH354 and 1 mg of *Lb*KRED can be regarded as sufficient, even though higher amounts of *Lb*KRED might furnish faster reactions, when comparing shorter periods of time (1 – 6 h). However, similar conversions of close to 90% were reached in all the cases after 24 h (Figure 3.24).

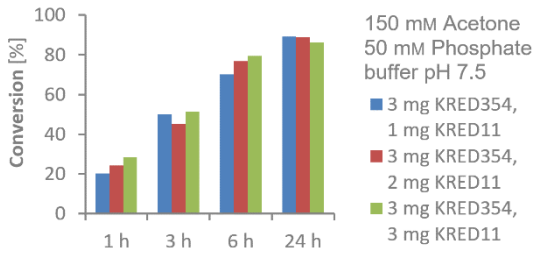

Figure 3.24 Measured conversion to lactone **135** with different enzyme ratios.

In a final experiment, it was investigated in which range reaction time needed to be prolonged to reach maximum conversion when utilizing only 1 mg of each enzyme as this information might be relevant for industrial use, where low amounts of enzymes can mean huge savings on costs. In this case, conversion measured by RP-HPLC showed a comparable yield of almost 90% after four days (Figure 3.25). Since in industry time is a crucial and valuable factor, a reaction time of four days can also mean high financial losses. Therefore, further reactions were conducted with the optimized enzyme amounts of 3 mg ADH354 and 1 mg *Lb*KRED per 300 μL reaction volume containing 100 mM of substrate.

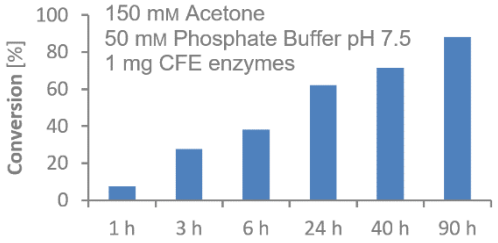

Figure 3.25 Measured conversion to lactone **135** after 1 – 90 h.

3. NADP$^+$-regeneration by a nicotinamide oxidase (NOX)

NAD(P)H oxidases (NOX) constitute a particularly suited NAD(P)$^+$-regeneration method for biocatalytic applications, as they simply require **oxygen as co-substrate** and thereby forming either hydrogen peroxide (type 1 NOX) or water (type 2 NOX) as single byproduct:[150]

$$\text{NAD(P)H} + O_2 + H^+ \rightarrow \text{NAD(P)}^+ + H_2O_2 \quad \text{(type 1 NOX)}$$
$$2\,\text{NAD(P)H} + O_2 + 2H^+ \rightarrow 2\,\text{NAD(P)}^+ + 2\,H_2O \quad \text{(type 2 NOX)}$$

Due to the driving force given by the high redox potential of molecular oxygen the reaction equilibrium is thermodynamically shifted towards NAD(P)$^+$-formation.[158] The unnecessity of additional substrates facilitates subsequent work-up procedures and helps to decrease costs while increasing purity and yield. However, as hydrogen peroxide, produced by type 1 NOXs, can cause enzyme damage or interfere within reactions, its removal is often required and can be achieved using an additional enzyme like a catalase.[150] On the other hand, **water-forming oxidases** are usually the preferred choice for cofactor recycling. Many of their representatives have been studied from sources like *Streptococcus*,[159] *Lactobacillus*,[160] *Lactococcus*,[161] *Clostridium*,[162] *Serpulina*,[163] *Leuconostoc*,[164] or *Bacillus*,[165] which are, however, all specific to NADH. There are only two known water-forming and one hydrogen peroxide forming native

NOXs that also tolerate NADPH as cofactor. Apart from these, a quintuple mutant of *Lb*NOX has also been reported to be highly specific towards NADPH.[166]
For our purpose, we utilized a water-forming NOX provided from *Prozomix Ltd* that tolerates both, NADH and NADPH (Pro-NOX001). The enzyme was successfully employed in the oxidation reaction of the PhAc-protected lactol **3a** (Scheme 3.19).

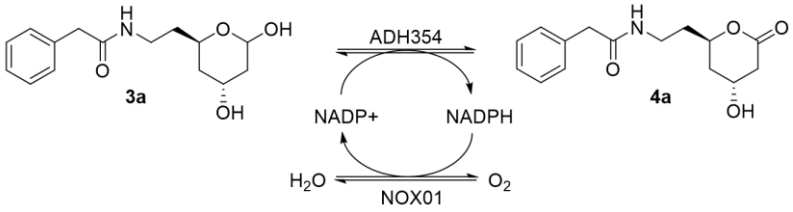

Scheme 3.19 ADH-catalyzed oxidation of **3a** with NOX employed for NAPD⁺ recycling.

In order to determine sufficient enzyme amounts, analytical scale reactions were studied with different amounts of NOX ranging from 5 – 20 mg CFE in 500 μL volume of 100 mM substrate. ADH354 was used at a concentration of 10 mg/mL and the reactions were monitored by RP-HPLC. Samples were taken after 10 and 24 h. Table 3.6 lists the different conversions reached.

Table 3.6 Conversions to **4a** measured after 10 h and 24 h at different enzyme amounts.

Enzyme amount	Conversion after 10 h	Conversion after 24 h
5 mg	45%	80%
10 mg	65%	100%
15 mg	80%	100%
20 mg	90%	100%

As can be seen, with 5 mg enzyme only, full conversion is still not reached after a reaction time of 24 h. Doubling the amount to 10 mg delivers 65% conversion after 10h and reaches 100% after 24 h. It is therefore, due to reasons of cost efficiency, not necessary to utilize more than 10 mg, even though 15 or 20 mg enzyme can reduce the reaction time dramatically.

3.4.3. ADH-catalyzed oxidation of DERA products

Following the protocols described in the previous chapters, the DERA products 3**a-g** were oxidized to the lactones via ADH-catalysis. Herein, $NADP^+$-cofactor recycling was provided by employing *Lb*KRED as a second enzyme and adding acetone as sacrificial co-substrate. This regeneration system was chosen, as *Lb*KRED is a commercially established catalyst and was available in greater quantities. However, in a proof-of-concept experiment, the PhAc-protected lactone **4a** was also obtained from a reaction conducted with NOX for cofactor recycling.
In all cases, the lactone products were achieved in high purity and high yields around 85-90%, although utilization of *Lb*KRED required smaller enzyme amounts than in the approach using NOX to achieve similar results.

3.5. A multienzymatic one-pot cascade for the synthesis of statins

Enzymatic one-pot reactions can save time and effort and reduce product loss and larger amounts of waste by avoiding unnecessary recovery of reaction intermediates. Herein, different strategies can be followed, including 'telescope reactions' and 'tandem reactions'.

3.5.1. One-pot telescoping reaction

A one-pot telescope reaction describes the performance of two or more reaction steps in a **serial, individual manner**, meaning that the catalyst(s)/reagent(s) for a subsequent reaction is only added after completion of the first. This offers the advantage that different reagents and catalyst cannot interfere with each other and can be chosen independently.[3c]

For proof of concept testing, this method was applied for the synthesis of PhAc-protected statin building block **4a**. After performing the DERA-catalyzed aldol addition step, ADH354 was added to the reaction mixture for lactol oxidation. During this, *Lb*KRED was utilized for cofactor recycling (Scheme 3.20).

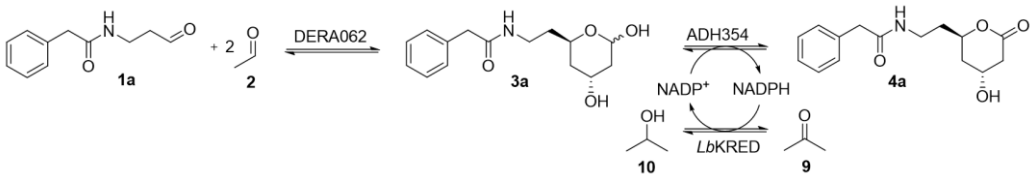

Scheme 3.20 One-pot telescope reaction towards PhAc-protected statin building block **4a**.

Conducting the aldol addition step and the oxidation of lactol **3a** in a separate, subsequent manner permitted the use of acetone as sacrificial substrate, even though acetone is also a potential DERA donor substrate and can be added to aldehyde **1a** generating an undesired side product. Therefore, it was of great importance to perform the DERA-catalyzed step until completion. This was achieved by monitoring the process by HPLC and finally conducting the reaction for 24 h. Direct addition of acetone and buffered enzyme solutions of ADH354 and *Lb*KRED to the reaction mixture without further work-up or isolation steps allowed for an easy and quick proceeding to the oxidation step. The method proved to be successful and a final yield of 50% of isolated product verified a more efficient and economically beneficial outcome than when performing single reaction steps in a classical fashion (45% final product yield).

3.5.2. One-pot tandem reaction

A one-pot tandem reaction is carried out in a **parallel manner**, where all reactants and catalysts are added directly from the beginning, enabling the reactions to proceed in a concurrent fashion.[3c]

In order to conduct statin synthesis in a tandem fashion, the enzymes' catalytic activities must not interfere within each other's processes. For example, it is required that the ADH does not consume the DERA aldehyde substrates in a reductive reaction. Hence, in a test reaction, the PhAc-protected aldehyde **1a** was incubated with ADH354 and the outcome was monitored via INT assay. No visible color formation after 6 h demonstrated that the enzyme did not consume the starting material and thus was suitable for employment during the DERA reaction. Assuming that the NOX will not interfere either, the reaction set-up was again tested on the PhAc-

protected substrate **1a** (Scheme 3.21). Here, the desired lactone product **4a** was successfully isolated after a reaction time of 24 h with a yield of 60%, marking the one-pot tandem reaction more efficient than the telescope reaction. However, the large amount of NOX required here was a minor drawback. Further reaction engineering would be necessary in order to optimize towards sufficient oxygen supply for an efficient operation of the enzyme. Possible effects can be achieved through temperature control, using lower substrate concentrations or applying a gradient. Anyhow, the positive reaction outcome represents a major success for statin synthesis by offering a simple and ecologically and economically friendly strategy with great industrial potential.

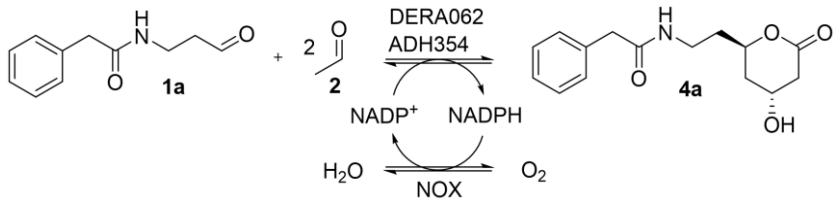

Scheme 3.21 One-pot tandem reaction towards PhAc-protected statin building block **4a**.

3.6. Penicillin G acylase-catalyzed cleavage of PhAc-protecting group

As will be subsequently discussed in chapter 4.1.1, penicillin acylases are known for their ability to **hydrolyze amide bonds** in penicillin antibiotics (Scheme 3.22).[130] According to their substrate specificity for penicillin V (phenoxymethyl penicillin) or G (benzyl penicillin), they are categorized into two classes: Type I and Type II penicillin acylases, respectively. Type II penicillin acylases (PGAs) can be further classified into two sub-categories: Type IIa, which act specifically on aromatic phenylacetyl moieties, and Type IIb, which prefer aliphatic moieties.[130]

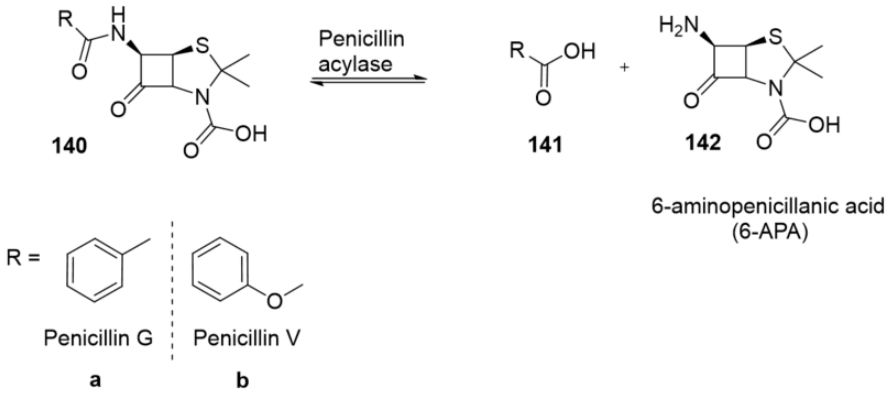

Scheme 3.22 Penicillin acylase-catalyzed hydrolysis of penicillin (**140**) to form 6-APA (**142**) and carboxylic acid **141**.[130]

In contrary to the limitations by the very specified acyl component, these enzymes tolerate a **broad variety of amines** as counterpart.[167] Thus, PGAs are not only one of the most commonly applied biocatalysts for the industrial production of β-lactam semisynthetic antibiotics[130] but can also be utilized for other amidation/hydrolysis processes.
Here, it was speculated that a PGA (type IIa) can be employed for the deprotection of statin precursor **4a** to give the free amine **143** (Scheme 3.23).

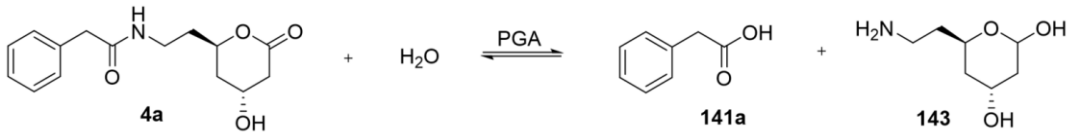

Scheme 3.23 PGA-catalyzed cleavage of PhAc-protecting group to furnish free amine **143**.

Herein, the reaction equilibrium is supposedly controlled by pH adjustment: Under basic conditions, the free phenyl acetic acid (**141a**) is deprotonated and should therefore not be consumed by the enzyme. Hence, the equilibrium is shifted towards hydrolysis. With decreasing pH, on the other hand, the amine's nucleophilicity is enhanced and reaction preferably takes place in synthesis direction. Thus, in order to find suitable conditions for the cleavage of the PhAc-group, it was mandatory to determine the enzyme's preferred pH range.

The PGA used in this work was of unknown source and was available as a stabilized preparation in ammonium sulfate solution (1.14 kU/mL, *Roche*). Initial experiments were conducted with 100 mM substrate and an enzyme concentration of 4.6 U/mL. The pH was varied between a range of 7 to 9 and reactions were carried out on 500 μL scale. A negative control without enzyme was conducted at ambient pH = 7.5 to exclude potential non-enzymatic processes. The reactions were monitored by HPLC analysis, which allowed for detection of the starting material **4a** as well as the cleavage product phenyl acetic acid (**141a**) via UV-measurement. As the enzyme-catalyzed cleavage reactions proceeded very fast and a conversion of around 75% was already reached after 1 h, samples taken after 15 minutes were utilized for analysis. The results summarized in Table 3.7 revealed that the reaction rate was by trend higher with increased pH until an optimum was reached at a slightly basic environment of around pH = 7.5. Increasing the pH above 8.5 led to a lower cleavage rate again.

Table 3.7 Conversions to lactone **143** after 15 min reaction time at different pH values.

pH	7.0	7.3	7.5	8.5	9.0
Conversion [%]	26	29	33	26	22

This finding verified the hypothesis that a rather basic environment is required for efficient cleavage reaction. However, a pH above 8.5 may not be beneficial for enzyme stability, leading to a decline of activity and lower conversion. It is assumed that the pH optimum lies somewhere between 7.5 and 8.5.

In order to verify successful cleavage by NMR analysis, a larger scale reaction was conducted to furnish amine **143** in sufficient amount. For this purpose, a buffered solution of pH = 7.7 was utilized. The enzyme amount and substrate concentration were kept the same and monitoring by HPLC showed full conversion after 1 h. The work-up was conducted by treating the reaction mixture with MeOH to precipitate the enzyme, which was then removed by filtration. In a preliminary proof of concept, the product was then isolated by simple removal of the aqueous phase via lyophilization. Analysis of the residue by NMR (Figure 3.26), in fact, showed the correct signals belonging to amine **143**. As expected, equally strong signals corresponding to the cleavage partner phenyl acetic acid (**141a**) were also present. Apart from that, an additional set of independent signals was found, which was also observed when just measuring the pure enzyme preparation. It is most likely that these signals belong to stabilizers added to the enzyme mixture and these signals were therefore not further investigated.

In order to separate the amine product from the acid after reaction completion and removal of the enzyme, various approaches were tested. The first attempt involved simple extraction of the aqueous phase with EtOAc. Contrary to our hope that the product would be absorbed to the organic phase while the acid would mainly stay in the aqueous phase, NMR analysis of the organic phase showed only signals corresponding to the acid. Thus, the aqueous phase was lyophilized and the obtained residue was directly resuspended in $CDCl_3$ for NMR analysis. Again, the chromatogram of the supernatant showed only the presence of phenyl acetic acid (**141a**). However, the residual solid, which was then resolved in D_2O and submitted to analysis, clearly constituted the target product, although not in perfect purity but enriched in 10 : 1 ratio to the acid. It is assumed that further washing steps are required during the work-up to furnish the product in higher purity. Although further extraction/purification experiments have not been conducted, a proof of principle was brought for the relevance of PGA-application in the production of amine-functionalized statin building block **143**.

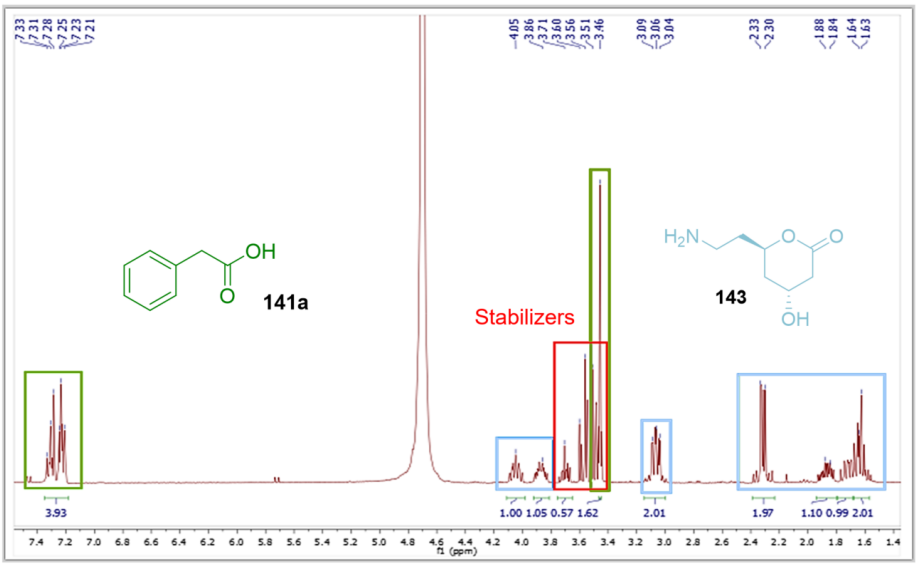

Figure 3.26 NMR chromatogram of isolated cleavage products **141a** and **143**.

3.7. Pharmacological activity of synthesized statins

In order to assess the pharmacological value of the synthesized statins, their **inhibitory activity towards HMG-CoA reductase** (HMGR) was tested *via* a commercial assay kit. The assay principle is based on the NADPH consumption of HMGR upon conversion of HMG-CoA (**20**) to mevalonate (**21**) (Scheme 3.24). Herein, the decrease of cofactor directly correlates with enzyme activity and can be detected at 340 nm, where the oxidized form $NAD(P)^+$ shows no absorption. Hence, successful inhibition is visualized by a steady NADPH absorption curve.

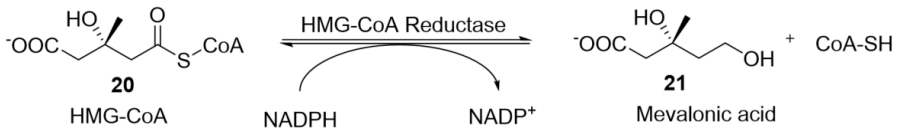

Scheme 3.24 Conversion of HMG-CoA (**20**) to mevalonic acid (**21**) by HMG-CoA reductase.

Prior to performing the assay, it was verified that, once resolved in an aqueous buffer solution, the cyclic lactones will hydrolyze to form the **active open chain formation** (Scheme 3.25). An NMR sample, which was directly measured after incubation of statin **4f** in D_2O at room temperature for 1 h verified this case by showing distinct signals of the acid functionality.

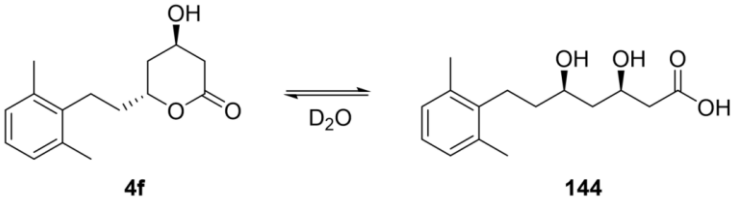

4f **144**

Scheme 3.25 Conversion to biologically active open chain upon hydrolysis in D_2O.

The HMG-CoA inhibition screening was finally performed in duplicate according to the protocol provided by the manufacturer (*Sigma Aldrich*). A control experiment with the commercial drug pravastatin, a blank without enzyme, and a control without inhibitor were performed in parallel. In initial experiments, when applying the statins at 1 nM concentration (suggested in the protocol), no inhibitory effects were detected for the synthesized statins including the literature known natural product solistatin (**4b**). However, after increasing the statin concentration to 1 mM (1000-fold compared to Pravastatin), most of the tested statins lead to inhibition of HMG-CoA reductase. Figure 3.27 visualizes the results measured over 12 min. The background data was subtracted from the blank measurement and normalized to the starting point of 0.5 arbitrary units.

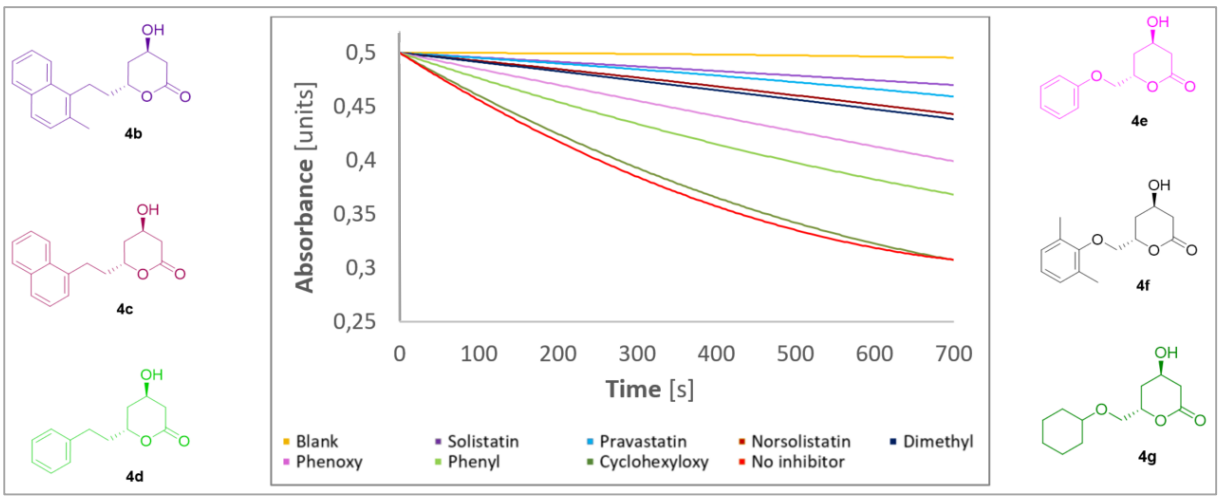

Figure 3.27 HMG-CoA inhibition assay conducted for synthesized statins **4b-g**.

As can be seen, solistatin (**4b**) showed the highest inhibitory property amongst the synthesized statins, followed by its non-methylated derivative norsolistatin (**4c**). Obviously, the bulky naphthalene core has a greater influence in substrate binding. Similar activity to **4c** was also found in the dimethylphenoxy substituted statin **4f.** Lower effects were observed for phenoxy-functionalized **4e** and last but not least phenyl-functionalized **4d**. The non-aromatic oxycyclohexyl **4g** appeared to be biologically inactive. This raised the hypothesis that π-stacking

effects by the aromatic ring structure in the core molecule must have greater influence in protein-ligand interaction and are relevant for effective binding. Indeed, my measuring electronic interaction energies through density-functional theory methods, KEE *et al.* have shown that the interactions between Tyr 479 and HMG-CoA are highly important (8 kcals/mol) and therefore suggest that π-π-stacking effects between protein ligand should be considered during the design of future statin drugs.[168]

By trend, introduction of an oxygen as ether functionality also seemed to have beneficial effects, which can probably be explained through higher polarity and solubility of the molecules.

Fascination arose, when the non-methylated statins **4c** and **4e** were compared to their methylated counterparts **4b** and **4f**: In both cases, the latter showed higher inhibitory effects. Apparently, the methyl group adjacent to the statin side chain plays an important role in stabilizing the substrate in the enzyme pocket by potentially inducing a conformational change. Indeed, when taking a look at the so far reported statins, it becomes evident that all of them, independently of being natural or synthetic products, feature an alkyl substitution at the mentioned position. While the first generation drugs typically bear a simple methyl group, the second generation statins carry a bulkier *iso*-propyl or cyclopropyl group (Figure 3.28). Interestingly, the alkyl substitutions of the non-aromatic statins are always cis-oriented to the statin side chain, giving higher evidence of their role in conformational induction.

X-ray crystallography of HMG-CoA reductase and complexes with statins show how the statin side chain binds to the HMG-CoA portion and interacts via hydrogen bonds while the hydrophobic groups are positioned in a shallow groove formed by the C-terminal residues of the enzyme. Additional binding interactions are exhibited in most of the synthetic statins via their fluorophenyl groups or in rosuvastatin via the electronegative sulfone group (see chapter 1.2).

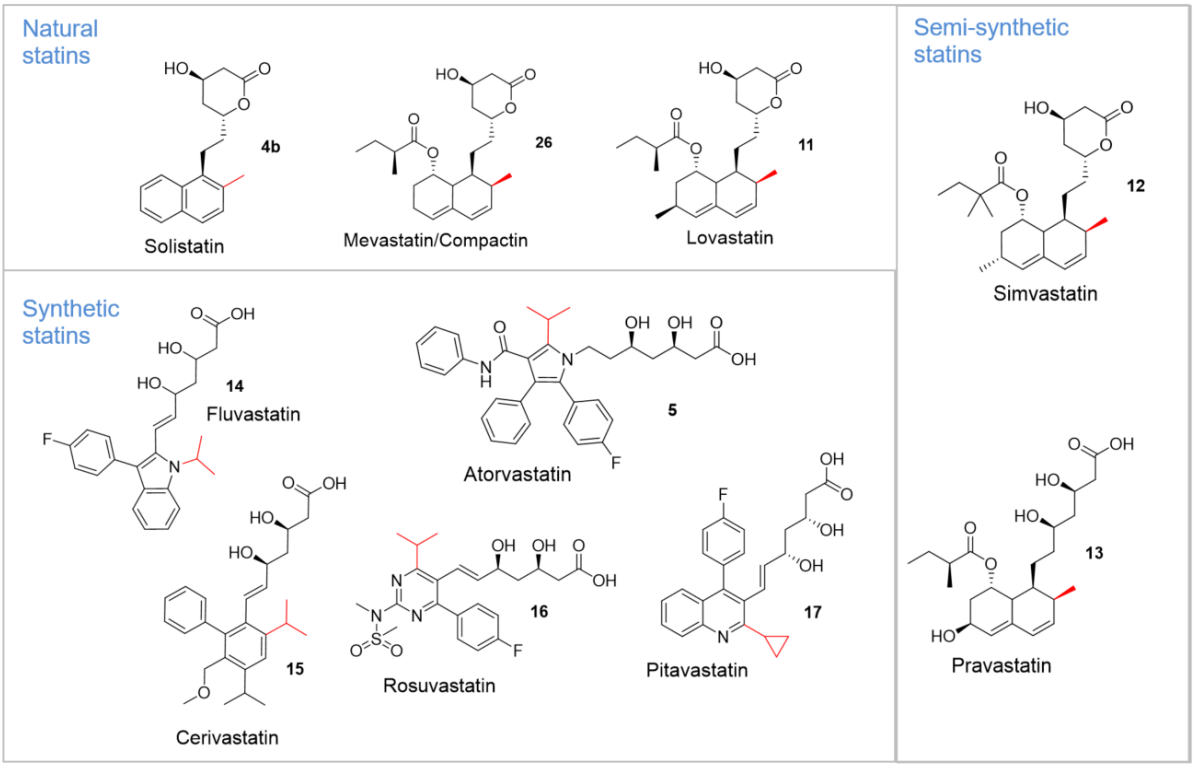

Figure 3.28 Molecular structures of reported and commercial statins. The alkyl substitutions adjacent to the statin side chains are highlighted in red.

4. Summary and outlook

In this work, an **efficient biocatalytic pathway** towards the synthesis of **simple statins** was developed by utilizing a novel DERA and a novel ADH in a **one-pot cascade manner**. This new strategy represents a major success for statin synthesis by offering a simple, fast and ecologically and economically friendly strategy with industrial potential.

Herein, DERA was applied for the **stereoselective sequential aldol addition** of two molecules of acetaldehyde to a set of different acceptor aldehydes, whereas an ADH was utilized for the **regioselective oxidation** of the furnished lactol intermediates with **cofactor recycling** by a second KRED or a NOX. The statins generated comprised the natural product solistatin (**4b**) and five of its simplified derivatives as well as an important amine-functionalized precursor **4a** to atorvastatin (**5**). Herein, with the exception of commercial phenyl propanal, all acceptor substrates were chemically synthesized from simple, readily available chemicals in a highly cost-efficient manner.

The aldol addition step, which represented the hardest challenge due enzyme deactivation and side product formation, was assessed in detail and successfully optimized in terms of reaction conditions towards higher product yield.

Part of the work also included the design of a **medium-throughput assay** in order to identify suitable DERAs from a large protein library. This was accomplished by using a **semi-automated HPTLC-assisted** screening strategy. The method offered **reliable qualitative and quantitative detection** of reaction products via color-density measurement of very distinct compound bands generated by a highly precise spray-on technique of reaction samples and an adapted plate development and staining process. The assay application led to the discovery of a **novel DERA** (by ANNA SZEKRENYI, FESSNER group) with notably high activity for acetaldehyde trimerization when compared to other reported DERAs and was therefore used in most of the DERA reactions in this work.

A **novel ADH**, which was suitable for the regioselective lactol oxidation step, was identified from a large protein library by **systematic screening** of a set of functionalized substrates via a **colorimetric assay**. In order to adapt the ADH-catalyzed process to industrial application, a cofactor recycling system was successfully implemented by either employing the literature known KRED from *Lactobacillus brevis* with acetone as sacrificial substrate or utilizing a water-forming oxygen-dependent NOX.

The application of *Lb*KRED brought the main advantage that this enzyme is already known and established for highly efficient conversion of small ketones upon generation of $NADP^+$. However, a small drawback lay in the fact that the same ketones can be consumed by DERA via aldol addition to the acceptor aldehydes. It was therefore mandatory to conduct the oxidation step in a one-pot telescope fashion after the starting material was fully converted by DERA.

The application of NOX brought the main advantage that no additional chemicals (apart from oxygen) were required in the reaction system, allowing for an unproblematic realization of a straight forward one-pot-three-enzyme tandem cascade, where all reagents and reactions partners were directly added from the beginning. However, large amounts of NOX were required for sufficient cofactor recycling (10 mg enzyme/mL reaction mixture).

In a proof of concept, both methods were successfully applied for the one-pot-three-enzyme synthesis of statin building block **4a** and represent a novel, simple, and efficient strategy with economically and ecologically friendly outcome, hence, moving towards a greener chemistry.

Ultimately, solistatin and its structurally simplified derivatives were tested for their **biological activity** via an **HMG-CoA reductase inhibition** assay. The results revealed that, apart from solistatin, many of the simpler statins exhibited inhibitory properties, as well. Interestingly, it was validated that, by trend, statins with alkyl groups adjacent to the statin side chain showed larger effects. This confirmed the importance and necessity of the studies conducted and deeply emphasized with this work's the objective, which was providing easier access to simple novel statins for the assessment of their different structural properties and the resulting effects on the biological activity.

Redesign of the *(R)*-Selective Ketoreductase from *Lactobacillus brevis* Relevant to Pharmaceutical Application

5. Theoretical background

5.1. Ticagrelor – An agent for anti-platelet therapy

Thrombocytes or platelets are small anuclear cells in our blood, which continuously patrol the vascular tree in order to act on injured vessels. Herein, they prevent excessive blood loss by aggregation and formation of blood clots.[169] Their fascinating molecular machinery has evolved to enable rapid shift from a non-adhesive to a pro-adhesive state after signal sensing.[170] This activation is primarily mediated by the glycoprotein VON WILLEBRAND factor (vWf) and collagen, which are both released at the site of vascular damage.[171] However, platelets exhibit a wide array of additional surface receptors for other agonists like thromboxane A2 (TxA2), thrombin, serotonin, and adenosine diphosphate (ADP), which amplify activation through unique intracellular signaling pathways.[172] However, by mischance, this highly complex interplay can malfunction and lead to unintended platelet adhesion/activation, which plays a pivotal role in atherothrombotic processes and **acute coronary artery syndrome** (ACS).[173]

In this context, aspirin (acetylsalicylic acid) was the first drug that gave insight into the role of platelets in health and disease and, for many years, has been used as the major treatment for ACS due to its ability to inhibit the formation of agonist thromboxane A2 from arachidonic acid.[174] Today, most anti-platelet pharmaceuticals either target the thromboxane- or the ADP-mediated signaling sequence. Amongst these, **ticagrelor** (Brillique®, *AstraZeneca*) entered the market as the first **reversible oral agent** in 2010 and reached sales of $619 million in 2015, which are envisioned to go as high as $3.5 billion by 2023,[175] even though common adverse effects like increased risk of bleeding[176] and shortness of breath[177] have been reported.

5.2. The development of ticagrelor

Ticagrelor belongs to the chemical class of cyclopentyltriazolo-pyrimidines and resembles ATP, the natural antagonist to the ADP-receptor $P2Y_{12}$, located on the platelet surface.[178] The drug functions as an **allosteric effector** molecule, meaning that it binds to a region different from the protein's actual active site, often referred to as the allosteric or regulatory site. This interaction induces conformational changes and inactivation of the receptor in a reversible manner, allowing for a controlled regulation of signal transduction with rapid on and offset of effects that closely follow drug exposure.[179]

The drug's structural design arose with the quest to find stable analogs of ATP. Hence, in ticagrelor the labile and charged triphosphate side chain was replaced for a nonacidic hydroxyl alkyl moiety. The metabolically labile ribose sugar unit was replaced for a more stable cyclopentyl ring while an additional nitrogen was joined to the purine system for higher affinity to the $P2Y_{12}$ receptor. However, the main difference was made by introducing a propyl thioether side chain in C2 position of the purine system and a fluorinated ***trans*-aryl cyclopropylamine** (CPA) unit to the amine group. Interestingly, cyclopropane ring systems are ubiquitously found in nature as an important structural framework and have been used as common design elements in medicinal chemistry.[14c, 180]

Scheme 5.1 shows the chemical structures of ATP in comparison to ticagrelor and depicts its retrosynthesis pathway via assembling of three individual subunits **146-148**. The production of the CPA unit **146** constitutes a greater challenge due to its **chirality**. The next chapters will

therefore cover this subject and give an insight into a selection of reported chemical and biochemical routes.

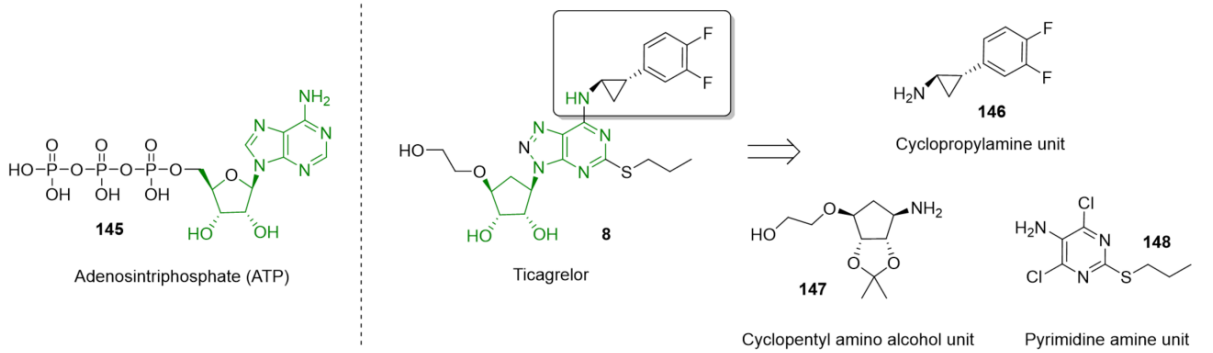

Scheme 5.1 Comparison between chemical structure of ATP (**145**) and ticagrelor (**8**). The common core present in both molecules is highlighted in green. The *trans*-aryl cyclopropylamine side chain is highlighted with a box.

5.2.1. Chemical synthesis of CPA building blocks

For the generation of the cyclopropylamine unit **146**, current classical synthesis strategies require **multiple reaction steps** that involve metal catalysts as well as chiral auxiliaries to obtain the specific *trans*-configuration of the substituents. Scheme 5.2 shows the reaction pathway realized by SPRINGTHORPE *et al.* at *AstraZeneca*.[14a]

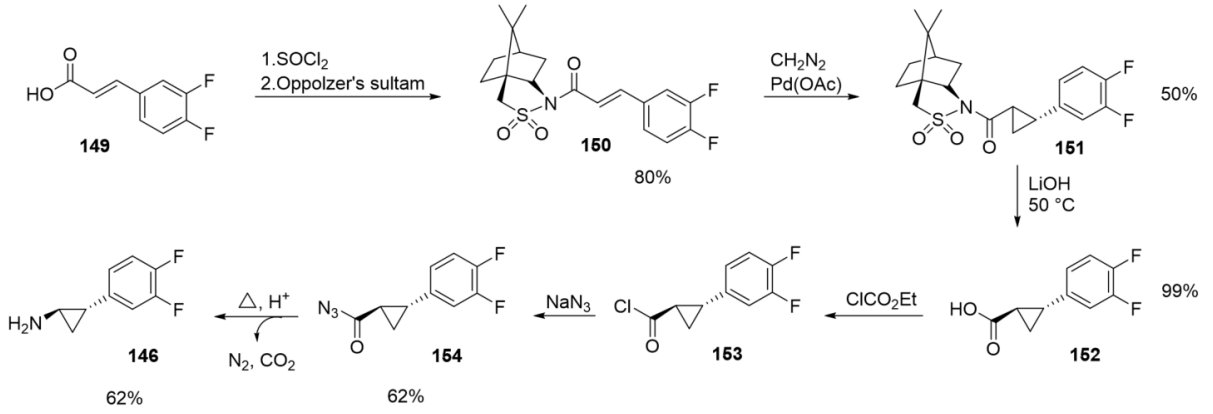

Scheme 5.2 Classical synthesis of the cyclopropylamine precursor **146** conducted by SPRINGTHORPE.[14a]

In the first step, difluoro-functionalized cinnamic acid **149** is derivatized with the **chiral auxiliary** OPPOLZER's sultam, allowing for a subsequent diastereoselective Pd-catalyzed cyclopropanation upon addition of a C_1-unit to yield **151**. Herein, diazomethane is used as carbon source. Saponification and generation of acyl azide **154** lays the ground for CURTIUS rearrangement to the desired CPA **146.**

However, this process is rather unattractive from industrial perspective, as it involves **explosive and hazardous chemicals**, such as diazomethane and NaN_3, making the process less suitable for larger scales. Besides, the employment of a toxic metal catalyst and the requirement for quantitative amounts of a chiral auxiliary reduces the process' appeal.

5.2.2. Biocatalytic routes towards CPA building blocks

Today, various biocatalytic routes towards CPA building blocks have been developed, which minimize laborous reaction steps and reduce the need for hazardous reaction components (Scheme 5.3).[12, 14b, 14c]

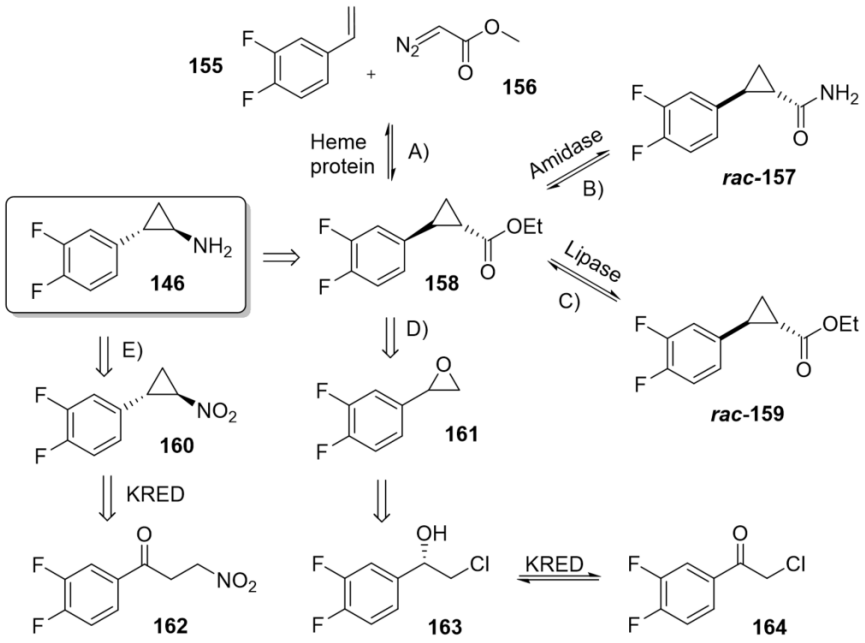

Scheme 5.3 Biocatalytical retrosynthesis pathways towards arylcyclopropylamine **146**.[12, 14b, 14c]

Pathway A relies on a **stereoselective cyclopropanation** reaction starting from commercially available difluorostyrene (**155**) and diazoacetate (**156**) and yields the *(R,R)*-configured ester **158** in a simple one-step process. The reaction is catalyzed by a **heme protein** from *B. subtilis* identified by the group of F. ARNOLD by screening of a larger panel of proteins from the same family. Further engineering by rational design furnished an efficient catalyst that exhibited high activity and excellent enantioselectivity (79% yield, 98% *ee*).[14b]

Route B and C follow the approach of **hydrolase-mediated resolution** of racemic precursors. Herein, the *(S)*-selective amidase from *R. rhodochrous* or the *(S)*-selective lipase from *T. lanuginosus* were employed to convert cyclopropyl amide ***rac*-157** or ester ***rac*-159**, respectively. Anyhow, without the possibility for a kinetic dynamic resolution, the maximum theoretical yield of 50% makes this appraoch less favourable.[12]

Route D and E are based on the **stereoselective reduction** of prochiral ketones to give the corresponding chiral alcohols. Herein, ketoreductases from different origins were employed. For example, an engineered **ketoreductase** from *Rhodococcus kyotonensis* was reported to consume the chloro-functionalized ketone **164** to form the *(S)*-configured alcohol **163**.[181] This intermediate can be transformed to the chiral oxiran **161**, which can undergo enantioselective cyclopropanation using triethylphosphonoacetate in a WADSWORTH–EMMONS type reaction to give the desired *trans*-configured ester **158**.[14c]

All the approaches mentioned so far (A-D) proceed via ester **158** as an intermediate state and, therefore, require transformation to an acyl azide analogous to the route of SPRINGTHORPE or treatment with NH_3, in order to perform a HOFMAN degradation. These pathways are thereby rather laborous and involve hazardous reagents.

In constrast, a KRED-catalyzed pathway starting from the nitro-functionalized ketone **162** represents a remarkably shorter and effective alternative.[12] Here, even both enantiomers of alcohol **165** are applicable for the production of the final amine **146.** Hence, ketoreductases with both, *(R)*- or *(S)*-selectivity, can be employed. However, the *(R)*-enantiomer of chiral alcohol **165** can be directly converted to the cyclic intermediate **160** by treatment with PPh_3 and DEAD in a MITSUNOBU type reaction,[182] whereas the *(S)*-alcohol ***(S)*-165** has to be transformed to the *(R)*-configured bromo-substituted precursor **166** prior to the APPEL cyclization reaction to give **160**. *(R)*-selective KREDs are therefore more preferrable, as they demand one less reaction step. In the final step, the amine product **146** can be obtained from the corresponding nitro compound **160** by simple reduction with e.g. zinc dust (Scheme 5.4).[12]

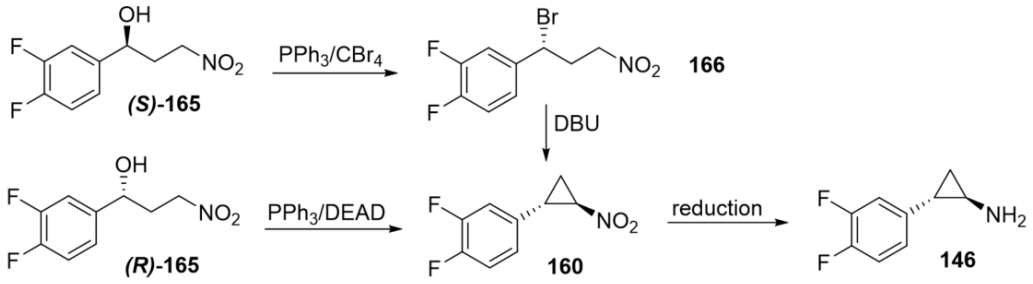

Scheme 5.4 Chemical transformation of *(S)*- and *(R)*-configured alcohols **165** to CPA **146**.[12]

5.3. State of the art: Ketoreductases for the synthesis of chiral alcohols

5.3.1. Introduction: Alcohol dehydrogenases and ketoreductases

Alcohol dehydrogenases (ADHs, EC 1.1.1.1) belong to the superfamily of **NAD(P)(H)-dependent oxidoreductases** and are present in many organisms, where they catalyze the interconversion between primary/secondary alcohols and aldehydes/ketones (Scheme 5.5).[183] In humans and animals, they mostly play a role in metabolizing alcohols that are otherwise toxic to the organism. However, in many bacteria, yeast, and plants, ADHs are responsible for the opposite reaction as part of fermentation processes, hence, are referred to as ketoreductases (KREDs).[29]

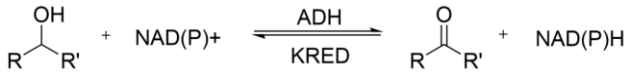

Scheme 5.5 ADH/KRED-catalyzed interconversion between alcohol and aldehyde/ketone. Nicotinamide is consumed as cofactor.

KREDs are attributed to great industrial potential due to their ability to catalyze asymmetric bioreductions of ketones for the production of chiral alcoholic precursors to many pharmaceuticals. Therefore, they are amongst the most commonly employed biocatalysts in industrial pharmaceutical synthesis.[184]

The enzyme's stereoselectivity originates from the substrate orientation in the active site and is mostly specific for prochiral ketones with substituents of fairly different size or, in some cases, different polarity, which will force the substrate to arrange accordingly. Hence, only one

prochiral face (*re* or *si* face) is presented for hydride transfer from NADPH, leading to single enantiomeric products (Scheme 5.6).[185]

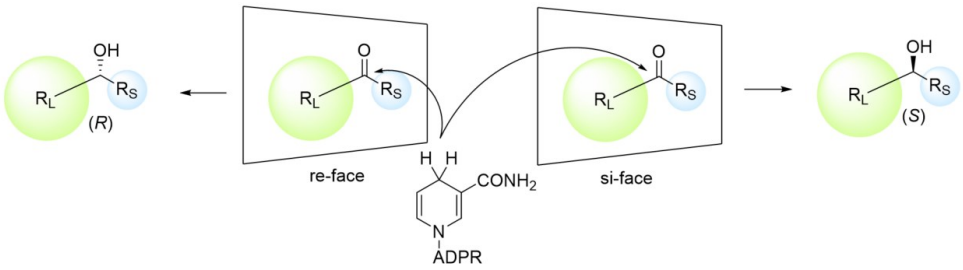

Scheme 5.6 Stereochemistry of hydride transfer from the nicotinamide group to the carbonyl. R_L: larger substituent; R_S: smaller substituent.

The most prominent KREDs/ADHs employed today are the *(S)*-selective catalysts from *Saccharomyces cerevisiae* (brewer's yeast, 1937)[186] and from horse liver (HLADH). The latter is often used as a model enzyme, as it was the first to be analyzed by X-ray crystallography.[183] Table 5.1 shows a set of chiral, pharmaceutically relevant compounds that are nowadays produced via KRED-catalysis on industrial scale.

Table 5.1 Chiral alcohols as pharmaceutical building blocks produced by KRED-catalysis on industrial scale.

Compound	Application	Microbial strain	*ee*	Yield	Ref.
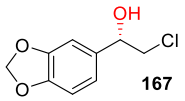 **167**	Endothelin receptor antagonist	*Rhodotorula piliminae*	99%	97%	[187]
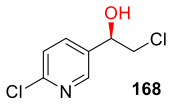 **168**	*β*-3-Adrenergic receptor agonist	Recombinant KRED of unknown source	99%	81%	[188]
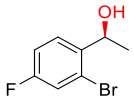 **169**	Anti-ALZHEIMER's drug	*Candida, Hansenula, Pichia, Rhodotorula, Saccharomyces, Sphingomonas*, Baker's yeast	99%	>90%	[189]
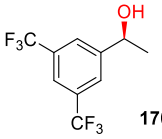 **170**	NK1 receptor antagonists	*Rhodococcus erythropolis*	99%	98%	[190]
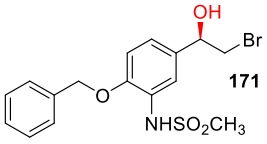 **171**	*β*-3-Adrenergic receptor agonist	*Sphingomonas. paucimobilis*	99%	80%	[191]

5.3.2. A ketoreductase for the synthesis of ticagrelor

The application of KREDs for the production of cyclopropylamine alcohol building block **165** has been followed only recently and is therefore not fully established yet.[12, 192] However, the research summarized in Table 5.2 reflects the great potential these enzymes comprise:

Table 5.2 Ketoreductases from different origins, screened for activity towards ticagrelor precursor **162**. The most promising candidates are *(S)*-selective and are highlighted in green.[12, 192]

Group (year)	Microbial strain	*ee*		Conv.
BANDICHHOR (2015)[192]	*Bacillus licheniformis*	-		0%
	Saccharomyces cerevisae	*(R)*	100%	6%
	Rhodococcus sp.	-		0%
	Pichia methanolica	*(R)*	73%	73%
	Rhodotorula sp.	-		-
	Candida tropicalis	*(S)*	82%	98%
	Candida rogusa	***(S)***	**91%**	**96%**
	Candida glabrata	*(R)*	68%	22%
	Candida boidinii	*(R)*	100%	5%
	Candida sonorensis	*(R)*	100%	7%
	Candida magnoliae	*(S)*	60%	5%
	Candida apis	*(R)*	62%	8%
	Candida maltosa	-	50%	10%
	Candida parapsilosis	***(S)***	**94%**	**98%**
	Candida etchellsii	***(R)***	**93%**	**76%**
	Candida utilis	*(R)*	*60%*	50%
	Candida pichia	*(R)*	73%	73%
TURNER (2016)[12]	*Ralstonia sp.*	*(S)*	92%	34%
	Codexis panel	***(S)***	**100%**	**100%**
	Codexis panel	*(R)*	73%	23%

In 2015, BANDICHHOR *et al.* screened through seven microbial strains from bacteria and fungi towards stereoselective reduction of ketone **162.** Amongst these, the *Candida* species showed the most promising results, as they exhibited superior activity (>96%) and selectivity (82% *ee*) in comparison to the other tested strains. Thus, by assessing eleven additional types from the *Candida* species, the *(S)*-selective KREDs from *C. parapsilosis* (*Cp*KRED) and *C. rugose* (*Cr*KRED) and an *(R)*-selective candidate from *C. etchellsii* were identified. The *(S)*-selective enzymes showed conversions between 96-98% and enantioselectivities of 94% and 91%, respectively. The *(R)*-selective KRED showed a very high *ee* of 93% but only a moderate conversion of 76%.[192]

In 2016, the group of N. TURNER tested a set of ketoreductases from a commercial panel provided by *Codexis* and the KRED from *Ralstonia sp.* (*Ras*KRED). *Ras*KRED showed decent *(S)*-enantioselectivity but unfortunately lacked adequate activity. From the commercial panel, a highly promising was an *(S)*-selective ketoreductase with quantitative conversion and an excellent enantiomeric excess of 100%. However, its applications required rather high catalyst loads (5 g/L).[12]

It is noticeable that most of the *(R)*-selective KREDs described here lack enantioselectivity and/or activity and are therefore of no use for industrial application. This finding is no surprise, as, by trend, most ketoreductases preferably produce *(S)*-enantiomers.[151, 193]

However, *(R)*-specific KREDs have been prevalently found in the strains of the *Lactobacillus* species, from which a very remarkable and promising candidate originates from *Lactobacillus brevis*.[151] As this enzyme will play a major role in this work, it will be portrayed in greater detail within the next chapter.

5.3.3. Ketoreductase from *Lactobacillus brevis*

The *(R)*-selective ketoreductase from *Lactobacillus brevis* (*Lb*KRED) was first identified by HUMMEL in 1997 and belongs to the superfamily of short-chain dehydrogenases/reductases (SDR) (EC 1.1.1.2).[151] It features a homotetrameric structure with subunits made of 251 amino acids or 26.6 kDa, each assembled in a ROSSMANN fold.[194] It catalyzes the enantioselective reduction of prochiral ketones to obtain the corresponding secondary alcohols in the presence of NADPH and Mg^{2+}. As shown by the group of SCHOMBURG, removal of Mg^{2+} by treatment with EDTA lead to a complete loss of functionality, although it has been shown that the magnesium ions have no interaction with the catalytic center. It is therefore assumed that their main purpose is to stabilize the protein fold as structural metal ions.[194-195]

Regarding the catalytic mechanism, the cycle starts with the formation of a complex between the enzyme and the NADPH cofactor, which then interacts with the carbonyl substrate upon hydride transfer from the nicotine amide to the ketone group, generating a carbanion intermediate. Crystallization studies revealed that the active site of *Lb*KRED consists of four amino acid residues, which form the catalytic machinery and lie in direct proximity to the substrate's carbonyl group and the nicotinamide moiety: N113, S142, Y155, and K159 (Figure 5.1 A)[185b, 196]

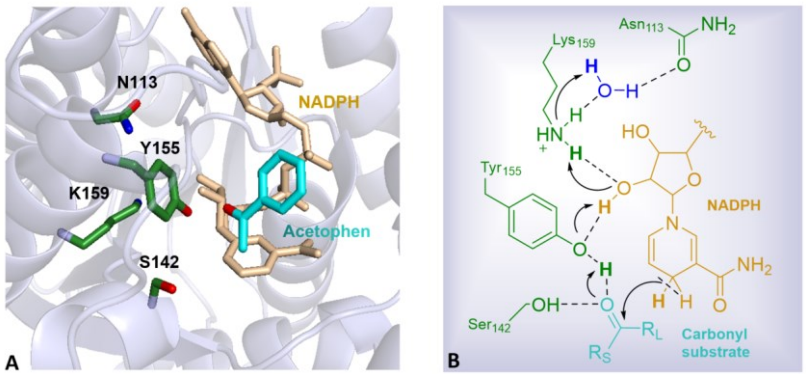

Figure 5.1 A) PyMOL generated visualization of *Lb*KRED active site. The acetophenone (cyan) carbonyl functionality (red) is in direct proximity to the catalytic residues N133, Y155, K159, and S142, visualized in green. The nicotinamide cofactor is depicted in light brown. B) Catalytic mechanism of *Lb*KRED-catalyzed reduction of carbonyl substrate (cyan) upon hydride transfer from NADPH (light brown). The protons acting within the proton relay system are highlighted in bold.[185b, 196]

While S142 is responsible for stabilizing the substrate by interaction with the carbanion group, Y155 is directly involved in the catalytic process by acting as a catalytic acid and proton donor, producing the final chiral alcohol. Herein, K159 lowers the pK_a value of the Tyr-OH group and, together with the N113, also functions as a part of an "extended proton relay system", which also comprises the OH-group of the nicotinamide ribose and a water molecule positioned at the N113. Restoring the original active site requires reprotonation of Y155 by the water molecule (Figure 5.1 B).[185b, 196]

While the physiological role and the *in vivo* substrate(s) of *Lb*KRED are still unknown,[195a] scientists have found that, *in vitro,* the wildtype enzyme can host alcohols and ketones with short side chains (R_S), limited to methyl, ethyl, small methyl and ethyl esters, and small halogenated methyl groups as one substituent, while in contrast, even bulky (often aromatic), highly variable moieties are tolerated as the other substituent (R_L) (Figure 5.2).[195b, 197]

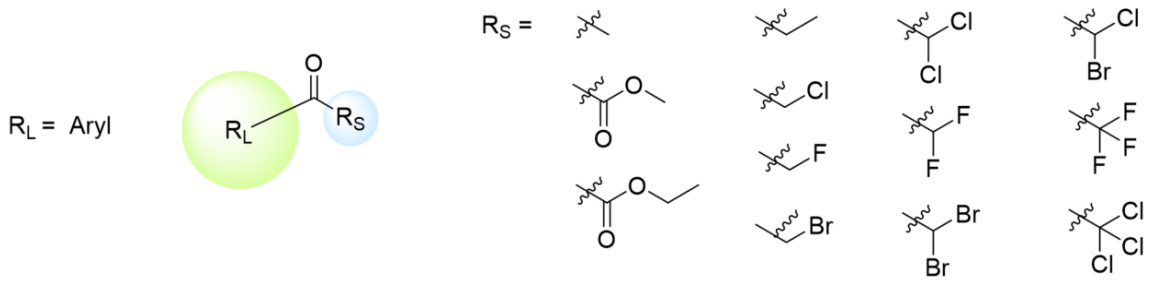

Figure 5.2 *Lb*KRED prochiral ketone substrates with large (R_L, highlighted in green) and small substituents (R_S, highlighted in blue).[195b, 197]

Analogous to other KREDs, these limitations are due to the distribution of the enzyme's active site, consisting of two hydrophobic pockets - a rather small, flexible chamber, and adjacently, an open, very spacious domain, forcing the substrate to arrange accordingly. 3D-Visualization by pyMOL shows the space distribution within the enzyme pocket (Figure 5.3) and explains why utilization of arylketones that show distinct size difference between the two substituents generally yields products with excellent optical purity (>99% *ee* for acetophenone).[198] Herein, *Lb*KRED is highlighted by its remarkable capability of preferably generating *(R)*-configured products,[151] while ketoreductases from most organisms occur to follow PRELOG's rule of producing the *(S)*-enantiomer, predominantly.[151, 193]

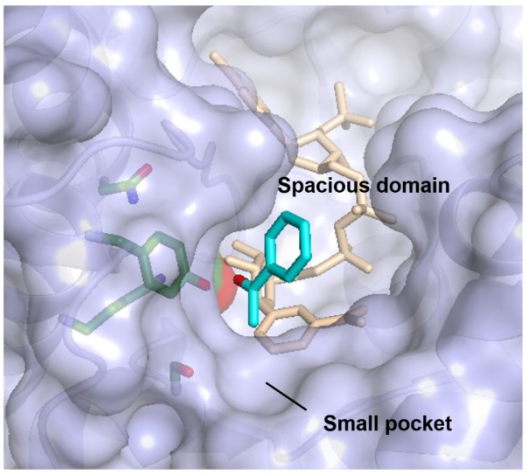

Figure 5.3 PyMOL generated visualization of *Lb*KRED active site. Acetophenone is shown as model substrate (cyan) and NADPH as cofactor (light brown). The methyl substituent on one side of the carbonyl group fits into the space inside the enzyme pocket. The larger aryl group is arranged at the entrance.

Atomic resolution (1.0 Å) of the *Lb*KRED structure[196a] as well as recent availability of technologies for protein engineering (see chapter 5.485) opened vast possibilities for structure-guided catalyst design, e.g. towards higher activity and/or substrate tolerance. As an example, scientists have engineered an *Lb*KRED variant

towards preference for NAD(H) instead of NADP(H) as cofactor, as the phosphor-substituted is more expensive and less stable. As a result, the mutant obtained (R38P) exhibited a four-fold increased activity with NAD(H)[194] and was successfully implemented for the oxidative kinetic resolution of phenylethanol upon cofactor regeneration by an NADH oxidase.[199] However, the catalyst's activity was still higher when utilizing NADP(H) as cofactor.[194]
Mirrored by the rising number of patents and publications referring to *Lb*KRED,[195b] this enzyme is a quite potential and versatile catalyst for the production of valuable intermediates in asymmetric organic synthesis and pharmaceutical chemistry. Apart from many applications of *Lb*KRED, e.g. for the reduction of a variety of keto-esters and acetophenone derivatives, this catalyst is, for example, industrially applied for the large scale production of ethyl-3*R*-hydroxy-butanoate (one ton per year).[195b]

5.4. Protein engineering

In the past decades, the employment of enzymes as green and sustainable catalysts for industrial processes has been dramatically fueled by the ability of scientists to create customized proteins with higher/novel catalytic activity, increased stability, broadened or altered substrate specificity, or improved or reversed stereoselectivity.[200] This modulation of structure to obtain a desired function is referred to as **protein engineering**. Better knowledge about the relation between protein structure and function as well as advances in methods for high-throughput screening have greatly expanded the possibilities within this field. Although it is still a young discipline, it comprises a large number of experimental techniques, which are applied within two general strategies - **directed evolution** and **rational design:**[201]

- Directed evolution is an iterative method that mimics the strategies of traditional evolution by introducing random mutations into the genetic material coding for a given enzyme and selecting improved candidates by (high-throughput) screening towards the desired phenotype. The hits can be used as parents for the next generation library in a repetitive manner until the goal is achieved or when no further improvements can be observed.[202]
  Directed evolution is, thereby, achieved by either introducing random mutations into single protein sequences (e.g. **error-prone PCR**) or by randomly recombining a set of related sequences (e.g. **gene shuffling**). Advantageously, structural information of the enzyme is not required in both cases and amino acid alterations can occur in any part of the sequence. This leads to potentially beneficial, unexpected variations that can also be distant from the active site. As a matter of course, this method relies on a high number of variants that have to be processed, which is both time and labor consuming, as a suitable high-throughput assay method has to be found, optimized and conducted.

- Rational design dates back only to the mid-1970s and relies on the distinct understanding of protein sequence and structure and the ability to predict resulting functions, which allows for proposing and generating the sequence needed. This can be either achieved by performing specific amino acid variations by site-saturation mutagenesis of existing native enzymes while maintaining most of the residues of the structure (**redesign**)[203] or, like in the newer approach of ***de novo* design**, the entire sequence is constructed from scratch without using any prior scaffolds.[204] In conclusion, rational design is strongly dependent on computer aided calculations and simulations. A big advantage is the resulting increased

probability for beneficial mutations as well as a significant reduction in library size. Therefore, this method is especially important in case a suitable high-throughput assay is not available.

Although the two strategies are often presented as competing methods, they are not always applied exclusively. Indeed, scientists will often utilize both, as a combination of these methods (**semi-rational design**) has often proven to be especially effective. Herein, the tools of rational design, such as structural and site-directed mutagenesis data or computational pre-screening results, can identify "hot spots" in the enzyme sequence. These regions can then be precisely aimed at during library construction by directed evolution. Thus, the mutant libraries have a smaller size but often accumulate a higher amount of unforeseeable hits. The three different methods are schematically outlined in Figure 5.4.[205]

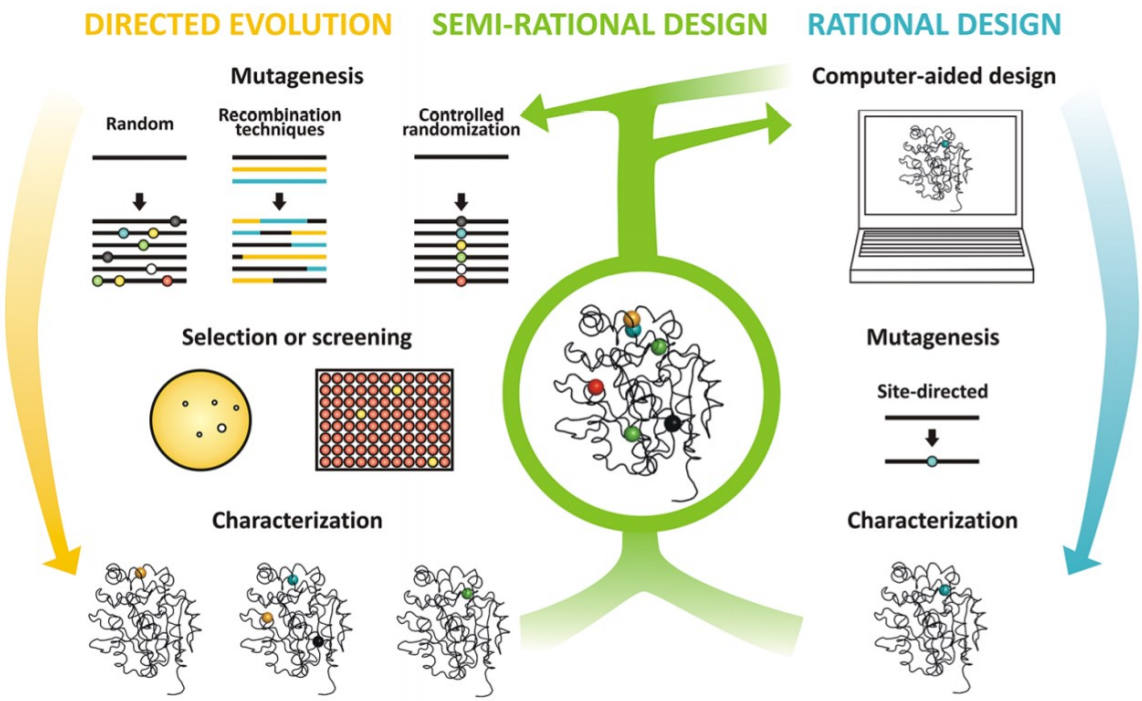

Figure 5.4 Schematic visualization of protein engineering strategies: Directed evolution, semi-rational design, and rational design.[205]

6. Objective

6.1. Main objective

As shown in chapter 5.3.2, many ketoreductases have been investigated and assessed for the production of the alcoholic ticagrelor precursor ***(R)*-165** through stereoselective reduction of the corresponding ketone **162.** Anyhow, a perfectly suitable candidate that meets the demands of pharmaceutical industry, e.g. excellent stereoselectivity, high activity, low catalyst load, and applicable cofactor recycling, has not been reported so far. Especially enzymes that specifically produce the *(R)*-enantiomer by acting in an anti-PRELOG manner while exhibiting high activity are completely absent.
Therefore, this part of the thesis is mainly dedicated to the engineering and employment of a suitable ketoreductase for the synthesis of chiral alcohol ***(R)*-165** (Scheme 6.1). As we aim for industrial feasibility of the process, attention will also be focused on factors like practicability, cost efficiency, reasonable cofactor recycling, and scalability.

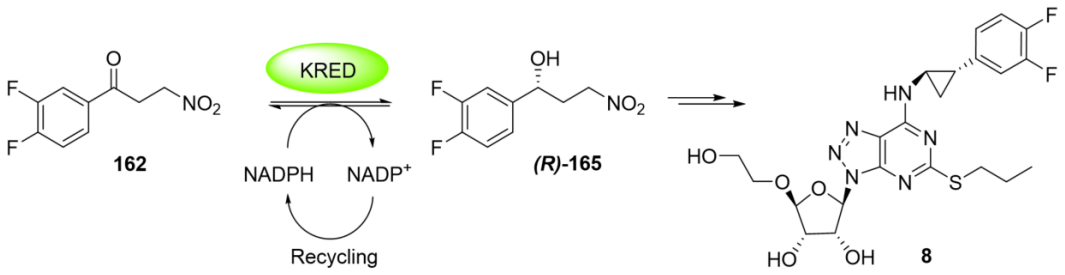

Scheme 6.1 KRED-catalysis towards chiral alcohol ***(R)*-165**. This valuable intermediate is used as a building block for ticagrelor (**8**).

6.2. Specific objectives

6.2.1. Protein engineering

As discussed in chapter 5.3.3, the KRED from *Lactobacillus brevis* inherits many beneficial characteristics, like *(R)*-enantioselectivity, broad substrate tolerance, and stability - plus it is already well-reviewed in the literature. These factors make this enzyme a very suitable scaffold for a redesign towards pharmaceutical application. For the protein engineering process, a combined approach of directed evolution and rational design is aimed for, in order to minimize time and effort while still furnishing applicable results.

6.2.2. Development of a high-throughput screening method

One of the main tasks lies in the development of a suitable high-throughput assay for a rapid screening of the constructed protein libraries. In the best case, an assay principle should rely on easily and directly detectable product formation and offer high sensitivity as in colorimetric assays, where colorful, UV- or fluorescent-active compounds are produced.
Since the pharmaceutical target substrate does not exhibit easily measurable change upon conversion and measuring of NADPH-consumption typically shows insufficient specificity due to its poor stability, an alternative method is required. In this context, molecules that resemble the actual substrate but are able to exhibit a color response upon conversion can act as

alternative targets in preliminary screenings. As reported by T. SCHEIDT, methoxy-functionalized naphthyl ketones feature strong, highly detectable fluorescent properties whereas the corresponding amines are inactive.[206] Hence, it is assumed that the corresponding alcohols will act likewise and may serve as fluorogenic proxy substrates. Therefore, it is aimed to utilize a set of methoxy naphthyl carbinols with alkyl substituted side chains of increasing bulkiness that mimic the target substrate during the initial screening processes. It is speculated that mutating and shaping the enzyme's active site in an iterative, controlled manner will finally furnish a candidate that also accepts the sterically similar nitro-functionalized substrate **162.**

6.2.3. Substrate synthesis

In order to obtain the different substrates with varying substituents, a simple and fast method was required for easy access. Therefore, a modular approach reported by SCHEIDT[206] is considered for substrate synthesis.
For the chemical synthesis of the pharmaceutical substrate standard procedures will be followed.

6.2.4. Overview

A schematic visualization of the project is shown in Figure 6.1. The four different tasks are highlighted in four different colors: Protein engineering, assay development and performance, substrate synthesis, and potential pharmaceutical application.

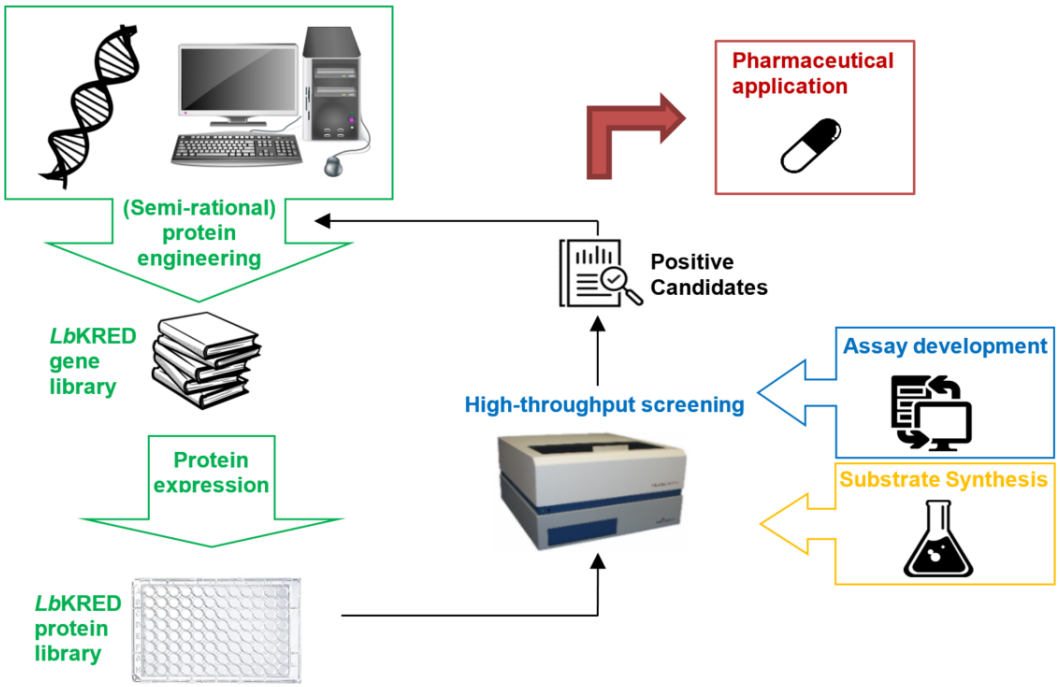

Figure 6.1 Project work flow. Four different tasks are crucial: Protein engineering, assay development & performance, substrate synthesis, and pharmaceutical application.

7. Results and discussion

7.1. Fluorescent assay development and substrate design

7.1.1. Fluorescent assay principle

Very often, the bottleneck of directed evolution is the lack of reliable assay methods for the survey of large protein libraries. In order to reduce time and effort, many methods for "high-throughput screenings" have evolved, in which the strategy applied can either rely on the detection of substrate or cofactor consumption. In discontinuous assays, reaction samples are taken in intervals and measured by, e.g. mass spectrometry (MS), nuclear magnetic resonance (NMR), high-performance liquid chromatography (HPLC), gas chromatography (GC), or radiology, while in continuous assays, the reaction progress is directly measured from the ongoing reaction, which offers higher convenience and is therefore applied more frequently. Herein, many approaches are based on the biochemical readouts of optical changes, such as shifts in UV/VIS-absorption, fluorescence, or chemiluminescence. However, these optical responses are often insignificant in the initial substrates and don't allow for sensitive measurements. To meet this issue, chemical modification of the substrate molecule by coupling with stronger chromogenic or fluorogenic labels that are released during the reaction allows for improved signal induction.[207]

Many KRED-assays reported in literature measure enzyme activity in reduction direction by monitoring the associated depletion of the NADPH cofactor at 340 nm. This method is very easily applicable but often lacks sufficient sensitivity (LOD = 1.7 nmol) while suffering from high interference due to the short UV wavelength of NADH and NADPH.[208] Alternatively, indirect, colorimetric approaches utilize coupled cofactor recycling systems with color active compounds, *e. g.* INT assay. This allows for signal amplification while the cofactor is continuously regenerated and therefore represent a more sensitive method.[153]

In this work, a highly sensitive, continuous, direct assay method was developed for the screening of large KRED libraries. Here, strongly fluorogenic methoxynaphthyl carbinols were utilized as substrates, which were designed to form delocalized π-electron systems upon conversion to the corresponding ketone. This change in the electronic properties induces a bright blue fluorescence emission at around 460 nm. Release of the fluorescence signal therefore directly correlates with enzyme activity and offers a notably high sensitivity at low substrate concentration. The assay principle and an exemplary 96-well assay test plate are depicted in Scheme 7.1.[13]

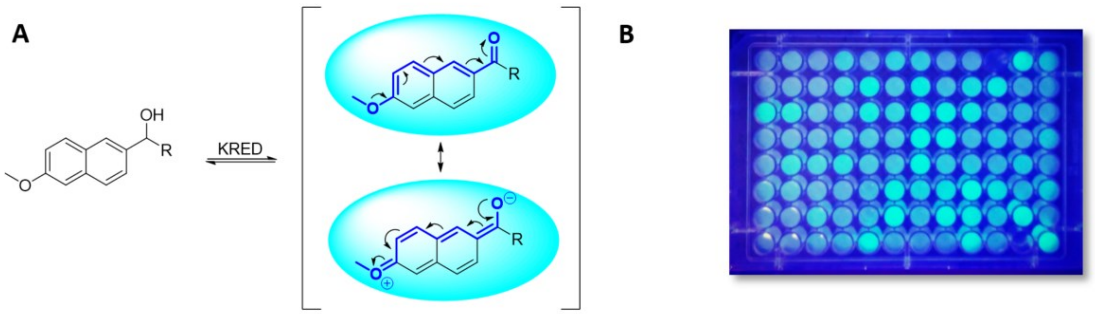

Scheme 7.1 A) Fluorogenic assay principle. B) Assay test plate upon UV-irradiation at λ = 362 nm.[13]

7.1.2. Substrate design and synthesis

Systematic structural variations of the fluorogenic substrates by altering the alkyl substituent (R-group) towards increased bulkiness allowed for a stepwise, methodical screening of the KRED libraries. Therefore, a simple synthesis strategy towards the applied substrate set was required. To address this need, a direct, modular approach of GRIGNARD addition of variable alkyl side chains to the commercially available naphthyl aldehyde **172** was employed. The reactions directly furnished the desired secondary alcohols **174a-g** (Scheme 7.2).

Following standard protocols for simple GRIGNARD reactions, products **174b-g** were obtained with good yields between 75-85% and very high purity after recrystallization.

The methyl substituted carbinol **174a** was achieved by borohydride reduction of the commercial ketone **173a.** An excellent yield of 96% was obtained by applying $CeCl_3$ as a LEWIS acid, which increased the electrophilicity of the carbonyl group by coordination to the oxygen.

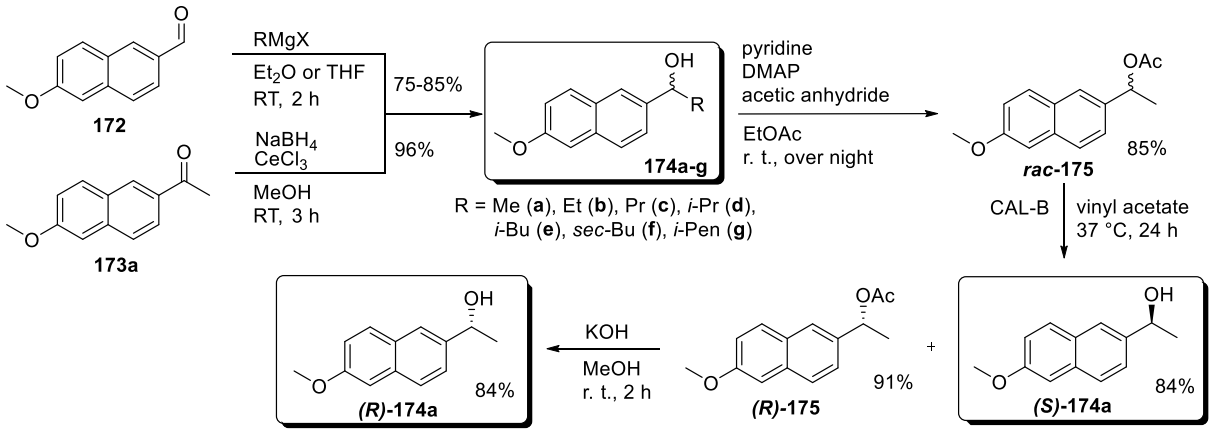

Scheme 7.2 Synthesis of fluorogenic methoxy naphthyl substrates. Carbinols **174b-g** with varies alkyl side chains were obtained by modular GRIGNARD addition. Methyl carbinol **174a** was synthesized from the corresponding ketone **173a** by borohydride reduction. The individual enantiomers were obtained by lipase resolution.

The individual *(R)*- and *(S)*-enantiomers of alcohol **174a** were generated by lipase resolution. Herein, lipase B from yeast *Candida antarctica* (CALB) represents a well-established enzyme that effectively catalyzes the stereoselective hydrolysis of carboxylic ester bonds.[133b] After chemical acetylation of the alcohol group by treatment with acetic anhydride, incubation with CALB at 37 °C for 24 h gave the *(S)*-carbinol ***(S)*-174** in high optical purity (100% *ee*). The reaction was monitored by chiral HPLC measurements. Separation from the remaining *(R)*-configured ester ***(R)*-175** was achieved by column chromatography. The ester was then chemically hydrolyzed to yield the *(R)*-alcohol ***(R)*-174.**

The ketones required as reference material for enzyme kinetic measurements were obtained by oxidation of the corresponding alcohols by utilizing pyridinium chlorochromate (PCC, COREY-SUGGS reagent[139]) as oxidizing agent. This represented an easy, fast and effective way and furnished yields around 95%.

All synthesized substrates were analyzed and verified by NMR analysis.

7.1.3. Assay development and application

Prior to assay performance, the optimal reaction conditions were determined. This included aspects like substrate concentration, cosolvent, pH-value, and cofactor recycling. Additionally,

detection parameters, e.g. optimal excitation and emission wavelength, signal linearity and limits of detection (LOD), were assessed:

- **Substrate concentration**
  The substrates applied in this assay bear the minor drawback of being very little soluble in plain water, as the hydrophobic character of the naphthyl moiety outweighs the polar property of the hydroxy functionality. The reaction mixtures were therefore prepared from concentrated DMSO stock solutions, giving final assay concentrations of 0.25 mM substrate in 10% DMSO as cosolvent. Working at this low concentration avoided potential internal quenching or inhibition effects and proved to be adequate for product quantification and comparison/evaluation of different catalysts.

- **pH-value**
  As discussed in chapter 5.3.3, the KRED-controlled interconversion between ketone and alcohol substrates is mechanistically mediated by the enzyme's lysine-tyrosine pair, which act as general base and acid, respectively. Hence, it was speculated that adjusting the pH to a slightly alkaline value of 7.5 can assist to shift reaction equilibrium towards ketone formation.

- **Cofactor-recycling**
  To guarantee full substrate conversion, it was mandatory to either apply the nicotinamide cofactor in stoichiometric quantities or provide *in situ* recycling.
  In biocatalysis, regeneration of $NAD(P)^+$ is often realized by embedding a "*coupled enzyme approach*" in which a second independent set of enzyme and substrate is employed. In this context, the most widely applied method involves glutamate dehydrogenases (GluDH), which catalyze the reductive amination of α-ketoglutarate (**139**) to give L-glutamate (**138**).[209] However, this approach requires high concentration of ammonia, which strongly enhances the pH and is not tolerated by all enzymes. An alternative is given by utilizing pyruvate (**72**) and a lactate dehydrogenase (LDH), which is less expensive and offers a higher specific activity but only accepts the non-phosphorylated NADH as cofactor.[210] The application of a nicotinamide oxidase (NOX)[211], which uses molecular oxygen to produce either water or H_2O_2 (see chapter 2.2.4), has been recently introduced but requires adequate equipment to guarantee sufficient circulation of oxygen in the reaction mixture. Scheme 7.3 summarizes the strategies mentioned.

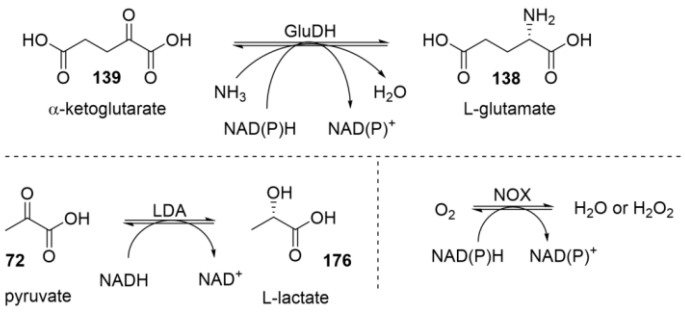

Scheme 7.3 Enzymatic regeneration of oxidized nicotinamide cofactors.

On the other hand, the so-called "*coupled substrate approach*" offers much more simplicity, as only one enzyme is utilized for both, product formation and cofactor recycling, by

converting a second, often simple, sacrificial substrate like acetone/*iso*-propanol in the opposite direction. The additional substrate is applied in large excess in order to shift the equilibrium into the desired direction. Therefore, higher amounts have to be tolerated by the enzyme.

In this work, the more appealing substrate coupled option was applied with acetone/*iso*-propanol as cosubstrate, as many KREDs are typically known to accept simple alcohols and ketones (Scheme 7.4).

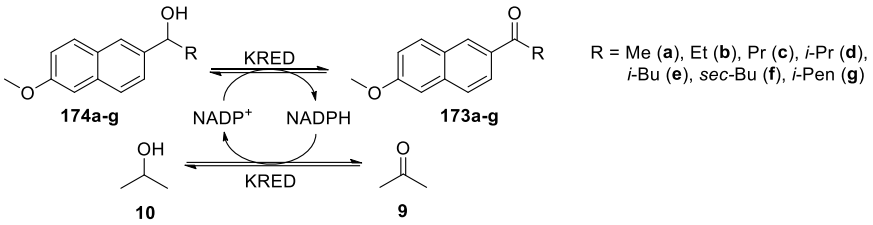

Scheme 7.4 NAD(P)+ regeneration upon conversion of acetone (**9**) to *iso*-propanol (**10**).

This system demonstrated many beneficial aspects: First, acetone/*iso*-propanol can assist as cosolvents to solubilize the hydrophobic substrates and are most likely accepted without activity decline at concentrations of up to 10%. Unlike DMSO, both can be easily removed from the reaction mixture by simple evaporation. Generation of *iso*-propanol does not induce pH changes, which is otherwise often the case when utilizing enzyme coupled approaches. Not to mention is of course the low cost and easy availability of acetone. Application of 10% acetone provided sufficient $NADP^+$ regeneration without the need for additional cofactor other than what was already present in the cell-free extracts.

- **Detection parameters**
  The maximal excitation and emission wavelength for ketone **173a** have been reported in the literature with a value of λ_{max} = 312 nm and λ_{max} = 441 nm, respectively.[212] However, due to the instrumental equipment that lacked the possibility to utilize the full spectrum of wavelengths, the measurements were performed using 330 nm excitation and 460 nm emission filters. Herein, a linear increase in fluorescence was observed with rising ketone concentration. Varying the amount of protein also confirmed a linear relation between signal intensity and enzyme activity, allowing for a continuous quantification of protein activity by correlating with a standard curve. The values for the limit of detection (LOD = 0.35 nmol/min) and the limit of quantification (LOQ =1.2 nmol/min) were determined by linear regression and confirmed a good assay performance.

In a proof of concept, the assay method was tested on a commercial KRED panel (*Prozomix Ltd*) containing environmental protein samples collected in the UK. The library was assorted based on a metagenomic approach and comprised catalysts that were classified as short chain dehydrogenases/reductases (SDR). This group of enzymes is especially known for having a wide substrate spectrum.[213]

For activity typing, substrate **174a** was applied as a racemic mixture. Utilizing the individual antipodes ***(S)*-174** and ***(R)*-174** under the same assay conditions also allowed for stereoselectivity typing.

The screening of the KRED collection was performed in 96 microtiter plate format utilizing a continuous fluorescence plate reader for reaction monitoring over a period of three hours. The

detection of fluorescence signals revealed a high fraction of biocatalysts to be active towards racemate **173a.** The most active candidates were found to catalyze the reaction with 90% total substrate conversion. More than half of the enzymes (53/96) reached at least 10% conversion relative to the best candidate and more than one quarter (27/96) yielded at least 50% relative conversion. In the negative controls with either absence of biocatalyst or substrate no signal change was detected, which excluded chemically catalyzed reactions or background fluorescence effects.

According to our expectations, enantioselectivity typing revealed almost all active enzymes to follow PRELOG's rule of being *(S)*-selective (42/96), while only two exhibited preferences for the *(R)*-enantiomer. Nine of the catalysts were found to accept both enantiomers.

The same enzyme panel was also screened against the homologous, sterically larger propyl carbinol substrate **174c.** In this case, the alcohol was converted by only around 20% of the enzymes (20/96), giving evidence that many candidates from the SDR family exhibit interesting substrate promiscuity distributed throughout the panel with no clear pattern.

Figure 7.1 shows the results of the stereoselectivity typing against methyl-carbinol **174a** and activity screening against the larger carbinol **174c.**

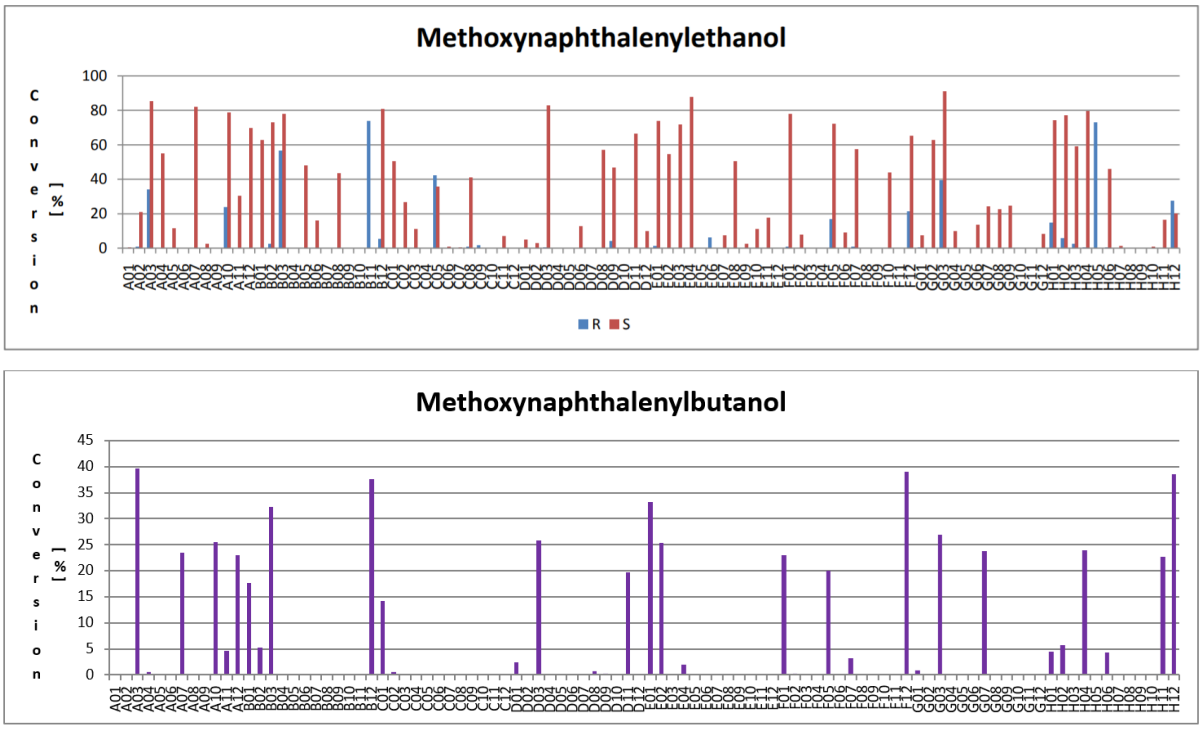

Figure 7.1 Screening results. A) Exemplary selectivity screening of a highly diverse metagenomic short-chain dehydrogenase/reductase (SDR) array in 96-well plate format (*Prozomix Ltd*) by using individual enantiomers ***(S)*-174a** and ***(R)*-174a**. Maximum substrate conversion after 1.5 h was 90% as determined by comparison against a fluorescence standard curve measured with ketone **173a** under identical assay conditions. B) Activity screening of the same plate against the bulkier substrate ***rac*-174c**.

In conclusion, the test screenings confirmed the assay format to be highly applicable for the assessment of activity as well as enantioselectivity of (unknown) enzymes. Determination of enzyme kinetics could also be conducted with the same assay format. In our case, each of the measured enzymes, which included one *(R)*-selective, one *(S)*-selective, and one non-selective one showed MICHAELIS-MENTEN-type kinetics with high substrate affinity towards the methyl-substrate **174a.**

7.2. *Lb*KRED library creation and screening

7.2.1. Library design

The native KRED of *Lactobacillus brevis* (*Lb*KRED$_{WT}$) is known to catalyze the reduction of the non-natural substrate acetophenone and many of its derivatives in a highly stereoselective manner (99% *ee*).[151] In this matter, *Lb*KRED$_{WT}$ is quite unique, as none of the other presently known commercially available KREDs accept this rather bulky substrate.[195a] Hence, acetophenone is often used as an interesting model substrate for *in vitro* studies.[195a, 196a, 198] Derivatives bearing nitro groups were so far not or only poorly accepted,[198] which makes the wildtype enzyme an interesting scaffold for a redesign towards tolerance for the pharmaceutically relevant nitro-functionalized acetophenone derivative **162.**

As discussed earlier, an approach of semi-rational design was chosen for the engineering process, offering a good compromise between library size/ screening capacity and maximized number of (unforeseeable) hits. Therefore, the first generation library was generated by site-saturation mutagenesis of residues rationally chosen based on their position in the crystal structure. Herein, it was speculated that randomizing those amino acids that are directly located at the substrate binding site will have the largest impact. However, in order to maintain the enzyme's catalytic activity, it was reasoned to only allow changes made to non-catalytic residues. 3D-modeling by pyMOL with acetophenone as standard substrate revealed six active site amino acids that met these criteria: I143, E144, L152, D149, Y189, and Y248. Figure 7.2 shows their positions at the substrate binding site, exhibiting distances between 3.7 – 7.9 Å to the acetophenone methyl side chain.

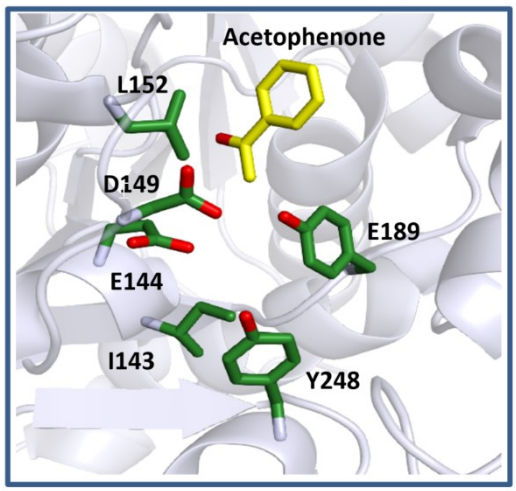

Figure 7.2 PyMOL 3D-model of *Lb*KRED active-site. Acetophenone is bound as model substrate (yellow). The six non-catalytic residues I143, E144, D149, L152, Y189, and Y248 that were selected for randomization are shown in green.

7.2.2. Mutagenesis

Individual randomization of the amino acids was achieved via polymerase chain reaction (PCR) using the *QuikChange II*® site saturation mutagenesis kit and protocol by *Agilent*. Herein, oligonucleotides that featured degenerated codons coding for all 20 proteinogenic amino acids were employed (NNK: N → G/C/T/A; K → T/G) and a pET-28a(+) vector featuring the native *Lb*KRED gene was used as DNA template. The oligonucleotide sequences are listed in the experimental part (chapter 9.4.2).

The success of the PCRs was verified by agarose gel electrophoresis. Figure 7.3 depicts the corresponding gel showing defined bands at the expected size of 6233 bp for all products.

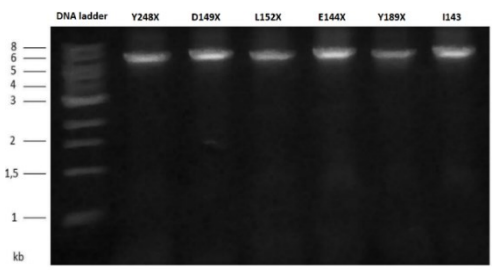

Figure 7.3 Agarose gel of PCR products after site-saturation mutagenesis. Visualization of the bands at 6233 bp under UV-light.

For sequence analysis, the plasmids were isolated from transformed commercial *E. coli* DH5α competent cells (NEB). This bacterial strain was chosen for plasmid amplification, because it is known for high transformation efficiency. Herein, transformation was conducted via heat shock and directly utilizing the linear PCR products, since *E. coli* is capable of *in vivo* ligation. This saved an additional manual step of generating circular DNA by phosphorylation. The DNA sequencing results provided by *GATC Biotech AG* verified the occurrence of all desired mutations necessary for all of the six targeted amino acid positions.

7.2.3. Protein expression

In order to create protein libraries from the mutant libraries, cells from the *E. coli* strain BL21 (DE3) were transformed with the isolated plasmids from the previous DH5α cultures. The BL21 strain was especially designed for high expression efficiency and was therefore chosen as host. Transformation was conducted using self-produced electro competent cells via electroporation. Subsequent cultivation on LB-agar plates furnished a sufficient amount of single colonies for each randomized position. To obtain the mutant sub-libraries, 95 single colonies were randomly picked from each of the six plates and cultivated in six round-bottom 96-well plates. Selecting this number of clones statistically covered all possible amino acid mutations with a probability of 95%. The last well on each plate was reserved for cells containing the wildtype gene as reference.
Protein expression was achieved by cell cultivation in an auto-induction medium (AIM). The composition contains a balanced amount of glucose for bacterial growth and lactose for protein expression. Herein, lactose can also be metabolized as carbon source, albeit with lesser preference than glucose, but mainly functions as an inducer for the expression of the T7 RNA polymerase, which generates the messenger-RNA needed for gene/protein expression.[214] Hence, this culture system brought the advantage of self-regulated bacterial multiplication and protein expression, avoiding the need for a manual inducement step after inoculation of the culture. Successful expression of sufficient amounts of protein was verified by SDS gel electrophoresis.

7.2.4. Screening of 1st generation protein library via fluorogenic assay

As the previous screenings applied on the commercial KRED panel from *Prozomix Ltd* was conducted using CFEs (chapter 7.1.3), it was first decided to also utilize CFEs for the mutant libraries. Therefore, a suitable method for cell lysis was required. Herein, the primary attempt comprised the standardized application of lysozyme (also muramidase or N-acetylmuramide glycanhydrolase), which is known to hydrolyze linkages in the bacterial cell wall and thereby force cell disruption. The approach was preliminary tested on cells containing wildtype enzyme only. For this purpose, the cultivated cells were treated with lysozyme and DNAse according to a standard protocol used in the FESSNER working group. However, analysis by gel electrophoresis revealed that hardly any target enzyme was present in the cell free extract. Figure 7.4 A depicts the related protein gel that was ran with samples containing the supernatant and the cell pellet obtained after lysis. The reference material (CFE of *Lb*KRED$_{WT}$) was provided by *Prozomix Ltd*. As can be seen, the protein band at approximately 32 kDA, which correlates to the protein of interest, can be mostly found in the lane containing the cell pellet.

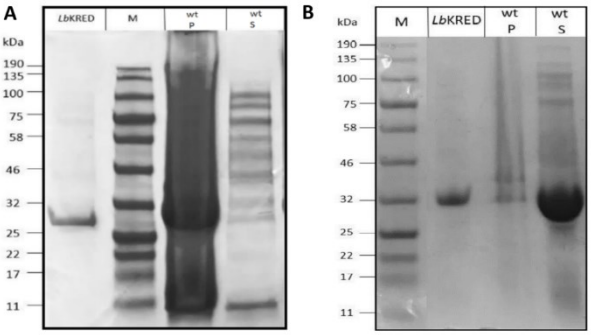

Figure 7.4 Agarose gel of samples obtained after lysis with lysozyme (A) and lysis by sonication (B). The Blue Prestained Protein Standard, Broad Range (NEB) was used as marker (M). CFE of *Lb*KRED$_{WT}$ was applied as a reference. Samples containing cell pellet material (P) and the supernatant (S) were analyzed.

It is assumed that either lysis failed or the freed protein was insoluble and therefore pelleted during the centrifugation step after lysis. This effect occurs when recombinant proteins accumulate intracellularly in aggregates called inclusion bodies.
Further attempts comprising different lysis buffers, like a commercial buffer from the *GenElute* Plasmid Miniprep Kit by *Sigma-Aldrich* or high concentrated lysozyme buffer (0.3 % w/v), which were supposed to help solubilizing proteins, remained unsuccessful. Also addition of urea, which can act as a denaturant and break disulfide bonds to help solubilizing aggregated proteins, was not fruitful. Experiments using commercial lysozyme from a different batch did not improve the outcome either.
In order to find a quick solution, a different approach for cell lysis was tested, which comprised ultrasound treatment. Sonication can be used to agitate the particles by sound energy, which leads to disruption of cellular membranes and release of cell contents. Herein, the setup applied contained a falcon tube with 10 mL of the buffered cell suspension, which was treated with ultrasound beams of 20 kHz in an interval of 1.5 s over 5 min. Analysis of the sample taken from the supernatant via agarose gel electrophoresis gave a clear protein band at the expected size (Figure 7.4 B) and verified the method to be finally successful. However, sonication was not applicable for our experimental setting when using 96-deep well plates, as a suitable sonotrode for this format was not available. Still, the method was later applied to obtain CFEs for kinetic measurements of selected candidates.
Regarding the assay, a direct application of resting cells instead brought the main advantage of avoiding the need for tedious work steps required during lysis and, in fact, proved to be fully viable for the activity screenings. Preliminary test assays conducted with resuspended cells in buffer showed that fluorescence signals could be clearly detected even in dense suspensions. Hence, all screenings were performed using resting cells that were cultivated in AIM in 96-well format, which considerably reduced time and effort and allowed for easy handling and quick screening of the large protein panels. Here, the cells were simply isolated from the cultivation broth by centrifugation and directly used after resuspension in the assay buffer. Another major advantage was brought by the fact that necessary compounds like cofactor or trace metals were already present in adequate amounts.
During first screenings, the protein libraries were each challenged with the six racemic alcohols **174a-f**, starting from the substrate featuring the smallest substituent (methyl group) and proceeding to the ones with higher sterical demand. In order to reduce time and effort, the largest substrate within the set, bearing the *iso*-pentyl substituent was not utilized in the initial screening but was applied later to assess pre-selected candidates only. The assay was performed in 10% DMSO as cosolvent and 10% acetone for potential cofactor recycling. The active candidates were spotted by the naked eye upon exposure to UV-light at 254 nm. Figure 7.5 exemplarily shows two screening plates of the D149X mutant library after a reaction time of 6 h. The plate on the left was screened towards the ethyl-substituted carbinol **174b**, resulting in approximately 40% of active enzymes while the plate on the right hand side was challenged

with the larger *iso*-butyl-substituted substrate **174e.** In this case, far fewer hits were observed (~16%). These discrepancies in activity met the expectation that larger substrates are generally less tolerated.

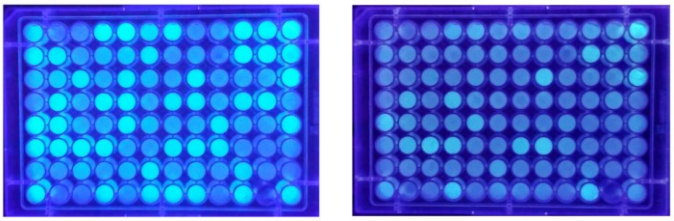

Figure 7.5 Fluorescent screening plates. The D149X sub-library is shown after a reaction time of 6 h. Positive hits are visualized by exposure to UV-light at 254 nm. The screening was performed towards the substrates **174b** (left) and **174e** (right).

Altogether, the screening furnished a multitude of enzymes that tolerated the smaller substrates **174a-c**. For the three larger carbinols **174d-f**, sequencing results revealed eight unique variants that gave high conversions. These candidates were distributed amongst the following four sub-libraries:

- **E144X** (4 hits: E → A, S, T, C)
- **D149X** (2 hits: D → N, Q)
- **L152X** (1 hit: L → R)
- **Y189X** (1 hit: Y → W)

As can be seen, most of the hits were found in the E144X library. Within these mutants, the rather large glutamic acid residue was swapped for a much smaller alanine, serine, threonine, or cysteine. Thus, in these cases, mutation obviously created essential space. In the hit enzymes of the D149X sub-library, however, the aspartic acid was altered to an asparagine or glutamine, which are similar or even larger in size but bear an amine-functionality instead of a negatively charged acid group. These changes can have an impact on the polarity of the active site and therefore influence the binding behavior. Also in the hit mutant of the L152X library the leucine was changed for a larger amino acid - an arginine. The unique guanidinium group present here most probably also has an effect on the substrate binding character. In the Y189X sub-library, the hit enzyme carries the switch from tyrosine to tryptophan. Both amino acids feature large aromatic side chains, but tryptophan additionally bears a secondary amine group that can provide hydrogen bonding effects. Changes made to the residues I143 and Y248 did not seem to furnish positive effects. When reassessing their positions in the active site via 3D-modeling, it became clear that their distance to the substrate is probably too large.

7.2.5. Creation and screening of 2nd generation library

Based on the initial screening results, a combinatorial library was created in order to investigate on potential cooperative effects. Herein, a smart construction approach was followed by embedding the most beneficial mutations and excluding the ones that were unlikely to yield further hits. As the greatest impact was most probably achieved by changes made to the residue E144, alterations to A, S, T and C were incorporated into all new clones. Switching the L152 to an arginine seemed worth being studied, as completely new substrate binding effects may occur. For the same reason, the trade of the aspartic acid at position 149 for an asparagine was also

included as a triple mutation. We resigned from permitting the change to the glutamine, though, as it is likely to feature the same characteristics like asparagine while only being bulkier. The swap from tyrosine to tryptophan at position 189 was also further investigated, as an additional amine-functionality can provide new binding properties. Hence, the following second generation library was designed:

- E144X/L152R X = A, S, T, C
- E144X/D149N/L152R
- E144X/Y189W

Herein, the experimental work of library construction was performed in close collaboration with my colleague Dr. ANNA SZEKRENYI. All mutations were conducted using the *QuikChange II* site directed mutagenesis kit from *Agilent*. The mutations at position 144 were accomplished by utilizing a degenerated codon: DST, where D stands for A, G, or T and S for G or C hence coding for all four desired amino acids (A, S, T, C) plus glycine.
The second generation library was created on a single 96-well plate and comprised of 72 picked clones plus the wildtype, with 24 clones belonging to each sub-library, giving a high probability of covering all desired combinations. Transformation and protein expression steps were performed analogously to the previous library.
Activity screening was again performed towards the six carbinols **174a-f**, except for this time, reaction monitoring was conducted over a period of 2 h with the help of a fluorescence plate reader for higher accuracy. Figure 7.6 A and B exemplarily show the detected increase in fluorescence intensity measured for the conversion of substrates **174c** and **174e** to their corresponding ketones. Again, conclusively, the larger *iso*-butyl-functionalized substrate **174e** was tolerated by far less mutants then the propyl substrate **174c**. From the combined data, the following positive hits were selected for assessment of their sequences: A7, E1, E5, F1, F3, and F8.
According to sequencing results, the screening furnished two unique genetic variants that were able to accept the bulkier carbinols **174d-f**: The double mutants E144A/L152R (A7) and E144A/Y189W (E5).

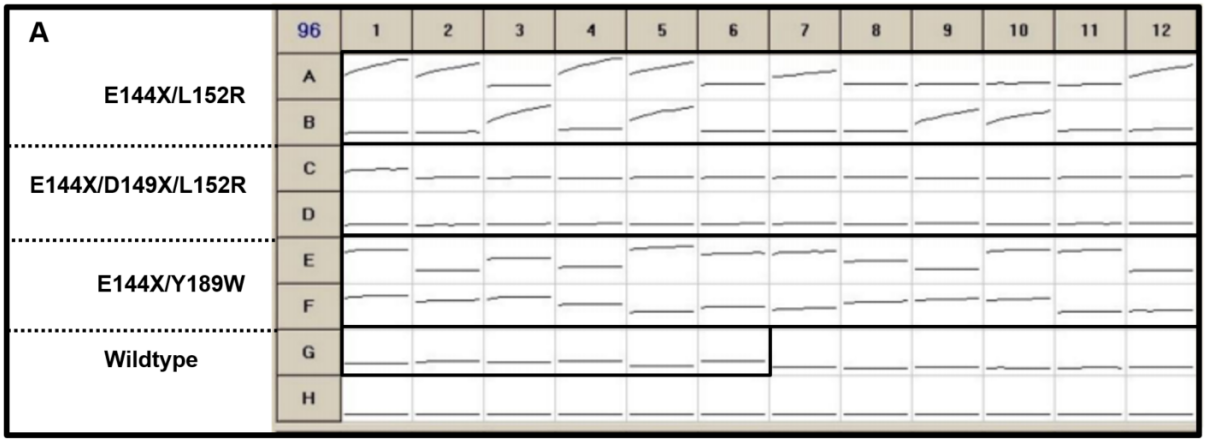

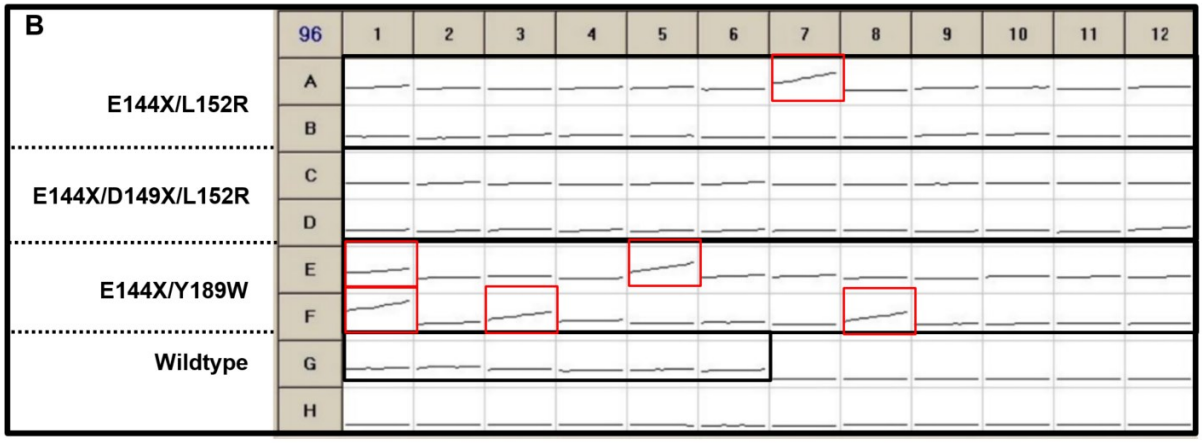

Figure 7.6 Results from activity screening of combinatorial library towards propyl-substituted **174c** (A) and *iso*-butyl-substituted **174e** (B). The increase in fluorescence was measured at an excitation wavelength of 330 nm and emission wavelength of 460 nm over a period of 2 h. The variants chosen for sequencing are highlighted in a red box.

7.2.6. Comparison of mutants from 1st and 2nd generation libraries

In order to allow direct comparison of enzymes from the 1st and 2nd generation library, all hits from both were expressed on a single plate in triplicate and rescreened towards the fluorogenic naphthyl substrates **174a-f**. In all cases, the E144A/L152R double mutant turned out to be the best candidate with the highest and fastest conversions, followed by the corresponding single mutant E144A and the double mutant E144A/Y189W. It is therefore apparent that the most beneficial mutation was the swap to alanine at position 144. However, alterations at position 152 and 189 obviously lead to synergistic effects.

Figure **7.7** exemplarily shows the increase in fluorescence over time measured for the substrates **174f** and **174e**.

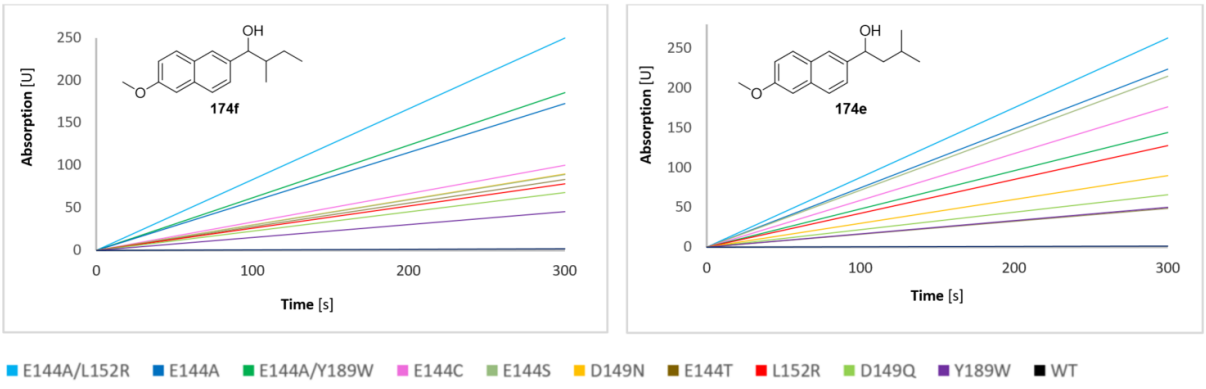

Figure 7.7 Fluorogenic screening of hit enzymes against *sec/iso*-butyl-substituted substrates **174f** and **174e.**

For further assessment, a smaller selection, comprising only the best hit from each single mutation sub library (E144A, L152R, D149N, Y189W) and the double mutants from the combinatorial library (E144A/L152R and E144A/Y189W) was challenged with the *iso*-pentyl-functionalized carbinol **174g.** Regarding the sterical configuration, its molecular structure directly translates to the one of the pharmaceutical target substrate **165** (see Figure 7.8). Thus, positive hits found here are considered as highly suitable candidates for the conversion of **165.**

Again, the screening was performed on a single plate using the same conditions as before. Figure 7.8 shows the measured increase in fluorescence over time (triplicate measurements). It was now revealed that the E144A variant was the best catalyst, followed by the E144A/L152R mutant. This finding can be well explained when just regarding the molecular size of leucine and arginine. Leucine possesses a shorter side chain, therefore offers more space in the active site. In the case of the sterically highly demanding substrate **174g**, this special effect actually became relevant. However, as all of the tested enzymes apart from the wildtype, which served as a control, showed at least minor activity towards **174g** and hydrogen bondings can play a major role they were all later considered for the pharmaceutical application (see chapter 7.3.2).

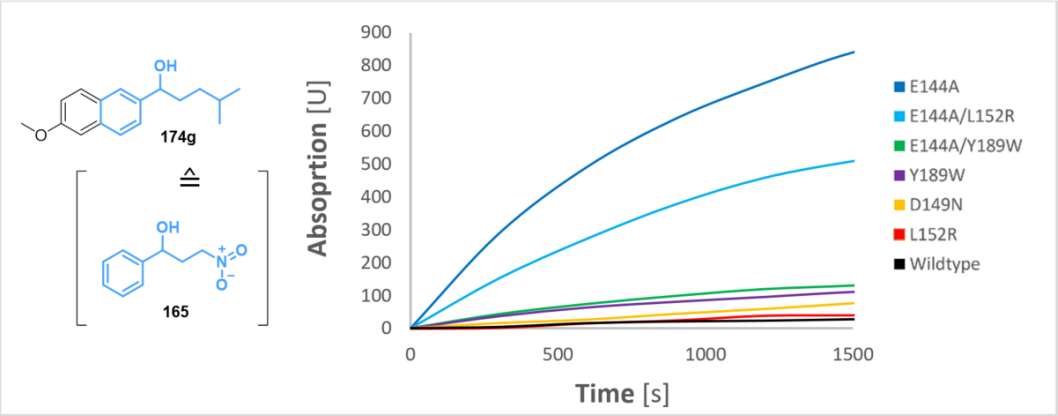

Figure 7.8 Fluorogenic screening of hit enzymes against *iso*-pentyl-functionalized substrate **174g**.

7.2.7. Determination of thermostability

In many enzyme-catalyzed processes a temperature-guided increase in activity is accompanied by a decrease in protein stability. This principle is also known as the *"activity-stability trade-off"*[215] and both factors, activity and protein stability, have to be taken into account when it comes to assessing an enzyme's suitability for industrial processes. A protein's stability can be regarded as its thermodynamic aspiration for maintaining the native folded state, whereas the thermostability is typically referred to as the melting temperature T_m, at which half of the proteins are unfolded due to heat caused disruption of intramolecular bonds in the tertiary and quaternary structure and serves as an indicator for the overall stability.[216]

In this context, nano-format differential scanning fluorimetry (nanoDSF) is a method, which allows for accurate determination of protein thermostability by applying a temperature ramp and monitoring the corresponding change in intrinsic fluorescence. During the protein's heat-induced unfolding process the close surroundings of the amino acids change and fluorescent residues like tyrosine and tryptophan undergo variations in fluorescence emission. The ratio of fluorescence intensity measured at the wavelengths $\lambda = 330$ nm and 350 nm describes the tryptophan emission shift and is characteristic during protein unfolding.[217]

For the T_m-determination via nanoDSF of the proteins of interest, samples were prepared by hypotonic enzyme extraction of whole cells, which represents a quick and simple method to attain small quantities of cell free material of adequate purity.[218] Sufficient protein content after lysis was verified by a qualitative BRADFORD test. During the T_m-measurements the

temperature was continuously increased from 20 °C to 75 °C in 1 °C/min steps. Table 7.1 summarizes the melting points obtained for the relevant enzymes. The values were found in an area ranging between 49.5 – 62.6 °C, with the wildtype enzyme's T_m of 53.9 °C positioned relatively at the average. This value also matches the data provided by SPIELMANN *et al.* quite well, who measured a T_m of 51.5 °C (via thermal shift assay with SYPRO orange).[219] The highest T_m was measured for the E144A variant, which nicely corresponded with the high conversion rates observed for this enzyme, while the lowest numbers were exhibited by the variants bearing the Y189W mutation. It seems that introduction of a tryptophan residue must have destabilizing effects. For all other mutants, the changes in T_m remained rather small. Interestingly, the double mutant E144/L152R exhibited a lower thermostability than both of its corresponding single variants.

Table 7.1 Protein melting points measured via nanoDSF.

Enzyme	T_m [°C]
E144A	62.6
D149N	57.7
L152R	56.6
Wildtype	53.9
E144A/L152R	51.7
E144A/Y189W	49.7
Y189W	49.5

7.2.8. Determination of kinetic parameters

The double mutants were further characterized by determination of their kinetic parameters for **174a** and the larger substrates **174d-g** according to the MICHAELIS-MENTEN model.[220] For this screening, cell-free extracts were prepared, as the application of whole cells would have otherwise bore several problematic factors, including uneven cell growth, which could have led to unsteady catalyst concentrations and irreproducibility of results. Further on, irregular substrate movement through cell walls as well as agglomeration effects needed to be considered, because small variations can already lead to biased results.

The K_m and V_{max} values were, apart from that, determined using the same assay conditions as for the activity screening. For the kinetic measurements the reactions were performed in triplicate at eight different substrate concentrations ranging between 0.1 – 1 mM at a fixed enzyme amount of 0.4 mg/well. Blank reactions without enzyme were included for each concentration in order to subtract background effects. The reactions were monitored by detection of fluorescence over a period of 1 h. A dilution series of the reference ketone was measured in order to correlate the conversions with mM concentrations. The raw data from the measurements were first evaluated via ***Excel*** (*Microsoft Office*) by plotting the fluorescence intensity against the time points and applying linear regression for the starting, "linear" parts of the curves. The obtained values for the slopes corresponded with the reaction's initial velocities V_0 and were further processed with Origin 9.1 (*OriginLab*) for hyperbolic fitting. This finally gave the V_{max} and the K_m values. Figure 7.9 A exemplarily shows the data analyzed for the E144A/L152R double mutant on the *iso*-butyl-substituted substrate **174e** at 0.25 mM concentration via *Excel*, including data plotting and linear regression. Subsequent hyperbolic fitting via *Origin 9.1* is shown in Figure 7.9 B.

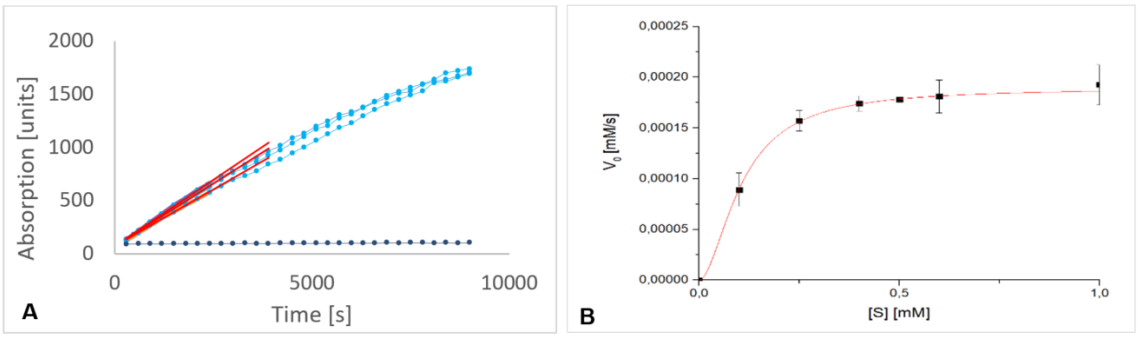

Figure 7.9 Measurements of MICHAELIS-MENTEN kinetics for E144A/L152R double mutant on the *iso*-butyl-substituted substrate **174e** at 0.25 mM concentration. (A) Measured data for fluorescence intensity plotted against corresponding time points (blue curves) and linear regression (red slope) via *Excel*. (B) Plotting of obtained V_0 -values against corresponding substrate concentrations (black dots) and hyperbolic fitting (red curve) via *Origin 9.1*.

Table 7.3 summarizes the values obtained for V_{max} and K_m for each mutant-substrate pair and the data for the native enzyme measured with the methyl-substituted substrate **174a.**

Table 7.3 MICHAELIS-MENTEN parameters of variant enzymes for carbinol substrates **174a** and **174d-g**.

R-substituent	Catalyst	V_{max} [mM/s]	K_m [mM]
Iso-pentyl (**174g**)	E144A/L152R	$(1.1 \pm 3.4) \times 10^{-5}$	0.5 ± 0.3
	E144A/Y189W	$(2.9 \pm 9.7) \times 10^{-5}$	1.5 ± 0.7
Sec-butyl (**174f**)	E144A/L152R	$(3.6 \pm 1.5) \times 10^{-4}$	0.9 ± 0.7
	E144A/Y189W	$(2.5 \pm 2.0) \times 10^{-4}$	3.0 ± 4.7
Iso-butyl (**174e**)	E144A/L152R	$(1.9 \pm 0.0) \times 10^{-4}$	0.1 ± 0.0
	E144A/Y189W	$(8.8 \pm 1.2) \times 10^{-5}$	0.6 ± 0.1
Iso-propyl (**174d**)	E144A/L152R	$(4.0 \pm 5.2) \times 10^{-5}$	0.8 ± 0.2
	E144A/Y189W	$(4.8 \pm 1.5) \times 10^{-4}$	0.7 ± 0.4
Methyl (**174a**)	E144A/L152R	$(5.4 \pm 0.2) \times 10^{-5}$	0.1 ± 0.0
	E144A/Y189W	$(2.7 \pm 0.8) \times 10^{-5}$	0.6 ± 0.3
	Wildtype	$(1.4 \pm 0.6) \times 10^{-3}$	0.4 ± 0.4

Regarding the V_{max}-parameters obtained with the methyl-substituted substrate **174a**, both double mutants showed approximately 100-times lower values than the wildtype, marking a much slower turn-over rate, as smaller concentrations already lead to a saturation of the enzyme's active site. When comparing the K_m values measured with **174a**, the E144A/L152R double mutant showed a more than three-fold lower MICHAELIS-MENTEN constant than the wildtype, referring to a three-fold increased affinity for the substrate. Even the K_m-value for the *iso*-butyl substituted substrate **174e** was found in the same range, meaning that this sterically demanding molecule is apparently also well accepted by this mutant and forms a stable substrate-enzyme complex. The K_m-value for the *iso*-pentyl substrate is with 0.45 mM a little higher but still indicates a strong substrate affinity. Regarding the potential application on the target molecule **165**, this finding was highly encouraging, as **174e** bears a very similar sterical orientation. Affinity for the *sec*-butyl and *iso*-propyl substrates **174f** and **174e** were approximately two times lower. It is assumed that the methyl group present in direct proximity to the ketone group hinders easy substrate entering and strong binding.

In comparison, the E144A/Y189W variant exhibited higher K_m-values in all cases except for the *iso*-propyl substrates **174g.** Taking this into account, the E144A/L152R mutant was regarded as the most promising candidate for further applications.

7.2.9. Stereoselectivity typing

In order to guarantee formation of optically pure alcohols, it was imperative to retain the enzyme's enantiospecificity after mutagenesis. Hence, a great challenge lay in meeting the fine line between creating just enough additional space in the enzyme pocket to host the substrate's nitro alkyl chain while distinctively preventing entrance of the substrate's larger aromatic moiety. To investigate if this matter was fulfilled, the selected hit enzymes were tested for stereoselectivity utilizing the same assay format as before. For this purpose, both enantiomers of methyl-substituted carbinol substrate **174a** were applied in individual reactions and samples containing the wildtype and no enzyme were utilized as controls. The reactions were performed in triplicate. Figure 7.11 shows the fluorescence measurements over a period of 30 minutes. As can be seen, only the reaction samples containing the *(R)*-alcohol showed an increase in fluorescence intensity, meaning that all candidates have proven to remain their anti-PRELOG specificity in oxidation direction.
In order to also proof *(R)*-stereoselectivity for the opposite direction, analytical scale reactions of the reduction of methyl-substituted ketone **173a** were performed and directly measured via chiral HPLC against the chiral references ***(R)*-174a** and ***(S)*-173a.** Here, the chromatograms showed single peaks only that referred to the *(R)*-configured reference material (Figure 7.11). This gave verification that all mutants, indeed, retained the enantiospecificity inherited from the native enzyme.

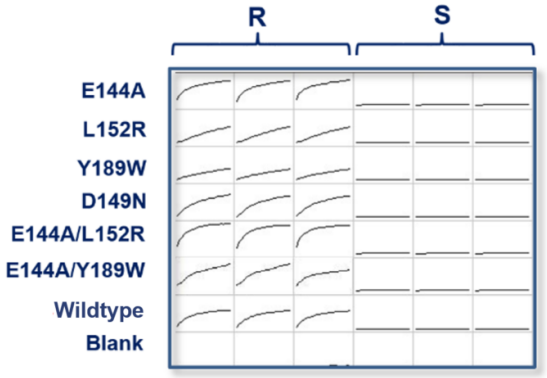

Figure 7.10 Stereoselectivity typing of selected variants. Individual enantiomers of alcohol **174a** were applied in triplicate measurements. Enzymatic activity was only observed when utilizing the *(R)*-enantiomer.

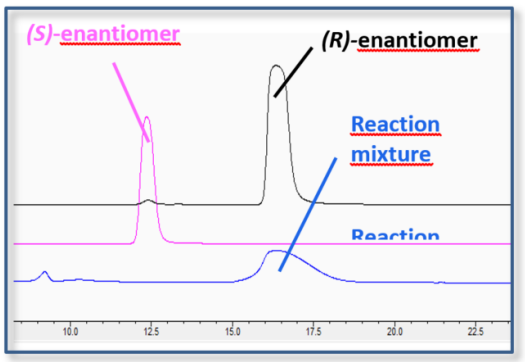

Figure 7.11 HPLC of sample taken directly from the E144A/L152R double mutant-catalyzed oxidation reaction of **173a.** The single peak correlates to the signal of the *(R)*-configured reference material.

7.3. Application of engineered enzymes in pharmaceutical synthesis

7.3.1. Synthesis of pharmaceutical substrate

Ketone **162** as well as the corresponding racemic alcohol ***rac*-165** were chemically synthesized following standard experimental protocols: The Cl-functionalized precursor **179** was obtained starting from FRIEDEL-CRAFTS acylation of commercially available 1,2-difluorobenzene (**177**) with 3-chloropropanoyl chloride (**178**). Subsequent treatment with sodium nitrite generated the desired nitro functionality (Scheme 7.5).

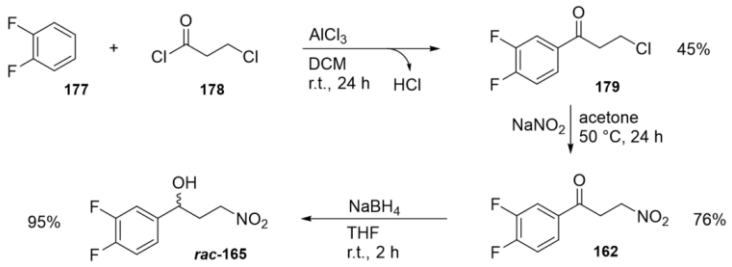

Scheme 7.5 Chemical pathway for the synthesis of ketone **162** and corresponding racemic alcohol ***rac*-165**.

The first step was performed following a standard procedure by the group of TURNER[12] and was catalyzed by stoichiometric amounts of the LEWIS acid $AlCl_3$. The low yield of only 45% obtained here was due to the presence of high amounts of trace water in the $AlCl_3$ used, which most likely caused the catalysts to transform to $Al(OH)_3$ and resulting in incomplete reaction. Anyhow, intermediate **179** was obtained in sufficient amount and purity, which was verified by NMR measurements.

The subsequent conversion of the chloride substitution to furnish the nitro group was conducted by treatment with $NaNO_2$ at 50 °C for 24 h according to a protocol by HUGENTOBLER[12] and gave the desired product **162** with a satisfactory yield of 76% after column chromatography. Attempts to shorten the process time by performing the reaction at 70 °C were aborted as higher temperatures triggered the elimination of nitrous acid and led to the formation of a double bond.

The racemic alcohol ***rac*-165** was produced by standard borohydride reduction of **162** with an excellent yield of 95%.

7.3.2. KRED-catalyzed analytical scale reactions

A) Reaction analysis

In speculation that some of the engineered enzymes may be suitable candidates for the biotransformation of precursor **162**, the preselected candidates from the fluorogenic screenings were finally tested for this purpose. Analytical scale reactions of 500 μL total volume were performed utilizing 10 mg resting cells in a buffered 10 mM substrate solution containing 10% DMSO as cosolvent. Monitoring was performed by HPLC analysis at different time points (0 h, 3 h, 6 h). Samples containing either no enzyme or the wildtype enzyme were used as negative controls.

To our satisfaction, three of the tested variants turned out to be active catalysts for the reduction of ketone **162**. Amongst these were the single mutant E144A and the double mutants

E144A/L152R and E144A/Y189W. Herein, the highest product formation was observed for the E144A/L152R variant. In this case, the ketone was almost fully converted to the corresponding alcohol after 6 h, providing almost quantitative yield. For the E144A variant and the E144A/Y189W double mutant measurements gave relative conversions of 68% and 12%, respectively. According to expectations, no product formation was observed when employing the native enzyme or no enzyme.

However, in all samples containing cells, two additional peaks were observed on the chromatograms, indicating the formation of two byproducts. Even in the case of the wildtype enzyme, the educt was fully consumed in favor of the mentioned. Very similar retention times of 15.6 and 16.3 minutes, compared to the target alcohol (15.9 minutes), led to the assumption that related alcoholic structures must have been formed, since the ketone exhibited a very distinguishable polarity and therefore different retention time of around 18 minutes. The HPLC chromatograms for the reactions catalyzed by the double mutants, the E144A variant, and the wildtype are shown in Figure **7.12**.

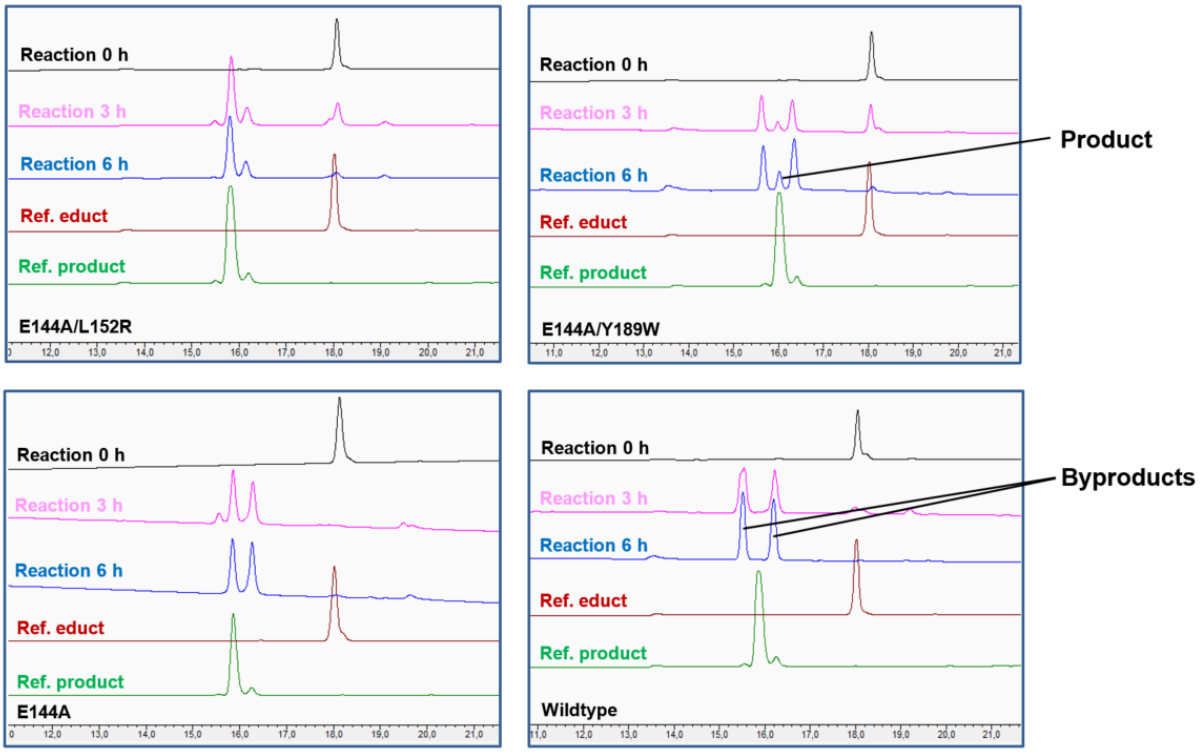

Figure 7.12 HPLC chromatograms of reductive transformations of nitro ketone **162**.

To further investigate on this matter, a larger scale reaction was performed with the wildtype enzyme as catalyst in order to isolate and analyze the unknown material. As a clean separation of the two side products turned out to be problematic due to too similar molecular properties, the compounds were analyzed as a mixture. Measurements by NMR (^{1}H, ^{13}C, ^{15}N) as well as mass spectrometry revealed structures that lacked the nitro group in both cases. Instead, signals that corresponded to alkyl and allyl groups were clearly assigned, matching the structures **180** and **181** shown in

Figure 7.13. Herein, the ratio between the two side products was 1 : 2 in favor of the saturated product.

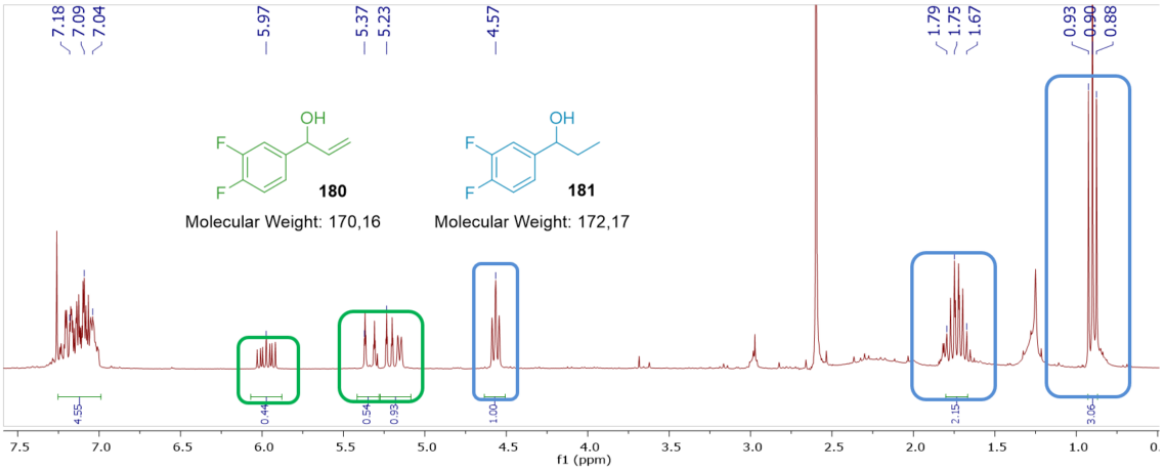

Figure 7.13 NMR spectrum of isolated byproducts **180** and **181** with proposed molecular structures.

This unexpected finding can be explained by proposing a two- and three enzyme cascade reaction that was mediated by additional enzymes co-expressed in the bacterial cells.
In this context, nitrosuccinate lyases have been reported to catalyze elimination of nitrous acid from nitrosuccinate (**182**). The catalytic mechanism is shown in Scheme 7.6 and involves a serine as catalytic base, which abstracts a proton from the beta-carbon, forming an enolate intermediate. Arginine then acts as a catalytic acid and donates a proton to stimulate the elimination of nitrous acid (**183**), which furnishes an allylic structure in the remaining molecule.[221]

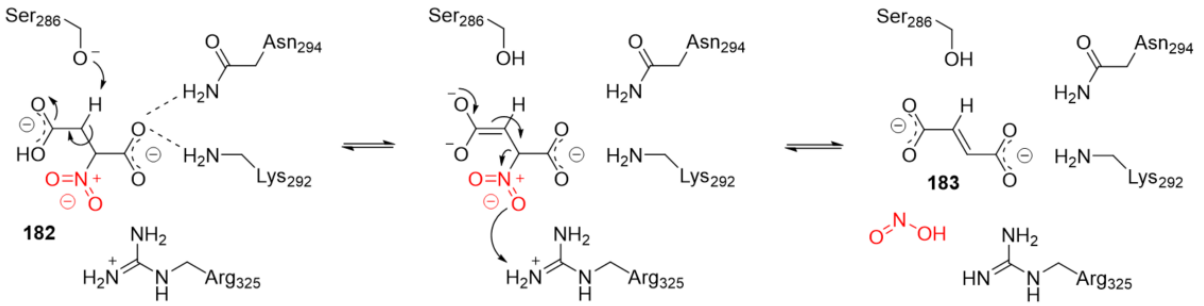

Scheme 7.6 Catalytic mechanism of lyase-mediated elimination of nitrous acid (**183**) from nitrosuccinate **182**.[221]

It is assumed that in our case, the same mechanism led to the formation of vinyl ketone **184**. Indeed, when the nitro alcohol ***rac*-165** was offered as a substrate instead of the ketone, no catalytic activity was observed. This confirmed that the first step relied on the formation of an enolate intermediate indicative for lyase catalysis.
The following step within the reaction cascade could now proceed with the shorter molecule, which was therefore well accepted by the ketoreductase and was transformed to the corresponding alcohol **180** as one of the detected side products. Concomitantly, reduction of vinyl ketone **184**, presumably by an enereductase (ER), gave the saturated derivative **185**,

which was again subsequently reduced via KRED-catalysis to generate the corresponding alcohol **181** as the second side product (Scheme 7.7).

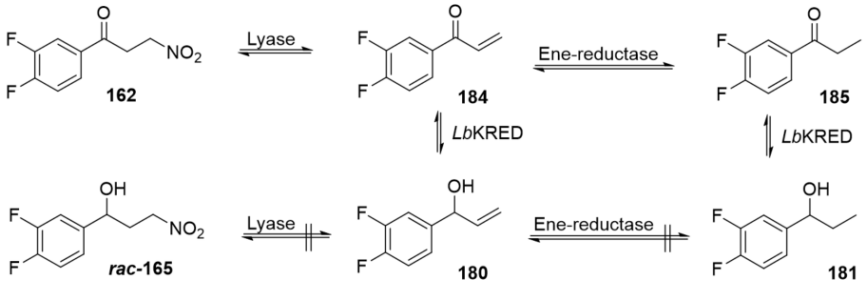

Scheme 7.7 Enzymatic cascade towards byproducts **180** and **181**. The reaction sequence is catalyzed by a nitro lyase, a ketoreductase, and an ene-reductase.

ERs are widespread in nature and have been identified from various origins, such as bacteria, yeasts, fungi, and plants. They are mostly flavin-dependent oxidoreductases and catalyze the reduction of α,β-unsaturated compounds that are activated through an electron withdrawing group (EWG) present in direct proximity to the double bond.[222] In our case, the carbonyl group plays the role of the activator. Consequently, the reaction cascade suggests a parallel (instead of a serial) reaction sequence to the byproducts **180** and **181**, as it is unlikely that the saturated alcohol was formed from the unsaturated via ER-catalysis. The alcohol moiety present in **180** functions as an electron donating group (EDG) and would rather have deactivating effects.
Anyhow, neither one of the ketones **184** and **185** were observed on the HPLCs, which indicated a rapid transformation to the corresponding alcohols once formed. Therefore, the lyase-mediated cleavage of nitrous acid marked the rate limiting step throughout the cascades.
When utilizing purified wildtype enzyme instead of resting cells, no reaction was observed, which brought the proof that the side products were, indeed, formed via a multienzymatic reaction sequence due to co-expressed catalysts.

B) Determination of enzyme kinetics

The variant E144A/L152R was further characterized by determining MICHAELIS-MENTEN parameters for alcohol **165.** For this purpose, the reaction progress was continuously measured by detecting NADPH-formation at 340 nm. The substrate concentration was varied between 10 - 40 mM while applying the enzyme at a fixed amount of 10 mg/mL. All data were obtained in triplicate and processed via Excel and Origin 9.1 for data plotting/linear regression and hyperbolic fitting (Figure 7.14).

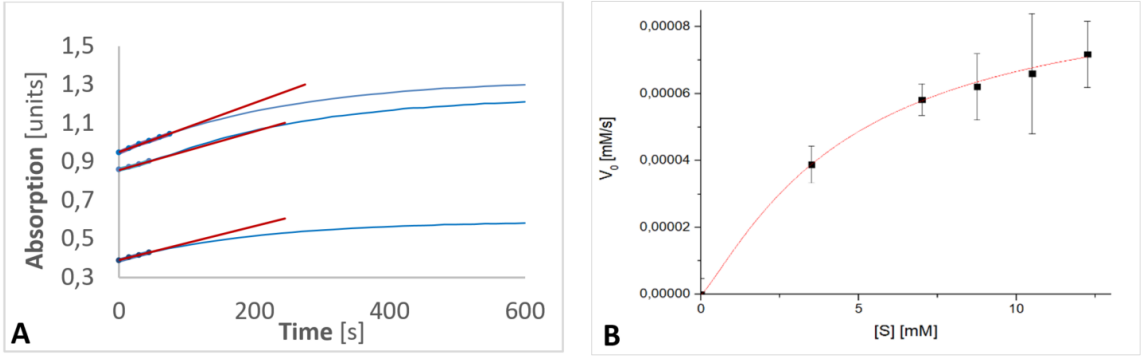

Figure 7.14 Processed results of kinetic measurements. (A) Fluorescence intensity was plotted against corresponding time points (blue curves) and linear regression (red slopes) was applied via *Excel*. (B) Plotting of obtained V_0-values against corresponding substrate concentrations (black dots) and hyperbolic fitting (red curve) via *Origin 9.1*.

Herein, the following kinetic parameters were obtained:

- $V_{max} = (9.3 \pm 0.96) \times 10^{-5}$ mM/s
- $K_m = 4.6 \pm 0.8$ mM

Compared to the alkyl substrates **174d-g**, the K_m-value here was higher, meaning a lower affinity to the nitro-functionalized side chain probably due to repulsive interactions. V_{max}, however, lay in the same range. Anyhow, incomparability of the results can be an issue, as a different and less sensitive detection method was used in this case.

C) Determination of stereoselectivity

Optical purity of the isolated product **165** was analyzed by chiral HPLC (Figure 7.15). As the chromatogram showed a single peak, only one enantiomer was produced and we can state with high confidence that the signal corresponded to the *(R)*-configured antipode. This assumption was consolidated not only by the original specificity provided by the native enzyme but also by our previous findings when stereotyping the catalyst using both optically pure individual antipodes of carbinol **174a.**

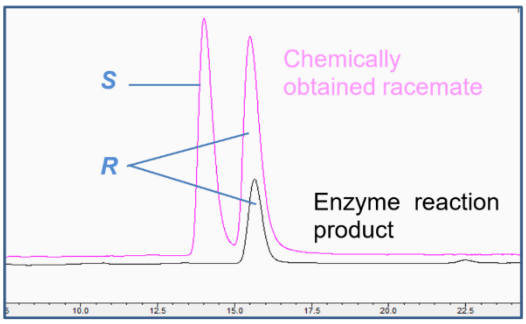

Figure 7.15 HPLC trace of chiral alcohol ***(R)*-174**, obtained from chemical synthesis (pink) and enantiopure compound, isolated from KRED-catalyzed reaction (black).

7.3.3. Preparative scale reaction

In order to scrutinize the variant's potential for application in industrial bioreduction processes, a preparative scale reaction at a higher, industrially relevant substrate concentration of 100 mM and a lower catalyst load of 5 g/L was performed. Utilization of resting cells obtained directly from the fermentation broth enabled cost-efficient and easy access to large amounts of catalyst. As industrially relevant processes are only economically feasible if a second catalytic cycle allows for *in situ* cofactor recycling, a "*coupled-substrate approach*" was applied. This included employing the same enzyme to convert *iso*-propanol (10%) as sacrificial alcohol for NADPH-cofactor regeneration (Scheme 7.8).

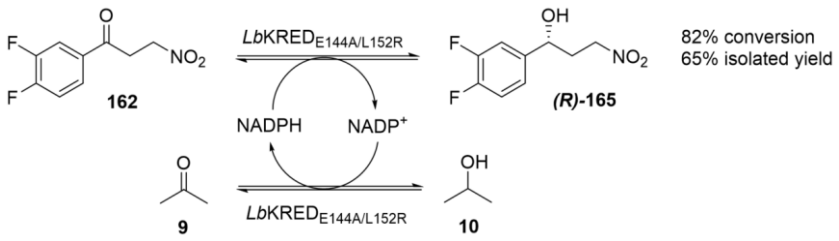

Scheme 7.8 *Lb*KRED-catalyzed conversion of ketone **162** to corresponding chiral alcohol ***(R)*-165** upon oxidation of NADPH by E144A/L152R variant. Cofactor regeneration is performed by employing *iso*-propanol as sacrificial substrate.

The up-scaled reaction was conducted at room temperature in 10% DMSO as additional cosolvent over a period of 24 h and gave 82% conversion (HPLC). An isolated yield of 79% based on conversion was reached after purification by silica column chromatography. Successful transformation was confirmed by NMR and chiral HPLC analysis of the isolated material.

7.3.4. Evaluation of mutagenesis effects

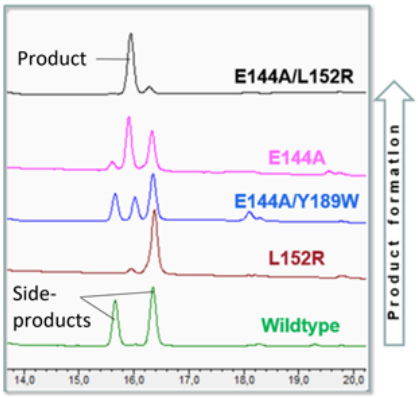

Figure 7.16 HPLCs of conversion of ketone **162** by different *Lb*KRED variants. Samples were taken after 6 h.

When comparing the different mutations, it is apparent that the reaction outcome is, on the one hand, controlled by sterical effects and, on the other hand, by electronic effects. Alanine, being one of the smallest amino acids, is the key residue for opening up additional space inside the enzyme's active site and therefore enabling entrance for larger substituents. Thus, as shown in the HPLCs in Figure 7.16, catalysts that carried the original glutamate residue at position 144 were not/hardly able to produce the target alcohol ***(R)*-165**. The wildtype and the L152R variant generated only byproducts, instead. Figure **7.18** highlights the size difference between alanine and glutamate and compares the pyMOL-simulated 3D-models of the native enzyme to the E144A/L152R variant, showing a significant difference in binding surface. Regarding the electronic effects, the guanidine group present in arginine changes the hydrophilic character of the active site. It is most likely responsible for polar interaction with the substrate's nitro group, hereby forming up to two hydrogen bonds (Figure 7.18 A). This is expected to notably stabilize substrate binding and orchestrating the molecule to arrange deeply inside the enzyme pocket. PyMOL simulations in Figure 7.18 B show how the R152 aligns sideways, leaving enough room for the substrate to enter while providing optimal possibility for interaction via hydrogen bond formation. This beneficial position enabled successful stereospecific reduction of the ketone group.

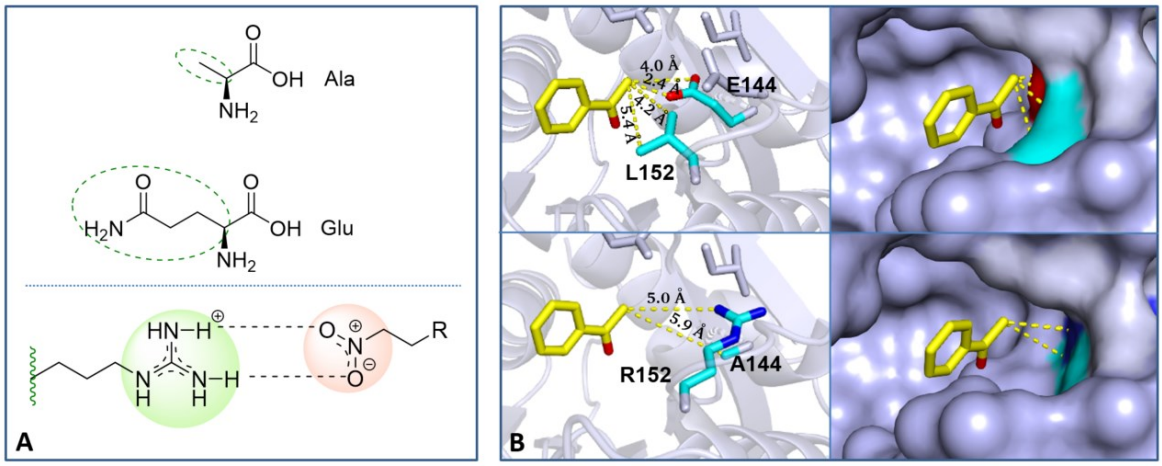

Figure 7.18 A) Molecular structure of alanine and glutamine (top) and dipolar interactions between guanidine group of arginine and nitro-functionality (bottom). B) Active site 3D-models of *Lb*KRED wildtype and variant E144A/L152R. Acetophenone is bound as model substrate (marked in yellow). The amino acid residues at the mutated positions 144 and 152 are highlighted in cyan. The variant's active site shows a significant increase in space with R152 aligning sideways.

8. Summary and Outlook

By following the approaches of directed evolution and rational design, a variant enzyme of *Lb*KRED was successfully engineered towards synthesis of the non-natural chiral precursor ***(R)*-165** to the anti-thrombotic drug ticagrelor (**8**) The employment of the engineered *(R)*-selective ketoreductase provided an attractive and much simpler alternative to classical chemical synthesis towards the target drug. By employing non-toxic aqueous media under mild conditions (ambient temperature, pH = 7.5) and avoiding hazardous reagents, this strategy prosperously follows the idea of green chemistry.
This achievement also validates the relevance and applicability of an assay strategy that was developed for high-throughput screening of large KRED panels.[13] For this highly sensitive and rapid assay, fluorogenic substrates with increased bulkiness were designed to incrementally mimic the target substrate, in order to subsequently shape the enzyme's active site within the next generation libraries. Part of the strategy included a very cost-effective and simple strategy for substrate synthesis by following a modular pathway of GRIGNARD addition reactions. The assay principle allowed not only for rapid activity typing of large enzyme libraries but also for selectivity typing and determination of enzyme kinetics.
Starting from the native enzyme, the first generation variant library was created by site-saturation mutagenesis of six non-catalytic amino acid residues present in direct surrounding of the substrate binding site, chosen via 3D-modeling. By recombining the hits obtained from this library, a second generation, smart library was constructed from which three active mutants were found to tolerate the pharmaceutically relevant ketone **162.** The best variant was identified as the double mutant E144A/L152R, which features an anti-PRELOG stereoselectivity of 100% *ee* and a sufficient substrate affinity, leading to a high conversion of 86% after 24 h. T_m measurements of the mutant via nanoDSF revealed a small loss in thermostability compared to the wildtype. Tolerance for higher substrate concentrations at 100 mM and cofactor regeneration by conversion of *iso*-propanol to acetone were tested and confirmed, making this catalyst highly suitable for industrial applications. Additionally, the option of employing whole cells at low catalyst load allowed for easy and cost-efficient enzyme access.

To our knowledge, no suitable, industrially relevant enzyme has so far been reported for the simpler *(R)*-selective KRED-catalyzed route to ticagrelor. Various KREDs from organisms like *Candida parapsilosis*[192] or *Ralstonia* species[12] have been presented, showing high enantioselectivity towards the *(S)*-enantiomer of alcohol **165.** However, very few of the more desirable *(R)*-selective candidates are known, from which very poor yields were observed (*e. g.* KRED from *Saccharomyces Cerivisiae*) while having to apply high catalyst loads.[192] Hence, our novel KRED constitutes a highly valuable tool for pharmaceutical synthesis of the ticagrelor building block.
Interestingly, the *trans*-aryl cyclopropylamine (CPA) building block can also be found in many other bioactive compounds, which mostly act as lysine-specific demethylase (LSD1) inhibitors or MAO blockers. Apart from ticagrelor (**8**) or the anti-depressant tranylcypromine (Parnate®) (**186**),[15a] which have already entered the market, other analogs are being tested in phase II clinical trials for cancer (ORY-1001/Rg6016 (**187**))[15b], Alzheimer's (ORY-2001 (**188**))[15c], and anti-myelofibrosis treatment (IMG-7289 (**189**))[15d] (Figure 8.1).

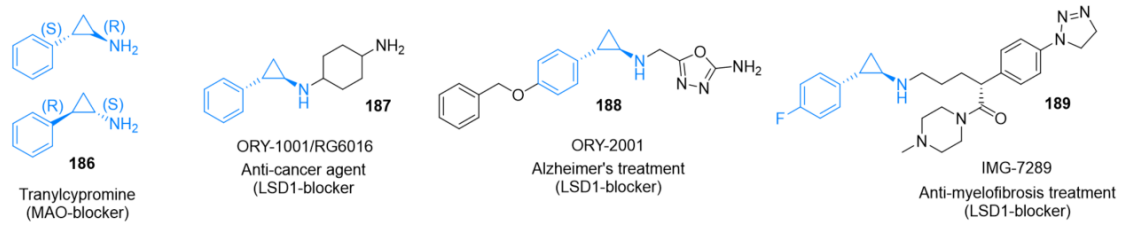

Figure 8.1 Pharmaceuticals bearing an aryl CPA building block highlighted in blue.[15]

As the molecular variations of the CPA units lie only in the substituents of the aromatic ring, it is highly expected that the engineered *LB*KREDs can as well be employed in their production. Chemical synthesis of the related precursors and activity test by HPLC analysis should prove these cases and open up further possibilities for the application of these unique and novel catalysts.

9. Experimental Part

9.1. General

9.1.1. Chemicals and reagents

Commercial chemicals and reagents were purchased from common providers, including *Sigma-Aldrich, TCI Europe, Fluka, Roth, VWR*, or *Acros* and were used without further purification if not mentioned.
For inert conditions, argon gas from *Linde* was applied. All solvents used in air or moisture-sensitive reactions were subjected to common drying processes and stored under inert atmosphere over 4 Å molecular sieves.

9.1.2. General reaction conditions

Reactions that demanded inert conditions were carried out using SCHLENK technique: Heat-dried reaction flasks were repeatedly (three times) purged by being subjected to a vacuum/argon line for removal of gases and trace water and refill with argon gas.
All reactions were conducted on a magnetic stirrer are shaker.
Temperatures above 40 °C were attained through a polyethylene glycol oil bath.

9.1.3. NMR measurements

^{1}H (300-500 MHz) and ^{13}C (75 MHz) NMR spectra were measured on an *AC300* or *DRX500* spectrometer from *Bruker*. Chloroform-d, Methanol-d^{4}, D_2O, or DMSO-d^{6} were used as NMR-solvents. The corresponding chemical shifts listed below are given in relation to the signal of tetramethylsilane as universal standard (δ = 0 ppm):[223]

- Chloroform-d: $\delta(^{1}H)$ = 7.26 ppm; $\delta(^{13}C)$ = 77.16 ppm
- D_2O: $\delta(^{1}H)$ = 4.79 ppm; -
- DMSO-d^{6}: $\delta(^{1}H)$ = 2.50 ppm; $\delta(^{13}C)$ = 39.52 ppm
- Methanol-d^{4}: $\delta(^{1}H)$ = 3.31 ppm; $\delta(^{13}C)$ = 49.00 ppm

In some cases, further characterization of the compounds was performed using typical gradient-enhanced 2D experiments like COSY, NOESY and HSQC.
For data analysis, the software *MestreNova* was employed.

9.1.4. Staining and derivatization reagents

Table 9.1 Composition of staining and derivatization reagents.

Reagent	Composition	Amounts
Anisaldehyde staining (kept at -20 °C, used for TLC staining)	EtOH	200 mL
	H_2SO_4 (conc.)	7.5 mL
	Glacial acetic acid	2.2 mL
	Anisaldehyde	7 mL
Hanessian's reagent (kept in dark flask, used for TLC staining)	Ammonium molybdate	5 g
	Cerium sulfate	1 g
	Sulfuric acid, conc.	10 mL
	H_2O	90 mL
Sample derivatization reagent (used for non-UV HPLC samples)	*O*-benzylhydroxylamine hydrochloride	1g
	Pyridine	33 mL
	Methanol	15 mL
	H_2O	2 mL
Coomassie Brilliant Blue staining (used for SDS-PAGE staining)	Coomassie (G250 Brilliant Blue)	75 mg
	H_2O	1 L

9.1.5. List of apparatus and devices

Table 9.2 List of apparatus and devices

Apparatus/device	Brand, specification
Fluorescence plate reader	*BMG*, Fluostar Optima
Freeze-dryer	*Telstar*, LyoQuest
Microplate-Reader	*Molecular Devices,* SpectraMax 190
UV-/VIS-Spectrophotometer	*Shimadzu,* UV-1800
Microplate incubator	*Heidolph,* Inkubator 1000
HPLC, gradient-system with MS-detector	*Shimadzu,* Prominence
HPLC, isocratic	*Shimadzu,* Prominence
Preparative flash/HPLC-system with UV- and ELS-detector	*Teledyne ISCO,* CombiFlash EZ Prep
HPTLC sampler and scanner	*CAMAG,* TLC Sampler ATS4
Fermenter	*Braun,* Biostat B
Autoclave	*Systec,* VX-150
Incubation shaker	*INFORS HT,* Ecotron
Vortex mixer	*IKA*, MS1Minishaker
NanoDSF-system	*NanoTemper,* Prometheus NT48
Protein purification by IMAC chromatography	*GE Healthcare,* HisTrap column
SDS-gelelectrophoresis	*Bio-Rad*, Mini Protean II
Ultrafiltration	*Stedim Biotech AG*, Vivacell 250 Sartorius
Eppendorf ultrafiltration	*Amicon* 8400, Membrane: YM 10
Centrifuge	*Eppendorf,* Centrifuge 5415D, 5804, 5810R
pH-meter	*SI Analytics,* TitroLine 7000

9.1.6. Media, buffers and solutions

Table 9.3 Constitution of media, buffers and solutions.

Medium*/Buffer	Composition	C in H_2O
LB-medium (LURIA-BERTANI) (pH 7.5) Rich medium that is extensively used in recombinant DNA work to culture *E. coli.*	Yeast extract	5 g/L
	Tryptone	10 g/L
	NaCl	5 g/L
For plate preparation	Agar	1.5 %
Auto-induction (AI)-medium (pH 7.5) Used for protein expression cultures. The principle of AIM is based on the different carbon sources that are metabolized differentially to promote high density cell growth (glucose consumption) and automatically induce protein expression (lactose consumption after glucose is used up) driven by the lac operon.	Yeast extract	5 g/L
	Tryptone	10 g/L
	NH_4Cl	2.68 g/L
	$NaSO_4$	0.71 g/L
	Glycerol	5 g/L
	Glucose	0.5 g/L
	Lactose	2g/L
	$MgSO_4$ solution (1 M)	1 mL/L
	K_2HPO_4 solution (1 M)	40 mL/L
	KH_2PO_4 solution (1 M)	10 mL/L
	Trace metal solution	1 mL/L
Trace metal solution (in 0,1 M HCl) Contains a mix of metal salts used for the preparation of AIM.	$FeCl_3$	50 mM
	$CaCl_2$	20 mM
	$MnCl_2$	20 mM
	$ZnSO_4$	10 mM
	$CoCl_2$	2 mM
	$CuCl_2$	2 mM
	$NiCl_2$	2 mM
SOC-medium Salt rich medium used primarily in the recovery step of *E. coli* competent cell transformations. The use of SOC maximizes the transformation efficiency of competent cells, if used for growing the recently transformed bacteria during incubation, before plating the culture.	Yeast extract	5 g/L
	Peptone	20 g/L
	NaCl	0.6 g/L
	KCl	0.2 g/L
	$MgCl_2$ solution (1 M)	10 ml/L
	$MgSO_4$ solution (1 M)	10 mL/L
	Glucose	3.6 g/L
HEPES-buffer, pH 7.5, 0.5 M Buffer action between pH = 6,8 - 8,2	HEPES	120 g/L
TEA-buffer, pH 7.5, 1 mM Stock solution used in enzymatic reaction	Triethanolamine	1 M
Phosphate assay-buffer, pH 7.4, 50 mM Buffer solution used in enzymatic reaction	KH_2PO_4 (1 M solution)	9.4 mL/L
	K_2HPO_4 (1 M solution)	40.6 mL/L
Phosphate wash-buffer, pH 7.4, 20 mM Buffer solution used in protein purification	$NaPO_4$	20 mM
	NaCl	0.5 M
Imidazol IMAC buffer, pH 7.4 Buffer solution used in protein purification	$NaPO_4$	20 mM
	NaCl	0.5 M
	Imidazole	30 mM
SDS-PAGE loading buffer Buffer solution used for sample preparation for SDS electrophoresis	Tris/HCl (1 M stock, pH 6.8)	0.5 M
	Glycerol	20%
	SDS	10%
	Bromphenolblue (2% in EtOH)	0.005%

	EDTA (from 0.5 M solution)	50 mM
SDS-PAGE Electrophoresis buffer Buffer solution used for SDS electrophoresis	TRIS	3 g/L
	Glycine	14 g/L
	SDS	1 g/L
Transformation buffer	PIPES	3 g/L
	$CaCl_2$	2.2 g/L
	KCl	18.6 g/L

*In most cases the media were complemented with antibiotics:
Herein, ampicillin, kanamycin, or tetracyclin were added to give concentrations of 100 µg/mL, 30 µg/mL, or 15 µg/mL, respectively.

9.1.7. Vector map

The pET-28a(+) vector used in this work features an N-terminal His-Tag and a T7 promoter. The vector map is shown in Figure 9.1.

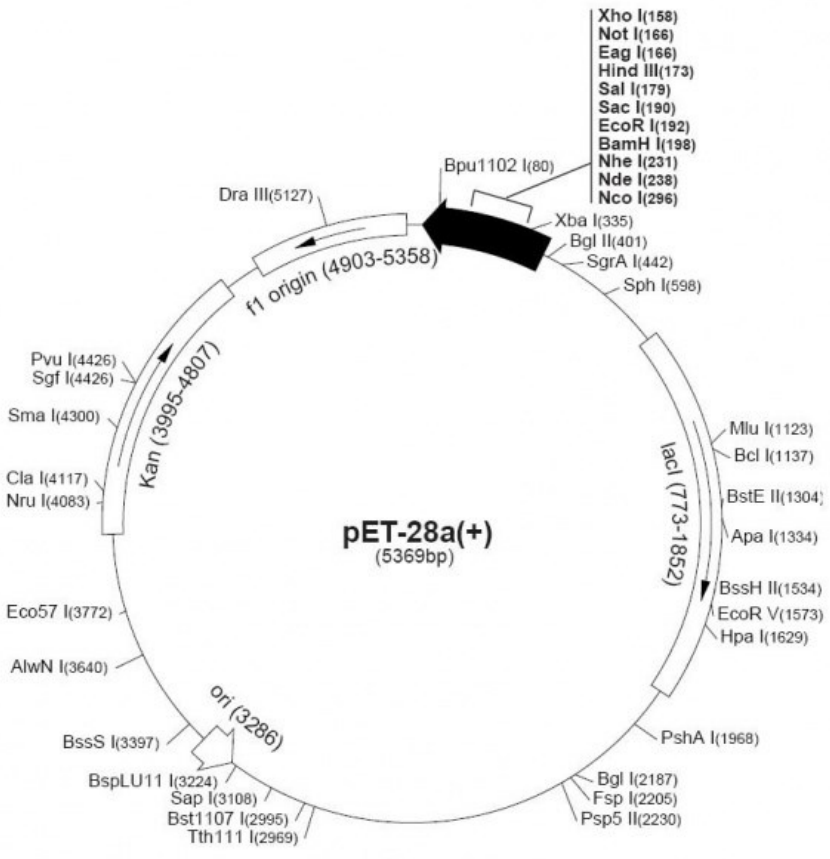

Figure 9.1 Vector map of pET-28a(+). Image provided by Novagen.

9.1.8. Microorganism strains

- ***E. coli* NEB 5-alpha** (*New England BioLabs*)

  For plasmid amplification in bacterial hosts *E. coli* NEB 5-alpha cells were used. This strain is known for high transformation efficiency and is widely used for cloning unmethylated PCR products.

  Genotype: fhuA2 a(argF-lacZ)U169 phoA glnV44 a80a(lacZ)M15 gyrA96 recA1 relA1 endA1 thi-1 hsdR17

- ***E. coli* BL21 (DE3)** (*New England BioLabs*)

  For protein expression, the *E. coli* BL2 (DE3) strain was employed. It is suitable for expression of genes from any T7 promoter-based expression vector. T7 RNA polymerase expression can be induced by the presence of lactose.

  Genotype: fhuA2 [lon] ompT gal (λ DE3) [dcm] ΔhsdS λ DE3 = λ sBamHIo ΔEcoRIB int::(lacI::PlacUV5::T7 gene1) i21 Δnin5

9.2. Standard operating procedures (SOPs)

9.2.1. Laboratorial and analytical techniques

SOP 1: Lyophilization

(Residual) water was removed from products and reaction intermediates as well as from bacterial cells and enzymes by freeze-drying. Herein, the aqueous sample was submitted to a round-bottom flask without exceeding more than half of its volume. The flask was immersed into liquid nitrogen upon continuous rotation until the sample was evenly frozen prior to placement onto the lyophilizer for 48 h.

SOP 2: High performance liquid chromatography (HPLC) measurements

For reverse phase HPLC measurements, an XbridgeTM C18 column (pore size: 3.5 μm, 3 x 150 mm) from *Waters* (Milford, USA) was used as stationary phase. The mobile phase contained water + 0.1% formic acid (solvent A) and acetonitrile + 0.1% formic acid (solvent B). The standard flow rate was set to 0.400 mL/min and the measurements were conducted at 40 °C.
Reaction samples were directly analyzed after dilution in MeOH (25-50 μL sample in 1 mL MeOH) and removal of precipitates via centrifugation.
Samples containing molecules without chromophores were derivatized prior to injection to the HPLC. For this purpose, the samples (10 -25 μL) were treated with an *O*-benzylhydroxylamine hydrochloride solution in pyridine (see Table 9.1) at 50 °C for 1 h. After dilution in MeOH (1 mL) and centrifugation, the supernatant was submitted to the HPLC.
For chiral HPLC measurements, a DaiCel Chiralpak IB column (4 × 250 mm) was used with cyclohexane/*iso*-propanol as mobile phase.

SOP 3: Gravity column chromatography

Gravity column chromatography was performed utilizing *silica gel 60* of 0.063 – 0.2 mm size (*Roth*) as stationary phase. The silica gel was dissolved in the apolar solvent and stirred until

homogeneous and gas-free. A column was slowly filled with the wet silica gel, which was then left to completely settle upon outflow of excess solvent. The product was either dissolved and directly pipetted onto the column or submitted as dry load bound on silica. A solvent gradient from apolar to polar was applied to elute the compounds.

SOP 4: Flash column chromatography

Flash column chromatography was performed employing a CombiFlash EZ Prep system from *Teledyne ISCO*, utilizing silica gel 60 of 0.04 – 0.063 mm size (*Roth*) as stationary phase. Herein, the column was manually prepared by subsequently filling small portions of dry silica upon bouncing the tube between each addition to guarantee a dense packing. The column was conditioned with the apolar solvent and the product was submitted onto the precolumn as dry load on silica. Elution was started and monitored over the software. Product fractions were detected via UV or ELS. Fractions containing the desired product were automatically collected.

SOP 5: Preparative thin layer chromatography (TLC)

Purification of small product amounts (10 – 50 mg) was achieved by preparative TLC. For this purpose, the sample was mixed with solvent (200 μL) and slowly and evenly subjected to the baseline of the preparative TLC plate (20 x 15 cm) using a pipette. After the solvent has fully evaporated, the TLC was placed into a chamber with the mobile phase and left to run for 30-45 minutes. After drying, the product was isolated from the plate by scratching off the product band (visualization by UV or staining of a small part of the plate) using a spatula. The silica gel containing the product was treated with EtOAc under shaking for 20 minutes. After removal of the solid by filtering, the organic solvent was evaporated to yield the product.

9.2.2. Molecular biology techniques

SOP 6: Site-directed (saturation) mutagenesis

Mutagenesis of the *Lb*KRED gene was achieved utilizing the QuikChange II Site-Directed Mutagenesis Kit by *Agilent* according to the manufacturer's protocol, and employing the pET-28a(+) vector featuring the gene for the native enzyme as DNA template. The general constitution of the reaction mixtures (25 μL total volume in standard 200 μL PCR vessels) is listed in Table 9.4 in the correct pipetting order. All pipetting steps were performed on ice. The thermocycler was preheated to 95 °C before adding the DNA polymerase as the last component. The temperature program applied during the amplification cycles is summarized in Table 9.5.

Table 9.4 constitution of the PCR mixtures.

Component	**Volume** [µL]
10 x reaction buffer	2.5
Plasmid	0.25 (5 ng)
Primer-forward	1 (50 ng)
Primer-reverse	1 (50 ng)
dNTP Mix (20 mm)	2.5
Sterilized H2O	17.5
pFU DNA polymerase (2.5 U/µL)	0.25

Table 9.5 Temperature program of PCR.

Segment		**Cycles**	**T** [°C]	**Time**
Initial denaturalization		1	95	2 min
Amplifi-cation	Denaturalization	16	95	20 sec
	Annealing		55	1 min
	Polymerization		68	1 min
Final extension		1	68	5 min

In order to remove parental (non-mutated) plasmids after the reaction, the mixtures were treated with the DpnI restriction enzyme (10 U, 1 μL) upon addition of buffer (5 μL) and sterilized water (19 μL) and incubated at 37 °C for 35 min on a shaker. Agarose gel electrophoresis (SOP 8) was used to verify a successful amplification outcome.

SOP 7: Isolation and purification of plasmid DNA (Miniprep)

Extraction of plasmid DNA was performed utilizing the commercial GenElute Plasmid Miniprep Kit from *Sigma-Aldrich* following the manufacturer's protocol. The principle is based on alkaline lysis. An *E. coli* overnight culture (3 mL) was centrifuged at 12000 x g for 1 min and the supernatant was discarded. The pellet was resuspended in the residual medium, following by addition of lysis buffer (200 μL) and gentle mixing by inverting the vessel 6-8 times. The mixture was incubated at room temperature for 3-5 minutes until a clear solution was obtained. Neutralizing buffer (350 μL) was added and the tube was gently inverted 3-4 times. The mixture was then centrifuged at 12000 x g for 10 min to remove cell debris. The supernatant (500 μL) was loaded onto a miniprep binding column, which was then placed into a microcentrifuge tube, and was centrifuged at 12000 x g for 1 minute. The flow-through was discarded and the column treated with two washing steps (500 μL and 750 μL wash solution, respectively, 12000 x g for 1 min, each). After the binding column was transferred to a fresh collection tube, elution buffer (30 μL) was added and the tube was again centrifuged at 12000 x g for 1 min. The plasmid was either directly used for DNA sequencing or transformation into E. coli BL21 cells, or otherwise stored at -20 °C for later purpose.

SOP 8: Agarose gel electrophoresis

Analysis of plasmids or PCR products was performed by agarose gel electrophoresis. For the preparation of the agarose gel (0,7%), agarose (350 mg) was mixed with TBE (0.5x, 50 mL) in a beaker and heated in the microwave oven until fully dissolved. The solution was left to cool down to approximately 50 °C, after which one drop of an ethidium bromide solution (0,5 mg/mL) was added. The gel was casted into a gel chamber (Wide Mini-Sub Cell GT System from *Bio-Rad*) and left to polymerize. TBE buffer was added to the chamber until the gel was fully covered. 2.0-2.5 μL of each DNA sample was mixed with 2 μL Gel Loading Dye (Purple, 6X, *NEB*) and filled up to 10 μL with nuclease-free water. The samples (10 μL) and a DNA standard mix (1 μL, Quick-Load® 1 kb DNA Ladder) were applied to the agarose gel pockets. The electrophoresis was performed at a voltage of 90 V for approximately 30 min. Visualization of the DNA bands was achieved under UV-light.

SOP 9: Plasmid transformation

Preparation of competent cells

Electrocompetent cells were obtained by growing an overnight culture of BL21 cells in LB medium (1.6 mL) at 37 °C. Fresh LB/Tet (12.5 μg/mL) medium (1.6 mL) was inoculated with the overnight culture (35 μL), which was then left to grow until an OD_{600} of 0.4 – 0.6 was reached. Afterwards, the cells were centrifuged at 10.000 rpm and the supernatant was discarded. Centrifugation was repeated and residual medium carefully removed with a pipette. The cells were washed with HEPES buffer (1.5 mL, 1 mM, pH 7.0,) and centrifuged at 10.000 rpm. The supernatant was removed and the pellet was resuspended in HEPES buffer

(50 μL,1 mM, pH 7.5). If the cells were not directly used for transformation, they were stored at -80 °C for later purpose.

Transformation of electro competent cell

For transformation, a cooled 2 mm cuvette was filled with the electrocompetent *E. coli* cells (50 μL, thawed on ice for 10 min), to which plasmid solution (1 μL), obtained from plasmid preparation, was added. The transformation step was executed by applying a 2.5 kV program using an electroporator (ECM 399 from *BTX*). The transformed cells were immediately transferred into pretempered (37 °C) SOC medium (950 μL) and left to regenerate in a vented Eppendorf vessel at 37 °C for 60 minutes. Part of the cells (100 μL) were then plated on an LB/Kan agar plate and incubated at 37 °C overnight to monitor the transformation efficiency. The remaining cell suspension (900 μL) was centrifuged at 4000 x g for 5 min and the supernatant was discarded. The pellet was resuspended in LB/Kan medium (100 μL) and again plated on an LB/Kan agar plate and incubated at 37 °C overnight. 95 single colonies were picked and transferred to a 96-well plate containing LB/Kan medium (200 μL per well). One well was inoculated with the *E. coli* BL21 wildtype plasmid as control. The plate was sealed with a perforated acetate foil and placed on a shaker at 37 °C overnight. For storage at -80°C, glycerol (85%, 35 μL) was added to each well.

Transformation by heat shock

Commercial NEB 5α Competent *E. coli* cells (NEB) (50 μL) were thawed on ice. The vector DNA (1 μL) was added and gently mixed by inverting the tube 4-5 times prior to incubation on ice for 30 minutes. A heat shock was applied for 30 seconds at 42 °C followed by incubation for another 5 minutes on ice. For regeneration, SOC medium (950 μL) was added and the mixture was incubated at 37 °C and 250 rpm for 60 minutes. The cells (100 μL) were finally plated on a preheated (37 °C) LB agar plate and incubated at 37 °C overnight to monitor the transformation efficiency. The remaining cells (900 μL) were centrifuged at 4000 rpm for 5 min and the supernatant was discarded. The cell pellet was resuspended in the residual medium, from which an overnight culture in LB-medium (3 mL) containing kanamycin (50 μg/mL) was inoculated and used for plasmid preparation.

SOP 10: Protein expression, lysis and purification

Protein expression on large scale

A sterile cultivation flask was filled with AI medium to which ampicillin/kanamycin (1 mL/L medium) and antifoam (1 mL/L medium) were added. The mixture was then inoculated with frozen cells using a toothpick and the flask was sealed with aluminium foil. Incubation was carried out in a shaker at 37 °C and 210 rpm for 22 h. The cell culture was then centrifuged at 4000 rpm for 30 min, after which the supernatant was discarded. The cell pellets were resuspended in phosphate buffer (20 mM, pH 7.5, 200 mL/1 L culture) and freeze-dried to yield resting cell powder or kept at -20 °C prior to lysis.

Cell lysis

Three different methods were used for cell lysis:

A) For lysis by lysozyme, the cells were thawed at room temperature, after which lysozyme (0.5 mg/mL pellet-buffer suspension) and DNAse (1 μL from DNAse stock solution [1 mg/mL] per mL pellet-buffer suspension) were added. The suspension was left to stir at 37 °C for 1 h. A solution of NaCl (5 M, 200 μL per mL cell suspension) and phosphate wash-buffer (800 μL/mL cell suspension) were added.
B) For lysis by sonication, the cells were thawed at room temperature and the suspension was treated with a sonotrode by applying ultra-sound beams at 20 kHz in an interval of 1.5 s for 5 min. After cell disruption, DNase (1 μL of DNAse stock solution [1 mg/mL] per mL pellet-buffer suspension) was added and the suspension was kept shaking at 37 °C for 1 h.
C) For hypotonic extraction, the frozen cell pellets were resuspended in ice-cold Tris buffer (1 mL/mL cells, 10 mM, pH 7.4) by vortexing and incubated on ice for 10 min.

In all cases, the resulting cell suspension was then centrifuged at 4000 rpm for 45 min and the cell supernatant was collected and freeze-dried for 48 h to give powdered cell-free extract or further purified by column purification.

Protein purification by affinity chromatography (IMAC)

Recombinant proteins containing a terminal sequence of polyhistidines (His-tag) can be purified by affinity chromatography. The principle is based on the histidine's ability to strongly coordinate metal ions, e.g. nickel.

For this purpose, the IMAC affinity column was first equilibrated with phosphate wash-buffer. The CFE solution was treated with a solution of imidazole (5 M) to give a final concentration of 30 mM (6 μL/mL CFE mixture) prior to loading onto the column. The column was washed with 10 column volumes of imidazole IMAC buffer and phosphate wash buffer, respectively. The protein of interest was finally eluted with phosphate wash-buffer containing EDTA (50 mM) as chelating agent until completion (BRADFORD-test). The enzyme solution was concentrated by ultrafiltration and freeze-dried to give purified protein powder. The column was regenerated by treatment with one column volume of $NiSO_4$-solution (100 mM) and five column volumes of IMAC wash buffer.

Protein expression on 96-well format (for library screening)

A 96-deep-well plate (MegaBlock, *Sarstedt*) was filled with AIM/kan (800 μL/well). Each well was inoculated with frozen cells from the mutant library. The plate was sealed with a perforated acetate foil and placed on a shaker at 37 °C overnight. The cells were then harvested by centrifugation at 4000 rpm for 15 minutes upon discarding of the supernatant and resuspending in washing buffer (200 μL). For screening, the cell suspensions were transferred to 96-well flat bottom plates (*Sarsted*) (100 μL per well).

9.2.3. Protein analysis

SOP 11: Sodium dodecyl sulfate–polyacrylamide gel electrophoresis (SDS-PAGE)

SDS-PAGE is a method to separate proteins by their molecular weight on a polymer gel and is used for the qualitative analysis of protein samples.

In this work, 10 % acrylamide/bis-acrylamide gels were used with the compositions listed in Table 9.6. The samples were prepared by homogenizing the protein solutions/suspensions (15 μL) in SDS-PAGE loading buffer (45 μL) in an Eppendorf vessel. The proteins were then denatured by applying a heat shock at 95 °C for 5 min (heat block). The protein mixtures (10 μL) were loaded into the wells of the gel along with a protein weight marker (Blue Prestained Protein Standard, Broad Range, *NEB*). The electrophoresis chamber was filled with SDS-PAGE electrophoresis buffer and an electric field of 200 V was applied until the bromophenol blue band reached the bottom of the gel. To visualize the different protein bands, the gel was treated with a solution of *Coomassie Brilliant Blue* dye upon microwaving for 30 s. Afterwards, the gel was left to shake at room temperature until an appropriate staining was achieved and the staining solution was discarded. The gel was then covered with water, again heated up for 30 s, and left to shake until the background was decolorized to generate well observable bands.

Table 9.6 Composition of SDS-PAGE

Composition	Amount
TRIS (760 mM, pH 7.4)	1 mL
Serine (1 M, pH 7.4)	1 mL
Glycine (1 M, pH 7.4)	1 mL
Asparagine	132 mg
Acrylamide (30%)	2.75 mL
Bis-acrylamide (2%)	1.16 mL
APS (10%)	60 µL
TEMED	10 µL
H_2O	3 mL

SOP 12: Qualitative analysis of protein samples - BRADFORD-test

The BRADFORD-test was used during protein purification for quick analytical assessment of residual protein amounts within eluted fractions. The principle is based on a colorimetric blue shift upon binding of the dye Coomassie Brilliant Blue G-250 to protein.
To perform the assay, the sample fraction (1-10 µL) was pipetted to a solution of BRADFORD reagent (1 : 4 dilution in H_2O, 50 μL, *Bio-Rad*) on a ceramic spot plate. Formation of a blue color corresponds with protein content.

SOP 13: Quantitative analysis of protein samples - Bicinchoninic Acid (BCA) Assay

The BCA assay is a colorimetric, analytical procedure for the accurate measurement of total protein concentrations. It relies on the reduction of copper(II)sulfate by peptide bonds and releasing the Cu^{1+}-species, which forms a purple-colored complex with two molecules of bicinchoninic acid.
The assay was performed using a commercial kit (*Thermo Scientific*) following the manufacturer's protocol: The assay solution was prepared by mixing 50 parts of bicinconic acid solution (A) with 1 part of copper sulfate solution (B). A dilution series, containing bovine serum albumin (BSA) as a standard was prepared from an aqueous BSA stock (1 mg BSA/mL, 0.15 M NaCl, 0.05% sodium azide) according to Table 9.7.

Table 9.7 Concentrations of BSA solutions.

Conc. *[µg/mL]*	V(BSA stock) *[µL]*	V(buffer) *[µL]*
0	-	100
200	20	80
400	40	60
600	60	40
800	80	20
1000	100	-

Analytical protein samples were prepared by dissolving the proteins in buffer (0.5 – 1 mg/mL). The assay was performed by filling a flat-bottom 96-well plate with the assay solution (200 μL per well) and quickly adding the protein solutions (25 μL) upon careful mixing. The plate was sealed with an acetate foil and left to incubate at 37 °C for 30 min on a shaker. Absorbance was measured at 562 nm using a plate reader.

SOP 14: T_m-measurements via nanoDSF

For determination protein melting temperatures, the Prometheus NT.48 instrument (*NanoTemper Technologies*) was used. Protein samples were prepared by dissolving 1 mg enzyme in 1 mL buffer solution. The glass capillaries were filled with 10 μL sample and placed on the sample holder. A temperature gradient of 1°C/min ranging between 20 to 90 °C was applied and the change in intrinsic protein fluorescence was monitored at 330 and 350 nm.

9.3. Experiments PART I

9.3.1. Screening of DERA protein panels

In each well of a 96-well plate enzyme cell free extracts (0.3 mg) were resuspended in TEA-buffer (100 μL, 50 mM, pH 7.5). Reactions were started by addition of the substrate from a buffered stock solution (10 μL) to give a final concentration of 100 mM. The plate was left to stand at room temperature for 24 h while reaction samples (10 μL) were taken after 3h, 6h, and 24h and each added to MeOH (40 μL) in a 96-well plate to precipitate the enzyme and stop the reaction. The plate was then centrifuged (15 min, 4000 rpm) and the supernatants transferred to a 96-well plate, which was submitted to the HPTLC auto-sampler. The device was programmed for spraying of 14 x 6 mm bands with 10 μL sample volumes on HPTCL silica plates (20 x 10 cm), from which two samples contained 1 mM and 2.5 mM product reference material as internal standard. The plates were developed in a solution of DMC/MeOH 10 : 1, carefully dried, and stained by dipping into anisaldehyde reagent and exposed to temperature treatment. In order to distribute the heat in a steady manner to guarantee equal staining, the plates were placed in an oven with their edges arranged on two glass rods to reduce direct surface contact as much as possible. The staining procedures were typically conducted at 120 °C and timed for 90 seconds, after which the plate was submitted to the HPTLC scanner for color density measurement.

9.3.2. Synthesis of DERA substrates

Synthesis of acetaldehyde dimer 130

4,4-dimethoxybutan-2-ol (190)

Yield: 91%
***R*$_f$-value:** 0.2 [EtOAc/Cy 1 : 3]

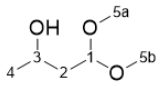

190

In a 500 mL flask, acetyl acetaldehyde dimethyl acetal (1 eq, 56.74 mmol, 7.5 g) was dissolved in MeOH (150 mL). A suspension of $NaBH_4$ (0.6 eq,34.04 mmol, 1.28 g) in H_2O (10mL) was carefully added via a syringe. The reaction mixture was left to stir in a water bath for 3 h. After completion, the mixture was concentrated under reduced pressure and the residue was diluted with H_2O (80 mL). $NaSO_4$ was added until saturated and the aqueous solution was extracted with ethyl acetate (3 x 60 mL) The combined organic layer was dried over Mg_2SO_4 and the solvent was removed under reduced pressure to yield acetal **190** as a colorless oil (6.9 g, 91 %)

^{1}H NMR (300 MHz, Chloroform-*d*) δ = 4.51 (td, *J* = 5.5, 2.1 Hz, 1H , 3-H), 3.99 – 3.82 (m, 1H, 1-H), 3.39 – 3.21 (m, 6H, 5a-, 5b-H), 2.99 (br, 1H, OH), 1.69 (m, 2H, 2H,), 1.21 – 1.04 (m, 3H, 4-H).
^{13}C NMR (75 MHz, $CDCl_3$) δ = 103.86 (C-1), 64.56 (C-3), 53.68 (C-5a), 52.89 (C-5b), 41.10 (C-2), 23.46 (C-4).

Racemic 3-hydroxybutanal (*rac*-130)

Yield: 91%
***R*$_f$-value:** 0.2 [EtOAc/Cy 1 : 3]

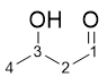

***rac*-130**

In a 25 mL flask, 3-hydroxybutanal dimethylacetal (**190**) (5.67 mmol, 500 mg) was dissolved in water (10 mL). Cation exchange resin (Dowex 50W X8, H^+ form) or HCl (5 mL, 1 N) was added and the reaction mixture was left to stir at room temperature for 3 h. After complete

deprotection (TLC), the resin was removed by filtration or the reaction mixture was neutralized with $NaCO_3$ (5 mL, 1 N). The obtained aqueous solution was directly used for enzymatic reactions. An NMR sample was measured from a reaction conducted in D_2O to verify a successful transformation.

^{1}H NMR (300 MHz, $CDCl_3$) δ = 9.76 (s, 1H, 1-H), 4.31-4.24 (m, 1H, 3-H), 2.55 (m, 2H, 2-H), 1.20 (m, 3H, 4-H).
^{13}C NMR (75 MHz, $CDCl_3$) δ = 202.54 (C-1), 42.73 (C-3), 37.34 (C-2), 23.15 (C-4).

Synthesis of *N*-(3-oxopropyl)-2-phenylacetamide (1a)

N-(3,3-diethoxypropyl)-2-phenylacetamide (108)

Yield: 83%
***R*$_f$-value:** 0.5 [EtOAc/Cy 1 : 4]

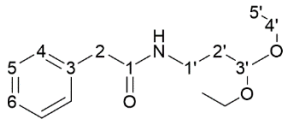

108

In a 25 mL round bottom flask, 3,3-diethoxypropan-1-amine (**105**) (476 mg, 523 μL, 3.23 mmol, 1 eq) was dissolved in a mixture of THF (5 mL) and a 2 M sodium carbonate solution (10 mL). After cooling to 4 °C, 2-phenyacetyl chloride (**104**) (500 mg, 427 μL, 3.23 mmol, 1 eq) was added dropwise and the reaction was allowed to stir at room temperature overnight.
After completion, the organic layer was separated and the aqueous phase was extracted with EtOAc (3 x 5 mL). The combined organic phase was successively washed with citric acid (5% w/v, 3 x 10 mL), $NaHCO_3$ (satd. solution, 3 x 10 mL), and brine (3 x 10 mL) and dried over $MgSO_4$. The solvent was removed under reduced pressure to yield the product as a yellow oil (710 mg, 83%).

^{1}H-NMR (300 MHz, Chloroform-d) δ = 7.28 – 7.14 (m, 5H, 4, 5, 6-H), 4.37 (t, J = 5.2 Hz, 1H, 3'-H), 3.49 (m, 2H, 2'-H), 3.46 (s, 2H, 2-H) 3.35 (dq, J = 7.0 Hz, 4H, 4'-H), 3.25 (q, J = 5.7 Hz, 2H, 2 x 1'-H), 1.72 – 1.63 (m, 2H, 2'-H), 1.04 (t, J = 7.0 Hz, 6H, 2 x 5'-H).
^{13}C-NMR (75 MHz, $CDCl_3$) δ = 170.72 (C-1), 135.05 (C-3), 129.41 (C-4), 128.88 (C-5), 127.17 (C-6), 102.27 (C-3'), 61.89 (C-4'), 43.95 (C-2), 35.58 (C-1'), 32.97 (C-2'), 15.23 (C-5').

Deprotection of N-(3,3-diethoxypropyl)-2-phenylacetamide (108)

Yield: 81%
***R*$_f$-value:** 0.33 [EtOAc/Cy 1 : 4]
Mp: 67°C

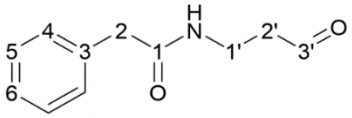

1a

In a round bottom flask acetal **108** (320 mg, 1.2 mmol) was dissolved in a mixture of THF (2 mL) and H_2O (2 mL). Dowex H^+-ion exchange (50 W8, 80 mg) was added and the reaction mixture was left to stir at room temperature for 2 h. After filtration from the resin, Na_2SO_4 was added until saturation and the mixture was extracted with EtOAc (3 x 2 mL). The combined organic phase was dried over $MgSO_4$ and removed under reduced pressure to yield a pale yellow solid (205 mg, 90%). The crude product was recrystallized from cyclohexane/ethyl acetate (8 : 1) to furnish colorless needles (185 mg, 81%).

^{1}H-NMR (300 MHz, $CDCl_3$) δ = 9.75 (s, 1H, 3'-H), 7.47 – 7.16 (m, 5H, 4-, 5-, 6-H), 3.54 (s, 2H, 2-H), 3.51 (q, J = 6.0 Hz, 2H, 2'-H), 2.69 (t, J = 5.6 Hz, 2H, 1'-H).
^{13}C NMR (75 MHz, $CDCl_3$) δ = 201.23 (C-3'), 171.21 (C-1), 134.81 (C-3), 129.33 (2 x C-4), 129.00 (2 x C-5), 127.36 (C-6), 43.70 (C-2), 43.67 (C-2'), 33.20 (C-1').

Synthesis of solistatin aldehyde 1b

N-tert-butyl-1-(2-methoxynaphthalen-1-yl)methanimine (116)

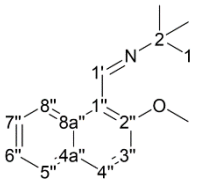

116

Yield: 93%

In a 5 mL-round bottom flask with reflux condenser, 2-methoxy-1-naphthaldehyde (**115**) (1 eq, 5 mmol, 931.04 mg) was treated with *tert*-butylamine (5 eq, 25 mmol, 2.65 mL). The reaction mixture was stirred at 100 °C overnight (mixture turns completely dark). Excess *tert*-butylamine was evaporated under reduced pressure. The residue was redissolved in DCM (20 mL) and the mixture was dried over $MgSO_4$. The solvent was removed under reduced pressure to give the product as a brown oil (1.12 g, 93%).

^{1}H NMR (300 MHz, Chloroform-*d*) δ = 9.09 (d, *J* = 9.1 Hz, 1H, H-5''), 8.97 (s, 1H, H-1'), 7.86 (d, *J* = 9.1 Hz, 1H, H-4''), 7.77 (d, *J* = 8.1 Hz, 1H, H-8''), 7.56 – 7.46 (m, 1H, H-7''), 7.37 (t, *J* = 7.5 Hz, 1H, H-6''), 7.26 (d, *J* = 9.1 Hz, 1H, H-3''), 3.97 (s, 3H, O-CH_3), 1.45 (s, 9H, H-1a, b, c).
^{13}C NMR (75 MHz, $CDCl_3$) δ = 157.39 (C-2''), 153.44 (C-1''), 132.19 (C-4a''), 131.66 (C-4''), 129.50 (C-8a''), 128.07 (C-5''), 127.69 (C-7''), 125.55 (C-6''), 123.92 (C-3''), 118.94 (C-1''), 112.96 (C-8''), 58.47 (C-2), 56.77 (O-CH_3), 30.06 (C-1).

2-Methyl-1-naphtaldehyde (112b)

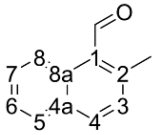

112b

Yield: 80%
***R*$_f$-value:** 0.23 [Acetone/Toluol 1:1]

To powdered $CrCl_2$ (0.1 eq, 61.45 mg, 0.5 mmol) in a Schlenck-flask was added a solution of imine **116** (1 eq, 1.21 g, 5 mmol) in dry diethyl ether (20 ml) under argon atmosphere. After stirring at room temperature for 5 min, the GRIGNARD reagent methylmagnesium bromide (3 M in Et_2O, 5 mL) was added dropwise under cooling (10 °C) and the resulting mixture was stirred at room temperature for 4 h. The reaction was quenched by addition of 3 M HCl (40 mL) and stirred for another 2 h at room temperature for hydrolysis. After completion, the mixture was extracted with EtOAc (3 x 20 mL) and the combined organic layer was dried over $MgSO_4$. The solvent was removed under vacuum to yield the crude product as brown oil (80%). Purification was performed by gravity column chromatography (DCM/MeOH).

^{1}H NMR (300 MHz, Chloroform-*d*) δ = 10.97 (s, 1H, H-C=O), 8.99 (d, *J* = 9.4 Hz, 1H, H-8), 7.94 (d, *J* = 8.4 Hz, 1H, H-5), 7.84 (d, *J* = 8.1 Hz, 1H, H-4), 7.67 – 7.60 (m, 1H, H-7), 7.51 (ddd, *J* = 8.0, 6.9, 1.1 Hz, 1H, H-6), 7.34 (d, *J* = 8.4 Hz, 1H, H-3), 2.81 (s, 3H, CH_3).
^{13}C NMR (75 MHz, $CDCl_3$) δ = 193.25 (C=O), 142.58 (C-2), 137.52 (C-4a), 134.30 (C-4), 132.48 (C-8a), 131.44 (C-1), 129.74 (C-3), 128.71 (C-7), 128.39 (C-5), 125.92 (C-6), 124.33 (8), 20.02 (CH_3).

2-((2-methylnaphthalen-1-yl)methylene)malonic acid (

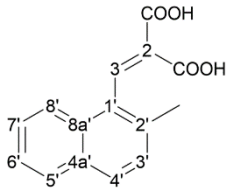

118

Yield: 78 %
***R*$_f$-value:** 0.064 [Acetone/Toluol 1:1]

In a 50 mL round bottom flask, a solution of 2-methyl-1-naphtaldehyde (**112b**) (1 eq, 5.9 mmol, 1 g) and malonic acid (**117**) (8 eq, 47 mmol, 4.90 g) in pyridine (20 mL) was heated to 50 °C. Piperidine (0.4 eq, 2.4 mmol, 200 mg) was added dropwise and the mixture was stirred at 50 °C overnight. The reaction mixture was cooled to 0 °C and poured into an ice-cold solution of concentrated hydrochloric acid in water (1:1, 10 mL). The resulting yellow suspension was extracted with EtOAc (3 x 5 mL). In order to separate from leftover starting material, the organic phase was washed with a saturated solution of $NaHCO_3$ (20 mL). The aqueous phase containing the product was acidified with conc. hydrochloric acid and again extracted with EtOAc (3 x 10 mL). The combined organic phase was dried over $MgSO_4$ and removed under reduced pressure to yield the product as a pale yellow solid (1.18 g, 78%).

^{1}H NMR (300 MHz, DMSO-*d*$_6$) *δ* = 7.98 (s, 1H, 3-H), 7.88 (dd, *J* = 6.6, 2.7 Hz, 1H, 5'-H), 7.82 (d, *J* = 8.4 Hz, 1H, 4'-H), 7.77 – 7.68 (m, 1H, 8'-H), 7.54 – 7.43 (m, 2H, 6'-, 7'-H), 7.40 (d, *J* = 8.4 Hz, 1H, 3'-H), 2.38 (s, 3H, CH_3).
^{13}C NMR (75 MHz, DMSO) *δ* = 166.32 (C-1a), 164.88 (C-1b), 140.28 (C-3), 134.04 (C-1'), 132.82 (C-2'), 131.31 (C-4a'), 130.33 (C-8a'), 130.05 (C-3'), 128.47 (C-5'), 128.03 (C-4'), 127.99 (C-7'), 126.32 (C-6'), 125.24 (C-8'), 124.82 (C-2), 20.12 (CH_3).

(*E*)-3-(2-methylnaphthalen-1-yl)acrylic acid (113b)

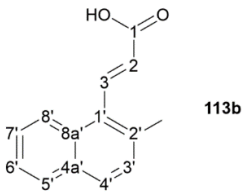

113b

Yield: 85 %
***R*$_f$-value:** 0.065 [Acetone/Toluol 1:1]

Bicarbonic acid **118** (1.5 g, 5.9 mmol) was dissolved in pyridine (50 mL), dimethylaminopyridine (10 %, 5 g) was added and the reaction mixture was stirred at 150 °C overnight. The mixture was cooled to room temperature and poured into an ice-cold solution of concentrated hydrochloric acid in water (1:1, 100 mL). The yellow suspension was extracted with EtOAc (3 x 50 mL). The combined organic layer was dried over $MgSO_4$ and removed under reduced pressure to yield the product as a pale yellow solid (85 %).

^{1}H NMR (300 MHz, Chloroform-*d*) *δ* = 10.98 (s, 1H, OH), 8.38 (d, *J* = 16.3 Hz, 1H, 3-H), 8.08 (d, *J* = 8.3 Hz, 1H, 5'-H), 7.85 (d, *J* = 7.8 Hz, 1H, 8'-H), 7.78 (d, *J* = 8.4 Hz, 1H, 4'-H), 7.60 – 7.41 (m, 2H, 6'-, 7'-H), 7.38 (d, *J* = 8.4 Hz, 1H, 3'-H), 6.33 (d, *J* = 16.3 Hz, 1H, 2-H), 2.57 (s, 3H, CH_3).
^{13}C NMR (75 MHz, $CDCl_3$) *δ* = 172.36 (C-1), 145.38 (C-3), 134.55 (C-1'), 132.25 (C-2'), 131.51 (C-8a'), 130.40 (C-4a'), 129.17 (C-3'), 129.06 (C-5'), 128.51 (C-4'), 126.90 (C-7'), 125.47 (C-6'), 124.79 (C-8'), 124.58 (C-2), 21.18 (CH_3).

3(-2-methylnaphthalen-1-yl)propan-1-ol (114b)

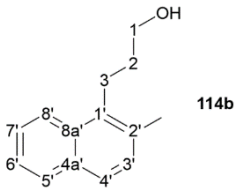

114b

Yield: 60%
***R*$_f$-value:** 0.73 [Acetone/Toluol 1:1]

To a suspension of $LiAlH_4$ (3 eq, 3 mmol, 107 mg) in anhydrous THF (5 mL) was slowly added a solution of (*E*)-3-(naphthalen-1-yl)acrylic acid (**113b**) (1 eq, 1 mmol, 200 mg) in anhydrous THF (5 mL). The resulting reaction mixture was refluxed for 3 h under argon atmosphere. After cooling to room temperature, the reaction was quenched by addition of H_2O (400 μL) and an aqueous KOH solution (15%, 400 μL). The suspension was washed with sat. aq. NH_4Cl, H_2O and brine (4 mL each) and dried over $MgSO_4$. The solvent was removed under reduced pressure to yield the product as a yellow oil (112 mg, 60%).

^{1}H NMR (300 MHz, Chloroform-*d*) δ = 7.95 (d, *J* = 8.4 Hz, 1H, 5'-H), 7.70 (d, *J* = 9.0 Hz, 1H, 8'-H), 7.53 (d, *J* = 8.4 Hz, 1H, 4'-H), 7.45 – 7.36 (m, 1H, 7'-H), 7.31 (t, *J* = 7.4 Hz, 1H, 6'-H), 7.20 (d, *J* = 8.4 Hz, 1H, 3'-H), 3.68 (t, *J* = 6.3 Hz, 2H, 1-H), 3.15 – 3.01 (m, 2H, 3-H), 2.41 (s, 3H, CH_3), 1.88 – 1.71 (m, 2H, 2-H).
^{13}C NMR (75 MHz, $CDCl_3$) δ = 135.07 (C-1'), 132.98 (C-2'), 132.61 (C-8'), 132.14 (C-8a'), 129.23 (C-3'), 128.62 (C-5'), 126.18 (C-4'), 125.91 (C-7'), 124.51 (C-6'), 123.55 (C-8'), 62.85 (C-1), 32.95 (C-2), 24.86 (C-3), 20.14 (CH_3).

3-(2-methylnaphthalen-1-yl)propanal (1b)

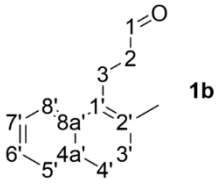

1b

Yield: 81%
***R*$_f$-value:** 0.97 [Acetone/Toluol 1:1]

In a 10 mL Schlenck-flask, PCC (1.5 eq, 0.75 mmol, 150 mg), $MgSO_4$ (0.5 g), NaOAc (1 eq, 0.5 mmol, 40 mg), and molecular sieves (400 mg) were suspended in dry DCM (4 mL) under argon atmosphere. A solution of alcohol **114b** (1 eq, 0.56 mmol, 112 mg) in dry DCM (1 mL) was slowly added and the reaction was stirred under inert gas at room temperature for 2 h (reaction mixture turns dark). After completion, the mixture was filtered through a short silica column. The solvent was removed under reduced pressure to yield aldehyde **1b** as a yellow oil (90 mg, 81%).

^{1}H NMR (300 MHz, Chloroform-*d*) δ = 9.91 (s, 1H, H-1), 7.95 (d, *J* = 8.5 Hz, 1H, 5'-H), 7.84 (d, *J* = 7.3 Hz, 1H, 8'-H), 7.67 (d, *J* = 8.4 Hz, 1H, 4'-H), 7.57 – 7.48 (m, 1H, 6'-H), 7.48 – 7.40 (m, 1H, 7'-H), 7.32 (d, *J* = 8.4 Hz, 1H, 3'-H), 3.49 – 3.34 (m, 2H, 3-H), 2.95 – 2.70 (m, 2H, 2-H), 2.52 (s, 3H. CH_3).
^{13}C NMR (75 MHz, $CDCl_3$) δ = 201.57 (C-1), 133.43(C-1'), 133.22(C-2'), 132.76(C-8a'), 131.87(C-4a'), 129.33 (C-3'), 128.92 (C-5'), 126.80 (C-4'), 126.38 (C-7'), 124.82 (C-6'), 123.08 (C-8'), 44.01 (C-3') 20.93 (C-3), 20.22 (CH_3).

Synthesis of norsolistatin aldehyde 1c

(E)-3-Naphthalene-1-yl)acrylic acid (113c)

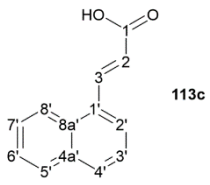

113c

Yield: 87%
***R*$_f$-value:** 0.23 [Acetone/Toluol 1:1]

In a 50 mL round bottom flask, a solution of 1-naphtaldehyde (**112c**) (1 eq, 30 mmol, 4.69 g) and malonic acid (**117**) (2 eq, 60 mmol, 6.24 g) in pyridine (20 mL) was heated to 90 °C. Piperidine (0.2 eq, 6 mmol, 510 mg) was added dropwise and the mixture was stirred for 2 h at 90 °C. After completion, the reaction mixture was cooled to 0 °C and poured into an ice-cold solution of concentrated hydrochloric acid in water (1:1, 75 mL). The resulting yellow

precipitate was filtered off and washed with cold water to yield the product as a pale yellow solid (87 %, 5.2 g).

^{1}H NMR (300 MHz, DMSO-d_6) δ = 8.40 (d, J = 15.8 Hz, 1H, 3-H), 8.18 (d, J = 8.1 Hz, 1H, 5'-H), 7.96 (dt, J = 13.6, 7.5 Hz, 3H, 2'-, 4'-, 8'-H), 7.66 – 7.49 (m, 3H, 3'-, 6'-, 7'-H), 6.60 (d, J = 15.7 Hz, 1H, 2-H).
^{13}C NMR (75 MHz, DMSO) δ = 167.38 (C-1), 140.16 (C-3), 133.23 (C-1'), 130.92 (C-4a'), 130.69 (C-8a'), 130.31 (C-3'), 128.66 (C-5'), 127.07 (C-4'), 126.23 (C-7'), 125.66 (C-6'), 125.15 (C-8'), 122.89 (C-2'), 121.83 (C-2).

3-(Naphthalen-1-yl)propan-1-ol (114c)

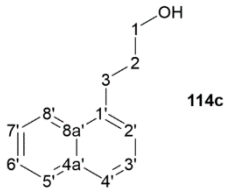

114c

Yield: 60%
***R*$_f$-value:** 0.66 [Acetone/Toluol 1:1]

To a suspension of $LiAlH_4$ (3 eq, 3 mmol, 115 mg) in anhydrous THF (5 mL) was slowly added a solution of (*E*)-3-(naphthalen-1-yl)acrylic acid (**113c**) (1 eq, 1 mmol, 200 mg) in anhydrous THF (5 mL). The resulting reaction mixture was refluxed for 3 h under argon atmosphere. After cooling to room temperature, the reaction was quenched by slow addition of H_2O (400 μL) and an aqueous KOH solution (15%, 400 μL). The resulting suspension was washed with satd. aq. NH_4Cl, H_2O and brine (4 mL each) and the organic phase was dried over $MgSO_4$. The solvent was evaporated under reduced pressure to yield the product as a yellow oil (112 mg, 60%).

^{1}H NMR (300 MHz, DMSO-d_6) δ = 8.15 – 8.02 (m, 1H, 8'-H), 7.90 (dd, J = 8.0, 1.5 Hz, 1H, 5'-H), 7.75 (dt, J = 8.0, 1.2 Hz, 1H, 4'-H), 7.58 – 7.45 (m, 3H, 3'-, 6'-, 7'-H), 7.45 – 7.27 (m, 1H, 2'-H), 3.51 (q, J = 6.2 Hz, 2H, 1-H), 3.10 - 3.05 (t, 2H, 3-H), 1.93 – 1.72 (m, 2H, 2-H).
^{13}C NMR (75 MHz, DMSO) δ = 138.31 (C-1'), 133.43 (C-8a'), 131.37 (C-4a'), 128.51 (C-3'), 126.22 (C-5'), 125.82 (C-4'), 125.80 (C-7'), 125.55 (C-6'), 125.45 (C-8), 123.70 (C-2'), 60.37 (C-1), 33.79 (C-2), 28.74 (C-3).

3-(Naphthalen-1-yl)propanal (1c)

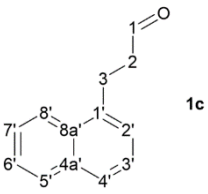

1c

Yield: 70%
***R*$_f$-value:** 0.94 [Acetone/Toluol 1:1]

In a 50 mL heat-dried Schlenck-flask, PCC (1.5 eq, 1.5 mmol, 323.34 mg), $MgSO_4$ (1 g), NaOAc (1 eq, 1 mmol, 82 mg), and molecular sieves (800 mg) were suspended in dry DCM (5 mL) under argon atmosphere. A solution of alcohol **114c** (1 eq, 1 mmol, 186.25 mg) in dry DCM (5 mL) was slowly added to the suspension and the reaction was stirred under inert atmosphere at room temperature for 3 h (reaction mixture turns dark). After completion, the mixture was filtered through a short silica column. The organic solvent was removed under reduced pressure to yield the product as a yellow oil (128 mg, 70%).

^{1}H NMR (300 MHz, Chloroform-*d*) δ = 9.78 (s, 1H, 1-H), 7.89 (d, J = 8.0 Hz, 1H, 8'-H), 7.78 (d, J = 7.4 Hz, 1H, 5'-H), 7.65 (d, J = 8.0 Hz, 1H, 4'-H), 7.47 – 7.36 (m, 2H, 3'-, 7'-H), 7.35 – 7.21 (m, 2H, 2'-, 6'-H), 3.32 (t, J = 7.6 Hz, 2H, 3-H), 2.89 – 2.71 (m, 2H, 2-H).
^{13}C NMR (75 MHz, $CDCl_3$) δ = 201.44 (C-1), 136.31 (C-1'), 133.94 (C-8a'), 131.56 (C-4a'), 128.97 (C-8'), 127.20 (C-3'), 126.16 (C-5'), 125.98 (C-4'), 125.68 (C-7'), 125.58 (C-6'), 123.26 (C-2'), 44.51 (C-3), 25.17 (C-2).

SOP for the synthesis of oxyacetaldehydes 1e-g

In a 25 mL round-bottom flask, the alcohol compound (**119**) (1 eq) was dissolved in dimethylacetamide (DMAC) (2 mL/mmol). Powdered KOH (2 eq) was added and the mixture was stirred vigorously. 2-Bromo-1,1-diethoxyethane (**120**) (1.5 eq) was added dropwise and the suspension was stirred under reflux for 3 h. The mixture was allowed to cool to room temperature prior to addition of H_2O (5 volumes) and extraction with Et_2O (3 x). The combined organic phase was washed with brine and dried over $MgSO_4$. The solvent was removed under reduced pressure to yield the acetal intermediate **121**.
Deprotection to the corresponding aldehydes **1e-g** was conducted by dissolving the acetal (925 mg, 4.4 mmol) in a mixture of THF (25 mL) and aqueous HCl (5%) (10 mL). The solution was left to stir under reflux for 3 h. After completion, water (25 mL) was added and the mixture was extracted with diethyl ether (3 x 25 mL). The combined ether phase was washed with NaOH (10%) and dried over $MgSO_4$. The solvent was removed under reduced pressure to yield the respective aldehyde product.

(2,2-diethoxyethoxy)benzene (121e)

Yield: 70%
***R*_f-value:** 0.94 [Acetone/Toluol 1:1]

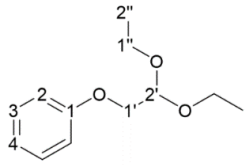

121e

^{1}H NMR (300 MHz, Chloroform-*d*) δ = 7.31 – 7.22 (m, 2H, 3-H), 6.93 (t, *J* = 8.9 Hz, 3H, 2-, 4-H), 4.83 (t, *J* = 5.2 Hz, 1H, 2'-H), 4.00 (d, *J* = 5.2 Hz, 2H, 1'-H), 3.88 – 3.50 (m, 4H, 1''-H), 1.24 (t, *J* = 7.1 Hz, 6H, 2''-H).
^{13}C NMR (75 MHz, $CDCl_3$) δ = 158.71 (C-1), 129.50 (C-3), 121.07 (C-4), 114.77 (C-2), 100.64 (C-2'), 68.62 (C-1'), 62.64 (C-1''), 15.42 (C-2'').

2-Phenoxyacetaldehyde (1e)

Yield: 80%
***R*_f-value:** 0.25 [EtOAc/Cy 1:3]

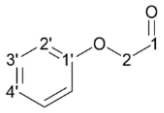

1e

^{1}H NMR (300 MHz, Chloroform-*d*) δ = 9.77 (s, 1H, 1-H), 7.32 – 7.17 (m, 2H, 3'-H), 6.97 (t, *J* = 7.4 Hz, 1H, 4'-H), 6.86 (t, *J* = 9.6 Hz, 2H, 2'-H), 4.48 (d, *J* = 0.8 Hz, 2H, 2-H).
^{13}C NMR (75 MHz, $CDCl_3$) δ = 199.34 (C-1), 157.66 (C-1'), 129.76 (C-3'), 121.95 (C-4'), 114.60 (C-2'), 72.60 (C-2).

2-(2,6-dimethylphenoxy)acetaldehyde (121f)

Yield: 87%
***R*_f-value:** 0.89 [EtOAc/Cy 1:3]

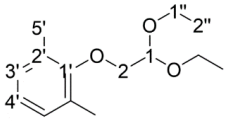

121f

1H NMR (300 MHz, Chloroform-d) δ = 7.00 (d, J = 7.4 Hz, 2H, 3'-H), 6.91 (dd, J = 8.4, 6.3 Hz, 1H, 4'-H), 4.86 (t, J = 5.2 Hz, 1H, 1-H), 3.84 (d, J = 5.2 Hz, 2H, 2-H), 3.82 – 3.60 (m, 4H, 1''-H), 2.31 (s, 6H. 5'-H), 1.27 (t, J = 7.0 Hz, 6H, 2''-H).
^{13}C NMR (75 MHz, $CDCl_3$) δ = 155.80 (C-1'), 130.91 (C-2'), 128.92 (C-3'), 123.95 (C-4'), 101.26 (C-1), 72.64 (C-2), 62.64 (C-1''), 16.38 (C-5'), 15.47 (C-2'').

2-(2,6-dimethylphenoxy)acetaldehyde (1f)

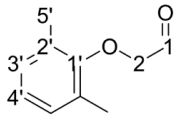

1f

Yield: 97%
***R*$_f$-value:** 0.4 [EtOAc/Cy 1:3]

^{1}H NMR (300 MHz, Chloroform-*d*) δ = 9.97 (s, 1H, 1-H), 7.11 – 6.78 (m, 3H, 2'-, 3'-, 4'-H), 4.40 (s, 2H, 2-H), 2.30 (s, 6H, 5'-H).
^{13}C NMR (75 MHz, $CDCl_3$) δ = 199.55 (C-1), 155.39 (C-1'), 130.51 (C-4'), 129.21 (C-3'), 124.69 (C-2'), 30.45 (C-2), 16.42 (C-5').

(2,2-diethoxyethoxy)cyclohexane (121g)

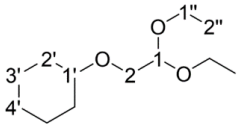

121g

Yield: 78%
***R*$_f$-value:** 0.73 [EtOAc/Cy 1:3]

(Purification by flash column chromatography (Cy/EtOAc 0 - 25%))

^{1}H NMR (300 MHz, Chloroform-*d*) δ = 4.64 (t, *J* = 5.3 Hz, 1H, 1-H), 4.05 (d, *J* = 5.3 Hz, 2H, 2-H), 3.66 (ddd, *J* = 9.3, 7.1, 2.2 Hz, 4H, 1''-H), 1.88 – 1.64 (m, 10H, 2'-, 3'-, 4'-H), 1.23 – 1.13 (m, 6H, 2''-H).
^{13}C NMR (75 MHz, $CDCl_3$) δ = 101.70 (C-1), 78.21 (C-1'), 70.26 (C-2), 62.26 (C-1''), 35.60 (C-2'), 25.54 (C-4'), 24.21 (C-3'), 15.30 (C-2'').

2-(Cyclohexyloxy)acetaldehyde (1g)

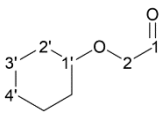

1g

Yield: 70%
***R*$_f$-value:** 0.73 [EtOAc/Cy 1:3]

(Purification by flash column chromatography (Cy/EtOAc 0 - 25%))

^{1}H NMR (300 MHz, Chloroform-*d*) δ = 9.73 (s, 1H, 1-H), 4.06 (d, *J* = 0.9 Hz, 2H, 2-H), 3.35 – 3.27 (m, 1H, 1'-H), 1.92 – 1.20 (m, 9H, 2'-, 3'-, 4'-H).
^{13}C NMR (75 MHz, $CDCl_3$) δ = 202.01 (C-1), 78.99 (C-1'), 73.85 (C-2), 32.06 (C-2'), 25.70 (C-4'), 24.03 (C-3).

Synthesis of tetrahydro-2H-pyran-2-ol (134)

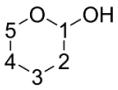

134

Yield: quantitative

In a round bottom flask, 3,4-dihydro-2H-pyran (1 eq, 2 mmol, 172 mg, 160 μL) was dissolved in water (10 mL) and indium trichloride (0.2 eq, 0.4 mmol, 88 mg) was added. The mixture was left to stir at room temperature for 16 h before extraction with DCM (3 x 5 mL). The organic layers were combined, washed with brine, dried over $MgSO_4$, and concentrated under vacuum to yield the product as a colorless fluid (204 mg, 100%).

^{1}H NMR (300 MHz, Chloroform-*d*) δ = 4.94 – 4.75 (m, 1H, 1-H), 3.99 (ddd, *J* = 11.0, 4.6, 3.1 Hz, 1H, 5-Ha), 3.87 (s, 1H, OH), 3.51 (dt, *J* = 11.6, 6.1 Hz, 1H, 5-Hb), 1.87 – 1.71 (m, 2H, 2-H), 1.55 – 1.44 (m, 4H, 3-, 4-H).
^{13}C NMR (75 MHz, $CDCl_3$) δ = 94.46 (C-1), 63.82 (C-5), 31.89 (C-2), 25.19 (C-3), 20.23 (C-4).

9.3.3. SOP 15 for DERA-catalyzed aldol reactions

Standard DERA-reactions were typically performed according to Table 9.8. If a cosolvent was applied, the substrates were first dissolved in the cosolvent prior to addition of the aqueous buffer (80% of total volume). The enzyme was reconstituted in the remaining buffer and added to the mixture as the last component.

Table 9.8 Constitution of DERA reactions.

Component	Final concentration
Acceptor substrate (1 eq)	25 – 100 mM
Donor substrate (3 eq)	75 – 300 mM
Cosolvent (DMSO/acetone)	0-10% each
Phosphate/TEA buffer	50 mM, pH 7.5
Enzyme	10 mg CFE/mL reaction volume

The substrates were typically added from 500 mM - 1M stock solutions or as solutions in DMSO to give a final concentration of 10% DMSO in case of the hydrophobic compounds and if acetone wasn't used as donor substrate. If necessary, the mixtures were sonicated for 5 min with 20 kHz beams to give macroemulsions.
Analytical reactions were carried out on 500 μL scale in Eppendorf vessels. The lids were sealed with a thermoplastic film (*Parafilm®*) to avoid evaporation of starting material or solvent. The samples were kept at room temperature on a shaker.
For preparative scales, closed reaction vessels were used to avoid evaporation. If acetaldehyde was applied as donor substrate, it was added from a 50 mM stock solution over the period of 8 h via a programmable syringe pump. If acetone was used as donor, it was directly added to give a total concentration of 10%. The reaction was left to shake at room temperature over a period of 24 h.
Reaction workup was performed by addition of two volumes of methanol and incubating the mixture at 0 °C for 20 minutes. Precipitated enzyme was removed by filtering through celite. The organic solvent was removed under reduced pressure and the aqueous layer was either extracted with EtOAc (3 x) or lyophilized to give the raw material. If necessary, the crude product was purified by (flash) column chromatography.

9.3.4. Acetone aldol products

(R)-4-hydroxyhexan-2-one (191)

Yield: 35%
***R*$_f$-value:** 0.31 [DCM/MeOH 10:1]

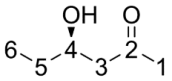

191

^{1}H NMR (500 MHz, Methanol-d_4) δ = 4.03 – 3.87 (m, 1H, 4-H), 2.59 (d, J = 7.3 Hz, 2H, 3-H), 2.19 (s, 4H, 1-H), 1.53 – 1.41 (m, 2H, 5-H), 0.94 (t, J = 7.4 Hz, 3H, 6-H).
^{13}C NMR (126 MHz, MeOD) δ = 212.08 (C-2), 70.26 (C-4), 51.33 (C-3), 49.00 (C-2), 30.99 (C-1), 10.21 (C-6).

(R)-4-hydroxyheptan-2-one (192)

Yield: 56%
***R*$_f$-value:** 0.33 [DCM/MeOH 10:1]

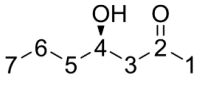

192

^{1}H NMR (500 MHz, Methanol-d_4) δ = 4.03 (p, J = 6.5 Hz, 1H, 4-H), 2.56 (d, J = 6.3 Hz, 2H, 3-H), 2.17 (s, 3H, 1-H), 1.55 – 1.31 (m, 4H, 5-, 6-H), 0.94 (t, J = 7.1 Hz, 3H, 7-H).
^{13}C NMR (126 MHz, MeOD) δ 210.87 (C-2), 68.69 (C-4), 51.95 (C-3), 40.69 (C-5), 30.80 (C-1), 19.82 (C-6), 14.42 (C-7).

(S)-4-hydroxy-4-phenylbutan-2-one (194)

Yield: 4%
***R*$_f$-value:** 0.40 [DCM/MeOH 10:1]

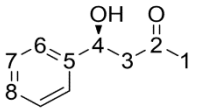

194

^{1}H NMR (300 MHz, DMSO-d_6) δ = 7.40 – 7.06 (m, 5H, 6-, 7-, 8-H), 5.53 (br, 1H, OH) 4.96 (dt, J = 8.6, 4.2 Hz, 1H, 4H), 2.83 – 2.37 (m, 2H, 3-H), 2.08 (s, 3H, 1-H).
^{13}C NMR (75 MHz, DMSO) δ = 206.85 (C-2), 145.25 (C-5), 128.06 (C-8), 126.88 (C-7), 125.69 (C-6), 68.96 (C-4), 52.95 (C-3), 22.99 (C-1).

4-hydroxy-6-phenylhexan-2-one (195)

Yield: 42%
***R*$_f$-value:** 0.30 [Cyclohexane/EtOAc 2:1]

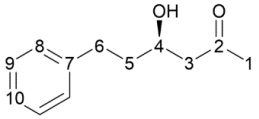

195

^{1}H NMR (300 MHz, Chloroform-d) δ = 7.43 – 7.18 (m, 5H, 8-, 9-, 10-H), 4.10 (tt, J = 8.4, 4.3 Hz, 1H, 4-H), 2.98 – 2.57 (m, 4H, 3-, 6-H), 2.20 (s, 3H, 1-H), 1.97 – 1.62 (m, 2H, 5-H).
^{13}C NMR (75 MHz, $CDCl_3$) δ = 209.88 (C-2), 141.89 (C-7), 128.52 (C-9), 128.48 (C-8), 125.94 (C-10), 66.90 (C-4), 50.04 (C-3), 38.09 (C-5), 31.81 (C-6), 30.78 (C-1).

(S,E)-4-hydroxy-6-phenylhex-5-en-2-one (196)

Yield: 2%
***R*$_f$-value:** 0.32 [DCM/MeOH 10:1]

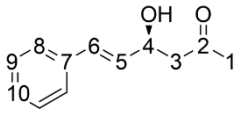

196

^{1}H NMR (500 MHz, Chloroform-d) δ = 7.23 – 6.85 (m, 5H, 8-, 9-, 10-H), 6.38 (d, J = 15.9 Hz, 1H, 6-H), 5.94 (dd, J = 15.9, 6.1 Hz, 1H, 5-H), 4.50 (q, J = 6.7 Hz, 1H, 4-H), 2.50 (d, J = 6.0 Hz, 2H, 3-H), 1.93 (d, J = 24.2 Hz, 3H, 1-H).
^{13}C NMR (126 MHz, $CDCl_3$) δ = 208.99 (C-2), 136.66 (C-7), 130.61 (C-6), 130.24 (C-5), 128.71 (C-8), 127.89 (C-10), 126.64 (C-9), 68.62 (C-4), 50.12 (C-3), 30.98 (C-1).

(R)-N-(3-hydroxy-5-oxohexyl)-2-phenylacetamide (197)

Yield: 82%
***R*$_f$-value:** 0.56 [acetone/toluol 5:1]

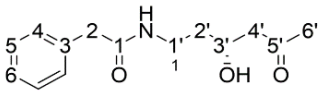

197

^{1}H NMR (300 MHz, Chloroform-d) δ = 7.49 – 7.15 (m, 5H, 4-, 5-, 6-H), 3.54 (s, 2H, 2-H), 3.34 (q, J = 6.4 Hz, 1H, 3'-H), 3.23 – 3.05 (m, 1H, 1'-H)., 2.64 – 2.28 (m, 2H, 4'-H), 2.14 (s, 3H, 3-H), 1.76 – 1.33 (m, 2H, 2'-H).
^{13}C NMR (75 MHz, $CDCl_3$) δ = 209.42 (C-5'), 172.03 (C-1), 134.89 (C-3'), 129.52 (C-4), 129.05 (C-5), 127.41 (C-6), 65.99 (C-3'), 49.89 (C-4'), 43.78 (C-2'), 36.95 (C-2'), 35.73 (C-1'), 30.86 (C-6').

9.3.5. Acetaldehyde addition products

(4R,6R)-6-methyltetrahydro-2H-pyran-2,4-diol (acetaldehyde trimer) (*(R,R)*-125)

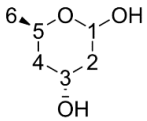

***(R,R)*-125**

Yield: 83%
***R*f-value:** 0.33 [DCM/MeOH 10:1]

^{1}H NMR (300 MHz, D_2O/DMSO 3:1) δ 6.64 (t, *J* = 2.9 Hz, 1H, 1-H, α-anomer), 6.52 (dd, *J* = 9.9, 2.4 Hz, 1H, 1-H, β-anomer), 5.87 (ddp, *J* = 12.2, 6.1, 3.0 Hz, 1H, 3-H, α-anomer), 5.75 – 5.61 (m, 1H, 5-H, β-anomer), 5.60 (p, *J* = 3.4 Hz, 1H, 5-H, α-anomer), 5.49 (dtt, *J* = 12.5, 6.3, 3.1 Hz, 1H, 3-H, β-anomer), 3.32 (ddt, *J* = 17.2, 12.1, 2.9 Hz, 2H, 2-H, β-anomer), 3.10 (dq, *J* = 13.9, 2.4 Hz, 2H, 2-H, α-anomer), 3.04 – 2.72 (m, 2H, 4-H, α+β-anomers).
^{13}C NMR (75 MHz, D_2O/DMSO 3:1) δ = 93.53 (C-1, α-anomer), 93.19 (C-1, β-anomer), 67.83 (C-5, β-anomer), 66.24 (C-3, β-anomer), 65.59 (C-5, α-anomer), 60.99 (C-3, α-anomer), 40.70 (C-2, α-anomer), 40.47 (C-2, β-anomer), 40.40 (C-4, β-anomer), 36.92 (C-4, α-anomer), 21.75 (C-6, β-anomer), 21.56 (C-6, α-anomer).

(4S,6R)-6-methyltetrahydro-2H-pyran-2,4-diol (acetaldehyde trimer) (*(S,R)*-125)

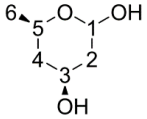

***(S,R)*-125**

Yield: 8%
***R*f-value:** 0.20 [DCM/MeOH 10:1]

^{1}H NMR (500 MHz, D_2O/DMSO 3:1) δ = 6.76 (dd, *J* = 3.8, 1.4 Hz, 1H, 1-H, α-anomer), 6.12 (d, *J* = 11.8 Hz, 1H, 1-H, β-anomer), 5.59 – 5.40 (m, 2H, 3-, 5-H, α+β-anomer), 5.23 (ddd, *J* = 15.9, 11.3, 4.7 Hz, 1H, 3-H β-anomer), 4.98 (dqd, *J* = 12.5, 6.2, 1.9 Hz, 1H, 5-H β-anomer), 3.62 – 3.51 (m, 1H, 2-H, β-anomer), 3.50 – 3.36 (m, 2H, 2-, 4-H, α-anomers), 3.32 (ddt, *J* = 12.5, 4.1, 1.9 Hz, 1H, 4-H, β-anomer), 2.88 (ddd, *J* = 12.7, 11.7, 3.6 Hz, 1H, 2-H, α-anomer), 2.63 (dd, *J* = 26.2, 6.3 Hz, 8H, 2-H, β-anomer, 4-H, α-anomer, 6-H, α+β-anomers), 2.59 – 2.42 (m, 1H, 4-H, β-anomer).
^{13}C NMR (126 MHz, D_2O/DMSO 3:1) δ = 95.22 (C-1, β-anomer), 93.35 (C-1, α-anomer), 69.80 (C-5, β-anomer), 67.36 (C-3, β-anomer), 65.64 (C-5, α-anomer), 64.08 (C-3, α-anomer), 43.44 (C-4, α-anomer), 42.69 (C-4, β-anomer), 42.57 (C-2, β-anomer), 40.13 (C-2, α-anomer), 21.86 (C-6, α-anomer), 21.68 (C-6, β-anomer).

(4R,6R)-6-((R)-2-hydroxypropyl)tetrahydro-2H-pyran-2,4-diol (acetaldehyde tetramer) (126)

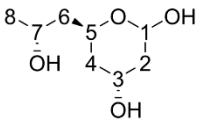

126

Yield: 4%
***R*f-value:** 0.10 [DCM/MeOH 10:1]

^{1}H NMR (300 MHz, Chloroform-*d*) δ = 5.33 (s, 1H, 1-H α-anomer), 5.20 (d, *J* = 9.8 Hz, 1H, β-anomer), 4.56 (t, *J* = 10.4 Hz, 1H, 7-H), 4.21-4.17 (m, 1H, 5-H), 4.11 – 4.00 (m, 1H, 3-h), 2.36 – 1.40 (m, 6H, 2-, 4-, 6-H), 1.22 (dd, *J* = 22.5, 4.9 Hz, 3H, 8-H).
^{13}C NMR (75 MHz, $CDCl_3$) δ = 92.61 (C-1, α-anomer), 92.40 (C-2, β-anomer), 71.69 (C-7, β-anomer), 68.50 (C-7 α-anomer), 65.27 (C-5, β-anomer), 64.63 (C-5, α-anomer), 64.14 (C-3, α-anomer), 62.64 (C-3, β-anomer), 44.47 (C-6, β-anomer), 43.94 (C-2, α-anomer), 43.74 (C-2, β-anomer), 39.64 (C-4, β-anomer), 38.70 (C-6, α-anomer), 35.10 (C-4, α-anomer), 23.80 (C-8, β-anomer), 23.49 (C-8, α-anomer).

6-(chloromethyl)tetrahydro-2H-pyran-2,4-diol (198)

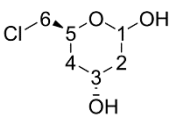

198

Yield: 78%
***R*f-value:** 0.24 [DCM/MeOH 10:1]

^{1}H NMR (300 MHz, Chloroform-*d*) δ = 5.36 (s, 1H, 1-H, β-anomer), 5.19 (d, *J* = 11.7 Hz, 1H, α-anomer), 4.82 (d, *J* = 4.6 Hz, 1H, OH), 4.48 (dtd, *J* = 12.2, 5.1, 2.6 Hz, 1H, 3-H, β-anomer), 4.35 (p, *J* = 3.0 Hz, 1H, 5-H, α-anomer), 4.26 (s, 1H, 5-H, β-anomer), 4.15 (dtd, *J* = 11.0, 5.4, 2.5 Hz, 1H, 3-H, α-anomer), 3.57 (dt, *J* = 5.9, 2.6 Hz, 2H, 6-H), 2.06 – 1.46 (m, 4H, 2-, 4-H).
^{13}C NMR (75 MHz, $CDCl_3$) δ = 93.15 (C-1, β-anomer), 92.66 (C-1, α-anomer), 70.62 (C-5, β-anomer), 64.98 (C-3, β-anomer), 64.61 (C-5, β-anomer), 63.35 (C-3, β-anomer), 50.75 (C-6, β-anomer) 47.86 (C-6, α-anomer), 47.15 (C-2, α-anomer), 39.41 (C-2, β -anomer), 35.49 (C-2, β-anomer), 35.23 (C-4, α-anomer), 34.92 (C-4, β-anomer).

PhAc-protected lactol (3a)

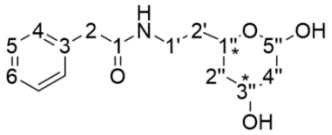

3a

Yield: 72-88%
***R*$_f$-value:** 0.46 [DCM/MeOH 10:1]

Diastereomer 1 *(R,R-x)*

^{1}H NMR (300 MHz, Chloroform-*d*) δ = 7.33 – 7.08 (m, 5H, 4-, 5-, 6-H), 4.96 (s, 1H, 5''-H), 4.16 (dd, *J* = 13.4, 5.9 Hz, 1H, 3''-H), 3.44 (s, 2H, 2-H), 3.35 (dt, *J* = 12.0, 6.1 Hz, 1H, 1''-H), 3.23 – 3.03 (m, 2H, 1'-H), 1.90 – 1.25 (m, 6H, 2'-, 2''-, 4''-H).
^{13}C NMR (75 MHz, $CDCl_3$) δ = 171.77 (C-1), 134.97 (C-3), 129.56 (C-4), 128.92 (C-5), 127.28 (C-6), 92.57 (C-5''), 64.67 (C-1''), 61.75 (C-3''), 43.79 (C-4''), 38.01 (C-2), 37.33 (C-2''), 35.12 (C-1), 34.50 (C-2').

Diastereomer 2 *(S,R)*

^{1}H NMR (500 MHz, Chloroform-*d*) δ 7.33 – 7.12 (m, 5H, 4-, 5-, 6-H), 5.05 (s, 1H, 5''-H), 4.05 – 3.95 (m, 1H, 3''-H), 3.46 (s, , 2H, 2-H), 3.34-3.39 (1H, 1''-H), 3.21 – 2.91 (m, 2H, 1'-H), 2.02 – 1.33 (m, 6H, 2'-, 2''-, 4''-H).
^{13}C NMR (126 MHz, $CDCl_3$) δ = 171.78 (C-1), 135.16 (C-3), 129.70 (C-4), 129.00 (C-5), 127.40 (C-6), 92.37 (C-5''), 66.56 C-1'', 63.31 (C-3''), 43.87 (C-4''), 41.03 (C-2), 39.37 (C-2''), 37.39 (C-1), 34.72 (C-2').

Solistatin lactol (3b)

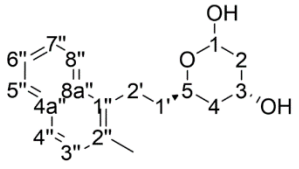

3b

Yield: 14%
***R*$_f$-value:** 0.46 [cyclohexanol/EtOAc 1:1]

^{1}H NMR (300 MHz, Chloroform-*d*) δ = 8.03 (d, *J* = 8.4 Hz, 1H, 8''-H), 7.75 (d, *J* = 7.9 Hz, 1H, 5''-H), 7.57 (d, *J* = 8.3 Hz, 1H, 4''-H), 7.39 (dt, *J* = 25.6, 7.0 Hz, 2H, 6''-, 7''-H), 7.22 (d, *J* = 5.7 Hz, 1H, 3''-H), 5.49 – 5.30 (m, 1H, 1-H), 4.47 – 4.32 (m, 1H, 3-H), 4.19 (s, 1H, 5-H), 3.37 – 2.99 (m, 2H, 2'-H), 2.03 – 1.45 (m, 6H, 1''-, 2-, 4-H).
^{13}C NMR (75 MHz, $CDCl_3$) δ = 135.39 (C-1''), 133.08 (C-8a''), 132.70 (C-4a''), 132.23 (C-2''), 129.37 (C-3''), 128.71 (C-5''), 126.23 (C-4''), 125.91 (C-7''), 124.59 (C-8''), 123.81 (C-6''), 93.12 (C-1), 65.18 (C-5), 62.81 (C-3), 38.30 (C-2), 36.01 (C-1'), 35.42 (C-4), 24.57 (C-2''), 20.21 (CH_3).

Norsolistatin lactol (3c)

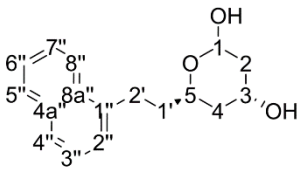

3c

Yield: 17%
***R*$_f$-value:** 0.45 [cyclohexanol/EtOAc 1:1]

^{1}H NMR (300 MHz, Chloroform-*d*) δ = 8.08 (d, *J* = 7.7 Hz, 1H, 2''-H), 7.85 (d, *J* = 8.9 Hz, 1H, 5''-H), 7.70 (d, *J* = 7.5 Hz, 1H, 6''-H), 7.57 – 7.43 (m, 21H, 3''-, 4''-H), 7.43 – 7.33 (m, 2H, 7''- 8''-H), 5.39 (d, *J* = 3.1 Hz, 1H, 1-H, α-anomer), 5.17 (dd, *J* = 9.8, 2.2 Hz, 1H, 1-H, β-anomer), 4.42 – 4.31 (m, 1H, 3-H, α-anomer), 4.31 – 4.27 (m, 1H, 5-H, β-anomer), 4.24 – 4.18 (m, 1H, 5-H, α-anomer), 3.99 (ddt, *J* = 11.1, 8.3, 3.1 Hz, 1H, 3-H, β-anomer), 3.21 (dddd, *J* = 55.4, 13.9, 10.6, 6.2 Hz, 2H, 2'-H,), 2.04 – 1.49 (m, 6H, 1'-, 2-, 4-H).
^{13}C NMR (75 MHz, $CDCl_3$) δ = 138.42 (C-1''), 134.01 (C-1a''), 131.96 (C-5a''), 128.88 (C-2''), 126.71 (C-5''), 126.14 (C-7''), 125.83 (C-3''), 125.70 (C-4''), 125.54 (C-6''), 123.98 (C-8''), 93.05 (C-2), 65.10 (C-6), 62.42 (C-4), 38.34 (C-3), 37.07 (C-5), 35.61 (C-1'), 28.87 (C-2').

(*4R,6R*)-6-phenethyltetrahydro-2H-pyran-2,4-diol (3d)

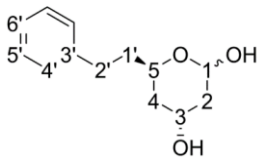

3d

Yield: 23%
***R*f-value:** 0.52 [acetone/toluol 1:1]

^{1}H NMR (300 MHz, Chloroform-*d*) δ = 7.43 – 7.02 (m, 5H, 4'-, 5'-, 6'-H), 5.34 (s, 1H, 1-H, β-anomer), 5.14 (d, *J* = 8.9 Hz, 1H, α-anomer), 4.49 – 4.10 (m, 2H, 3-, 5-H), 2.95 – 2.55 (m, 2H, 2'-H), 2.14 – 1.39 (m, 6H, 1'-, 2-, 4-H).
^{13}C NMR (75 MHz, $CDCl_3$) δ = 142.19 (C-3'), 128.53 (C-4'), 128.47 (C-5'), 125.90 (C-6'), 92.99 (C-1, β-anomer), 92.50 (C-1, α-anomer), 69.87 (C-5 α-anomer), 65.09 (C-3, α-anomer) 65.07 (C-5, β-anomer), 62.23 (C-3, β-anomer), 39.95 (C-2, α-anomer), 38.26 (C-2, β-anomer), 37.92 (C-4, α-anomer), 37.70 (C-4, β-anomer), 37.53 (C-1', α-anomer), 35.41 (C-1', β-anomer), 31.86 (C-2', α-anomer), 31.77 (C-2', β-anomer).

(4R,6S)-6-(phenoxymethyl)tetrahydro-2H-pyran-2,4-diol (3e)

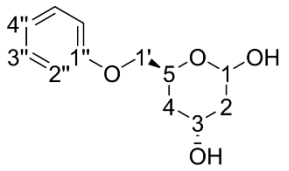

3e

Yield: 34%
***R*f-value:** 0.56 [DCM/MeOH 10:1]

^{1}H NMR (300 MHz, Chloroform-*d*) δ = 7.27 – 7.09 (m, 2H, 3''-H), 7.01 – 6.71 (m, 3H, 2''-, 4''-H), 5.33 (s, 1H, 1-H), 4.62 (dd, *J* = 14.3, 4.9 Hz, 1H, 5-H), 4.39 – 4.11 (m, 1H, 3-H), 4.07 – 3.74 (m, 2H, 1'-H), 1.99 – 1.46 (m, 4H, 2-, 4-H).
^{13}C NMR (75 MHz, $CDCl_3$) δ = 158.79 (C-1''), 129.57 (C-3''), 121.17 (C-2''), 114.77 (C-4''), 93.06 (C-1), 71.07 (C-1'), 64.58 (C-5), 62.20 (C-3), 35.09 (C-2), 34.55 (C-4).

6-((2,6-dimethylphenoxy)methyl)tetrahydro-2H-pyran-2,4-diol (3f)

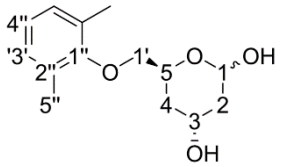

3f

Yield: 32%
***R*f-value:** 0.58 [DCM/MeOH 10:1]

^{1}H NMR (300 MHz, Chloroform-*d*) δ = 7.09 – 6.83 (m, 3H, 3''-, 4''-H), 5.44 (d, *J* = 3.1 Hz, 1H, 1-H, β-anomer), 5.27 (dd, *J* = 9.6, 2.2 Hz, 1H, 1-H, α-anomer), 4.68 (ddt, *J* = 12.2, 6.3, 3.4 Hz, 1H. 3-H, β-anomer), 4.42 – 4.38 (m, 1H, 5-H, α-anomer), 4.35 (m, 1H, 3-H, α-anomer), 4.31 – 4.25 (m, 1H, 5-H, α-anomer), 3.92 – 3.67 (m, 2H, 1'-H), 2.29 (s, 6H, 5''-H), 2.14 – 1.69 (m, 4H, 2-, 4-H).
^{13}C NMR (75 MHz, $CDCl_3$) δ = 155.50 (C-1''), 130.98 (C-2''), 128.99 (C-3''), 124.13 (C-4''), 93.12 (C-1, β-anomer), 92.59 (C-1, α-anomer), 74.87 (C-1', β-anomer), 74.56 (C-1', α-anomer), 70.04 (C-3, α-anomer), 65.23 (C-5-α-anomer), 64.70 (C-3, β-anomer), 62.80 (C-5, β-anomer), 39.72 (C-2, α-anomer), 35.16 (C-2, β-anomer), 34.59 (C-4, β-anomer), 29.81 (C-4, α-anomer), 16.36 (C-5'').

(4R,6S)-6-((cyclohexyloxy)methyl)tetrahydro-2H-pyran-2,4-diol (3g)

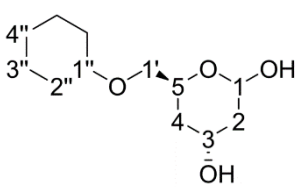

3g

Yield: 14%
***R*f-value:** 0.58 [cyclohexanol/EtOAc 1:1]

^{1}H NMR (300 MHz, Chloroform-*d*) δ = 5.31 (s, 1H, 1-H, α-anomer), 5.24 (s, 1H, 1-H, β-anomer), 4.38 (dt, *J* = 12.2, 6.2 Hz, 1H, 3-H, α-anomer), 4.32 – 4.23 (m, 1H, 3-H, β-anomer), 4.13–4.04 (m, 2H, 5'-H), 3.62 – 3.33 (m, 2H, 1'-H), 3.18 (td, *J* = 9.1, 4.0 Hz, 1H, 1''-H), 2.06 – 1.07 (m, 14H, 2-, 4-, 2''-, 3''-, 4''-H).
^{13}C NMR (75 MHz, $CDCl_3$) δ = 92.81 (C-1, α-anomer), 92.32 (C-1. β-anomer), 78.60 (C-1'', α-anomer), 78.48 (C-1'', β-anomer), 71.24 (C-1', α-anomer), 70.98 (C-1'', β-anomer), 65.01 (C-5, β-anomer), 64.56 (C-5, β-anomer), 63.32 (C-3, β-anomer), 62.87 (C-3, α-anomer), 35.15 (C-2), 34.74 (C-4), 32.14 (C-2''), 25.80 (C-4''), 24.31 (C-3'').

9.3.6. Chemical oxidation of PhAc-protected lactol 3a

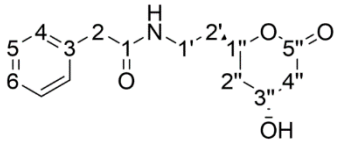

4a

Yield: 83%
***R*$_f$-value:** 0.70 [acetone/toluol 1:1]

In a reaction vessel, lactol **3a** (0.54 mmol, 150 mg) was dissolved in glacial acetic acid (720 μL). An aqueous solution of NaOCl (14% chlorine, 318 μL) was added dropwise and the reaction mixture was left to stir at room temperature for 3 h.
After completion, the mixture was neutralized with solid sodium bicarbonate and extracted with ethyl acetate (3 x 500 μL). The organic fraction was dried over $MgSO_4$ and removed under reduced pressure to yield the product as yellow oil (125 mg, 83%).

^{1}H NMR (300 MHz, Chloroform-*d*) δ = 7.42 – 7.15 (m, 5H, 4-, 5-, 6-H), 4.34 – 4.17 (m, 1H, 1''-H), 3.52 (s, 2H, 2-H), 3.35 (p, *J* = 6.6 Hz, 1H, 3''-H), 2.60 (d, *J* = 4.1 Hz, 2H, 1'-H), 2.02 – 1.41 (m, 6H,2'-, 2''-, 4''-H).
^{13}C NMR (75 MHz, $CDCl_3$) δ = 171.94 (C-1), 170.87 (C-5''), 134.93 (C-3), 129.38 (C-4), 128.98 (C-5), 127.33 (C-6), 74.32 (C-1''), 62.21 (C-3''), 43.63 (C-2), 38.44 (C-4''), 36.13 (C-1'), 35.64 (C-2''), 35.11 (C-2').

9.3.7. SOP for INT assay (96-well format)

For one assay plate, 20 mL of a INT solution in phosphate buffer was prepared (0.25 mg INT/mL buffer, 50 mM, pH 7.5). To 10 mL of the INT solution, the target alcohol (50 mg or 50 μL) was added and stirred until fully dissolved. 100 μL of the INT/alcohol solution was pipetted to each well of a 96-well plate containing enzyme (using a multi-channel pipette for whole plates) and mixed carefully to reconstitute the freeze-dried enzymes. A blank plate was prepared the same way using 100 μL of the plain INT solution for each well.
The plates were incubated at ambient temperature for up to 24 h and were inspected by holding above a white sheet of paper or analyzed using a microplate reader at 492 nm.

9.3.8. SOP for ADH-catalyzed oxidation of DERA products

Depending on each substrate, a solution of 25 – 100 mM final substrate concentration in 10% acetone in phosphate buffer (50 mM, pH 7.5) was prepared. CFE of ADH354 (30 mg/mL) and *Lb*KRED (10 mg/mL) or NOX (30 mg/mL) were added and the mixture was left to shake at room temperature for 24 h. As the CFE used here contained sufficient amounts of cofactor, no additional $NADP^+$ was required. After reaction completion, the enzyme was precipitated by addition of acetone (2 volumes) and removed by filtration through celite. After evaporation of acetone, the aqueous layer was extracted with EtOAc (3 x). The combined organic layer was dried over $MgSO_4$ and the solvent was evaporated to yield the lactone product. Table 9.9 lists the concentrations applied for each substrate.

Table 9.9 Substrate concentrations applied in KRED-catalyzed oxidation reactions.

Substrate	C [mM]	Substrate	C [mM]
Solistatin	25	Phenoxy	100
Norsolistatin	25	Cyclohexyloxy	100
Phenyl	100	PhAc	100
Dimethylphenoxy	100		

Solistatin (4b)

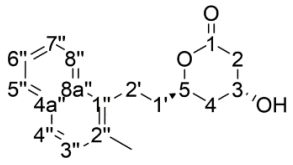

4b

Yield: 70%
***R*f-value:** 0.43 [cyclohexanol/EtOAc 1:1]

^{1}H NMR (300 MHz, Chloroform-*d*) δ = 7.98 (d, *J* = 8.4 Hz, 1H, 8''-H), 7.75 (d, *J* = 7.8 Hz, 1H, 5''-H), 7.59 (d, *J* = 8.3 Hz, 1H, 4''-H), 7.52 – 7.30 (m, 2H, 6''-, 7''-H), 7.22 (d, *J* = 6.8 Hz, 1H, 3''-H), 4.91 – 4.69 (m, 1H, 3-H), 4.35 (p, *J* = 3.6 Hz, 1H, 5-H), 3.47 – 3.03 (m, 2H, 2'-H), 2.74 (dd, *J* = 17.6, 4.9 Hz, 1H, 2H), 2.46 (s, 3H, CH_3), 2.09 – 1.68 (m, 1'-, 4-H).
^{13}C NMR (75 MHz, $CDCl_3$) δ = 170.48 (C-1), 133.26 (C-1''), 132.74 (C-8a''), 132.11 (C-4a''), 129.36 (C-2''), 128.79 (C-3''), 126.57 (C-5''), 126.27 (C-4''), 124.74 (C-7''), 123.49 (C-8''), 123.49 (C-6''), 75.70 (C-5), 62.95 (C-3), 38.87 (C-2), 36.24 (C-1'), 35.82 (C-4), 24.17 (C-2''), 20.27 (CH_3).

Norsolistatin (4c)

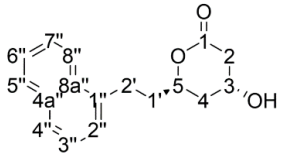

4c

Yield: 72%
***R*f-value:** 0.42 [cyclohexanol/EtOAc 1:1]

^{1}H NMR (300 MHz, Chloroform-*d*) δ = 8.04 (d, *J* = 8.0 Hz, 1H, 8''-H), 7.86 (d, *J* = 7.5 Hz, 1H, 5''-H), 7.73 (d, *J* = 7.6 Hz, 1H, 4''-H), 7.50 (pd, *J* = 6.9, 1.5 Hz, 2H, 6''-, 7''-H), 7.43 – 7.31 (m, 2H, 2'', -3''-H), 4.79 (ddt, *J* = 11.6, 8.0, 3.6 Hz, 1H, 3-H), 4.38 (p, *J* = 3.6 Hz, 1H, 5-H), 3.41 (ddd, *J* = 14.7, 9.9, 5.2 Hz, 1H, 2'-H_a), 3.17 (ddd, *J* = 14.1, 9.6, 6.8 Hz, 1H, 2'-H_b), 2.76 (dd, *J* = 17.6, 5.0 Hz, 1H, 2-H_a), 2.64 (ddd, *J* = 17.7, 3.7, 1.5 Hz, 1H, 2-H_b), 2.22 – 1.90 (m, 2H, 4-H), 1.80 (ddd, *J* = 14.5, 11.2, 3.4 Hz, 1H, 1'-H).
^{13}C NMR (75 MHz, $CDCl_3$) δ = 170.58 (C-1), 137.30 (C-1''), 134.08 (C-8a''), 131.84 (4a'-H'), 128.98 (C-8''), 127.09 (C-5''), 126.38 (C-4''), 126.14 (C-3''), 125.72 (C-7''+8''), 123.75 (C-2''), 75.36 (C-5), 62.92 (C-3), 38.81 (C-2), 36.75 (C-1), 36.25 (C-4'), 28.48 (C-2').

(4R,6R)-4-hydroxy-6-phenethyltetrahydro-2H-pyran-2-one (4d)

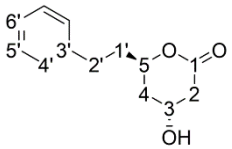

4d

Yield: 82%
***R*f-value:** 0.50 [acetone/toluol 1:1]

^{1}H NMR (300 MHz, Chloroform-*d*) δ = 7.31 – 6.90 (m, 5H, 4'-, 5', 6'-H), 4.63 (ddt, *J* = 11.4, 7.8, 3.9 Hz, 1H, 3-H), 4.28 (p, *J* = 3.7 Hz, 1H, 5H), 2.96 – 2.49 (m, 4H, 2-, 2'-H), 1.94 – 1.59 (m, 4H, 1'-, 4-H).
^{13}C NMR (75 MHz, $CDCl_3$) δ = 170.85 (C-1), 141.06 (C-3'), 128.51 (C-4'+C-5'), 126.09 (C-6'), 76.63 (C-5), 62.57 (C-3), 38.61 (C-2), 37.29 (C-4), 35.95 (C-1'), 31.12 (C-2').

(4R,6S)-4-hydroxy-6-(phenoxymethyl)tetrahydro-2H-pyran-2-one (4e)

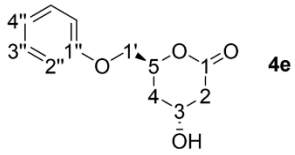

4e

Yield: 85%
***R_f*-value:** 0.52 [cyclohexanol/EtOAc 1:1]

^{1}H NMR (300 MHz, Chloroform-*d*) δ = 7.27 (td, *J* = 8.9, 8.2, 1.8 Hz, 2H, 3''-H), 7.05 – 6.79 (m, 3H, 2'', -4''-H), 5.14 – 4.97 (m, 1H, 5-H), 4.52 – 4.42 (m, 1H, 3-H), 4.20 – 4.02 (m, 2H, 1'-H), 2.81 – 2.47 (m, 2H, 2-H), 2.14 – 1.69 (m, 2H, 4-H).
^{13}C NMR (75 MHz, $CDCl_3$) δ = 170.58 (C-1), 158.48 (C-1''), 129.66 (C-3''), 121.48 (C-4''), 114.63 (C-2''), 74.38 (C-5), 69.34 (C-1), 62.49 (C-3), 38.61 (C-2), 31.97 (C-4).

(4R,6S)-6-((2,6-dimethylphenoxy)methyl)-4-hydroxytetrahydro-2H-pyran-2-one (4f)

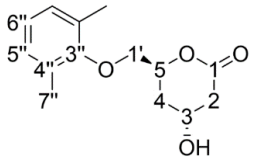

4f

Yield: 86%
***R_f*-value:** 0.53 [DCM/MeOH 10:1]

^{1}H NMR (300 MHz, Chloroform-*d*) δ = 7.08 – 6.84 (m, 3H, 3''-, 4*'-H), 5.02 (dq, *J* = 11.1, 3.9 Hz, 1H, 5-H), 4.59 – 4.44 (m, 1H, 3-H), 4.05 – 3.86 (m, 2H, 1'-H), 2.78 – 2.54 (m, 2H, 2-H), 2.27 (s, 6H, 5'-H), 2.26 – 2.11 (m, 2H, 4-H).
^{13}C NMR (75 MHz, $CDCl_3$) δ = 170.66 (C-1), 155.34 (C-1''), 131.36 (C-2''), 129.52 (C-3''), 124.82 (C-4''), 75.31 (C-5, 73.33 (C-1'), 63.19 (C-3), 39.22 (C-2), 32.43 (C-4), 16.74 (C-5'').

(3R,5S)-6-(2,6-dimethylphenoxy)-3,5-dihydroxyhexanoic acid (144)

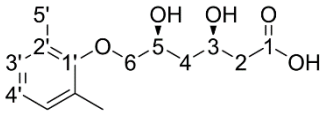

144

^{1}H NMR (300 MHz, DMSO/D_2O 1:1) δ = 7.07 – 6.77 (m, 3H, 3'-, 4'-H), 4.49 – 4.38 (m, 2H, 6-H), 3.87– 3.84 (m, 1H, 5-H), 3.63 – 3.61 (m, 2H, 3-H), 2.79 – 2.27 (m, 2H, 2-H), 2.13 (s, 6H, 5'-H), 2.07 – 1.54 (m, 2H, 4-H).
^{13}C NMR (75 MHz, DMSO/D_2O 1:1) δ = 174.26 (C-1), 154.65 (C-1'), 130.50 (C-2'), 128.75 (C-3'), 124.26 (C-4'), 75.47 (C-6), 72.84 (C-5), 65.26 (C-3), 41.55 (C-2), 29.88 (C-4), 15.35 (C-5').

(4R,6S)-6-((cyclohexyloxy)methyl)-4-hydroxytetrahydro-2H-pyran-2-one (4g)

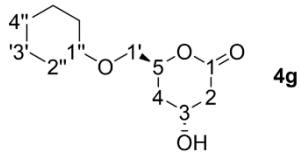

4g

Yield: 78%
***R_f*-value:** 0.54 [cyclohexanol/EtOAc 1:1]

^{1}H NMR (300 MHz, Chloroform-*d*) δ = 4.85 – 4.72 (m, 1H, 3-H), 4.48 – 4.38 (m, 1H, 5-H), 3.33 (dd, *J* = 19.3, 7.3 Hz, 1H, 1'-H), 2.82 – 2.50 (m, 1H, 1''-H), 2.07 – 1.63 (m, 1H, 2-, 4-H), 1.61 – 1.13 (m, 10H, 2''-, 3'', 4''-H).
^{13}C NMR (75 MHz, $CDCl_3$) δ = 170.25 (C-2), 78.48 (C-1''), 75.30 (C-1'), 69.64 (C-6), 62.89 (C-4), 38.93 (C-3), 32.79 (C-5), 32.16 (C-2''), 25.87 (C-4''), 24.02 (C-3'').

9.3.9. SOP 16 for enzymatic one-pot tandem cascade reactions

Reactions were conducted in 10 - 50 mL total volume. The acceptor aldehydes were added to phosphate buffer (50 mM, pH = 7.5) from stock solutions to give final concentrations of 50 – 100 mM substrate (see Table 9.9). In case of hydrophobic substrates 10% DMSO was used as cosolvent and the mixtures were sonicated for 5 min with 20 kHz beams. A solution of DERA062, ADH354 and NOX (cell free extracts) in buffer was added to give final amounts of 10, 30, and 30 mg enzyme/mL, respectively. The reactions were started by allowing a continuous feed of acetaldehyde to enter the flask via syringe pump over a period of 8 hours (2 eq from a 1 M buffered stock solution). The mixtures were left to shake at room temperature for additional 16 h. The enzymes were precipitated by addition of two volumes of methanol and incubation at 0 °C for 15 min after which the solids were removed by filtration through celite. The organic solvent was evaporated under reduced pressure and the aqueous layers were extracted with EtOAc. The combined organic layers were dried over $MgSO_4$ and the solvents were evaporated to yield the final lactone products.

9.3.10. HMG-CoA inhibition assay

The HMG-CoA inhibition assay was conducted according to the manufacturer's protocol with a total volume of 100 μL in each well:

Sample	Assay buffer	Statin	NADPH	HMG-CoA	HMGR
Blank	92 µL	-	2 µL	6 µL	-
Activity	91 µL	-	2 µL	6 µL	1 µL
Inhibition	81 µL	10 µL	2 µL	6 µL	1 µL

The reagents were added to the wells in the following order:

a) 1×Assay buffer was added to each well.
b) The inhibitors were pipetted to the inhibition samples from 10 mM stocks solutions in assay buffer with 10% DMSO (10 μM stock in the case of the control pravastatin).
c) Reconstituted NADPH (16,7 mg/mL) was pipetted into all samples.
d) The substrate solution (HMG-CoA) was added to all samples.
e) HMG-CoA reductase (HMGR, 0.5-0.7 mg/mL) was added to the activity and inhibition samples.

The samples were mixed thoroughly and the plate was placed into the plate reader. Absorbance was measured every 30 s over a period of 15 min at 340 nm. Herein, the plate was shaken thoroughly before each read.

9.4. Experiments PART II

9.4.1. Synthesis of KRED substrates

Synthesis of 1-(6-Methoxynaphthalen-2-yl)ethan-1-ol (*rac*-174a)

Yield: 96%
***R*f-value:** 0.18 [EtOAc/Cy 1:5]

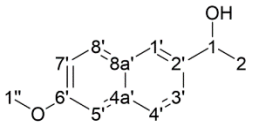

174a

In a 1 L-round bottom flask, 1-(6-methoxynaphthalen-2-yl)ethanone (**173a**) (5 g, 25 mmol, 1 eq) was dissolved in MeOH (500 mL). The solution was cooled to 0°C, and $CeCl_3 \cdot 7H_2O$ (12.71 g, 33.71 mmol, 1.35 eq) was added followed by slow addition of $NaBH_4$ (5 g, 132.35 mmol, 5.3 eq). The mixture was allowed to stir at room temperature for 1 h, then the reaction was terminated by addition of a satd. aq. NH_4Cl solution (150 mL). After removal of methanol under reduced pressure, the aqueous phase was extracted with DCM (3 x 80 mL). The combined organic layer was dried over $MgSO_4$ and evaporated to furnish the product as a colorless solid (4.7 g, 96%).

^{1}H NMR (300 MHz, $CDCl_3$) δ = 7.74 – 7.70 (m, 3H, 1'-, 4'-, 8'-H), 7.47 (d, *J* = 8.5 Hz, 1H, 5'-H), 7.17 – 7.12 (m, 2H, 3'-, 7'-H), 5.02 (q, *J* = 6.4 Hz, 1H, 1-H), 3.92 (s, 3H, OCH_3), 2,06 (br, 1H, OH), 1.57 (d, *J* = 6.5 Hz, 3H, 2-H).
^{13}C NMR (75 MHz, $CDCl_3$) δ = 157.75 (C-6'), 141.07 (C-2'), 134.16 (C-4a'), 129.51 (C-8), 128.87 (C-8a'), 127.26 (C-1'), 124.49 (C-4'), 123.87 (C-3'), 119.03 (C-7'), 105.85 (C-5'), 70.59 (C-1), 55.41 (OCH_3), 25.17 (C-2).

Synthesis of 1-(6-Methoxynaphthalen-2-yl)ethyl acetate (*rac*-175)

Yield: 85%

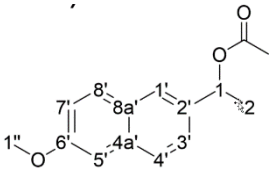

***rac*-175**

In a 100 mL-round bottom flask, racemic 1-(6-methoxynaphthalen-2-yl)ethanol (***rac*-174a**) (500 mg, 2.47 mmol, 1 eq) was dissolved in ethyl acetate (50 mL). The solution was cooled to at 0°C, then pyridine (293 mg, 3.7 mmol, 1.5 eq) and DMAP (60 mg, 49.1 mmol, 0.2 eq) were added, followed by addition of acetic anhydride (505 mg, 5 mmol, 2 eq). The reaction mixture was allowed to stir at room temperature overnight and then quenched by addition of H_2O (50 mL). The organic phase was washed with brine, dried over $MgSO_4$, and evaporated under reduced pressure. Purification was performed by column chromatography over silica gel (ethyl acetate/cyclohexane 1:5) to furnish the product as a colorless solid (513 mg, 85%).

^{1}H NMR (300 MHz, $CDCl_3$) δ = 7.66-7.63 (m, 3H, 1'-, 4'-, 8'-H), 7.38-7.35 (m, 1H, 5'H), 7.08-7.04 (m, 2H, 3'-, 7'H), 5.98-5.91 (q, 1H, 1-H), 3.83 (s, 3H, OCH_3), 2.01 (s, 3H, CH_3), 1.54 (d, 3H, CH_3).
^{13}C NMR (75 MHz, $CDCl_3$) δ 170.36 (C=O), 157.86 (C-6'), 136.70 (C-2'), 134.21 (C-4a'), 129.49 (C-8'), 128.62 (C-1'), 127.15 (C-4'), 124.99 (C-3'), 124.72 (C-8a'), 119.04 (C-7'), 105.67 (C-5'), 72.45 (C-1), 55.30 (OCH_3), 22.08 (CH_3), 21.40 (CH_3).

Lipase resolution of *rac*-174

Yield: 91%

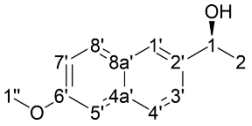

***(S)*-174a**

To a solution of racemic 1-(6-methoxynaphthalen-2-yl)ethyl acetate (***rac*-175**) (4 g, 20 mmol) in vinyl acetate (130 mL) was added 5 g of immobilized CAL-B and the mixture was shaken at 37 °C on a rotary shaker for 24 h. The catalyst was filtered off and the solvent was evaporated under reduced pressure. The residue obtained was submitted to flash column chromatography on silica gel (cyclohexane/ethyl acetate 10-20%) to give the *(S)*-configured alcohol ***(S)*-1a** (1.67 g, 84%) and the *(R)*-configured acetate ***(R)*-175** (2.21 g, 91%) as colorless solids.

Hydrolysis of *(R)*-175

Yield: 92%

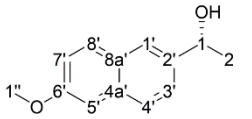

***(R)*-174a**

(R)-1-(6-methoxynaphthalen-2-yl)ethyl acetate (***(R)*-175**) (1 g, 4.1 mmol, 1 eq) was dissolved in methanol (25 mL). To this solution KOH (1.5 g, 27.5 mmol, 6.7 eq) was added under vigorous stirring and the mixture was left to react at room temperature for 2 h. After neutralization using conc. hydrochloric acid, the organic solvent was removed under reduced pressure and the aqueous phase was extracted with diethyl ether (3 x 10 mL). The combined organic layer was dried over $MgSO_4$ and the solvent was evaporated to furnish the product as a colorless solid (760 mg, 92%).

SOP 17 for the synthesis of methoxynaphthylcarbinols 174b-g via GRIGNARD reaction

In a 250 mL round bottom flask, 6-methoxy-2-naphthaldehyde (**172**) (5 g, 26.85 mmol, 1 eq) was dissolved in dry THF or Et_2O (75 ml) under argon atmosphere and a solution of commercial GRIGNARD reagent (43 mmol, 1.1 eq) was added slowly at 0 °C. The mixture was allowed to stir at room temperature for two hours and then was quenched by addition of satd. aq. NH_4Cl (45 mL). After removal of the organic solvent under reduced pressure the aqueous phase was extracted with diethyl ether (3 x 100 mL). The combined organic layer was dried over $MgSO_4$ and then evaporated under reduced pressure. The crude product was recrystallized from n-heptane/toluene (1:1) to yield the product as a solid.

1-(6-methoxynaphthalen-2-yl)propan-1-ol (174b)

Yield: 76%
***Rf*-value:** 0.24 [EtOAc/Cy 1:5]

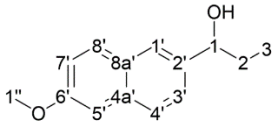

174b

^{1}H NMR (300 MHz, $CDCl_3$) δ = 7.72 (m, 3H, 1‘,-4‘-8‘-H), 7.44 (dd, *J* = 8.5, 1.7 Hz, 1H, 5‘-H), 7.20 – 7.09 (m, 2H, 3‘-, 7‘-H), 4.72 (t, *J* = 6.6 Hz, 1H, 1-H), 3.92 (s, 1H, 1‘‘-H), 2.06 (br, 1H, OH), 1.87 (ddd, *J* = 16.9, 13.8, 6.9 Hz, 2H, 2-H), 0.94 (t, *J* = 7.4 Hz, 3H, 3-H).
^{13}C NMR (75 MHz, $CDCl_3$) δ = 157.95 (C-6‘), 140.02 (C-2‘), 134.42 (C-4a‘), 129.71 (C-8’), 129.04 (C-8a’), 127.38 (C-1’), 125.02 (C-4’), 124.96 (C-3’), 119.20 (C-7’), 106.05 (C-5’), 76,45 (C-1,) 55.62 (OCH_3), 32.06 (CH_2), 10.51 (CH_3).

1-(6-methoxynaphthalen-2-yl)butan-1-ol (174c)

Yield: 85%
***Rf*-value:** 0.3 [EtOAc/Cy 1:5]

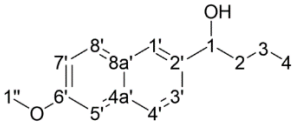

174c

^{1}H NMR (300 MHz, $CDCl_3$) δ = 7.76 – 7.63 (m, 3H, 1'-, 4'-, 8'-H), 7.45 (dd, *J* = 8.5, 1.7 Hz, 1H, 5'-H), 7.19 – 7.10 (m, 2H, 3'-, 7'-H), 4.80 (t, *J* = 6.7 Hz, 1H, 1-H), 3.92 (s, 3H, OCH_3), 1.95 – 1.66 (m, 2H, 2-H), 2.12 (br, 1H, OH) 1.55 – 1.24 (m, 2H, 3-H), 0.95 (t, *J* = 7.3 Hz, 3H, CH_3).
^{13}C NMR (75 MHz, $CDCl_3$) δ = 157.71 (C-6'), 140.11 (C-2'), 134.19 (C-4a'), 129.50 (C-8), 128.81 (C-8a'), 127.20 (C-1'), 124,79 (4'), 124.65 (C-3'), 119.02 (C-7'), 105.78 (C-5'), 74.66 (C-1), 55.42 (OCH_3), 41.18 (C-2), 19.22 (C-3), 14.13 (CH_3).

1-(6-methoxynaphthalen-2-yl)-2-methylpropan-1-ol (174d)

Yield: 76%
***Rf*-value:** 0.36 [EtOAc/Cy 1:5]

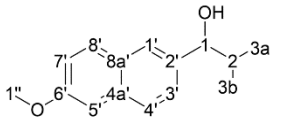

174d

^{1}H NMR (300 MHz, $CDCl_3$) δ = 7.81 – 7.60 (m, 3H, 1'-, 4'-, 8'-H), 7.42 (d, *J* = 6.8 Hz, 1H, 5'-H), 7.22 – 7.06 (m, 2H, 3'-, 7'-H), 4.47 (d, *J* = 7.0 Hz, 1H, 1-H), 3.92 (s, 3H, 1''-H), 2.13 – 1.96 (m, 1H, 2-H), 1.05 (d, *J* = 6.7 Hz, 3H, 3a-H), 0.82 (d, *J* = 6.8 Hz, 3H, 3b-H).
^{13}C NMR (75 MHz, $CDCl_3$) δ = 157.58 (C-6'), 138.87 (C-2'), 134.04 (C-4a'), 129.40 (C-8'), 128.60 (C-8a'), 126,81 (C-1'), 125.31 (C-4'), 125.19 (C-3'), 118.86 (C-7'), 105.64 (C-5'), 80.21 (C-1'), 55.31 (CH_3), 35.21 (C-2), 19.14 (C-3a), 18.41 (C-3b).

1-(6-methoxynaphthalen-2-yl)-3-methylbutan-1-ol (173e)

Yield: 82%
***Rf*-value:** 0.4 [EtOAc/Cy 1:5]

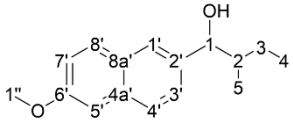

173e

^{1}H NMR (300 MHz, Chloroform-*d*) δ = 7.80 – 7.60 (m, 3H, 1'-, 4'-, 8'-H), 7.48 – 7.35 (m, 1H, 5'-H), 7.21 – 7.07 (m, 2H, 3'-, 7'-H), 4.60 (dd, *J* = 26.6, 6.6 Hz, 1H, 1-H),3.92 (s, 3H, 1''-H), 1.98 (br, 1H, OH), 1.92 – 1.65 (m, 1H), 1.32 – 1.07 (m, 0H), 1.03 – 0.68 (m, 3H).
^{13}C NMR (75 MHz, $CDCl_3$) δ = 157.69 (C-6'), 138.95 (C-2'), 134.15 (C-4a'), 129.50 (C-8'), 128.70 (C-8a'), 126.92 (C-1'), 125.57 (C-4'), 125.16 (C-3'), 118.97 (C-7'), 105.76 (C-5'), 79.06 (C-1), 55.43 (C-1''), 41.70 (C-2), 25.09 (C-3), 15.37 (C-5), 11.47 (C-4).

1-(6-methoxynaphthalen-2-yl)-3-methylbutan-1-ol (173f)

Yield: 75%
***Rf*-value:** 0.38 [EtOAc/Cy 1:5]

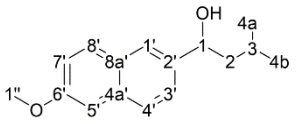

173f

^{1}H NMR (300 MHz, $CDCl_3$) δ 7.81 – 7.61 (m, 3H, 1'-,4'-, 8'-H), 7.45 (dd, *J* = 8.5, 1.7 Hz, 1H, 5'-H), 7.21 – 7.07 (m, 2H, 3'-, 7'-H), 4.87 (dd, *J* = 8.1, 5.6 Hz, 1H, 1-H), 3.92 (s, 1H, 1''-H), 1.98 (br, 1H, OH), 1.89 – 1.67 (m, 2H, 2-H), 1.66 – 1.54 (m, 1H, 3-H), 0.97 (dd, *J* = 6.4, 3.8 Hz, 6H, 4a-, 4b-H).
^{13}C NMR (75 MHz, $CDCl_3$) δ = 157.73 (C-6'), 140.40 (C-2'), 134.19 (C-4a'), 129.49 (C-8'), 128.83 (C-8a'), 127.26 (C-1'), 124.78 (C-4'), 124.59 (C-3'), 119.03 (C-7'), 105.80 (C-5'), 73.02 (C-1), 55.42 (C-1''), 48.27 (C-2), 24.99 (C-3), 23.24 (C-4a), 22.49 (C-4b).

1-(6-methoxynaphthalen-2-yl)-3-methylpentan-1-ol (173g)

Yield: 57%
***Rf*-value:** 0.75 [EtOAc/Cy 1:1]

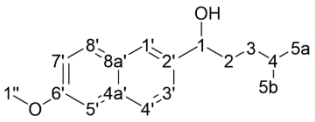

173g

^{1}H NMR (300 MHz, $CDCl_3$) δ = 7.74 – 7.55 (m, 3H, 8'-, 4'-, 1'-H), 7.36 (d, *J* = 8.5 Hz, 1H, 3'-H), 7.12 – 7.00 (m, 2H, 3'-, 7'-H), 4.66 (t, *J* = 6.7 Hz, 1H, 1-H), 3.82 (s, 1H, 1''-H), 1.95 (s, 1H, -OH) 1.91 – 1.60 (m, 2H, 2-H), 1.59 – 1.36 (m, 1H, 4-H), 1.35 – 1.17 – 0.96 (m, 2H, 3-H), 0.78 (dd, *J* = 6.6, 2.7 Hz, 6H, 5a-H + 5b-H).
^{13}C NMR (75 MHz, $CDCl_3$) δ 157.62 (C-6'), 140.02 (C-2'), 134.08 (C-4a'), 129.40 (C-8'), 128.70 (C-8a'), 127.11 (C-1'), 124.66 (C-4'), 118.90 (C-7'), 105.69 (C-5'), 75.12 (C-1), 55.31 (C-1''), 36.80 (C-2), 34.97 (C-3), 28.04 (C-4), 22.57 (C-5a +C-5b).

1-(6-methoxynaphthalen-2-yl)-2-phenylethanol (198)

Yield: 75%
mp: 133 °C

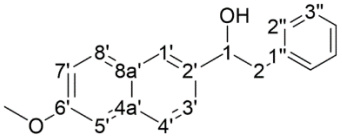

198

^{1}H NMR (300 MHz, $CDCl_3$): δ = 7.67-7.61 (m, 3H, 8'-, 4'-, 1'-H), 7.40-7.37 (d, 1H, 3'-H), 7.22-7.12 (m, 5H, Ph),7.09-7.08 (d, 1H, 7'-H), 4.97 (s, 1H, 5'-H), 4.97-4.93 (q, 1H, 1-H), 3.84 (s, 3H, OCH_3), 3.07-2.98 (m, 2H, 2-H);
^{13}C-NMR ($CDCl_3$, 75 MHz): δ = 157,69 (C-6'), 138,96 (C-1''), 138,08 (C-2'), 134,14 (C-4a'), 129,53 (C-8'), 128,7 (C-8a'), 129,44 (C-3" 2x), 128,73 (C-3'), 127,03 (C-1'), 126,61 (C-2" 2x), 124,65 (C-4"), 124,45 (C-4'), (118,93 (C-7'), 105,71 (C-5'), 76,45 (C-1), 55,3 (OCH_3), 46,01 (C-2).

SOP 18 for the synthesis of methoxynaphthylketones 173d-g via PCC-oxidation

In a heat dried 25 mL round bottom flask pyridinium chlorochromate (353 mg, 1.6 mmol, 1.6 eq.), $MgS0_4$ (1 g), NaOAc (100 mg) were added to dry DCM (4 mL) under argon atmosphere. To the resulting suspension, a solution of the carbinol (1 mmol, 1 eq.) in dry DCM (1 mL) was added dropwise and the reaction mixture was stirred at room temperature for 3 h. The reaction mixture was filtered through a short silica column to remove precipitations and the organic solvent was removed under reduced pressure to yield the ketone product.

1-(6-methoxynaphthalen-2-yl)-2-methylpropan-1-one (173d)

Yield: 95%
***Rf*-value:** 0.81 [Cy/EtOAc 1:1]

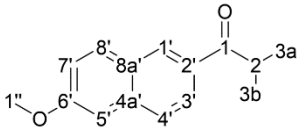

173d

^{1}H NMR (300 MHz, $CDCl_3$) δ = 8.40 (s, 1H, 1'-H), 8.01 (d, *J* = 8.6 Hz, 1H, 4'-H), 7.84 (d, *J* = 8.9 Hz, 1H, 8'-H), 7.77 (d, *J* = 8.6 Hz, 1H, 3'-H), 7.20 (d, *J* = 11.1 Hz, 1H, 7'-H), 7.15 (s, 1H, 5'-H), 3.94 (s, 3H, 1''-H), 3.70 (p, *J* = 6.8 Hz, 1H, 2-H), 1.27 (d, *J* = 6.8 Hz, 6H, 3a + 3b-H).
^{13}C NMR (75 MHz, $CDCl_3$) δ 204.29 (C-1), 159.78 (C-6'), 137.27 (C-4a'), 131.69 (C-8a'), 131.22 (C-8), 129.70 (C-1'), 128.06 (C-2'), 127.25 (C-3'), 125.20 (C-4'), 119.74 (C-7'), 105.84 (C-5'), 55.53 (C-1''), 35.32 (C-2), 19.51 (C-3a+3b).

1-(6-methoxynaphthalen-2-yl)-2-methylbutan-1-one (173e)

Yield: 92%
***Rf*-value:** 0.82 [Cy/EtOAc 1:1]

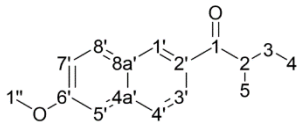

173e

^{1}H NMR (300 MHz, $CDCl_3$) δ = 8.40 (s, 1H, 1'-H), 8.01 (d, *J* = 10.4 Hz, 1H, 4'-H), 7.85 (d, *J* = 8.9 Hz, 1H, 8'-H), 7.77 (d, *J* = 8.6 Hz, 1H, 3'-H), 7.24 – 7.18 (m, 1H,7'-H), 7.16 (s, 1H, 5'-H), 3.94 (s, 3H, 1''-H), 3.55 (q, *J* = 6.8 Hz, 1H, 2-H), 1.89 (dt, *J* = 14.0, 6.8 Hz, 1H, 3-H), 1.58 (dt, *J* = 13.8, 7.1 Hz, 1H, 3-H), 1.25 (d, *J* = 6.9 Hz, 3H, 5-H), 0.95 (t, *J* = 7.4 Hz, 3H, 4-H).
^{13}C NMR (75 MHz, $CDCl_3$) δ = 204.25 (C-1), 159.79 (C-6'), 137.28 (C-4a'), 132.36 (C-8a'), 131.25 (C-8), 129.64 (C-1'), 128.07 (C-2'), 127.26 (C-3'), 125.14 (C-4'), 119.74 (C-7'), 105.85 (C-5'), 55.54 (C-1''), 42.11 (C-2), 27.03 (C-3), 17.18 (C-5), 11.99 (C-4).

1-(6-methoxynaphthalen-2-yl)-4-methylbutan-1-one (173f)

Yield: 90%
***Rf*-value:** 0.80 [EtOAc/Cy 1 : 1]

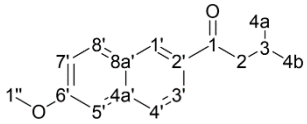

173f

^{1}H NMR (300 MHz, $CDCl_3$) δ = 8.38 (s, 1H, 1'-H), 8.01 (d, *J* = 8.6 Hz, 1H, 4'-H), 7.85 (d, *J* = 8.9 Hz, 1H, 8'-H), 7.76 (d, *J* = 8.6 Hz, 1H, 3'-H), 7.25 – 7.18 (m, 1H, 7'-H), 7.15 (s, 1H, 5'-H), 3.94 (s, 3H, 1''-H), 2.93 (d, *J* = 6.9 Hz, 2H, 2-H), 2.36 (dp, *J* = 13.4, 6.7 Hz, 1H, 3-H), 1.04 (d, *J* = 6.6 Hz, 6H, 4a-H, 4b-H).
^{13}C NMR (75 MHz, $CDCl_3$) δ = 200.04 (C-1'), 159.80 (C-6'), 137.30 (C-4a'), 133.02 (C-8a'), 131.23 (C-8'), 129.68 (C-1'), 128.00 (C-2'), 127.19 (C-3'), 124.88 (C-4'), 119.77 (C-7'), 105.87 (C-5'), 55.53 (C-1''), 47.55 (C-2), 25.54 (C-3), 22.98 (C-4a+4b).

1-(6-methoxynaphthalen-2-yl)-4-methylpentan-1-one (173g)

Yield: 95%
***Rf*-value:** 0.83 [Cy/EtOAc 1:1]

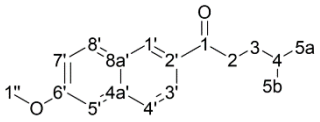

173g

^{1}H NMR (300 MHz, $CDCl_3$) δ = 8.39 (s, 1H, 1'-H), 8.01 (d, *J* = 10.4 Hz, 1H, 4'H), 7.85 (d, *J* = 9.0 Hz, 1H, 8'-H), 7.76 (d, *J* = 8.7 Hz, 1H, 3'-H), 7.23 – 7.11 (m, 2H, 5'-, 7'-H), 3.94 (s, 3H, 1''-H), 3.13 – 2.99 (m, 2H, 2-H), 1.69 (t, *J* = 7.2 Hz, 3H, 3-, 4-H), 0.98 (d, *J* = 6.5 Hz, 6H, 5a-H + 5b-H).
^{13}C NMR (75 MHz, $CDCl_3$) δ = 200.52 (C-1'), 159.79 (C-6'), 137.30 (C-4a'), 132.68 (C-8a'), 131.21 (C-8'), 129.56 (C-1'), 128.03 (C-2'), 127.19 (C-3'), 124.87 (C-4'), 119.76 (C-7'), 105.90 (C-5'), 55.53 (C-1''), 36.67 (C-2), 33.66 (C-3), 28.08 (C-4), 22.62 (C-5a + 5b).

Synthesis of 3-chloro-1-(3,4-difluorophenyl)propan-1-one (164):

Yield: 45%
***Rf*-value:** 0.30 [Cy/EtOAc 10:1]

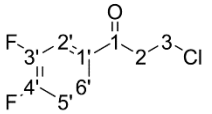

164

In a 50 mL round bottom flask, aluminiumchloride (1.91 g, 14.30 mmol, 1.1 eq) was dissolved in DCM (15 mL) and the mixture was cooled down to 0 °C. A solution of chloropropanoyl chloride (**178**) (1.37 mL, 14.3 mmol, 1.1 eq) and 1,2-diflourobenzene (**177**) (1.27 mL, 13 mmol, 1 eq) was added dropwise without exceeding a temperature of 10 °C. The reaction mixture was then left to stir at room temperature overnight. After completion, the mixture was

cooled to 0 °C and quenched by addition of water (10 mL). The aqueous phase was separated from the organic layer and extracted with DCM (3 x 5 mL). The combined organic layer was washed with satd. aq. $NaHCO_3$ (2 x 25 mL), dried over $MgSO_4$, and the solvent was removed under reduced pressure to yield the product as a brown oil.

^{1}H NMR (300 MHz, $CDCl_3$): δ=7.76-7.65 (m, 2H, 5´,6´-H), 7.21 (q, *J*=9.5 Hz, 1H, 2´-H), 3.34 (t, *J*=7 Hz, 2H, 3-H), 2.83 (t, *J*=7 Hz, 2H, 2-H) ppm.
^{13}C-NMR ($CDCl_3$, 75 MHz): δ= 194.28 (1-C), 155.83 (4´-C), 152.40 (3´-C), 148.89 (1´-C), 133.89 (6´-C), 125.16 (5´-C), 117.95 (2´-C), 41.27 (2-C), 38.43 (3-C) ppm.

Synthesis of 1-(3,4-difluorophenyl)-3-nitropropan-1-one (162):

Yield: 76%
***Rf*-value:** 0.54 [Cy/EtOAc 7:1]

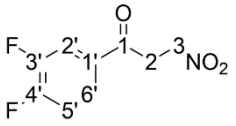

162

In a 100 mL round bottom flask, 3-chloro-1-(3,4-difluorophenyl)propan-1-one (**164**) (1.2 g, 5.9 mmol, 1 eq) was dissolved in acetone (50 mL). Sodiumnitrite (485 mg, 7 mmol, 1.2 eq) was added under stirring and the reaction mixture was left to stir at 45 °C for 6 h. The solvent was removed under reduced pressure and the raw product was purified by silica-column chromatography (cyclohexane/ethylacetate 10 – 50%) to yield nitro compound **162** as a yellow solid.

^{1}H NMR (300 MHz, $CDCl_3$): δ= 7.82-7.68 (m, 2H, 5´,6´-H), 7.27-7.19 (q, ^3J=9 Hz, 1H, 2´-H), 4.75 (t, J=7 Hz, 2H, 3-H), 3.53 (t, J=7 Hz, 2H, 2-H) ppm.
^{13}C-NMR ($CDCl_3$, 75 MHz): δ= 192.72 (1-C), 154.50 (3´-C), 149.12 (4´-C), 132.91 (1´-C), 125.47 (6´-C), 117.51(5´-C), 69.12 (3-C), 34.85 (2-C) ppm.

Synthesis of racemic 1-(3,4-difluorophenyl)-3-nitropropan-1-ol (*rac*-165):

Yield: 95%
***Rf*-value:** 0.64 [Cy/TEA/EtOAc 20:1:80]

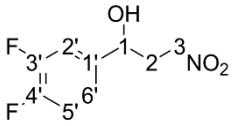

***rac*-165**

Nitropropanone **162** (500 mg, 2.3 mmol, 1 eq) was dissolved in THF/water 1 : 1 (11 mL) and the solution was cooled to 0 °C. $NaBH_4$ (108 mg, 2.3 mmol, 1 eq) was slowly added and the reaction mixture was allowed to stir at room temperature for 2 h. After completion, NH_4Cl (1 g) was added to quench the reaction. After gas formation has stopped, the mixture was extracted with Et_2O. The organic layer was dried over $MgSO_4$ and the solvent was removed under reduced pressure to obtain the product as yellow oil.

^{1}H NMR (300 MHz, $CDCl_3$): δ= 7.19- 7.00 (m, 3H, 2´,5´,6´-H), 4.77-4.74 (q, *J*=4.2 Hz, 1H, 1-H), 4.60-4.34 (m, 2H, 3-H), 2.39-2.15 (m, 2H, 2-H) ppm.
^{13}C-NMR ($CDCl_3$, 75 MHz): δ= 152.25 (3´-C), 148.24 (4´-C), 140.11 (1´-C), 121.54 (6´-C), 117.69 (5´-C), 114.51 (2´-C), 72.00 (3-C), 70.00 (1-C), 36.00 (2-C) ppm.

9.4.2. Creation of *Lb*KRED library

Site-directed saturation mutagenesis of the *Lb*KRED gene was individually performed for each amino acid following SOP6 using six according sets of primers with degenerated codons (NNK/MNN). All primers were designed using the QuikChange Primer Design Webtool provided by *Agilent* and were purchased from *Sigma Aldrich*. The primer sequences used are listed in Table 9.10.

Table 9.10 Primer sequences used for saturation mutagenesis.

Primer	Sequence
I143X-f	5'- CAT CAA CAT GTC TTC GNN KGA AGG CTT TGT GGG TG -3'
I143X-r	5'- CAC CCA CAA AGC CTT CMN NCG AAG ACA TGT TGA TG -3'
E144X-f	5'- CAA CAT GTC TTC GAT CNN KGG CTT TGT GGG TGA TCC -3'
E144X-r	5'- GGA TCA CCC ACA AAG CCM NNG ATC GAA GAC ATG TTG -3'
D149X-f	5'- GAT CGA AGG CTT TGT GGG TNN KCC TAG CTT AGG GG -3'
D149X-r	5'- CCC CTA AGC TAG GMN NAC CCA CAA AGC CTT CGA TC -3'
L152X-f	5'- GTG GGT GAT CCT AGC NNK GGG GCT TAC AAC GCA TC -3'
L152X-r	5'- GAT GCG TTG TAA GCC CCM NNG CTA GGA TCA CCC AC -3'
Y189X-f	5'- CAC TGT TCA CCC TGG CNN KAT CAA GAC ACC ATT GG -3'
Y189X-r	5'- CCA ATG GTG TCT TGA TMN NGC CAG GGT GAA CAG TG -3'
Y248X-f	5'- GAA TTT GTA GTT GAT GGT GGT NNK ACC GCT CAA TAA C -3'
Y24X8-r	5'- GTT ATT GAG CGG TMN NAC CAC CAT CAA CTA CAA ATT C -3

9.4.3. Fluorogenic protein activity assay

Protein libraries were obtained from each mutant sub-library according to SOP 10.
The high-throughput assays were performed as triplicate for each sub-library and substrate. The enzymatic reactions were started by addition of the substrate solution (10 μL of a 2.5 mM stock in DMSO). The reactions were monitored by utilizing a FluoStar Optima plate reader (*BMG Labtech*) with 330 nm filters for excitation and 460 nm filters for emission. The gain factor was set between 800 - 950. Data points were measured every 5 minutes over a period of 2 - 3 h at room temperature.

9.4.4. Fluorogenic enzyme kinetics assay

Kinetic measurements were performed in triplicate utilizing crude cell free extracts of selected clones and were conducted in triplicate. The reactions were performed in 96-well plates with a total volume of 200 μL per well. A dilution series for each substrate ranging from 1 – 10 mM in TEA-buffer was created. Each dilution (20 μL) was transferred to the assay plate. DMSO (20 μL) and acetone (10 μL) were pipetted to the wells to serve as cosolvent and sacrificial ketone for cofactor recycling. $NADP^+$ was added in equimolar amount to the substrate (10 μL, dissolved in TEA-buffer). The wells were filled up with TEA-buffer (130 μL) and the reactions were started by addition of the enzyme (400 μg, dissolved in 10 μL TEA-buffer). For each substrate concentration a blank reaction without enzyme served as control. The reactions were monitored by utilizing a FluoStar Optima plate reader (*BMG Labtech*) with 330 nm filters for excitation and 460 nm filters for emission. The gain factor was set between 800 - 950. Data points were measured every 30 s over a period of 1 h at room temperature.

The raw data was processed with *Excel* (Microsoft Office) by plotting the fluorescence intensity against the corresponding time points. Linear regression was applied for the initial, "linear" parts of the curves and the slopes corresponding with the reaction's initial velocities V_0 were determined. These values were further processed with *Origin 9.1* (OriginLab) for hyperbolic fitting according to the Michaelis-Menten equation:

$$y = V_{max} \times \frac{x^n}{k^n + x^n}$$

9.4.5. Protein stereoselectivity typing

Protein libraries were obtained according to SOP 10.
The assays were performed as triplicate for each enantiomer of substrate (**174a**) using the same conditions as in the activity assay.

9.4.6. NADPH-dependent enzyme kinetic assay

MICHAELIS-MENTEN kinetics for the non-fluorescent substrate **165** were determined by measuring the NADPH-formation during the oxidation reaction. For this purpose, reaction mixtures with the following final substrate concentration ranging between 0 – 12 mM in 50 mM TEA buffer and 10% DMSO were used: $NADP^+$ was added at 12 mM concentration to provide a sufficient amount of cofactor. The enzyme content was chosen at a fixed amount of 1 mg/mL of 15 minutes. Data points were taken every 20 s, between which the plate was shook for 2 s. The data was processed as described in 9.4.4.

9.4.7. Analytical scale reactions of selected mutants

Selected mutant enzymes were tested for activity towards the pharmaceutically relevant substrate **162**. For this purpose, reactions were carried out in an analytical volume of 500 μL in Eppendorf vessels with a substrate concentration of 10 mM in 50 mM TEA buffer, equimolar amounts of cofactor, 10% DMSO, 5 mM $MgCl_2$, and 20 mg/mL catalyst. The substrate (1 mg) was dissolved in DMSO (50 μL). H_2O (250 μL), NADPH (4 mg in 50 μL H_2O), TEA-buffer (25 μL from 1 M stock), and a $MgCl_2$ solution (25 μL from a 100 mM stock) were added before pipetting the enzyme solutions (5 mg resting cells in 100 μL H_2O) to the composition. Reactions containing the wildtype enzyme (resting cells and purified enzyme) and no catalyst were used as controls. The reactions were left to gently shake at room temperature for 24 h. HPLC samples were taken after 1, 3, 6, and 24 h and compared with reference material.

9.4.8. Preparative enzyme reaction towards alcohol *(R)*-165

For the preparative synthesis of ***(R)*-165**, the E144A/L152R double mutant was employed. The reaction was carried out in a total volume of 5 mL with 100 mM substrate concentration, 10% DMSO, 10% *iso*-propanol as sacrificial alcohol, 5 mM $MgCl_2$, 50 mM TEA-buffer, and an enzyme amount of 10 mg/mL (resting cells). Ketone **162** (100 mg) was dissolved in DMSO (500 μL) and *iso*-propanol (500 μL). H_2O (2.5 mL), TEA buffer (250 μL from 1 M stock), $MgCl_2$ (250 μL from a 100 mM stock) were added. The reaction was started by addition of the catalyst (50 mg in 1 mL H_2O) and was carried out at room temperature in a closed glass vessel to prohibit

evaporation of solvents. After 24 h, the enzyme was precipitated by incubation in MeOH (10 mL) for 20 minutes. The solids were then removed by filtration over celite, after which the organic solvent was evaporated under reduced pressure. For product isolation, the aqueous phase was extracted with EtOAc (3 x 5 mL) and the combined organic phase was dried over $MgSO_4$. The solvent was removed under reduced pressure to yield the crude product as yellow oil. Purification was achieved by column chromatography (Cy/EtOAc, gradient: 0-50% to give a yield of 85% relative to conversion.

References

[1] D. G. Blackmond, *Cold Spring Harb Perspect Biol* **2010**, *2*.
[2] L. A. Nguyen, H. He, C. Pham-Huy, *Int J Biomed Sci* **2006**, *2*, 85-100.
[3] a) W. Jiang, B. Fang, *Applied Biochemistry and Biotechnology* **2020**, *192*, 146-179; bR. Kourist, *Angewandte Chemie International Edition* **2015**, *54*, 12547-12547; cK. Faber, *in Biotransformations in Organic Chemistry, Springer Nature* **2018**, *7th Edition*, 204-217.
[4] H. Gröger, Y. Asano, in *Enzyme Catalysis in Organic Synthesis*, Wiley-VCH Verlag GmbH & Co. KGaA, **2012**, pp. 1-42.
[5] A. L. Margolin, *Enzyme and Microbial Technology* **1993**, *15*, 266-280.
[6] G. Prelich, *Genetics* **2012**, *190*, 841-854.
[7] M. T. Reetz, *Journal of the American Chemical Society* **2013**, *135*, 12480-12496.
[8] A. Endo, *Proc Jpn Acad Ser B Phys Biol Sci* **2010**, *86*, 484-493.
[9] E. Istvan, *Atherosclerosis Supplements* **2003**, *4*, 3-8.
[10] M. Haridas, E. M. M. Abdelraheem, U. Hanefeld, *Appl Microbiol Biotechnol* **2018**, *102*, 9959-9971.
[11] J. J. Nawarskas, S. M. Clark, *Cardiology in Review* **2011**, *19*, 95-100.
[12] K. G. Hugentobler, H. Sharif, M. Rasparini, R. S. Heath, N. J. Turner, *Organic & Biomolecular Chemistry* **2016**, *14*, 8064-8067.
[13] Y. C. Thai, A. Szekrenyi, Y. Qi, G. W. Black, S. J. Charnock, W. D. Fessner, *Bioorg Med Chem* **2018**, *26*, 1320-1326.
[14] a) B. Springthorpe, A. Bailey, P. Barton, T. N. Birkinshaw, R. V. Bonnert, R. C. Brown, D. Chapman, J. Dixon, S. D. Guile, R. G. Humphries, S. F. Hunt, F. Ince, A. H. Ingall, I. P. Kirk, P. D. Leeson, P. Leff, R. J. Lewis, B. P. Martin, D. F. McGinnity, M. P. Mortimore, S. W. Paine, G. Pairaudeau, A. Patel, A. J. Rigby, R. J. Riley, B. J. Teobald, W. Tomlinson, P. J. H. Webborn, P. A. Willis, *Bioorganic & Medicinal Chemistry Letters* **2007**, *17*, 6013-6018; b) K. E. Hernandez, H. Renata, R. D. Lewis, S. B. J. Kan, C. Zhang, J. Forte, D. Rozzell, J. A. McIntosh, F. H. Arnold, *ACS Catalysis* **2016**, *6*, 7810-7813; c) P. Kumar, A. Dubey, A. Harbindu, *Organic & Biomolecular Chemistry* **2012**, *10*, 6987-6994.
[15] a) R. M. Atkinson, K. S. Ditman, *Clinical Pharmacology & Therapeutics* **1965**, *6*, 631-655; b) T. Maes, C. Mascaró, I. Tirapu, A. Estiarte, F. Ciceri, S. Lunardi, N. Guibourt, A. Perdones, M. M. P. Lufino, T. C. P. Somervaille, D. H. Wiseman, C. Duy, A. Melnick, C. Willekens, A. Ortega, M. Martinell, N. Valls, G. Kurz, M. Fyfe, J. C. Castro-Palomino, C. Buesa, *Cancer Cell* **2018**, *33*, 495-511.e412; c) T. Maes, C. Mascaró, D. Rotllant, F. Cavalcanti, E. Carceller, A. Ortega, C. Molinero, C. Buesa, *Alzheimer's & Dementia* **2016**, *12*, P1192; d) K. Pettit, N. Curtin, M. Tartaczuch, J. Shortt, J. Watts, W. Stevenson, A. Gerds, K. Burbury, A. Yacoub, A. Jones, J. Peppe, D. Ross, H. Rienhoff, *HemaSphere* **2019**, *3*, 369-370.
[16] N. Imani, M. Donn, B. Vale, *Biomimicry as Innovation: a systematic review*, **2017**.
[17] E. S. Istvan, J. Deisenhofer, *Science* **2001**, *292*, 1160-1164.
[18] D. P. B. T. B. Strik, H. V. M. Hamelers, J. F. H. Snel, C. J. N. Buisman, *International Journal of Energy Research* **2008**, *32*, 870-876.
[19] S. Basak, *Bio-Design and Manufacturing* **2020**, *3*, 148-154.
[20] G. Hughes, J. C. Lewis, *Chemical Reviews* **2018**, *118*, 1-3.
[21] R. Pörtner, *Nachrichten aus der Chemie* **2006**, *54*, 1025-1026.
[22] D. Vasic-Racki, in *Industrial Biotransformations*, Wiley-VCH Verlag GmbH & Co. KGaA, **2006**, pp. 1-36.
[23] a) J. M. Sperl, V. Sieber, *ACS Catalysis* **2018**, *8*, 2385-2396; b) R. Cutlan, S. De Rose, M. N. Isupov, J. A. Littlechild, N. J. Harmer, *Biochimica et Biophysica Acta (BBA) - Proteins and Proteomics* **2020**, *1868*, 140322.
[24] S. Datta, L. R. Christena, Y. R. S. Rajaram, *3 Biotech* **2013**, *3*, 1-9.

[25] H. Sun, H. Zhang, E. L. Ang, H. Zhao, *Bioorganic & Medicinal Chemistry* **2018**, *26*, 1275-1284.
[26] R. N. Patel, *Biomolecules* **2013**, *3*, 741-777.
[27] B. Borup, T. Daussmann, S. Collier, in *Encyclopedia of Industrial Biotechnology*, Wiley & Sons, pp. 1-36.
[28] B. Mathew, R. Daniel, *Libyan J Med* **2008**, *3*, 63-63.
[29] J. L. T. Jeremy M. Berg, Lubert Stryer, *Stryer Biochemie* **2015**, *7*.
[30] M. Brown, J. Goldstein, *Science* **1986**, *232*, 34-47.
[31] R. Zetterström, *Acta Paediatrica* **2009**, *98*, 1223-1227.
[32] a) J. W. Gofman, H. B. Jones, F. T. Lindgren, T. P. Lyon, H. A. Elliott, B. Strisower, *Circulation* **1950**, *2*, 161-178; b) J. L. Goldstein, M. S. Brown, *Cell* **2015**, *161*, 161-172.
[33] M. Oliver, *Br J Clin Pharmacol* **2012**, *74*, 907-910.
[34] a) S. Schandelmaier, M. Briel, R. Saccilotto, K. K. Olu, A. Arpagaus, L. G. Hemkens, A. J. Nordmann, *Cochrane Database Syst Rev* **2017**, *6*, CD009744-CD009744; b) S. H. Ganji, V. S. Kamanna, M. L. Kashyap, *The Journal of Nutritional Biochemistry* **2003**, *14*, 298-305.
[35] C. A. Liacouras, P. M. Coates, P. R. Gallagher, J. A. Cortner, *The Journal of pediatrics* **1993**, *122*, 477-482.
[36] B. Hamprecht, K. R. Bruckdorfer, C. Nüßler, F. Lynen, in *Membrane-Bound Enzymes: Proceedings of an International Symposium held in Pavia, Italy May 29–30, 1970* (Eds.: G. Porcellati, F. di Jeso), Springer US, Boston, MA, **1971**, pp. 135-146.
[37] A. G. Brown, T. C. Smale, T. J. King, R. Hasenkamp, R. H. Thompson, *Journal of the Chemical Society. Perkin transactions 1* **1976**, 1165-1170.
[38] D. Kalaria, W. Wassenaar, *CMAJ* **2002**, *167*, 737-737.
[39] T. P. Stossel, *Cell* **2008**, *134*, 903-905.
[40] a) M. Bifulco, A. Endo, *Pharmacological Research* **2014**, *88*, 1-2; bP. Hoyos, V. Pace, A. Alcántara, *Catalysts* **2019**, *9*, 260.
[41] M. Demasi, *British Journal of Sports Medicine* **2018**, *52*, 1282-1282.
[42] A. Endo, *Nature Medicine* **2008**, *14*, 1050-1052.
[43] T. B. Vree, E. Dammers, I. Ulc, S. Horkovics-Kovats, M. Ryska, I. Merkx, *TheScientificWorldJournal* **2003**, *3*, 1332-1343.
[44] J. Latimer, J. A. Batty, R. D. G. Neely, V. Kunadian, *Journal of Thrombosis and Thrombolysis* **2016**, *42*, 405-419.
[45] W. März, M. E. Kleber, H. Scharnagl, T. Speer, S. Zewinger, A. Ritsch, K. G. Parhofer, A. von Eckardstein, U. Landmesser, U. Laufs, *Clinical Research in Cardiology* **2017**, *106*, 663-675.
[46] H. H. Wang, G. Garruti, M. Liu, P. Portincasa, D. Q. Wang, *Ann Hepatol* **2017**, *16*, s27-s42.
[47] L. Tabernero, V. W. Rodwell, C. V. Stauffacher, *J Biol Chem* **2003**, *278*, 19933-19938.
[48] C. Stancu, A. Sima, *J. Cell. Mol. Med.* **2001**, *5*, 378-387.
[49] N. Mohammadkhani, S. Gharbi, H. Fatima, A. Farzaneh, G. Mahjoob, A. Hoseinsalari, E. Korsching, *European Journal of Pharmacology* **2019**, *863*, 172704.
[50] R. Deichmann, C. Lavie, S. Andrews, *Ochsner J* **2010**, *10*, 16-21.
[51] R. Bitzur, H. Cohen, Y. Kamari, D. Harats, *Diabetes Care* **2013**, *36 Suppl 2*, S325-S330.
[52] a) D.-x. Bu, G. Griffin, A. H. Lichtman, *Current Opinion in Lipidology* **2011**, *22*, 165-170; b) E. Diamantis, G. Kyriakos, L. V. Quiles-Sanchez, P. Farmaki, T. Troupis, *Curr Cardiol Rev* **2017**, *13*, 209-216.
[53] C. Ulivieri, C. T. Baldari, *Pharmacological Research* **2014**, *88*, 41-52.
[54] J.-S. Rachoin, E. Cerceo, R. P. Dellinger, *Crit Care* **2013**, *17*, 105-105.
[55] Y. Zhang, A. D. Bradley, D. Wang, R. A. Reinhardt, *Pharmacological Research* **2014**, *88*, 53-61.

[56] K. V. Radha, D. Lakshmanan, *Asian Journal of Pharmaceutical and Clinical Research* **2013**, *6*.
[57] a) J. T. Zacharia, T. Tanaka, M. Hayashi, *The Journal of Organic Chemistry* **2010**, *75*, 7514-7518; b) Y. Wu, M.-J. Liu, H.-Q. Huang, G.-X. Huang, F.-J. Xiong, F.-E. Chen, *European Journal of Organic Chemistry* **2017**, *2017*, 3681-3688.
[58] P. Hoyos, V. Pace, A. Alcántara, *Catalysts* **2019**, *9*.
[59] N. P. Money, in *The Fungi (Third Edition)* (Eds.: S. C. Watkinson, L. Boddy, N. P. Money), Academic Press, Boston, **2016**, pp. 401-424.
[60] H. Mukhtar, S. S. Ijaz, H. Ikram ul, *Cell Biochemistry and Biophysics* **2014**, *70*, 309-320.
[61] Z. Casar, *Current Organic Chemistry* **2010**, *14*, 816-845.
[62] K.-M. Chen, G. E. Hardtmann, K. Prasad, O. Repič, M. J. Shapiro, *Tetrahedron Letters* **1987**, *28*, 155-158.
[63] E. R. Burkhardt, K. Matos, *Chemical Reviews* **2006**, *106*, 2617-2650.
[64] V. B. Boralli, E. B. Coelho, S. A. Sampaio, M. P. Marques, V. L. Lanchote, *The Journal of Clinical Pharmacology* **2009**, *49*, 205-211.
[65] G. Wess, K. Kesseler, E. Baader, W. Bartmann, G. Beck, A. Bergmann, H. Jendralla, K. Bock, O. Holzstein, H. Kleine, M. Schnierer, *Tetrahedron Letters* **1990**, *31*, 2545-2548.
[66] H.-w. Choi, H. Shin, *Synlett* **2008**, *2008*, 1523-1525.
[67] S. Rádl, J. Stach, J. Hajicek, *Tetrahedron Letters* **2002**, *43*, 2087-2090.
[68] G. Beck, K. Kesseler, E. Baader, W. Bartmann, A. Bergmann, E. Granzer, H. Jendralla, B. Von Kerekjarto, R. Krause, *Journal of Medicinal Chemistry* **1990**, *33*, 52-60.
[69] M. Müller, *Angewandte Chemie International Edition* **2005**, *44*, 362-365.
[70] R. N. Patel, A. Banerjee, C. G. McNamee, D. Brzozowski, R. L. Hanson, L. J. Szarka, *Enzyme and Microbial Technology* **1993**, *15*, 1014-1021.
[71] A. J. Blacker, C. R.A. Holt, D. Reeve, *(Avecia Pharmaceuticals), WO 01/85975* **2001**.
[72] Y. Yasohara, N. Kizaki, J. Hasegawa, M. Wada, M. Kataoka, S. Shimizu, *Tetrahedron: Asymmetry* **2001**, *12*, 1713-1718.
[73] A. Schallmey, M. Schallmey, *Applied microbiology and biotechnology* **2016**, *100*, 7827-7839.
[74] R. Öhrlein, G. Baisch, *Advanced Synthesis & Catalysis* **2003**, *345*, 713-715.
[75] S. Bergeron, D. Chaplin, J. Edwards, B. Ellis, C. Hill, K. Holt-Tiffin, J. Knight, T. Mahoney, A. Osborne, G. Ruecroft, *Organic Process Research & Development - ORG PROCESS RES DEV* **2006**, *10*.
[76] M. Schürmann, in *Industrial Enzyme Applications* (Eds.: A. Vogel, O. May), Wiley, **2019**, pp. 385-403.
[77] J. Podlech, *Angewandte Chemie International Edition* **2010**, *49*, 6490-6495.
[78] M. Wurtz, *Soc. Chim. Fr* **1872**, *17*, 436-442.
[79] M. Braun, in *Modern Aldol Reactions* (Ed.: R. Mahrwald), **2004**, pp. 1-61.
[80] N. Yoshikawa, Y. M. A. Yamada, J. Das, H. Sasai, M. Shibasaki, *Journal of the American Chemical Society* **1999**, *121*, 4168-4178.
[81] B. List, R. A. Lerner, C. F. Barbas, *Journal of the American Chemical Society* **2000**, *122*, 2395-2396.
[82] a) R. Lerner, S. Benkovic, P. Schultz, *Science* **1991**, *252*, 659-667; b) Y. Yamashita, T. Yasukawa, W.-J. Yoo, T. Kitanosono, S. Kobayashi, *Chemical Society Reviews* **2018**, *47*, 4388-4480.
[83] Karlheinz Drauz, Harald Groeger, O. May., *Enzyme Catalysis in Organic Synthesis, Wiley-VCH Verlag GmbH & Co. KGaA* **2012**
[84] W.-D. Fessner, E. (R. Mahrwald, *Enzyme-catalyzed Aldol Additions in Modern Aldol Reactions, Wiley-VCH, Weinheim* **2004**, 201-272.
[85] T. Gefflaut, C. Blonski, J. Perie, M. Willson, *Progress in Biophysics and Molecular Biology* **1995**, *63*, 301-340.

[86] W.-D. Fessner, A. Schneider, H. Held, G. Sinerius, C. Walter, M. Hixon, J. V. Schloss, *Angewandte Chemie International Edition in English* **1996**, *35*, 2219-2221.
[87] O. T. B. L. Horecker, C. Y. Lai, *in The Enzymes, Academic Press, New York,* **1972,**, *Vol. VII (Ed.: P. D. Boyer)*, .213–258.
[88] a) J. Sygusch, D. Beaudry, M. Allaire, *Proceedings of the National Academy of Sciences of the United States of America* **1987**, *84*, 7846-7850; b) S. J. Gamblin, G. J. Davies, J. M. Grimes, R. M. Jackson, J. A. Littlechild, H. C. Watson, *J Mol Biol* **1991**, *219*, 573-576; c) Š. Janeček, Š. Baláž, *Journal of Protein Chemistry* **1993**, *12*, 509-514; d) A. R. Dalby, D. R. Tolan, J. A. Littlechild, *Acta crystallographica. Section D, Biological crystallography* **2001**, *57*, 1526-1533; e) M. Dick, R. Hartmann, O. H. Weiergraber, C. Bisterfeld, T. Classen, M. Schwarten, P. Neudecker, D. Willbold, J. Pietruszka, *Chem Sci* **2016**, *7*, 4492-4502; f) A. Heine, J. G. Luz, C. H. Wong, I. A. Wilson, *J Mol Biol* **2004**, *343*, 1019-1034; g) A. C. Joerger, C. Gosse, W.-D. Fessner, G. E. Schulz, *Biochemistry* **2000**, *39*, 6033-6041.
[89] C. L. Windle, M. Muller, A. Nelson, A. Berry, *Curr Opin Chem Biol* **2014**, *19*, 25-33.
[90] Y. Li, H. Yu, H. Cao, K. Lau, S. Muthana, V. K. Tiwari, B. Son, X. Chen, *Applied microbiology and biotechnology* **2008**, *79*, 963-970.
[91] M. Cheriyan, E. J. Toone, C. A. Fierke, *Biochemistry* **2012**, *51*, 1658-1668.
[92] I. Baburina, G. Dikdan, F. Guo, G. I. Tous, B. Root, F. Jordan, *Biochemistry* **1998**, *37*, 1245-1255.
[93] N. Appaji Rao, M. Ambili, V. R. Jala, H. S. Subramanya, H. S. Savithri, *Biochimica et Biophysica Acta (BBA) - Proteins and Proteomics* **2003**, *1647*, 24-29.
[94] P. Clapés, W.-D. Fessner, G. A. Sprenger, A. K. Samland, *Current Opinion in Chemical Biology* **2010**, *14*, 154-167.
[95] M. D. Bednarski, E. S. Simon, N. Bischofberger, W. D. Fessner, M. J. Kim, W. Lees, T. Saito, H. Waldmann, G. M. Whitesides, *Journal of the American Chemical Society* **1989**, *111*, 627-635.
[96] a) L. Babich, A. F. Hartog, L. J. van Hemert, F. P. Rutjes, R. Wever, *ChemSusChem* **2012**, *5*, 2348-2353; b) D. Crestia, C. Guérard, J. Bolte, C. Demuynck, *Journal of Molecular Catalysis B: Enzymatic* **2001**, *11*, 207-212.
[97] T. Kajimoto, K. K. C. Liu, R. L. Pederson, Z. Zhong, Y. Ichikawa, J. A. Porco, C. H. Wong, *Journal of the American Chemical Society* **1991**, *113*, 6187-6196.
[98] M. D. Bednarski, in *Comprehensive Organic Synthesis* (Eds.: B. M. Trost, I. Fleming), Pergamon, Oxford, **1991**, pp. 455-473.
[99] M. Schurmann, G. Sprenger, *J Biol Chem* **2001**, *276*, 11055-11061.
[100] a)J. A. Castillo, J. Calveras, J. Casas, M. Mitjans, M. P. Vinardell, T. Parella, T. Inoue, G. A. Sprenger, J. Joglar, P. Clapés, *Organic Letters* **2006**, *8*, 6067-6070; b) D. Güclü, A. Szekrenyi, X. Garrabou, M. Kickstein, S. Junker, P. Clapés, W.-D. Fessner, *ACS Catalysis* **2016**, *6*, 1848-1852.
[101] L. Salleron, G. Magistrelli, C. Mary, N. Fischer, A. Bairoch, L. Lane, *Biochimica et Biophysica Acta (BBA) - Molecular Cell Research* **2014**, *1843*, 2913-2925.
[102] aC. F. Barbas, C.-H. Wong, Y.-F. Wang, *J. Am. Chem. Soc.* **1990**, *112*, 2013-2014; bH. J. M. Gijsen, C.-H. Wong, *Journal of the American Chemical Society* **1995**, *117*, 7585-7591.
[103] D. Chambre, C. Guérard-Hélaine, E. Darii, A. Mariage, J.-L. Petit, M. Salanoubat, V. de Berardinis, M. Lemaire, V. Hélaine, *Chemical Communications* **2019**, *55*, 7498-7501.
[104] a) E. A. Stura, S. Ghosh, E. Garcia-Junceda, L. Chen, C.-H. Wong, I. A. Wilson, *Proteins: Structure, Function, and Bioinformatics* **1995**, *22*, 67-72; b) A. Heine, G. DeSantis, J. G. Luz, M. Mitchell, C. H. Wong, I. A. Wilson, *Science* **2001**, *294*, 369-374.
[105] N. K. Lokanath, I. Shiromizu, N. Ohshima, Y. Nodake, M. Sugahara, S. Yokoyama, S. Kuramitsu, M. Miyano, N. Kunishima, *Acta Crystallographica Section D* **2004**, *60*, 1816-1823.

[106] H. Sakuraba, H. Tsuge, I. Shimoya, R. Kawakami, S. Goda, Y. Kawarabayasi, N. Katunuma, H. Ago, M. Miyano, T. Ohshima, *J Biol Chem* **2003**, *278*, 10799-10806.
[107] H. J. M. Gijsen, C.-H. Wong, *Journal of the American Chemical Society* **1994**, *116*, 8422-8423.
[108] a) M. Oslaj, J. Cluzeau, D. Orkic, G. Kopitar, P. Mrak, Z. Casar, *PLoS One* **2013**, *8*, e62250; b) C.-H. Wong, E. Garcia-Junceda, L. Chen, O. Blanco, H. J. M. Gijsen, D. H. Steensma, *Journal of the American Chemical Society* **1995**, *117*, 3333-3339; c) B. Grabner, Y. Pokhilchuk, H. Gruber-Woelfler, *Catalysts* **2020**, *10*, 137.
[109] V. Laurent, V. Hélaine, C. Vergne-Vaxelaire, L. Nauton, M. Traikia, J.-L. Petit, M. Salanoubat, V. de Berardinis, M. Lemaire, C. Guérard-Hélaine, *ACS Catalysis* **2019**, *9*, 9508-9512.
[110] R. N. Patel, *Bioorg Med Chem* **2018**, *26*, 1252-1274.
[111] a) S. Jennewein, M. Schurmann, M. Wolberg, I. Hilker, R. Luiten, M. Wubbolts, D. Mink, *Biotechnology journal* **2006**, *1*, 537-548; b) H. Fei, G. Xu, J.-P. Wu, L.-R. Yang, *Journal of Molecular Catalysis B: Enzymatic* **2015**, *116*, 148-152.
[112] L. Chen, D. P. Dumas, C. H. Wong, *Journal of the American Chemical Society* **1992**, *114*, 741-748.
[113] W. A. Greenberg, A. Varvak, S. R. Hanson, K. Wong, H. Huang, P. Chen, M. J. Burk, *Proceedings of the National Academy of Sciences of the United States of America* **2004**, *101*, 5788.
[114] Z.-Y. You, Z.-Q. Liu, Y.-G. Zheng, Y.-C. Shen, *Journal of Industrial Microbiology & Biotechnology* **2013**, *40*, 29-39.
[115] G. DeSantis, J. Liu, D. P. Clark, A. Heine, I. A. Wilson, C. H. Wong, *Bioorg Med Chem* **2003**, *11*, 43-52.
[116] J. Liu, C.-C. Hsu, C.-H. Wong, *Tetrahedron Letters* **2004**, *45*, 2439-2441.
[117] J. T. G. Kierkels, D. Mink, S. Panke, F. A. M. Lommen, D. Heemskerk, *DSM, WO 03/006 656*.
[118] J. Li, J. Yang, Y. Men, Y. Zeng, Y. Zhu, C. Dong, Y. Sun, Y. Ma, *Appl Microbiol Biotechnol* **2015**, *99*, 7963-7972.
[119] H. Sakuraba, K. Yoneda, K. Yoshihara, K. Satoh, R. Kawakami, Y. Uto, H. Tsuge, K. Takahashi, H. Hori, T. Ohshima, *Appl Environ Microbiol* **2007**, *73*, 7427-7434.
[120] I. Kullartz, J. Pietruszka, *J Biotechnol* **2012**, *161*, 174-180.
[121] X.-C. Jiao, J. Pan, G.-C. Xu, X.-D. Kong, Q. Chen, Z.-J. Zhang, J.-H. Xu, *Catalysis Science & Technology* **2015**, *5*, 4048-4054.
[122] X.-C. Jiao, J. Pan, X.-D. Kong, J.-H. Xu, *Biochemical and Biophysical Research Communications* **2017**, *482*, 159-163.
[123] A. F. S. A. Habeeb, R. Hiramoto, *Archives of Biochemistry and Biophysics* **1968**, *126*, 16-26.
[124] J. Bramski, M. Dick, J. Pietruszka, T. Classen, *Journal of Biotechnology* **2017**, *258*, 56-58.
[125] J. T. Davies, S. F. Delfino, C. E. Feinberg, M. F. Johnson, V. L. Nappi, J. T. Olinger, A. P. Schwab, H. I. Swanson, *Lipid Insights* **2016**, *9*, 13-29.
[126] J. Clayden, N. Greeves, S. Warren, *Organic Chemistry*, Springer Spektrum, **2013**.
[127] X. Chen, F. Xiong, W. Chen, Q. He, F. Chen, *The Journal of Organic Chemistry* **2014**, *79*, 2723-2728.
[128] H. Waldmann, P. Braun, H. Kunz, *Biomed Biochim Acta* **1991**, *50*, S243-248.
[129] H. Waldmann, A. Heuser, S. Schulze, *Tetrahedron Letters* **1996**, *37*, 8725-8728.
[130] K. Srirangan, V. Orr, L. Akawi, A. Westbrook, M. Moo-Young, C. P. Chou, *Biotechnol Adv* **2013**, *31*, 1319-1332.
[131] P. T. Bandeira, J. C. Thomas, A. R. M. de Oliveira, L. Piovan, *Journal of Chemical Education* **2017**, *94*, 800-805.

[132] D. Manova, F. Gallier, L. Tak-Tak, L. Yotava, N. Lubin-Germain, *Tetrahedron Letters* **2018**, *59*, 2086-2090.
[133] a) B. Stauch, S. J. Fisher, M. Cianci, *J Lipid Res* **2015**, *56*, 2348-2358; b) A. Kundys, E. Białecka-Florjańczyk, A. Fabiszewska, J. Małajowicz, *Journal of Polymers and the Environment* **2018**, *26*, 396-407.
[134] N. J. Oppenheimer, G. T. M. Henehan, in *Enzymology and Molecular Biology of Carbonyl Metabolism 5* (Eds.: H. Weiner, R. S. Holmes, B. Wermuth), Springer US, Boston, MA, **1995**, pp. 407-415.
[135] P. Domínguez de María, C. Carboni-Oerlemans, B. Tuin, G. Bargeman, A. van der Meer, R. van Gemert, *Journal of Molecular Catalysis B: Enzymatic* **2005**, *37*, 36-46.
[136] D. Sørensen, T. Ostenfeld Larsen, C. Christophersen, P. H. Nielsen, U. Anthoni, *Phytochemistry* **1999**, *51*, 1027-1029.
[137] X. Cong, H. Tang, X. Zeng, *J Am Chem Soc* **2015**, *137*, 14367-14372.
[138] M.-M. Wang, X.-S. Ning, J.-P. Qu, Y.-B. Kang, *ACS Catalysis* **2017**, *7*, 4000-4003.
[139] E. J. Corey, J. W. Suggs, *Tetrahedron Letters* **1975**, *16*, 2647-2650.
[140] N. Sun, P. Huang, Y. Wang, W. Mo, B. Hu, Z. Shen, X. Hu, *Tetrahedron* **2015**, *71*, 4835-4841.
[141] A. Švarc, Z. Findrik Blažević, Đ. Vasić-Rački, A. Szekrenyi, W. D. Fessner, S. J. Charnock, A. Vrsalović Presečki, *Journal of Chemical Technology & Biotechnology* **2019**, *94*, 1832-1842.
[142] M. Karplus, *Journal of the American Chemical Society* **1963**, *85*, 2870-2871.
[143] a) M. K. Sharma, D. O. Shah, in *Macro- and Microemulsions, Vol. 272*, American Chemical Society, **1985**, pp. 1-18; b) S. G. Gaikwad, A. B. Pandit, *Ultrasonics Sonochemistry* **2008**, *15*, 554-563; c) J. P. Canselier, H. Delmas, A. M. Wilhelm, B. Abismaïl, *Journal of Dispersion Science and Technology* **2010**, *23*, 333-349.
[144] N. Pravdić, H. G. Fletcher, *Carbohydrate Research* **1971**, *19*, 339-352.
[145] T.-J. Lee, *Tetrahedron Letters* **1985**, *26*, 4995-4996.
[146] D. L. J. Clive, K. S. K. Murthy, A. G. H. Wee, J. S. Prasad, G. V. J. Da Silva, M. Majewski, P. C. Anderson, R. D. Haugen, L. D. Heerze, *Journal of the American Chemical Society* **1988**, *110*, 6914-6916.
[147] M. Sharma, R. J. Bernacki, B. Paul, W. Korytnyk, *Carbohydrate Research* **1990**, *198*, 205-221.
[148] S. Rajagopal, S. Vancheesan, J. Rajaram, J. C. Kuriacose, *Journal of Molecular Catalysis* **1992**, *75*, 199-208.
[149] Y. Mori, M. Suzuki, *Journal of the Chemical Society, Perkin Transactions 1* **1990**, 1809-1812.
[150] F. S. Aalbers, M. W. Fraaije, *ChemBioChem* **2019**, *20*, 51-56.
[151] W. Hummel, *Adv Biochem Eng Biotechnol* **1997**, *58*, 145-184.
[152] T. Vajdič, M. Ošlaj, G. Kopitar, P. Mrak, *Metabolic Engineering* **2014**, *24*, 160-172.
[153] C. Luo, X. Wang, J. Long, J. Liu, *J Biochem Biophys Methods* **2006**, *68*, 101-111.
[154] J. Dong, E. Fernández-Fueyo, F. Hollmann, C. E. Paul, M. Pesic, S. Schmidt, Y. Wang, S. Younes, W. Zhang, *Angewandte Chemie International Edition* **2018**, *57*, 9238-9261.
[155] A. Plaitakis, E. Kalef-Ezra, D. Kotzamani, I. Zaganas, C. Spanaki, *Biology (Basel)* **2017**, *6*, 11.
[156] E. Fossati, F. Polentini, G. Carrea, S. Riva, *Biotechnology and Bioengineering* **2006**, *93*, 1216-1220.
[157] K. Edegger, H. Mang, K. Faber, J. Gross, W. Kroutil, *Journal of Molecular Catalysis A: Chemical* **2006**, *251*, 66-70.
[158] B. Petschacher, N. Staunig, M. Müller, M. Schürmann, D. Mink, S. De Wildeman, K. Gruber, A. Glieder, *Comput Struct Biotechnol J* **2014**, *9*, e201402005-e201402005.
[159] H. Gao, M. K. Tiwari, Y. C. Kang, J. K. Lee, *Bioorg Med Chem Lett* **2012**, *22*, 1931-1935.
[160] W. Hummel, B. Riebel, *Biotechnol Lett* **2003**, *25*, 51-54.

[161] B. R. Riebel, P. R. Gibbs, W. B. Wellborn, A. S. Bommarius, *Advanced Synthesis & Catalysis* **2002**, *344*, 1156-1168.
[162] S. Kawasaki, J. Ishikura, D. Chiba, T. Nishino, Y. Niimura, *Archives of microbiology* **2004**, *181*, 324-330.
[163] T. B. Stanton, R. Sellwood, *Anaerobe* **1999**, *5*, 539-546.
[164] M. Sakamoto, T. Uchimura, K. Komagata, *Journal of Fermentation and Bioengineering* **1996**, *82*, 531-537.
[165] L. Wang, H. Chong, R. Jiang, *Appl Microbiol Biotechnol* **2012**, *96*, 1265-1273.
[166] V. Cracan, D. V. Titov, H. Shen, Z. Grabarek, V. K. Mootha, *Nature chemical biology* **2017**, *13*, 1088-1095.
[167] A. Pessina, P. Lüthi, P. L. Luisi, J. Prenosil, Y.-S. Zhang, *Helvetica Chimica Acta* **1988**, *71*, 631-641.
[168] E. A. Kee, M. C. Livengood, E. E. Carter, M. McKenna, M. Cafiero, *The Journal of Physical Chemistry B* **2009**, *113*, 14810-14815.
[169] K. Laki, *Annals of the New York Academy of Sciences* **1972**, *202*, 297-307.
[170] L. Stefanini, W. Bergmeier, *Journal of thrombosis and haemostasis : JTH* **2018**, *16*, 220-230.
[171] M. Bryckaert, J.-P. Rosa, C. V. Denis, P. J. Lenting, *Cell Mol Life Sci* **2015**, *72*, 307-326.
[172] K. Sangkuhl, A. R. Shuldiner, T. E. Klein, R. B. Altman, *Pharmacogenet Genomics* **2011**, *21*, 516-521.
[173] L. K. Jennings, *The American journal of cardiology* **2009**, *103*, 4a-10a.
[174] D. A. Mistry, A. Chandratreya, P. Y. F. Lee, *Surg J (N Y)* **2017**, *3*, e191-e196.
[175] K. E. Hernandez, H. Renata, R. D. Lewis, S. B. Jennifer Kan, C. Zhang, J. Forte, D. Rozzell, J. A. McIntosh, F. H. Arnold, *ACS catalysis* **2016**, *6*, 7810-7813.
[176] R. C. Becker, J. P. Bassand, A. Budaj, D. M. Wojdyla, S. K. James, J. H. Cornel, J. French, C. Held, J. Horrow, S. Husted, J. Lopez-Sendon, R. Lassila, K. W. Mahaffey, R. F. Storey, R. A. Harrington, L. Wallentin, *European Heart Journal* **2011**, *32*, 2933-2944.
[177] R. F. Storey, R. C. Becker, R. A. Harrington, S. Husted, S. K. James, F. Cools, P. G. Steg, N. S. Khurmi, H. Emanuelsson, A. Cooper, R. Cairns, C. P. Cannon, L. Wallentin, *European Heart Journal* **2011**, *32*, 2945-2953.
[178] K. Huber, B. Hamad, P. Kirkpatrick, *Nature Reviews Drug Discovery* **2011**, *10*, 255-256.
[179] a) K. Birkeland, D. Parra, R. Rosenstein, *J Blood Med* **2010**, *1*, 197-219; b) B. S. Cooperman, in *Encyclopedia of Biological Chemistry (Second Edition)* (Eds.: W. J. Lennarz, M. D. Lane), Academic Press, Waltham, **2013**, pp. 71-74.
[180] S. J. Chawner, M. J. Cases-Thomas, J. A. Bull, *European journal of organic chemistry* **2017**, *2017*, 5015-5024.
[181] J. Hu, G. Li, C. Liang, S. Shams, S. Zhu, G. Zheng, *Process Biochemistry* **2020**, *92*, 232-243.
[182] O. Mitsunobu, M. Yamada, *Bulletin of the Chemical Society of Japan* **1967**, *40*, 2380-2382.
[183] S. B. Raj, S. Ramaswamy, B. V. Plapp, *Biochemistry* **2014**, *53*, 5791-5803.
[184] J. P. Adams, M. J. B. Brown, A. Diaz-Rodriguez, R. C. Lloyd, G.-D. Roiban, *Advanced Synthesis & Catalysis* **2019**, *361*, 2421-2432.
[185] a) A. Vogel, O. May, *Industrial Enzyme Applications*, Wiley, **2019**; b) J. An, Y. Nie, Y. Xu, *Critical Reviews in Biotechnology* **2019**, *39*, 366-379.
[186] O. de Smidt, J. C. du Preez, J. Albertyn, *FEMS Yeast Research* **2008**, *8*, 967-978.
[187] B. Krulewicz, D. Tschaen, P. Devine, S. S. Lee, C. Roberge, R. Greasham, M. Chartrain, *Biocatalysis and Biotransformation* **2001**, *19*, 267-279.
[188] D. Zhu, C. Mukherjee, L. Hua, *Tetrahedron: Asymmetry* **2005**, *16*, 3275-3278.
[189] R. N. Patel, A. Goswami, L. Chu, M. J. Donovan, V. Nanduri, S. Goldberg, R. Johnston, P. J. Siva, B. Nielsen, J. Fan, W. He, Z. Shi, K. Y. Wang, R. Eiring, D. Cazzulino, A. Singh, R. Mueller, *Tetrahedron: Asymmetry* **2004**, *15*, 1247-1258.

[190] D. Pollard, M. Truppo, J. Pollard, C.-y. Chen, J. Moore, *Tetrahedron: Asymmetry* **2006**, *17*, 554-559.
[191] R. N. Patel, A. Banerjee, L. Chu, D. Brozozowski, V. Nanduri, L. J. Szarka, *Journal of the American Oil Chemists' Society* **1998**, *75*, 1473-1482.
[192] M. Singh, H. Krishnen, U. K. Neelam, K. Charugondla, G. Gilla, K. Holt-Tiffin, R. Bandichhor, *RSC Advances* **2016**, *6*, 35086-35090.
[193] M. D. Truppo, F. Escalettes, N. J. Turner, *Angewandte Chemie International Edition* **2008**, *47*, 2639-2641.
[194] R. Machielsen, L. L. Looger, J. Raedts, S. Dijkhuizen, W. Hummel, H.-G. Hennemann, T. Daussmann, J. van der Oost, *Eng. Life Sci.* **2009**, *9*, 38-44.
[195] a) K. Niefind, J. Müller, B. Riebel, W. Hummel, D. Schomburg, *Journal of Molecular Biology* **2003**, *327*, 317-328; b) S. Leuchs, L. Greiner, *Chem. Biochem. Eng Q.* **2011**, *25*, 267–281.
[196] a) N. H. Schlieben, K. Niefind, J. Muller, B. Riebel, W. Hummel, D. Schomburg, *J Mol Biol* **2005**, *349*, 801-813; b) R. Buller, E. Medina, W. K. Chan, A. Michine, R. Sheldon, T. Moody, A. Buthe, M. Schurmann, F. Moris, R. Snajdrova, *Biocatalysis: An Industrial Perspective*, Royal Society of Chemistry, **2017**.
[197] M. Wolberg, W. Hummel, M. Müller, *Chemistry-a European Journal - CHEM-EUR J* **2001**, *7*, 4562-4571.
[198] C. Rodríguez, W. Borzęcka, J. H. Sattler, W. Kroutil, I. Lavandera, V. Gotor, *Organic & Biomolecular Chemistry* **2014**, *12*, 673-681.
[199] B. Geueke, B. Riebel, W. Hummel, *Enzyme and Microbial Technology* **2003**, *32*, 205-211.
[200] S. Lutz, S. M. Iamurri, in *Protein Engineering: Methods and Protocols* (Eds.: U. T. Bornscheuer, M. Höhne), Springer New York, New York, NY, **2018**, pp. 1-12.
[201] T. S. Farmer, P. Bohse, D. Kerr, *Journal of Student Research* **2018**, *6*, 31-38.
[202] S. B. Rubin-Pitel, C. M. H. Cho, W. Chen, H. Zhao, in *Bioprocessing for Value-Added Products from Renewable Resources* (Ed.: S.-T. Yang), Elsevier, Amsterdam, **2007**, pp. 49-72.
[203] F. Cedrone, A. Ménez, E. Quéméneur, *Curr Opin Struct Biol* **2000**, *10*, 405-410.
[204] C. A. Floudas, H. K. Fung, S. R. McAllister, M. Mönnigmann, R. Rajgaria, *Chemical Engineering Science* **2006**, *61*, 966-988.
[205] V. Stepankova, S. Nevolova, T. Koudelakova, Z. Prokop, R. Chaloupkova, J. Damborský, *ACS Catalysis* **2013**, *3*, 2823–2836.
[206] T. Scheidt, H. Land, M. Anderson, Y. Chen, P. Berglund, D. Yi, W.-D. Fessner, *Advanced Synthesis & Catalysis* **2015**, *357*, 1721-1731.
[207] Y. V. Sheludko, W.-D. Fessner, *Current Opinion in Structural Biology* **2020**, *63*, 123-133.
[208] K. Chamchoy, D. Pakotiprapha, P. Pumirat, U. Leartsakulpanich, U. Boonyuen, *BMC Biochem* **2019**, *20*, 4-4.
[209] W. Zhang, K. Connor, D. I. C. Wang, Z. Li, *Applied and Environmental Microbiology* **2009**, *75*, 687.
[210] N. Richter, A. Zienert, W. Hummel, *Engineering in Life Sciences* **2011**, *11*, 26-36.
[211] Y.-H. Paik, K. Iwaisako, E. Seki, S. Inokuchi, B. Schnabl, C. H. Österreicher, T. Kisseleva, D. A. Brenner, *Hepatology* **2011**, *53*, 1730-1741.
[212] D. J. Yee, V. Balsanek, D. R. Bauman, T. M. Penning, D. Sames, *Proceedings of the National Academy of Sciences* **2006**, *103*, 13304.
[213] S. Roth, M. B. Kilgore, T. M. Kutchan, M. Müller, *ChemBioChem* **2018**, *19*, 1849-1852.
[214] F. W. Studier, *Protein Expr Purif* **2005**, *41*, 207-234.
[215] K. S. Siddiqui, *Critical Reviews in Biotechnology* **2017**, *37*, 309-322.
[216] T. Ku, P. Lu, C. Chan, T. Wang, S. Lai, P. Lyu, N. Hsiao, *Computational Biology and Chemistry* **2009**, *33*, 445-450.
[217] G. Chattopadhyay, R. Varadarajan, *Protein Science* **2019**, *28*, 1127-1134.

[218] A. O. Magnusson, A. Szekrenyi, H.-J. Joosten, J. Finnigan, S. Charnock, W.-D. Fessner, *The FEBS Journal* **2019**, *286*, 184-204.
[219] A. Spielmann, Y. Brack, H. van Beek, L. Flachbart, L. Sundermeyer, M. Baumgart, M. Bott, *AMB Express* **2020**, *10*, 14.
[220] A. Cornish-Bowden, *Perspectives in Science* **2015**, *4*, 3-9.
[221] Y. Katsuyama, Y. Sato, Y. Sugai, Y. Higashiyama, M. Senda, T. Senda, Y. Ohnishi, *Febs j* **2018**, *285*, 1540-1555.
[222] H. S. T. Tanja Knaus, and Nigel S. Scrutton, in *Green Biocatalysis*, **2016**, pp. 473-488.
[223] G. R. Fulmer, A. J. M. Miller, N. H. Sherden, H. E. Gottlieb, A. Nudelman, B. M. Stoltz, J. E. Bercaw, K. I. Goldberg, *Organometallics* **2010**, *29*, 2176-2179.

Annex

List of frequently used abbreviations

ADH	Alcohol dehydrogenase
ACS	acute coronary artery syndrome
AIM	Auto induction medium
ATP, ADT	Adenosine triphosphate, diphosphate
BCA	bicinchoninic acid
β-CD	β-cyclodextrine
BSA	Bovine serum albumin
CalB	*Candida antarctica* Lipase B
CE	Crude extract
CFE	Cell free extract
CPA	Cyclopropylamine
CoA	Coenzyme A
DCM	Dichloromethane
DERA	2-Deoxyribose-5-phosphate aldolase
D-G3P	D-glyceraldehyde 3-phosphate
DHAP	Dihydroxyacetone phosphate
DMAC	Dimethylacetamide
DMAP	Dimethylamino pyridine
DMSO	Dimethylsulfoxide
DNA	Deoxyribonucleic acid
D-R5P	2-deoxy- D-ribose 5-phosphate
DTT	Dithiothreitol
E. coli	*Eschericchia coli*
ee	enantiomeric excess
e.g.	(lat.) *exempli gratia*
eq	equivalents
et al.	(lat.) *et alii* or *et aliae*
EDG	Electron donating group
EDTA	Ethylenediaminetetraacetic acid
EWG	Electron-withdrawing group
ER	Enereductase
FSA	D-Fructose-6-phosphat aldolase
GDH	Glucose/glutamate dehydrogenase
3-HB	3-Hydroxybutanal
HHD	Halohydrine dehydrogenase
HMG	3-Hydroxy-3-methylglutaryl
HMGR	3-Hydroxy-3-methylglutaryl-CoA reductase
HPLC	High performance liquid chromatography
(HP)TLC	(High performance) thin layer Chromatography
INT	Iodonitrotetrazolium
KRED	Ketoreductase
LB	Lysogeny broth
Lb	*Lactobacillus brevis*
LDL	Low density lipoprotein
LOD	Limit of detection
LOQ	Limit of quantification
MS	Mass spectrometry
NAD(P)H	Nicotinamide adenine dinucleotide (phosphate), reduced form
nanoDSF	Nanoscale differential scanning fluorimetry
NMR	Nuclear magnetic resonance
NOX	Nicotinamide oxidase
PCC	Pyridinium chlorochromate
PCR	Polymerase chain reaction
PGA	Penicillin G acylase
PhAc	Phenylacetyl
ppm	parts per million
rpm	revolutions per minute
RC	Resting cells
RT	Room temperature
R_f	Retention factor
SDR	short-chain reductases
SDS-PAGE	sodium dodecyl sulfate polyacrylamide gel electrophoresis
SOP	Standard operating procedure
TEA	Triethanolamine
THF	Tetrahydrofurane
TLC	Thin layer chromatography
Tm	*Thermotoga maritima*
UV	ultra violet
WT	wildtype

NMR spectra of statin products (Part I)

PhAc-protected lactone 4a

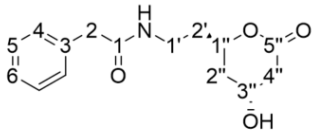

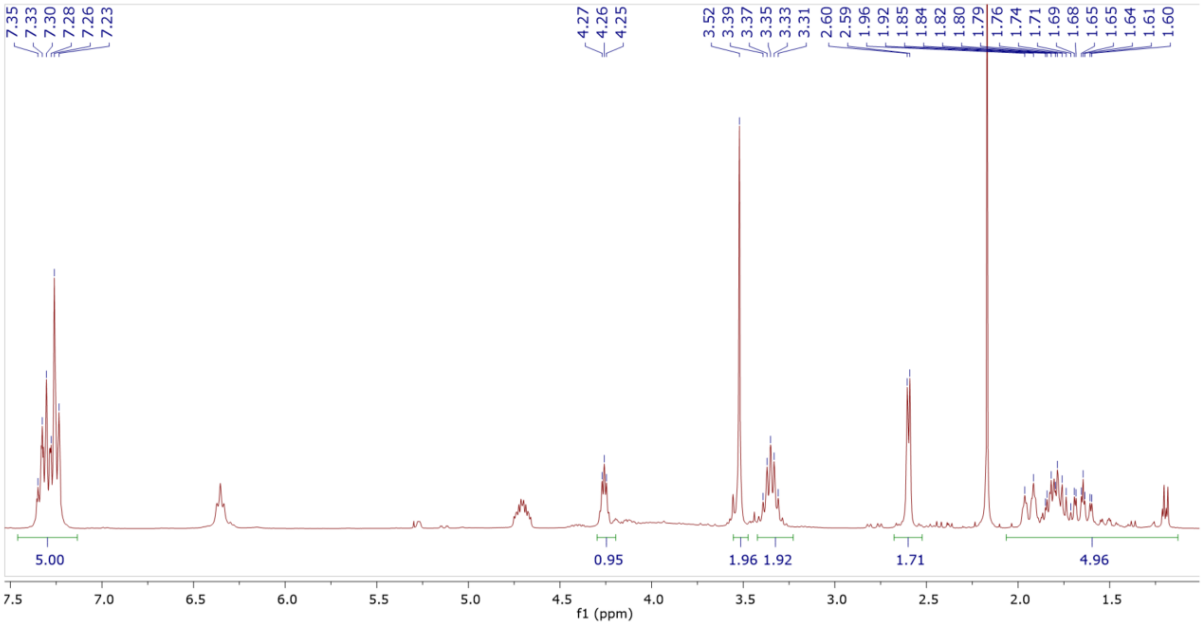

^{1}H NMR (300 MHz, Chloroform-*d*) δ = 7.42 – 7.15 (m, 5H, 4-, 5-, 6-H), 4.34 – 4.17 (m, 1H, 1’’-H), 3.52 (s, 2H, 2-H), 3.35 (p, *J* = 6.6 Hz, 1H, 3’’-H), 2.60 (d, *J* = 4.1 Hz, 2H, 1’-H), 2.02 – 1.41 (m, 6H,2’-, 2’’-, 4’’-H).

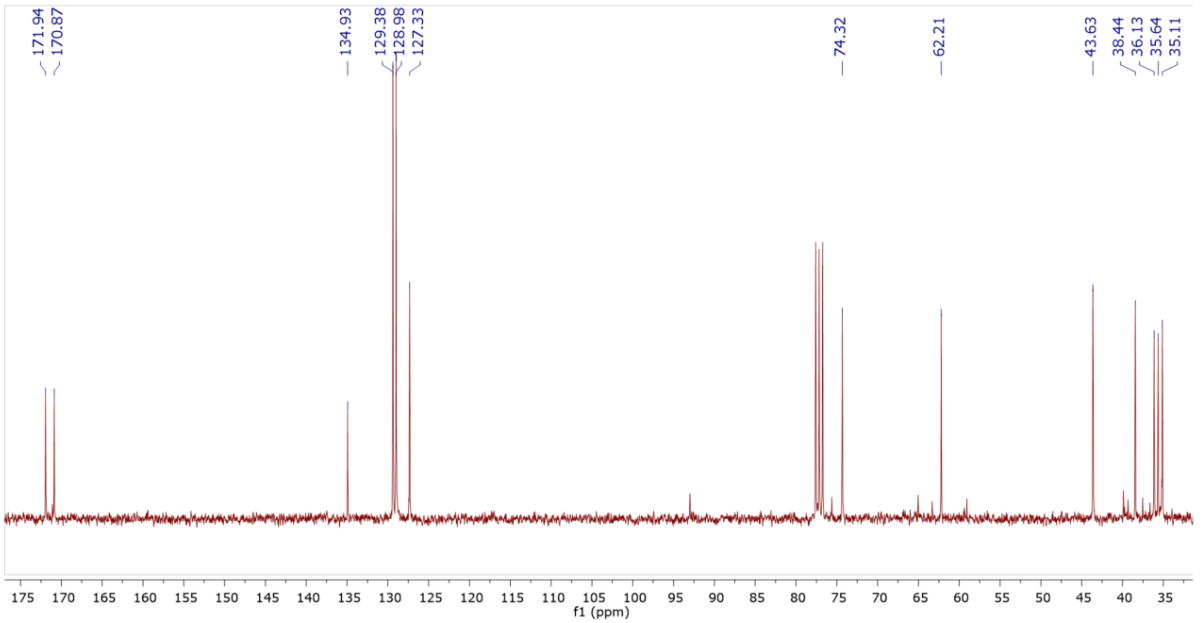

^{13}C NMR (75 MHz, $CDCl_3$) δ = 171.94 (C-1), 170.87 (C-5’’), 134.93 (C-3), 129.38 (C-4), 128.98 (C-5), 127.33 (C-6), 74.32 (C-1’’), 62.21 (C-3’’), 43.63 (C-2), 38.44 (C-4’’), 36.13 (C-1’), 35.64 (C-2’’), 35.11 (C-2’).

Solistatin (4b)

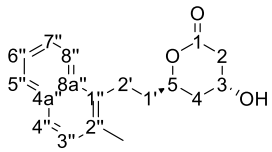

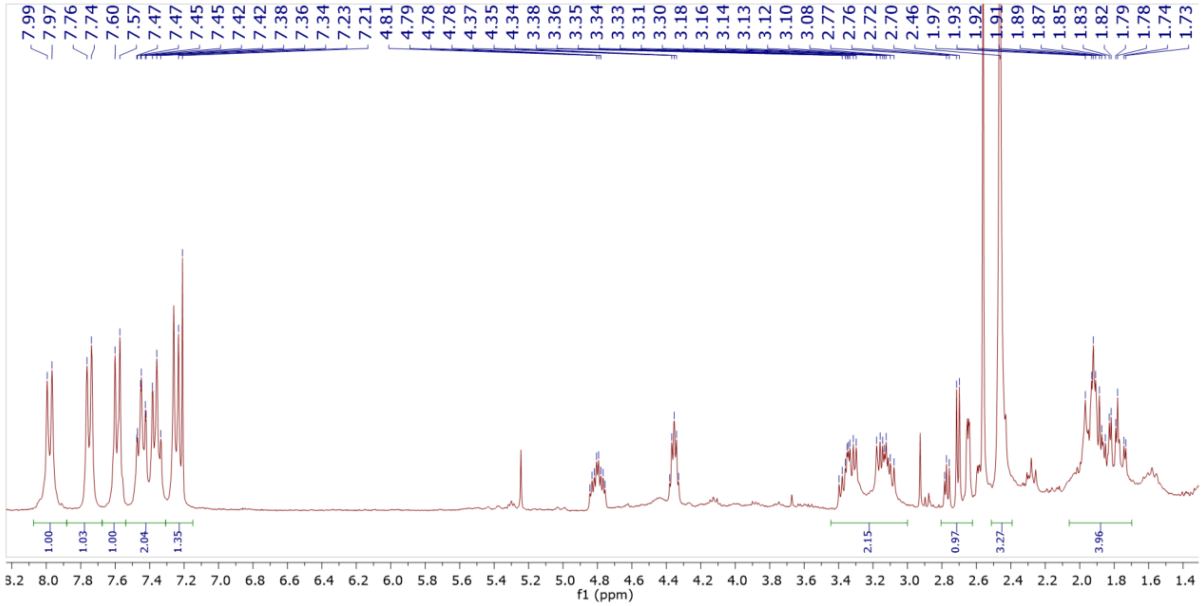

[1]H NMR (300 MHz, Chloroform-*d*) δ = 7.98 (d, *J* = 8.4 Hz, 1H, 8‘‘-H), 7.75 (d, *J* = 7.8 Hz, 1H, 5‘‘-H), 7.59 (d, *J* = 8.3 Hz, 1H, 4‘‘-H), 7.52 – 7.30 (m, 2H, 6‘‘-, 7‘‘-H), 7.22 (d, *J* = 6.8 Hz, 1H, 3‘‘-H), 4.91 – 4.69 (m, 1H, 3-H), 4.35 (p, *J* = 3.6 Hz, 1H, 5-H), 3.47 – 3.03 (m, 2H, 2‘-H), 2.74 (dd, *J* = 17.6, 4.9 Hz, 1H, 2H), 2.46 (s, 3H, CH_3), 2.09 – 1.68 (m, 1‘-, 4-H).

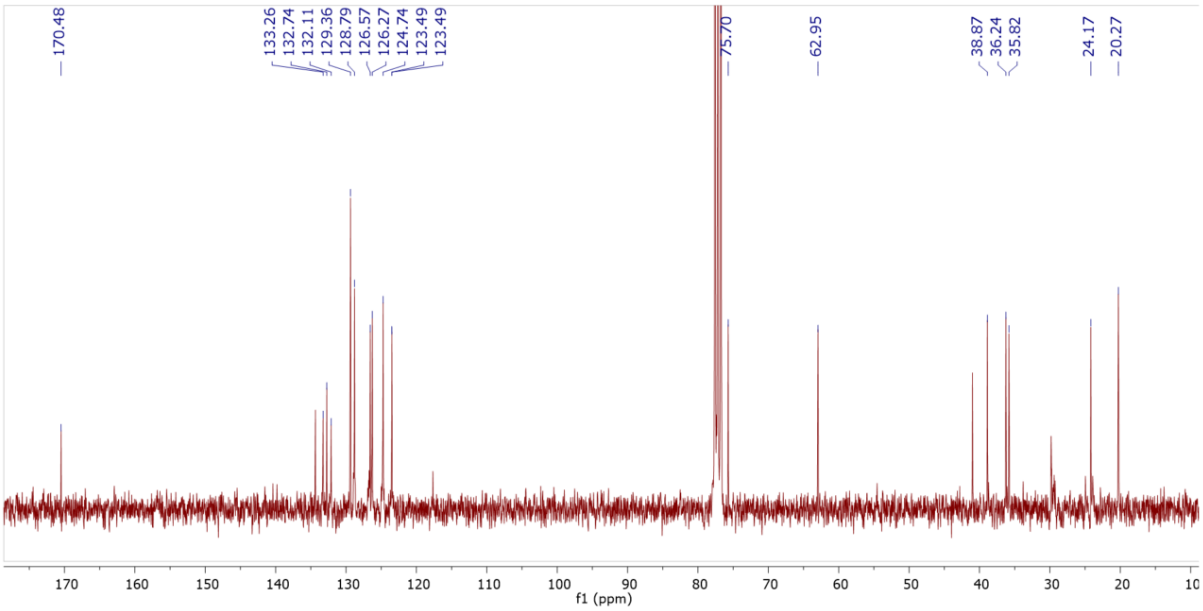

[13]C NMR (75 MHz, $CDCl_3$) δ = 170.48 (C-1), 133.26 (C-1‘‘), 132.74 (C-8a‘‘), 132.11 (C-4a‘‘), 129.36 (C-2‘‘), 128.79 (C-3‘‘), 126.57 (C-5‘‘), 126.27 (C-4‘‘), 124.74 (C-7‘‘), 123.49 (C-8‘‘), 123.49 (C-6‘‘), 75.70 (C-5), 62.95 (C-3), 38.87 (C-2), 36.24 (C-1’), 35.82 (C-4), 24.17 (C-2‘‘), 20.27 (CH_3).

Norsolistatin (4c)

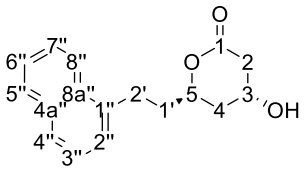

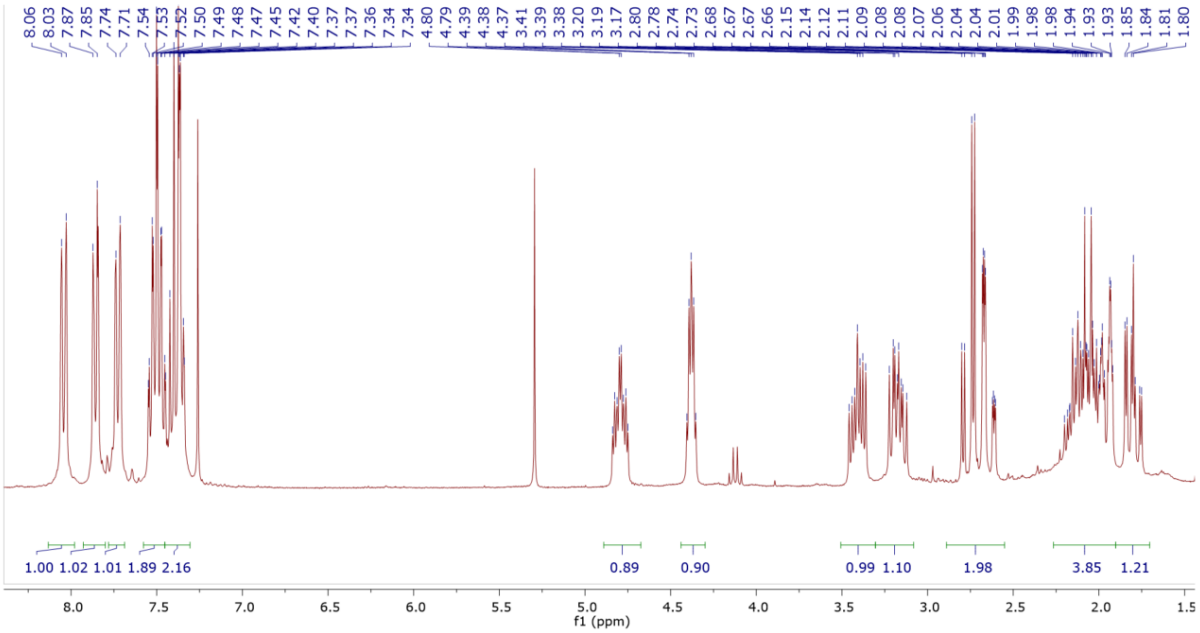

^{1}H NMR (300 MHz, Chloroform-*d*) δ = 8.04 (d, *J* = 8.0 Hz, 1H, 8''-H), 7.86 (d, *J* = 7.5 Hz, 1H, 5''-H), 7.73 (d, *J* = 7.6 Hz, 1H, 4''-H), 7.50 (pd, *J* = 6.9, 1.5 Hz, 2H, 6''-, 7''-H), 7.43 – 7.31 (m, 2H, 2'', -3''-H), 4.79 (ddt, *J* = 11.6, 8.0, 3.6 Hz, 1H, 3-H), 4.38 (p, *J* = 3.6 Hz, 1H, 5-H), 3.41 (ddd, *J* = 14.7, 9.9, 5.2 Hz, 1H, 2'-H_a), 3.17 (ddd, *J* = 14.1, 9.6, 6.8 Hz, 1H, 2'-H_b), 2.76 (dd, *J* = 17.6, 5.0 Hz, 1H, 2-H_a), 2.64 (ddd, *J* = 17.7, 3.7, 1.5 Hz, 1H, 2-H_b), 2.22 – 1.90 (m, 2H, 4-H), 1.80 (ddd, *J* = 14.5, 11.2, 3.4 Hz, 1H, 1'-H).

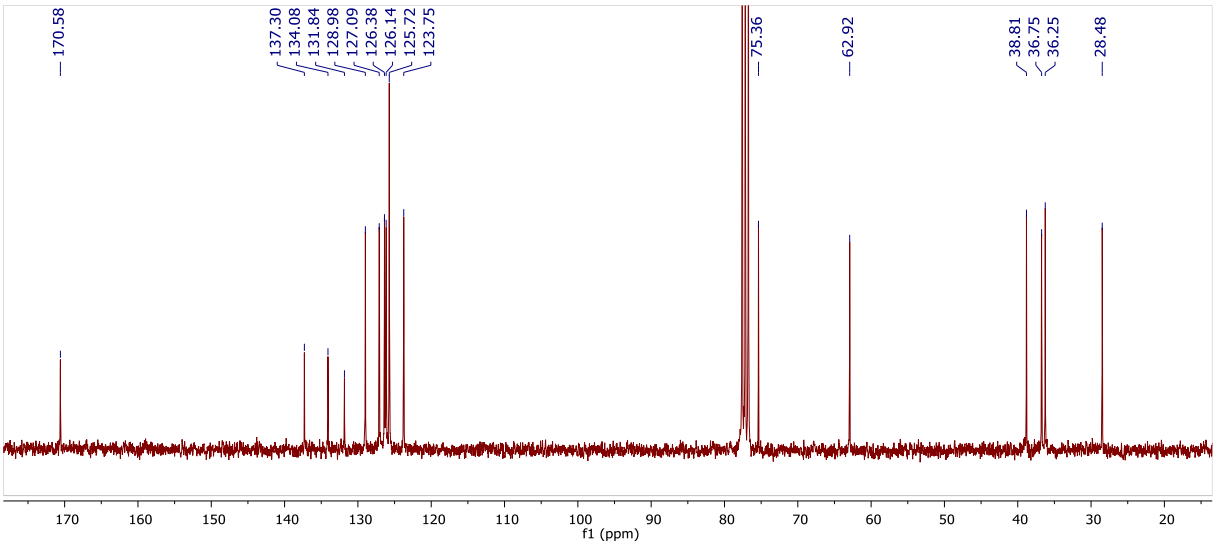

^{13}C NMR (75 MHz, $CDCl_3$) δ = 170.58 (C-1), 137.30 (C-1''), 134.08 (C-8a''), 131.84 (4a'-H'), 128.98 (C-8''), 127.09 (C-5''), 126.38 (C-4''), 126.14 (C-3''), 125.72 (C-7''+8''), 123.75 (C-2''), 75.36 (C-5), 62.92 (C-3), 38.81 (C-2), 36.75 (C-1), 36.25 (C-4'), 28.48 (C-2').

(4R,6R)-4-hydroxy-6-phenethyltetrahydro-2H-pyran-2-one (4d)

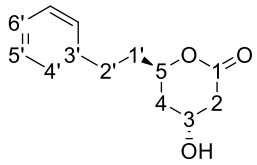

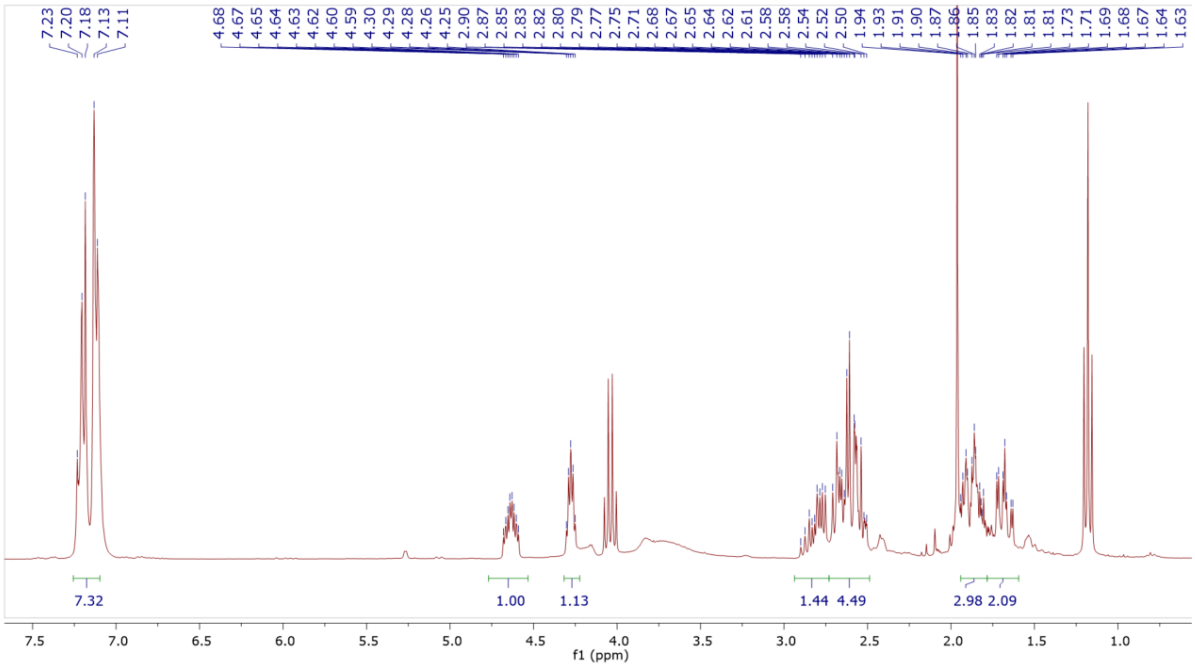

^{1}H NMR (300 MHz, Chloroform-*d*) δ = 7.31 – 6.90 (m, 5H, 4'-, 5', 6'-H), 4.63 (ddt, *J* = 11.4, 7.8, 3.9 Hz, 1H, 3-H), 4.28 (p, *J* = 3.7 Hz, 1H, 5H), 2.96 – 2.49 (m, 4H, 2-, 2'-H), 1.94 – 1.59 (m, 4H, 1'-, 4-H).

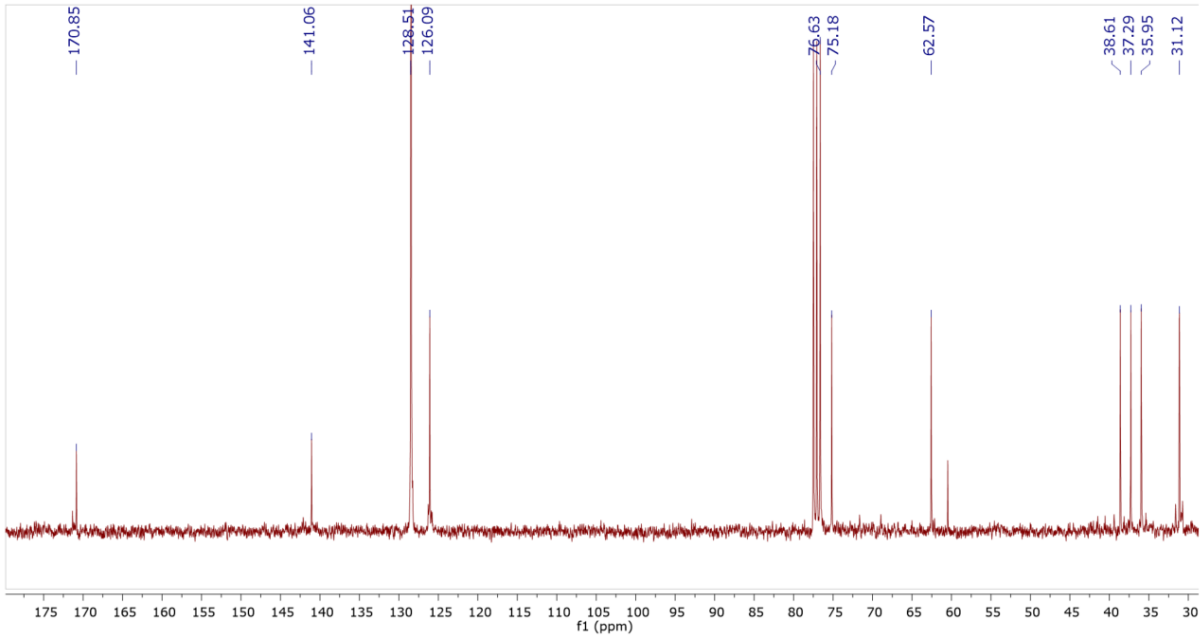

^{13}C NMR (75 MHz, $CDCl_3$) δ = 170.85 (C-1), 141.06 (C-3'), 128.51 (C-4'+C-5'), 126.09 (C-6'), 76.63 (C-5), 62.57 (C-3), 38.61 (C-2), 37.29 (C-4), 35.95 (C-1'), 31.12 (C-2').

(4R,6S)-4-hydroxy-6-(phenoxymethyl)tetrahydro-2H-pyran-2-one (4e)

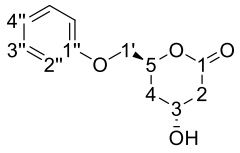

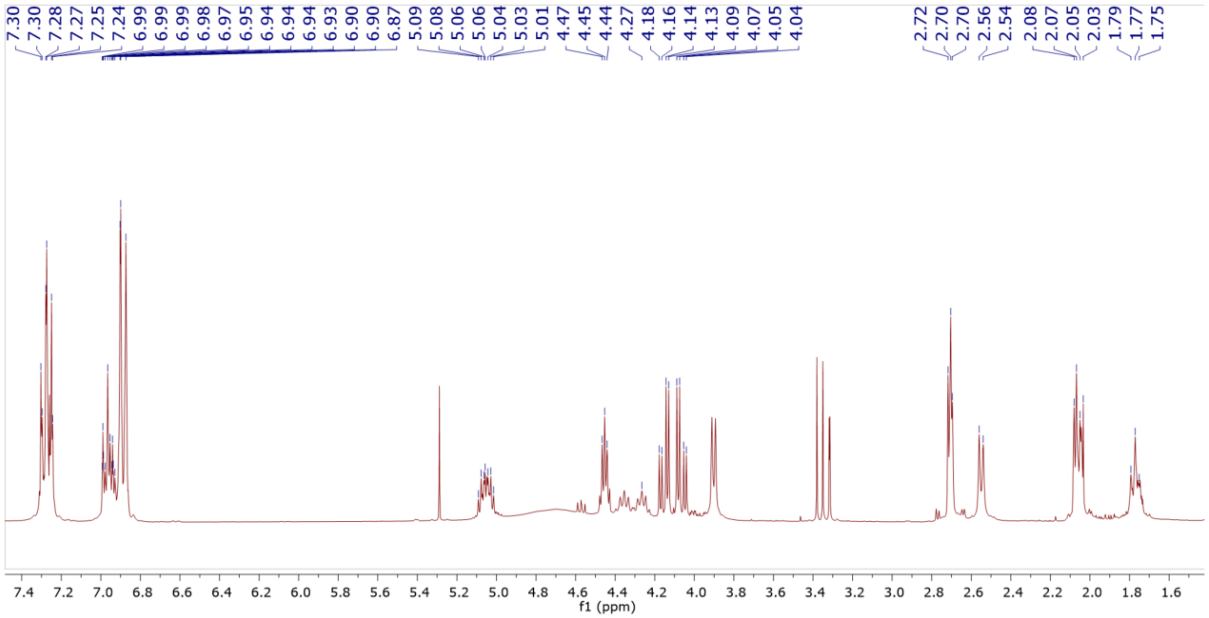

^{1}H NMR (300 MHz, Chloroform-*d*) δ = 7.27 (td, *J* = 8.9, 8.2, 1.8 Hz, 2H, 3''-H), 7.05 – 6.79 (m, 3H, 2'', -4''-H), 5.14 – 4.97 (m, 1H, 5-H), 4.52 – 4.42 (m, 1H, 3-H), 4.20 – 4.02 (m, 2H, 1'-H), 2.81 – 2.47 (m, 2H, 2-H), 2.14 – 1.69 (m, 2H, 4-H).

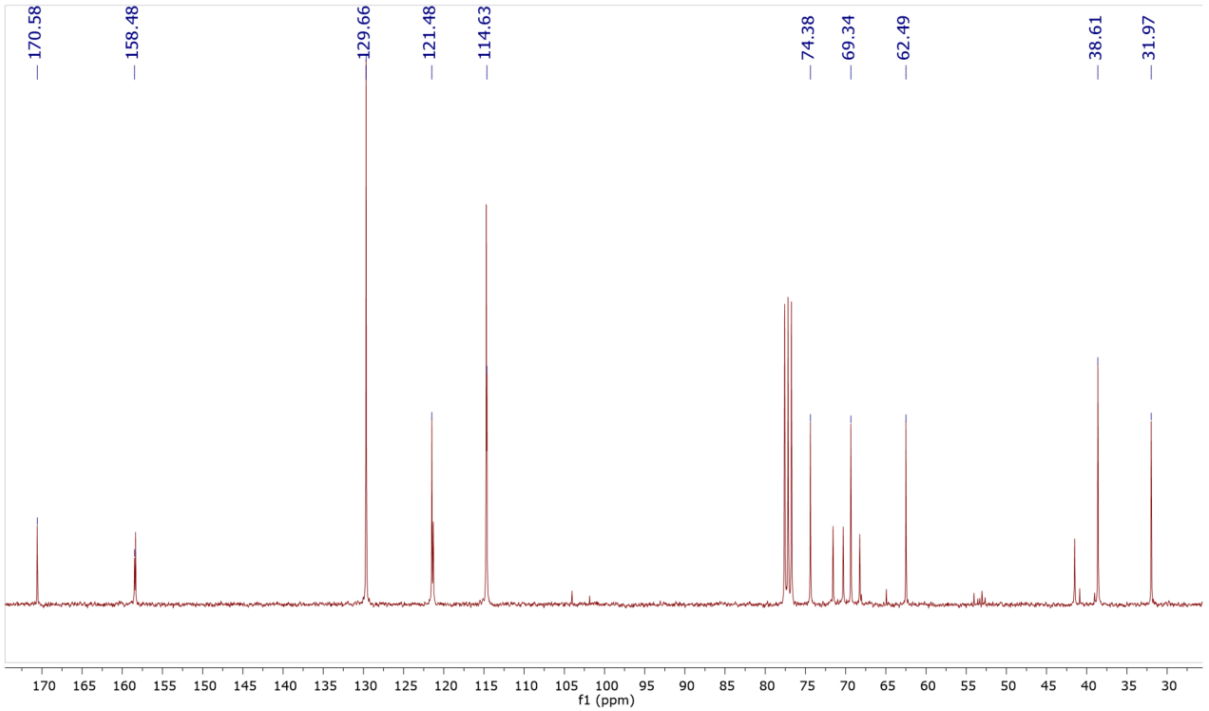

^{13}C NMR (75 MHz, $CDCl_3$) δ = 170.58 (C-1), 158.48 (C-1''), 129.66 (C-3''), 121.48 (C-4''), 114.63 (C-2''), 74.38 (C-5), 69.34 (C-1), 62.49 (C-3), 38.61 (C-2), 31.97 (C-4).

(4R,6S)-6-((2,6-dimethylphenoxy)methyl)-4-hydroxytetrahydro-2H-pyran-2-one (4f)

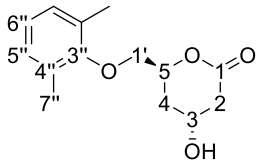

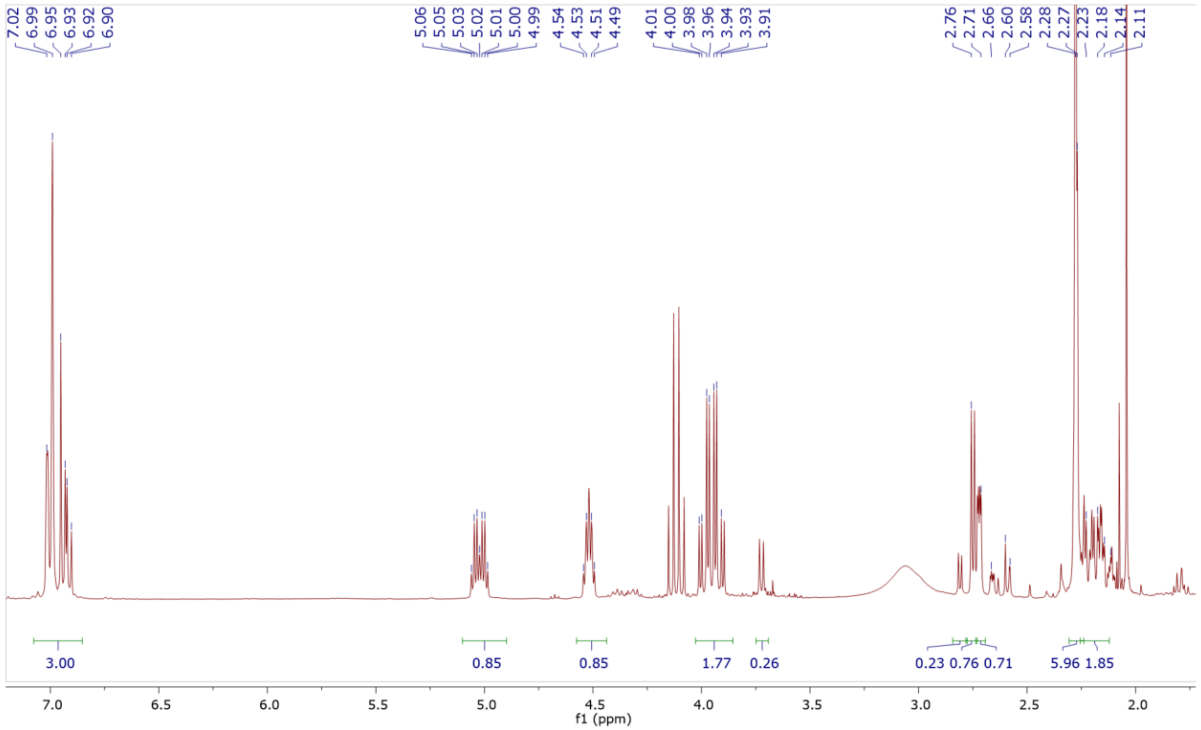

^{1}H NMR (300 MHz, Chloroform-*d*) δ = 7.08 – 6.84 (m, 3H, 3''-, 4*'-H), 5.02 (dq, *J* = 11.1, 3.9 Hz, 1H, 5-H), 4.59 - 4.44 (m, 1H, 3-H), 4.05 – 3.86 (m, 2H, 1'-H), 2.78 – 2.54 (m, 2H, 2-H), 2.27 (s, 6H, 5'-H), 2.26 – 2.11 (m, 2H, 4-H).

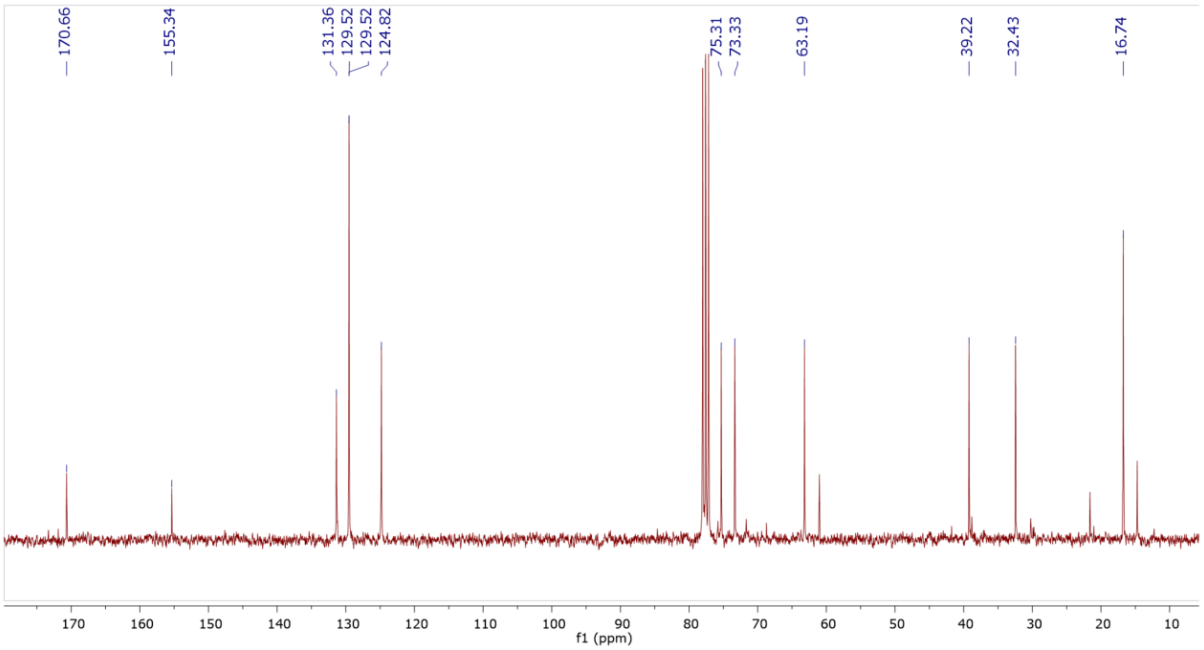

^{13}C NMR (75 MHz, $CDCl_3$) δ = 170.66 (C-1), 155.34 (C-1''), 131.36 (C-2''), 129.52 (C-3''), 124.82 (C-4''), 75.31 (C-5, 73.33 (C-1'), 63.19 (C-3), 39.22 (C-2), 32.43 (C-4), 16.74 (C-5'').

(4R,6S)-6-((cyclohexyloxy)methyl)-4-hydroxytetrahydro-2H-pyran-2-one (4g)

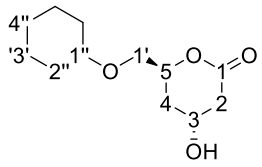

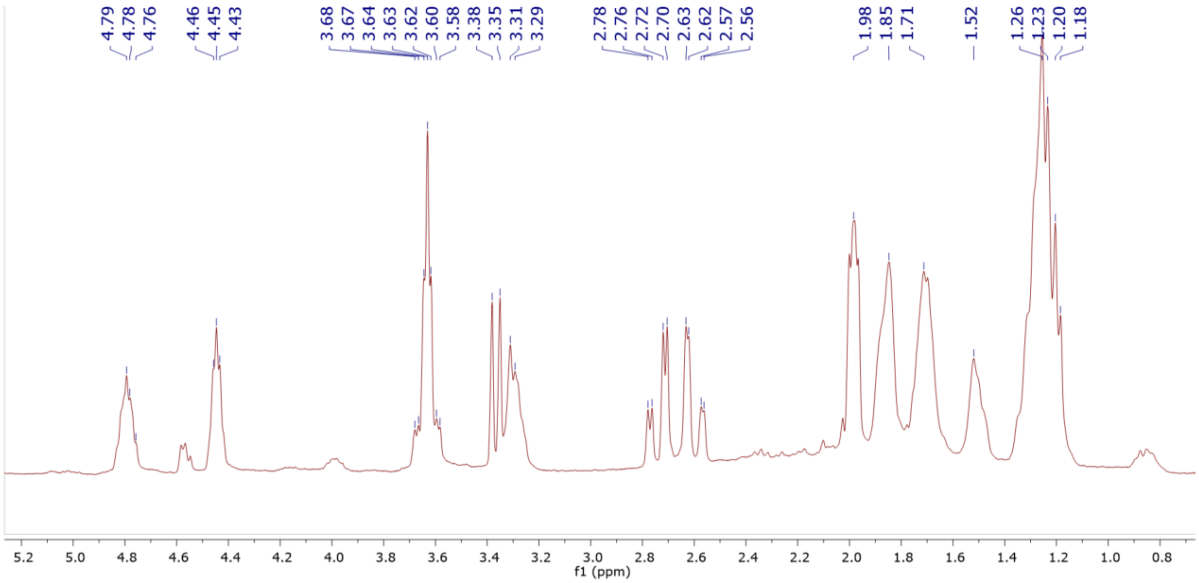

^{1}H NMR (300 MHz, Chloroform-*d*) δ = 4.85 – 4.72 (m, 1H, 3-H), 4.48 – 4.38 (m, 1H, 5-H), 3.33 (dd, *J* = 19.3, 7.3 Hz, 1H, 1'-H), 2.82 – 2.50 (m, 1H, 1''-H), 2.07 – 1.63 (m, 1H, 2-, 4-H), 1.61 – 1.13 (m, 10H, 2''-, 3'', 4''-H).

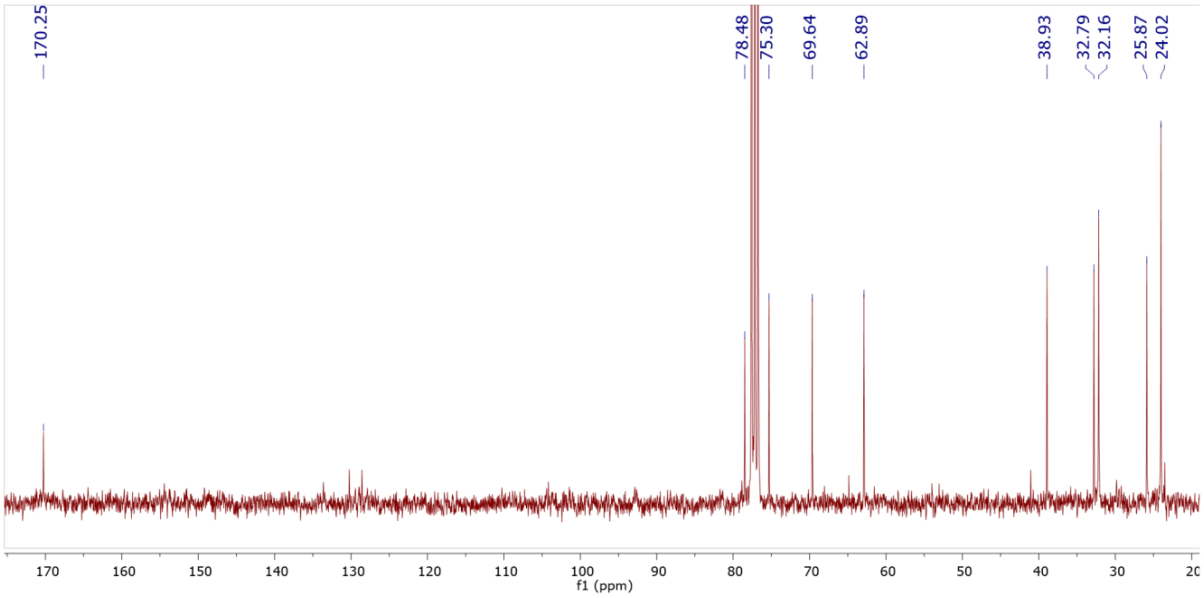

^{13}C NMR (75 MHz, $CDCl_3$) δ 170.25 (C-2), 78.48 (C-1''), 75.30 (C-1'), 69.64 (C-6), 62.89 (C-4), 38.93 (C-3), 32.79 (C-5), 32.16 (C-2''), 25.87 (C-4''), 24.02 (C-3'').

1-(6-methoxynaphthalen-2-yl)ethanol (174a)

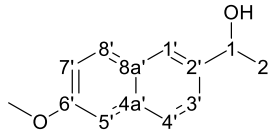

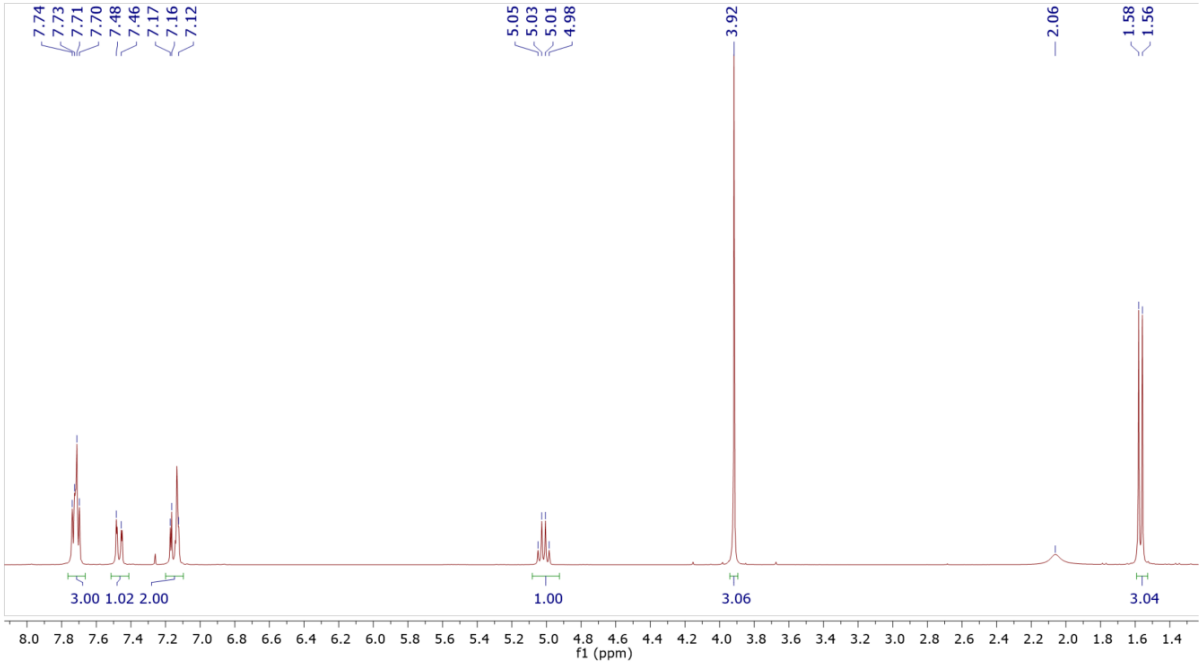

^{1}H NMR (300 MHz, Chloroform-*d*) δ = 7.74 – 7.70 (m, 3H, 1'-, 4'-, 8'-H), 7.47 (d, *J* = 8.5 Hz, 1H, 5'-H), 7.17 – 7.12 (m, 2H, 3'-, 7'-H), 5.02 (q, *J* = 6.4 Hz, 1H, 1-H), 3.92 (s, 3H, 1''-H), 2,06 (br, 1H, OH), 1.57 (d, *J* = 6.5 Hz, 3H, 2-H).

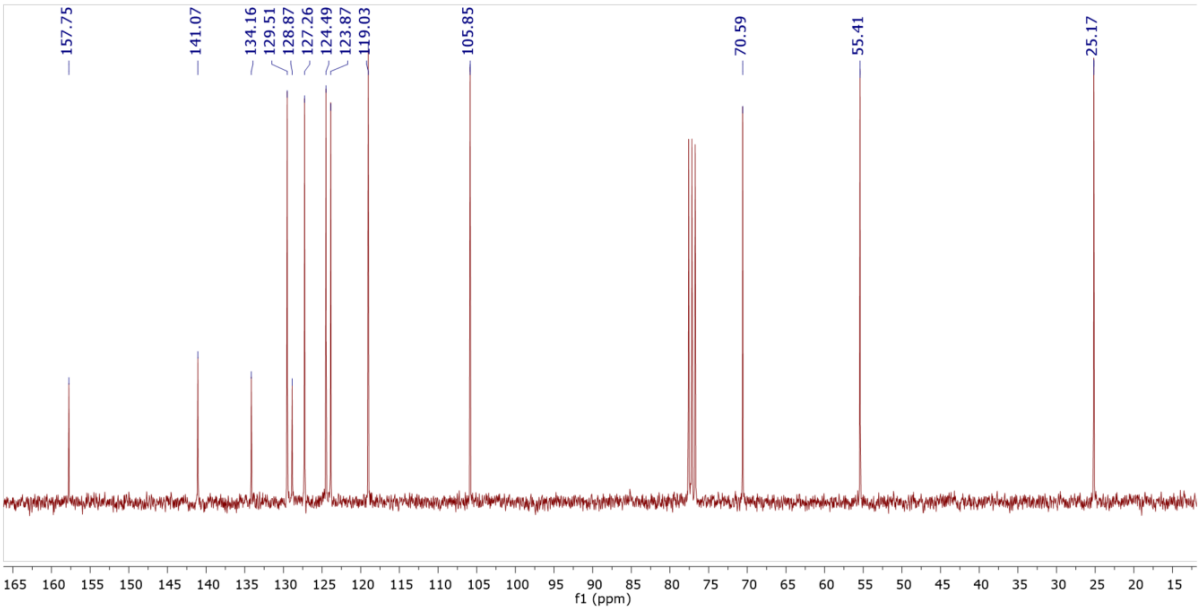

^{13}C NMR (75 MHz, $CDCl_3$) δ = 157.75 (C-6'), 141.07 (C-2'), 134.16 (C-4a'), 129.51 (C-8), 128.87 (C-8a'), 127.26 (C-1'), 124.49 (C-4'), 123.87 (C-3'), 119.03 (C-7'), 105.85 (C-5'), 70.59 (C-1), 55.41 (OCH_3), 25.17 (C-2).

1-(6-methoxynaphthalen-2-yl)propan-1-ol (174b)

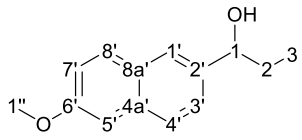

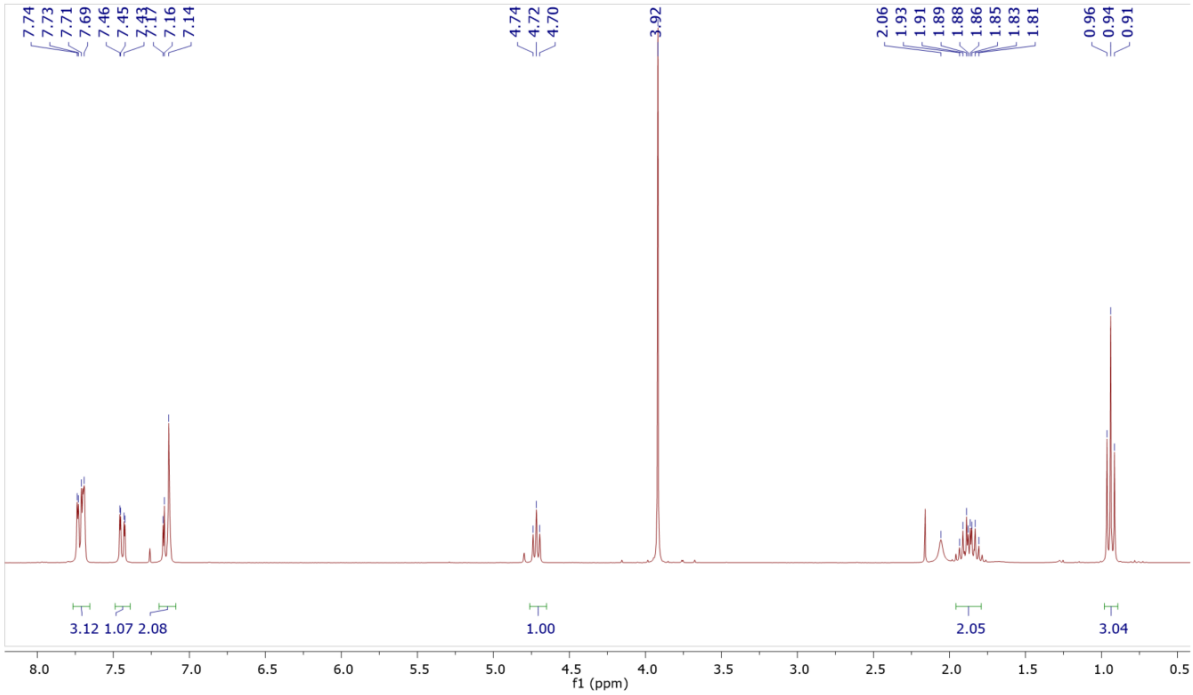

^{1}H NMR (300 MHz, Chloroform-*d*) δ 7.72 (m, 3H, 1‘,-4‘-8‘-H), 7.44 (dd, *J* = 8.5, 1.7 Hz, 1H, 5‘-H), 7.20 – 7.09 (m, 2H, 3‘-, 7‘-H), 4.72 (t, *J* = 6.6 Hz, 1H, 1-H), 3.92 (s, 1H, 1‘‘-H), 2.06 (br, 1H, OH), 1.87 (ddd, *J* = 16.9, 13.8, 6.9 Hz, 2H, 2-H), 0.94 (t, *J* = 7.4 Hz, 3H, 3-H).

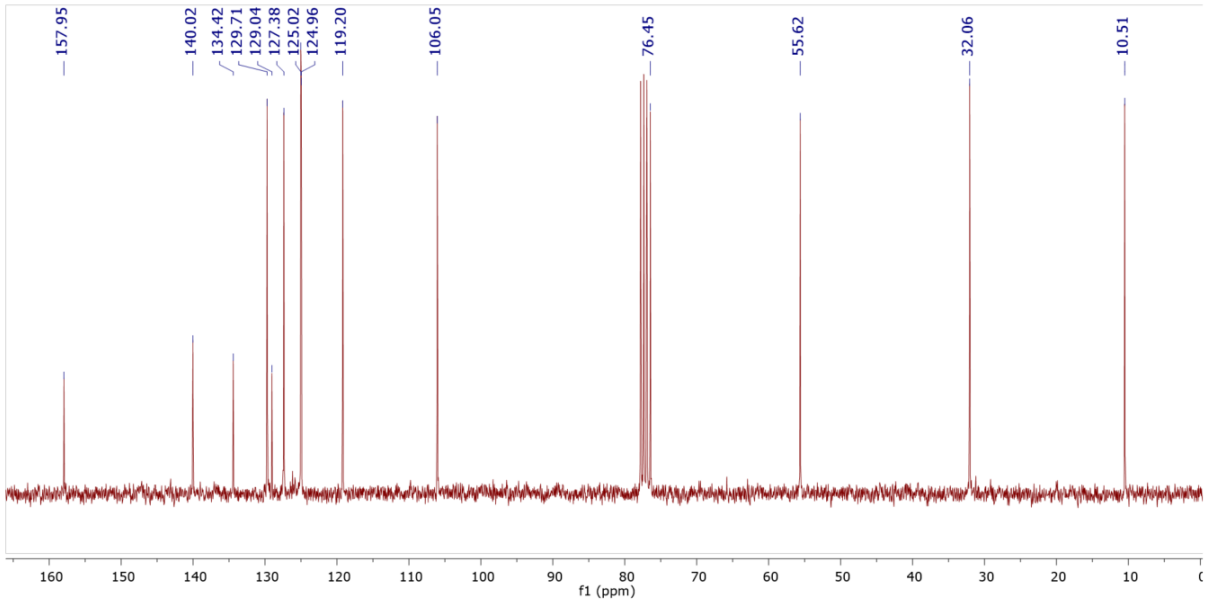

^{13}C NMR (75 MHz, $CDCl_3$) δ = 157.95 (C-6‘), 140.02 (C-2‘), 134.42 (C-4a‘), 129.71 (C-8‘), 129.04 (C-8a‘), 127.38 (C-1‘), 125.02 (C-4‘), 124.96 (C-3‘), 119.20 (C-7‘), 106.05 (C-5‘), 76,45 (C-1,) 55.62 (C-1‘‘), 32.06 (C-2), 10.51 (C-3).

1-(6-methoxynaphthalen-2-yl)butan-1-ol (174c)

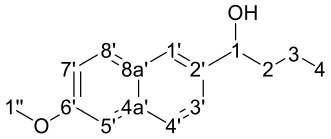

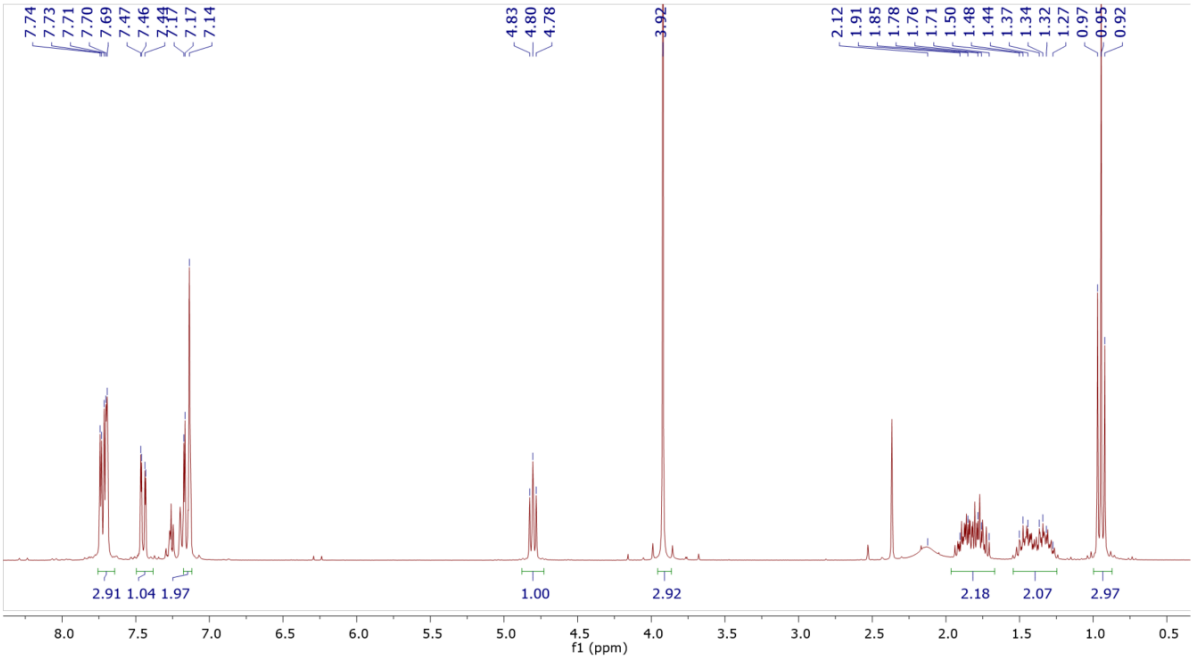

^{1}H NMR (300 MHz, Chloroform-*d*) δ = 7.76 – 7.63 (m, 3H, 1'-, 4'-, 8'-H), 7.45 (dd, *J* = 8.5, 1.7 Hz, 1H, 5'-H), 7.19 – 7.10 (m, 2H, 3'-, 7'-H), 4.80 (t, *J* = 6.7 Hz, 1H, 1-H), 3.92 (s, 1H, 1''-H), 1.95 – 1.66 (m, 2H, 2-H), 2.12 (br, 1H, OH) 1.55 – 1.24 (m, 2H, 3-H), 0.95 (t, *J* = 7.3 Hz, 3H, 4-H).

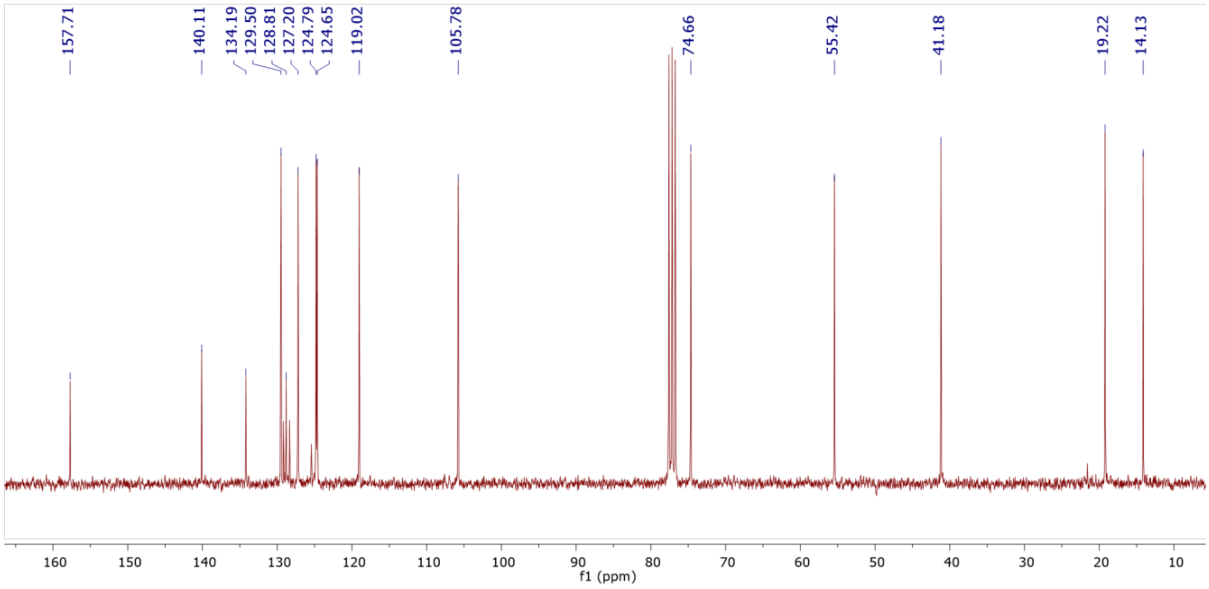

^{13}C NMR (75 MHz, $CDCl_3$) δ = 157.71 (C-6'), 140.11 (C-2'), 134.19 (C-4a'), 129.50 (C-8), 128.81 (C-8a'), 127.20 (C-1'), 124,79 (4'), 124.65 (C-3'), 119.02 (C-7'), 105.78 (C-5'), 74.66 (C-1), 55.42 (C-1''), 41.18 (C-2), 19.22 (C-3), 14.13 (C-4).

1-(6-methoxynaphthalen-2-yl)-2-methylpropan-1-ol (174d)

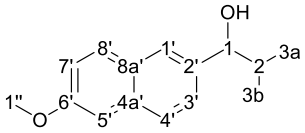

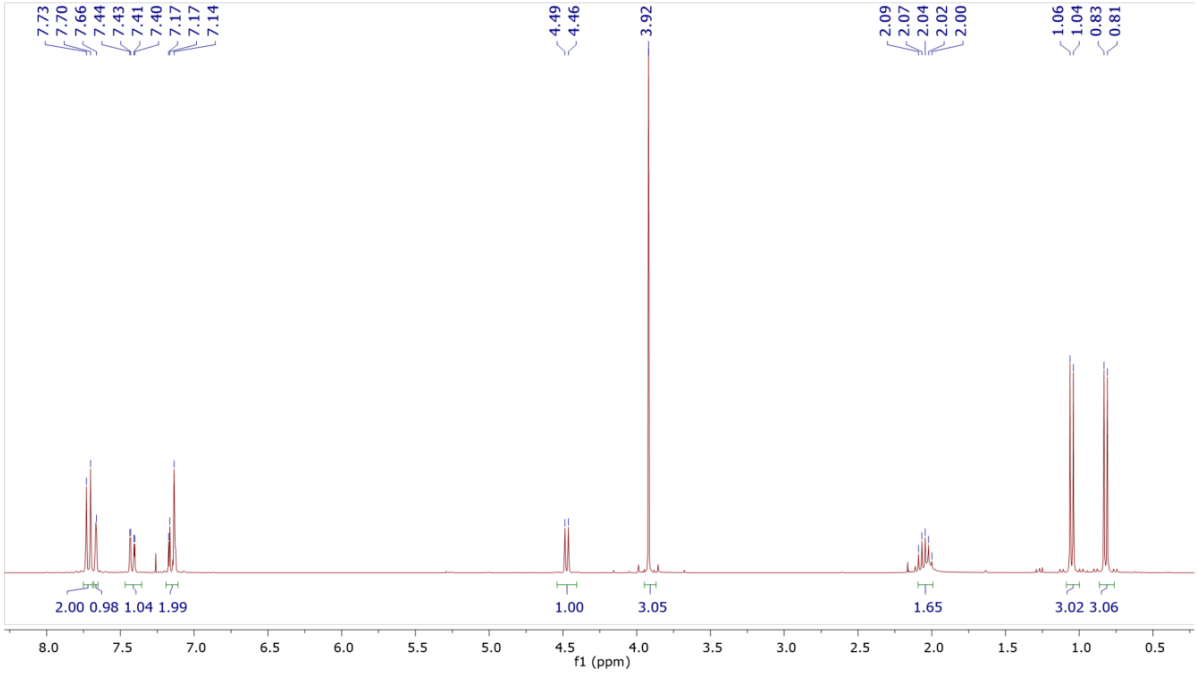

[1]H NMR (300 MHz, Chloroform-*d*) δ = 7.76 – 7.61 (m, 3H, 1‘-, 4‘-, 8‘-H), 7.42 (dd, *J* = 8.4, 1.7 Hz, 1H, 5‘-H), 7.21 – 7.09 (m, 2H, 3‘-, 7‘-H), 4.47 (d, *J* = 7.0 Hz, 1H, 1-H), 3.92 (s, 3H, 1‘‘-H), 2.04 (dt, *J* = 13.5, 6.8 Hz, 1H, 2-H), 1.05 (d, *J* = 6.7 Hz, 3H, 3a-H), 0.82 (d, *J* = 6.8 Hz, 3H, 3b-H).

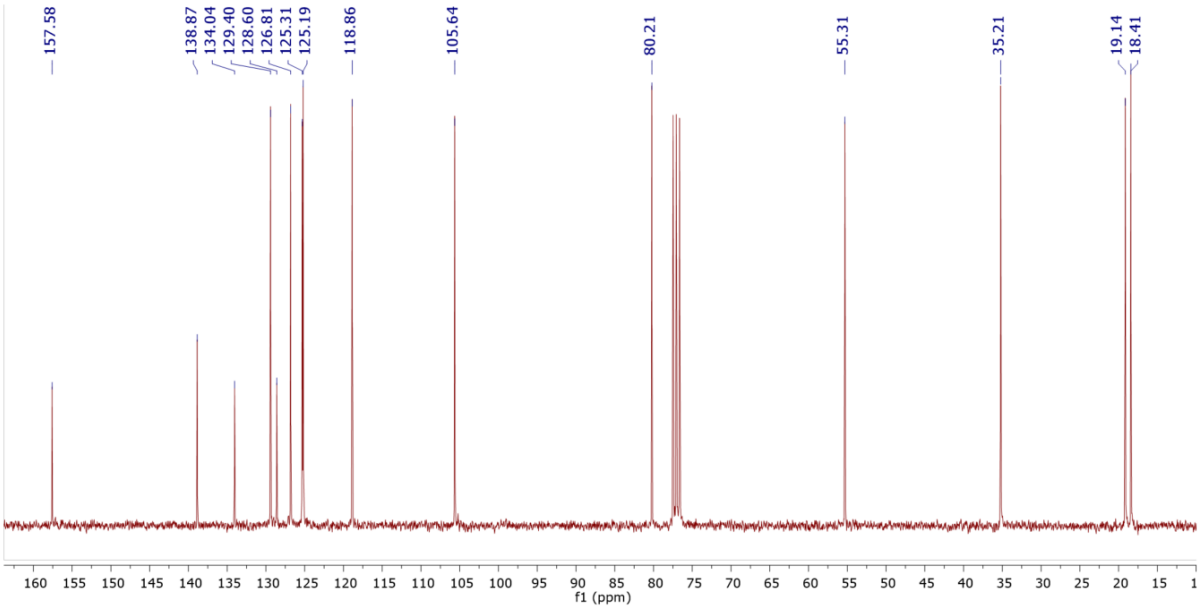

[13]C NMR (75 MHz, $CDCl_3$) δ = 157.58 (C-6‘), 138.87 (C-2‘), 134.04 (C-4a‘), 129.40 (C-8‘), 128.60 (C-8a‘), 126,81 (C-1‘), 125.31 (C-4‘), 125.19 (C-3‘), 118.86 (C-7‘), 105.64 (C-5‘), 80.21 (C-1‘), 55.31 (C-1‘‘), 35.21 (C-2), 19.14 (C-3a), 18.41 (C-3b).

1-(6-methoxynaphthalen-2-yl)-2-methylbutan-1-ol (174e)

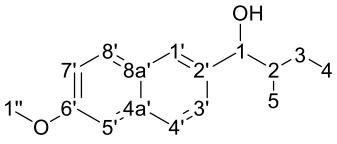

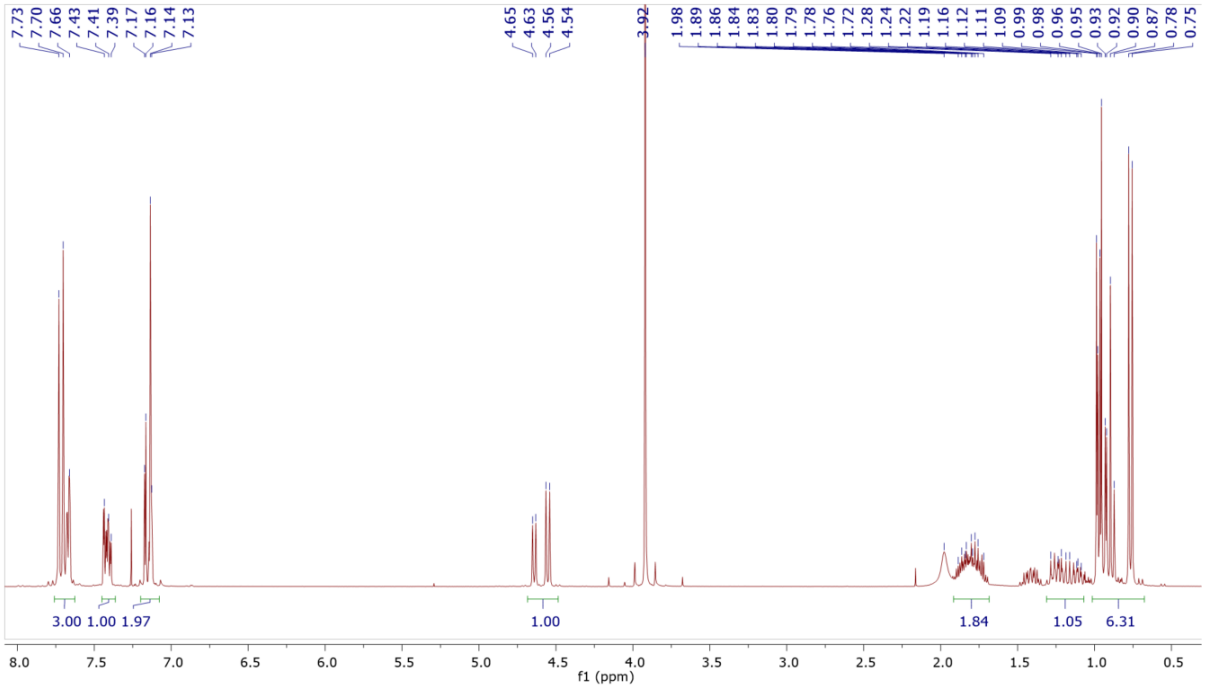

^{1}H NMR (300 MHz, Chloroform-*d*) δ 7.80 – 7.60 (m, 3H, 1‘-, 4‘-, 8‘-H), 7.48 – 7.35 (m, 1H, 5‘-H), 7.21 – 7.07 (m, 2H, 3‘-, 7‘-H), 4.60 (dd, *J* = 26.6, 6.6 Hz, 1H, 1-H),3.92 (s, 3H, 1‘‘-H), 1.98 (br, 1H, OH), 1.92 – 1.65 (m, 1H), 1.32 – 1.07 (m, 0H), 1.03 – 0.68 (m, 3H).

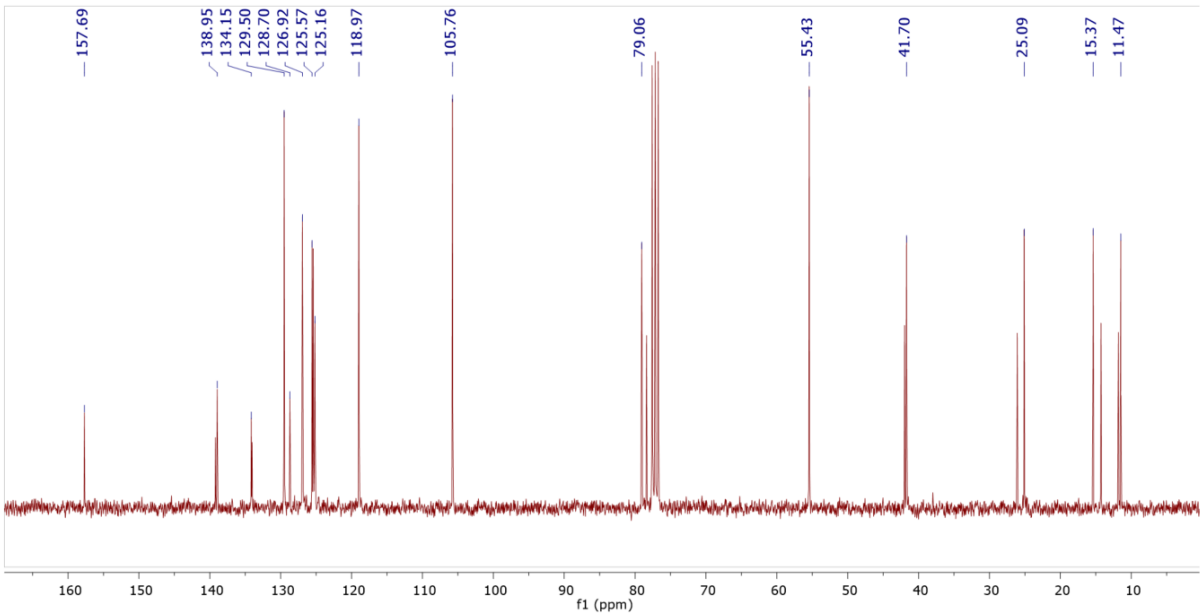

^{13}C NMR (75 MHz, $CDCl_3$) δ = 157.69 (C-6‘), 138.95 (C-2‘), 134.15 (C-4a‘), 129.50 (C-8‘), 128.70 (C-8a’), 126.92 (C-1’), 125.57 (C-4’), 125.16 (C-3’), 118.97 (C-7’), 105.76 (C-5’), 79.06 (C-1), 55.43 (C-1’’), 41.70 (C-2), 25.09 (C-3), 15.37 (C-5), 11.47 (C-4).

1-(6-methoxynaphthalen-2-yl)-3-methylbutan-1-ol (174f)

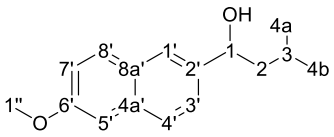

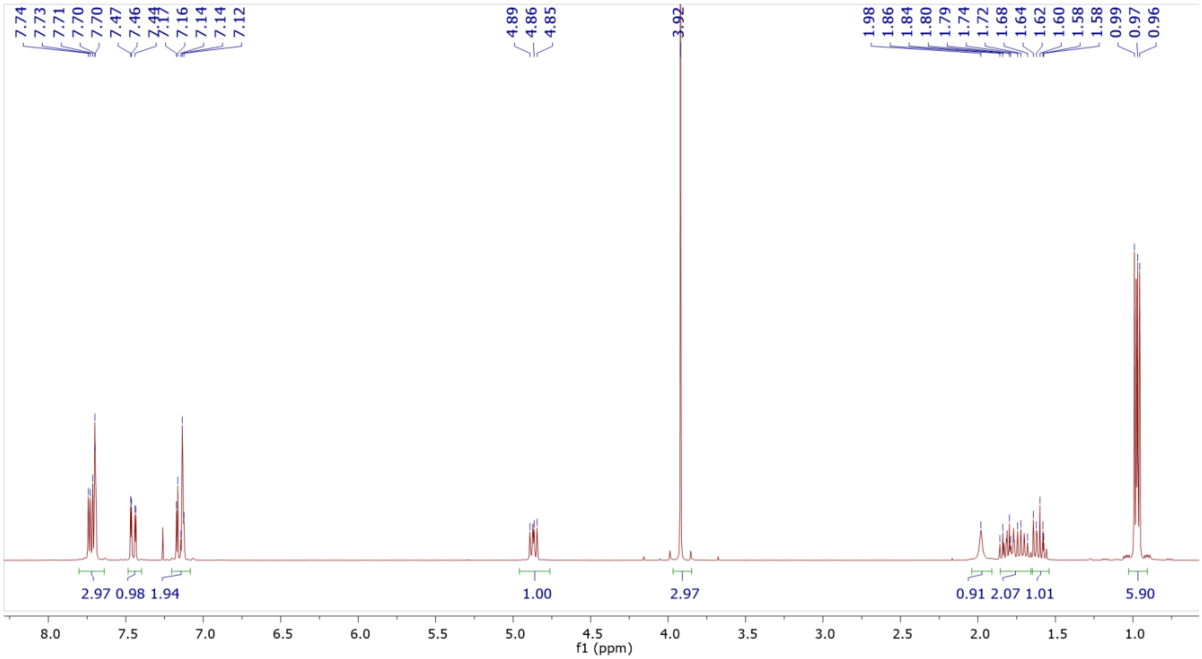

^{1}H NMR (300 MHz, Chloroform-*d*) δ 7.81 – 7.61 (m, 3H, 1‘-,4‘-, 8‘-H), 7.45 (dd, *J* = 8.5, 1.7 Hz, 1H, 5‘-H), 7.21 – 7.07 (m, 2H, 3‘-, 7‘-H), , 4.87 (dd, *J* = 8.1, 5.6 Hz, 1H, 1-H), 3.92 (s, 1H, 1‘‘-H), 1.98 (br, 1H, OH), 1.89 – 1.67 (m, 2H, 2-H), 1.66 – 1.54 (m, 1H, 3-H), 0.97 (dd, *J* = 6.4, 3.8 Hz, 6H, 4a-, 4b-H).

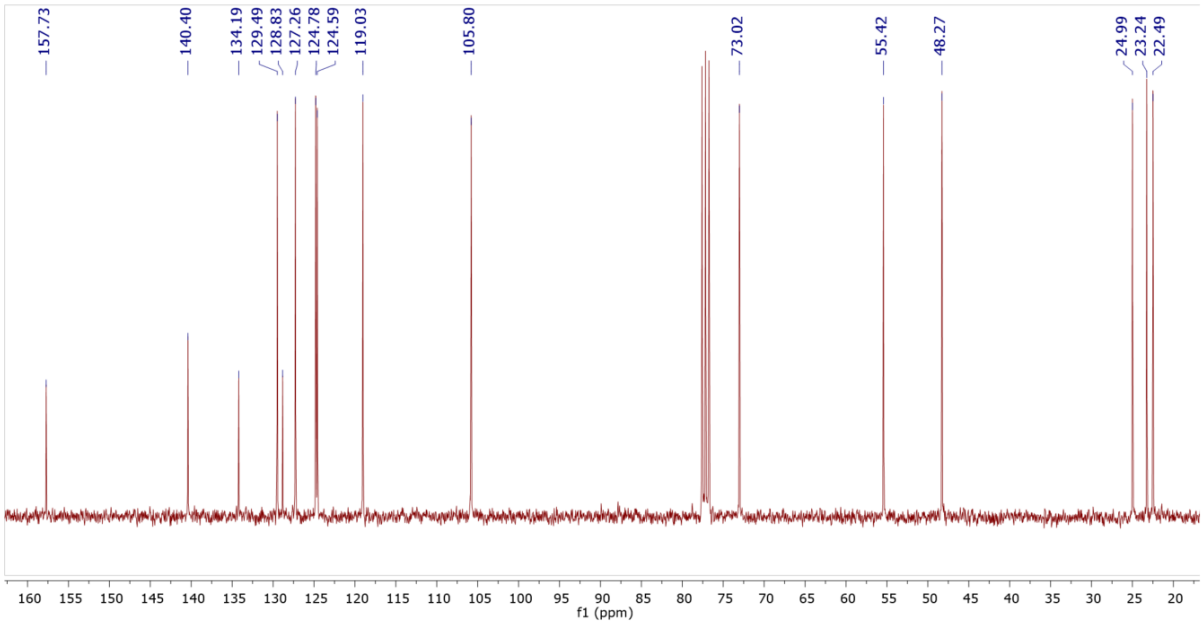

^{13}C NMR (75 MHz, $CDCl_3$) δ = 157.73 (C-6‘), 140.40 (C-2‘), 134.19 (C-4a‘), 129.49 (C-8‘), 128.83 (C-8a’), 127.26 (C-1’), 124.78 (C-4’), 124.59 (C-3’), 119.03 (C-7’), 105.80 (C-5’), 73.02 (c-1), 55.42 (C-1’’), 48.27 (C-2), 24.99 (C-3), 23.

1-(6-methoxynaphthalen-2-yl)-3-methylpentan-1-ol (174g)

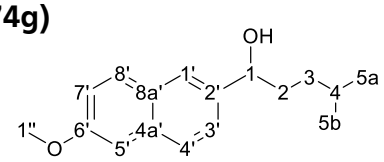

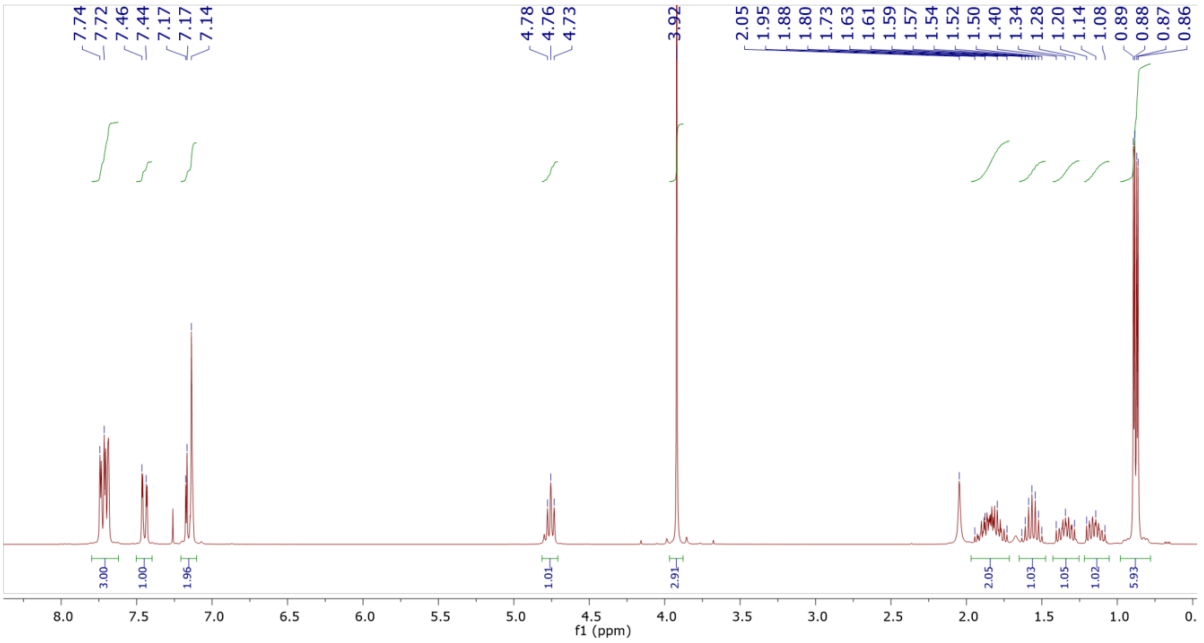

^{1}H NMR (300 MHz, $CDCl_3$) δ = 7.74 – 7.69 (m, 3H, 8'-, 4'-, 1'-H), 7.45 (d, *J* = 8.5 Hz, 1H, 3'-H), 7.17 – 7.14 (m, 2H, 3'-, 7'-H), 4.76 (t, *J* = 6.7 Hz, 1H, 1-H), 3.92 (s, 1H, 1''-H), 2.05 (s, 1H, -OH) 1.95 – 1.73 (m, 2H, 2-H), 1.57 (dp, J = 13.2, 6.6 Hz, 1H, 4-H), 1.35 – 1.17 – 0.96 (m, 2H, 3-H), 0.78 (dd, *J* = 6.6, 2.7 Hz, 6H, 5a-H + 5b-H).

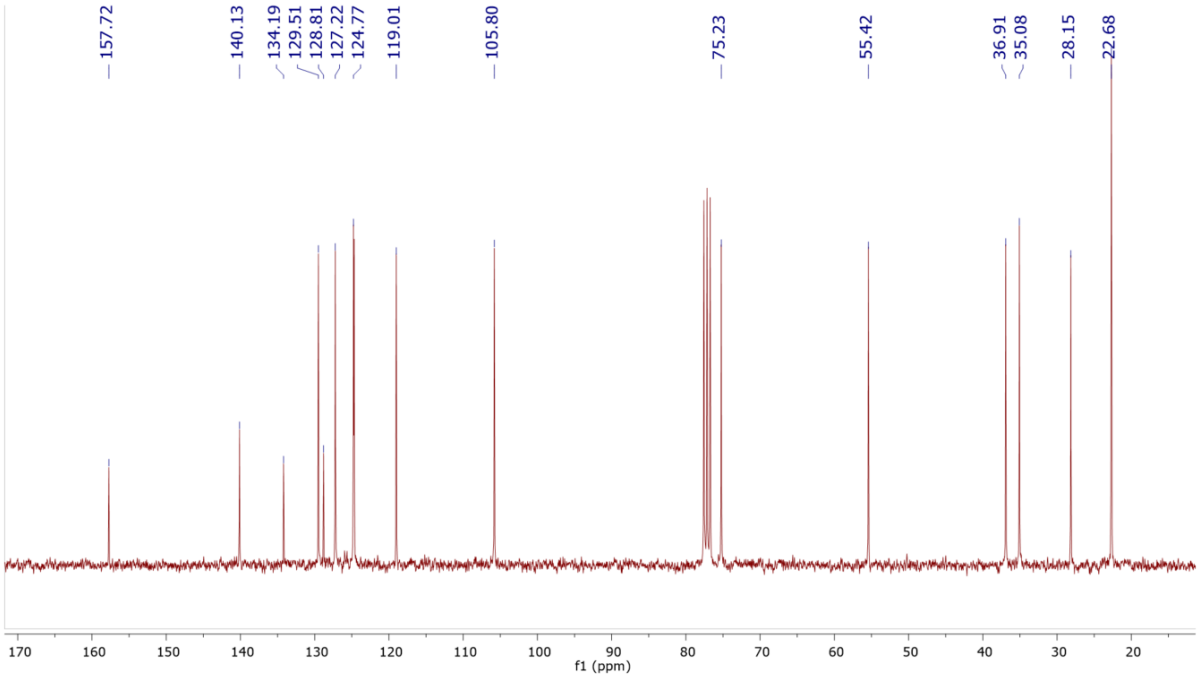

^{13}C NMR (75 MHz, $CDCl_3$) δ 157.72 (C-6'), 140.13 (C-2'), 134.19 (C-4a'), 129.51 (C-8'), 128.81 (C-8a'), 127.22(C-1'), 124.77 (C-4'), 119.01 (C-7'), 105.80 (C-5'), 75.23 (C-1), 55.42 (C-1''), 36.91 (C-2), 35.08 (C-3), 28.15 (C-4), 22.68 (C-5a +C-5b).

3-chloro-1-(3,4-difluorophenyl)propan-1-one (164)

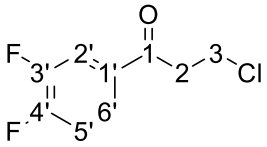

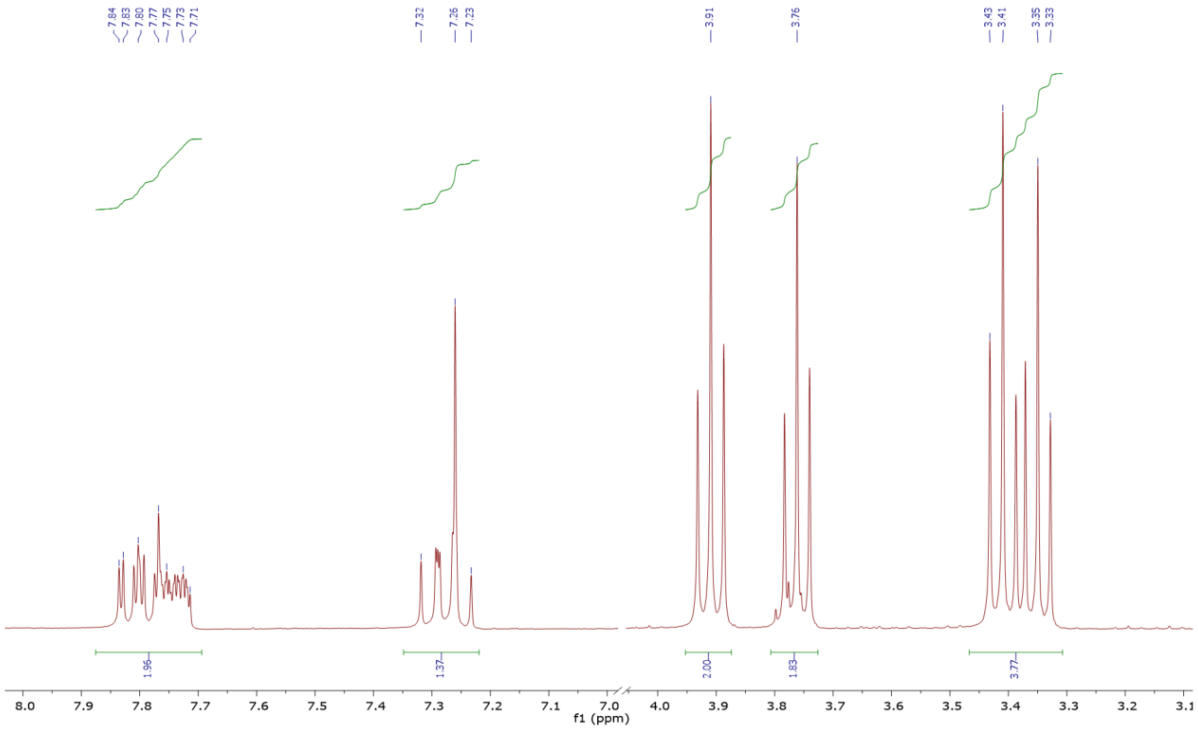

^{1}H NMR (300 MHz, $CDCl_3$): δ = 7.76-7.65 (2H, m, 5´,6´-H), 7.21 (q, J=9.5 Hz, 1H, 2´-H), 3.34 (t, J=7 Hz, 2H, 3-H), 2.83 (t, J=7 Hz, 2H, 2-H), ppm.

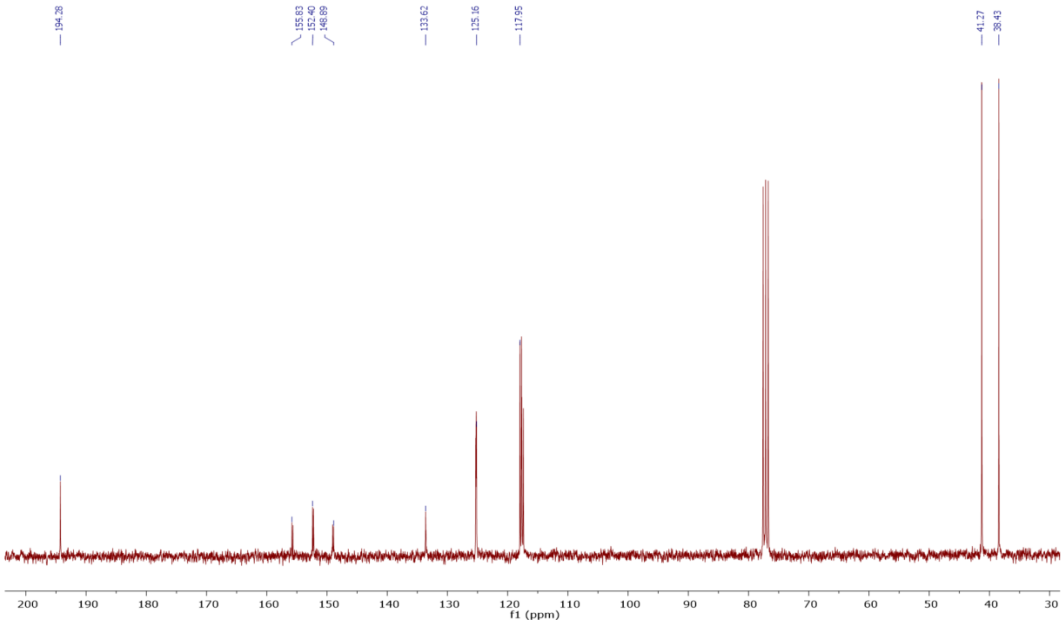

^{13}C-NMR ($CDCl_3$, 75 MHz): δ = 194.28 (C-1), 155.83 (C-4´), 152.40 (C-3´), 148.89 (C-1´), 133.89 (C-6´), 125.16 (C-5´), 117.95 (C-2´), 41.27 (C-2), 38.43 (C-3) ppm.

1-(3,4-difluorophenyl)-3-nitropropan-1-ol (165):

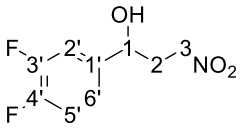

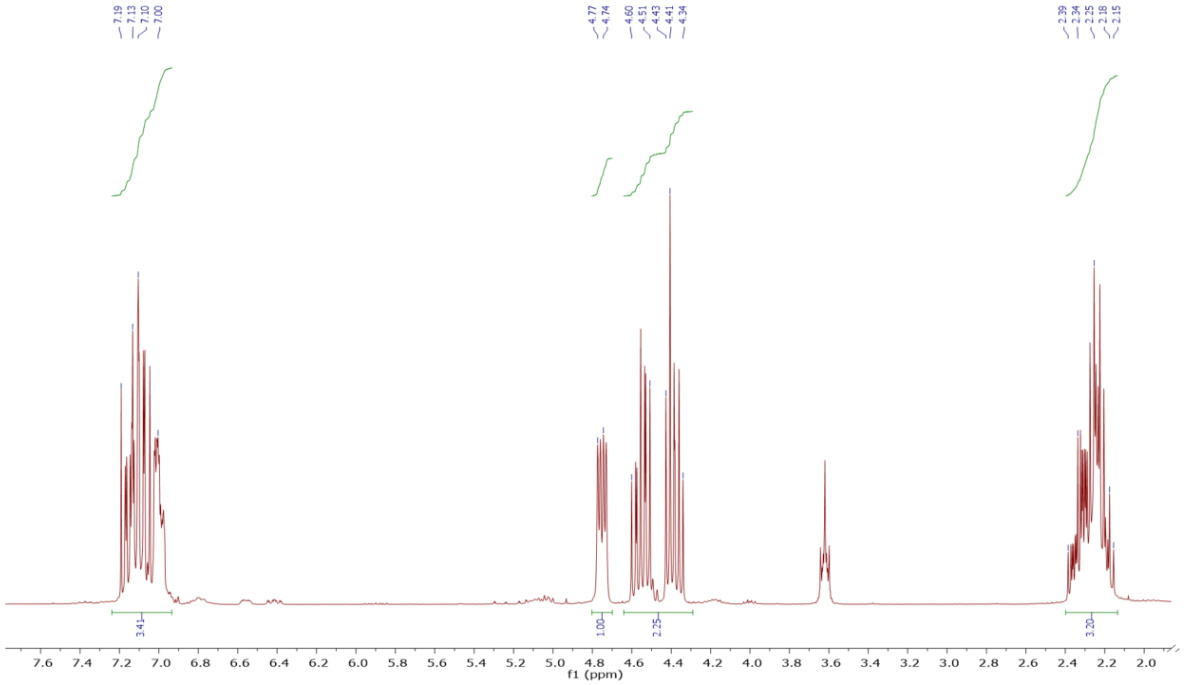

^{1}H NMR (300 MHz, $CDCl_3$): δ= 7.19- 7.00 (m, 3H, 2´,5´,6´-H), 4.77-4.74 (q, *J*=4.2 Hz, 1H, 1-H), 4.60-4.34 (m, 2H, 3-H), 2.39-2.15 (m, 2H, 2-H) ppm.

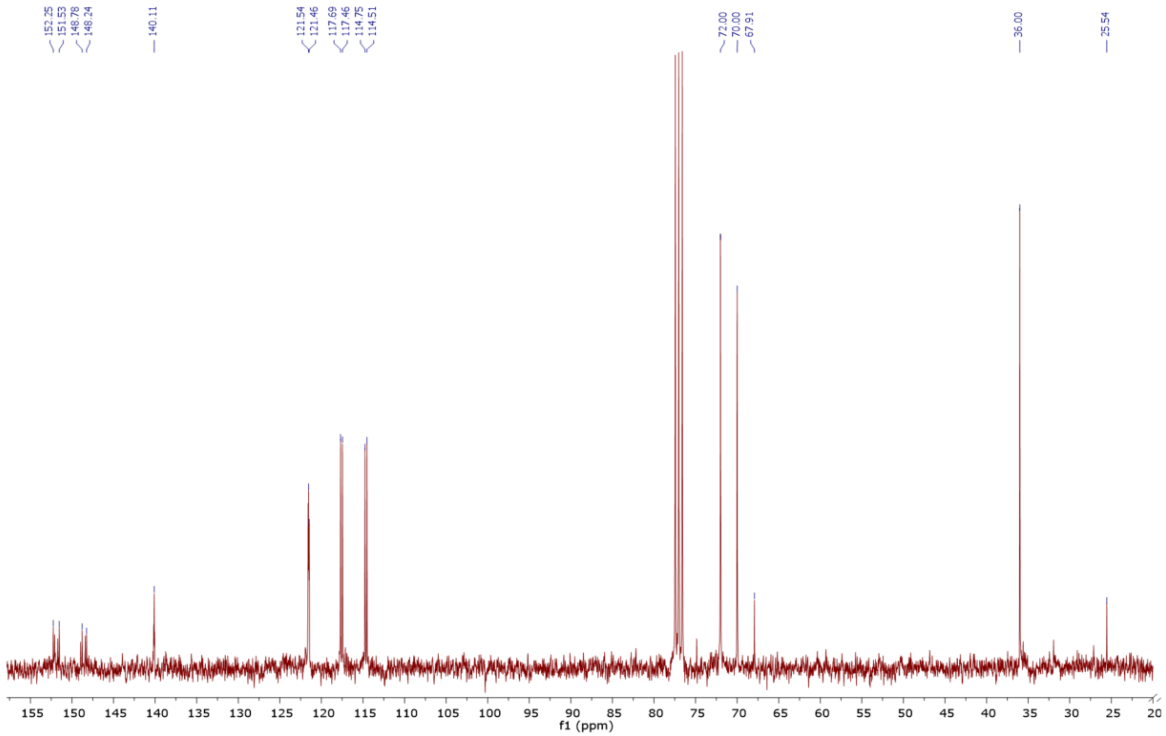

^{13}C-NMR ($CDCl_3$, 75 MHz): δ = 152.25 (C-3), 148.24 (C-4'), 140.11 (C-1´), 121.54 (C-6´), 117.69 (C-5'), 114.51 (C-2´), 72.00 (C-3), 70.00 (C-1), 36.00 (C-2) ppm.

-(3,4-difluorophenyl)-3-nitropropan-1-one (162):

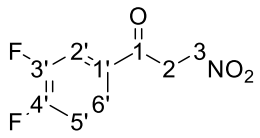

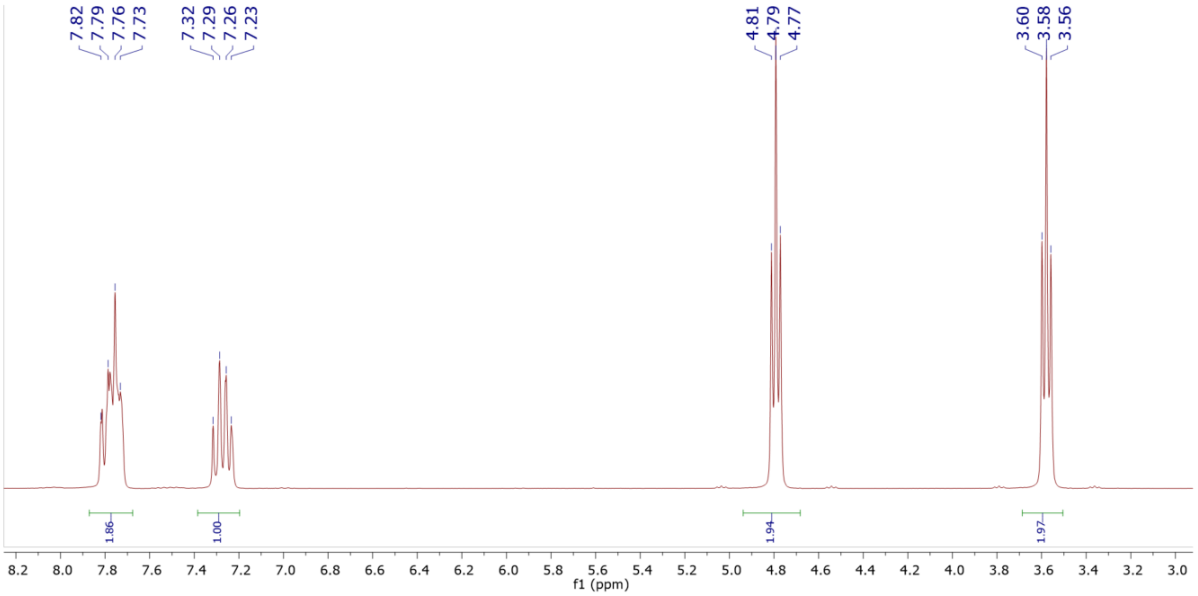

^{1}H NMR (300 MHz, $CDCl_3$): δ= 7.82-7.68 (m, 2H, 5´,6´-H), 7.27-7.19 (q, ^{3}J=9 Hz, 1H, 2´-H), 4.75 (t, J=7 Hz, 2H, 3-H), 3.53 (t, J=7 Hz, 2H, 2-H) ppm.

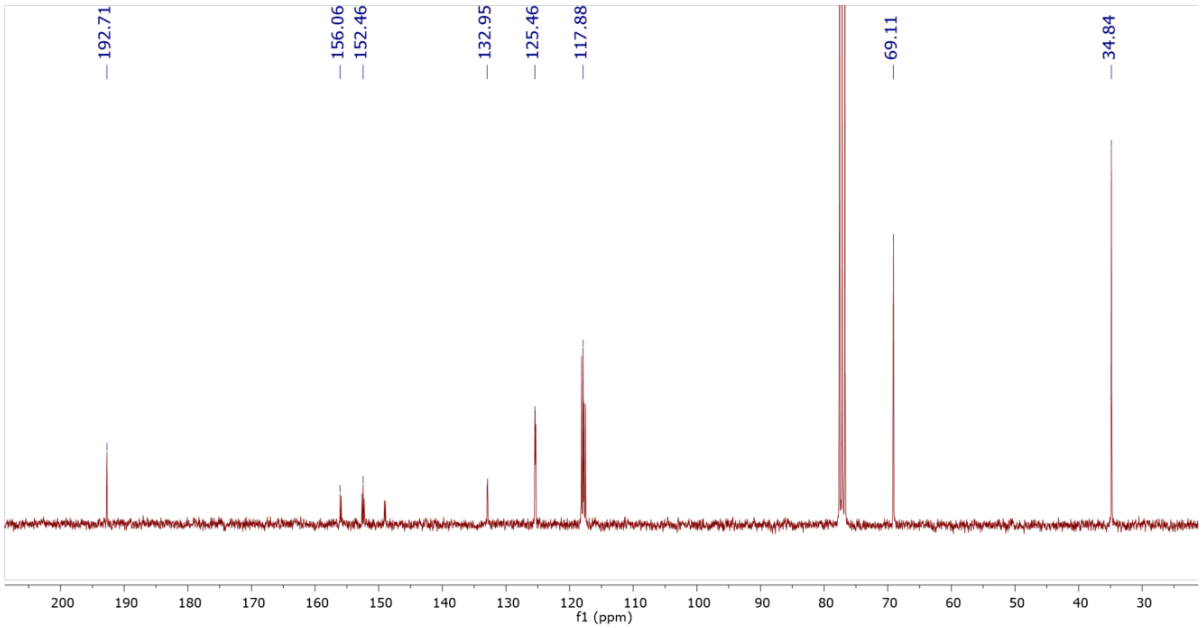

^{13}C-NMR ($CDCl_3$, 75 MHz): δ= 192.72 (C-1), 154.50 (C-3´), 149.12 (C-4´), 132.91 (C-1´), 125.47 (C-6´), 117.51(C-5´), 69.12 (C-3), 34.85 (C-2) ppm.

Byproducts 180 and 181

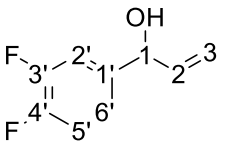

180

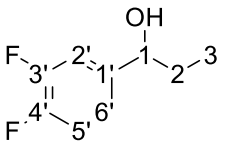

181

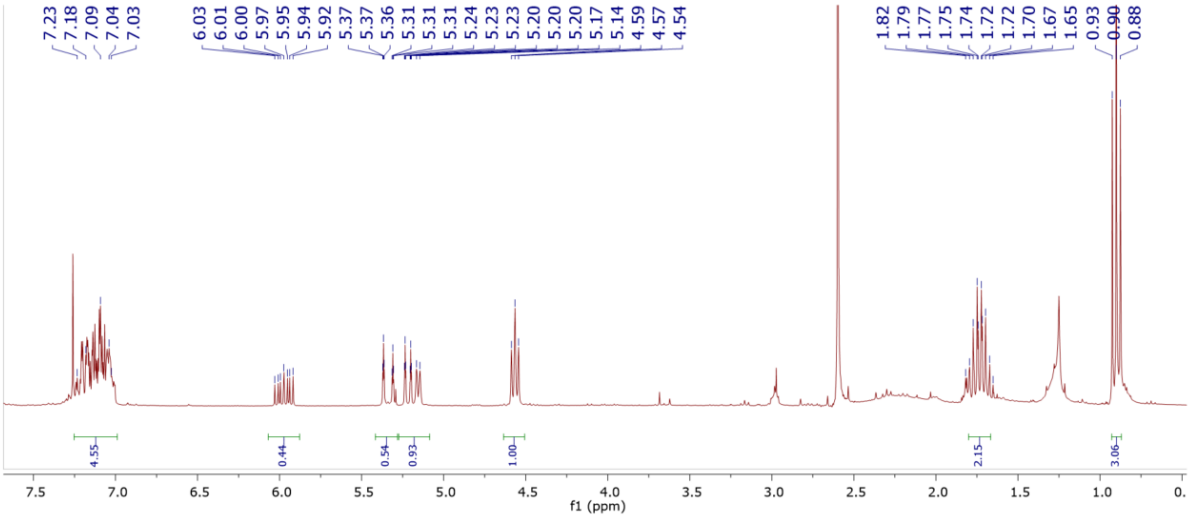

Unsaturated product 180:
^{1}H NMR (300 MHz, Chloroform-*d*) δ = 7.25 – 6.95 (m, 3H, 2‘, 5‘, 6‘-H), 6.05 – 5.88 (m, 1H, 2-H), 5.34 (dt, *J* = 17.1, 1.3 Hz, 1H, 1-H), 5.22 (dt, *J* = 10.3, 1.2 Hz, 1H, 3-H$_a$), 5.16 (d, *J* = 6.2 Hz, 1H, 3-H$_b$).

Saturated product 181:
^{1}H NMR (300 MHz, Chloroform-*d*) δ = 7.27 – 6.85 (m, 3H, 2‘, 5‘, 6‘-H), 4.57 (t, *J* = 6.5 Hz, 1H, 1-H), 1.99 – 1.56 (m, 2H, 2-H), 0.90 (t, *J* = 7.4 Hz, 3H, 3-H).

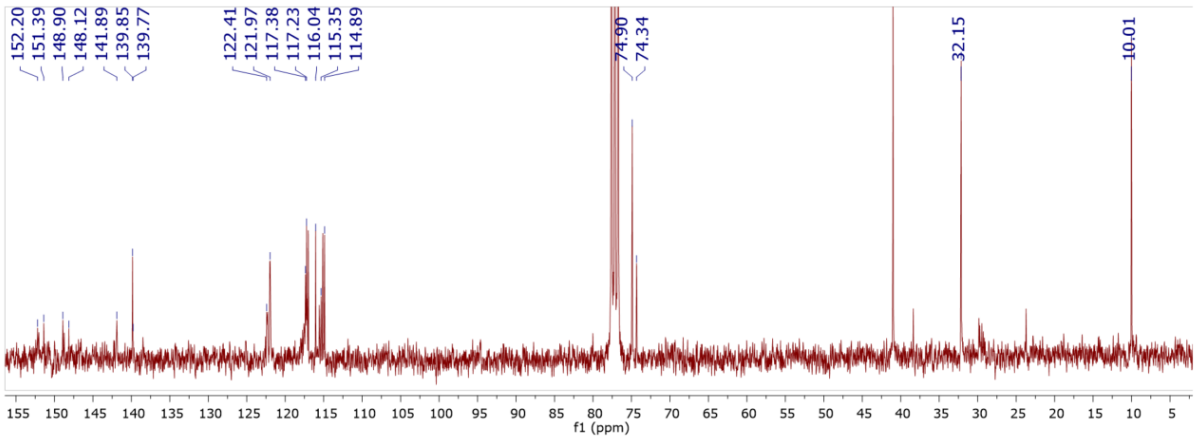

Unsaturated product 180:
^{13}C NMR (75 MHz, $CDCl_3$) δ = 152.20 (C-3‘), 148.12 (C-4‘), 141.89 (C-2), 139. 77 (C-1‘), 122.41 (C-6‘), 117.38 (C-5‘), 116.04 (C-3), 115.35 (C-2‘), 74.34 (C-1).

Saturated product 181:
^{13}C NMR (75 MHz, $CDCl_3$) δ = 151.39 (C-3’), 148.90 (C-4’), 139.85 (C-1’), 122.02 (C-6’), 117.23 (C-5’), 114.89 (C-2’), 74.90 (C-1), 32.15 (C-2), 10.01 (C-3).

EI mass spectrum of byproducts 180 and 181

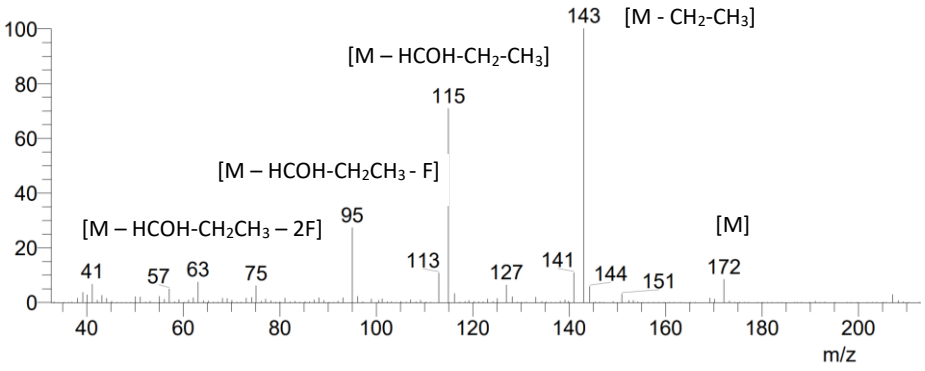

$C_9H_8F_2O$ $[M^+]$ = 170

$C_9H_{10}F_2O$ $[M^+]$ = 172

Data from library screenings

Fluorogenic screening plates of 1st generation libraries (KREDs)

E144X Library

Ethyl-substrate **174b**

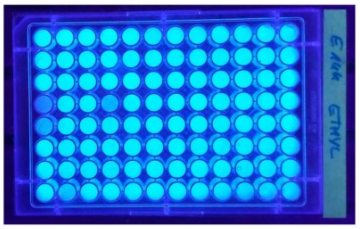

Propyl-substrate **174c**

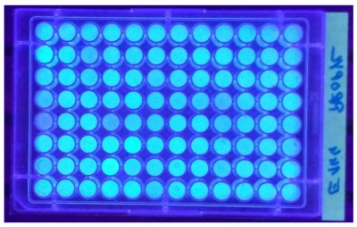

Iso-propyl-substrate **174d**

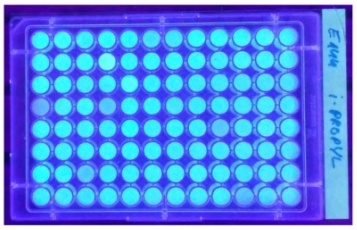

Sec-butyl-substrate **174e**

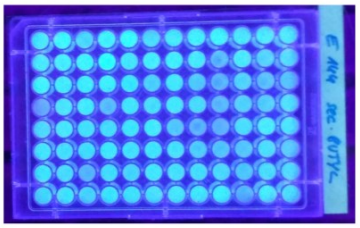

Iso-butyl-substrate **174f**

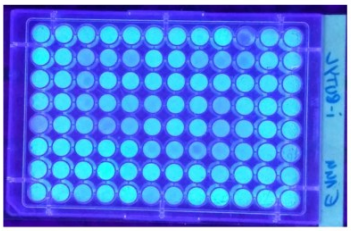

D149X Library

Ethyl-substrate **174b**

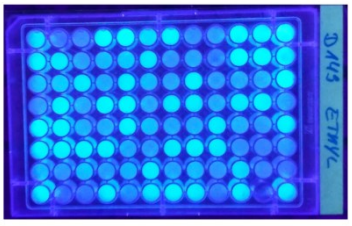

Propyl-substrate **174c**

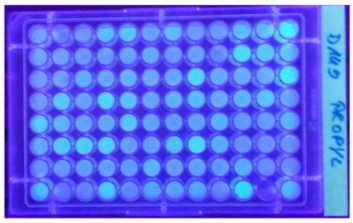

Iso-propyl-substrate **174d**

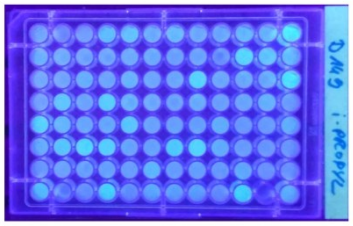

Sec-butyl-substrate **174e**

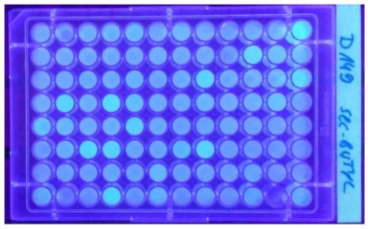

Iso-butyl-substrate **174f**

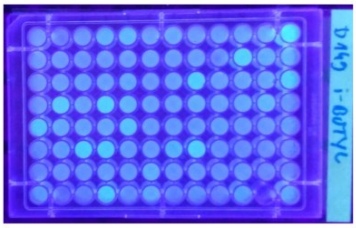

L152X Library

Ethyl-substrate **174b**

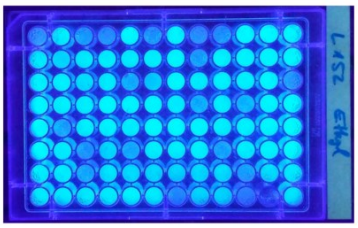

Propyl-substrate **174c**

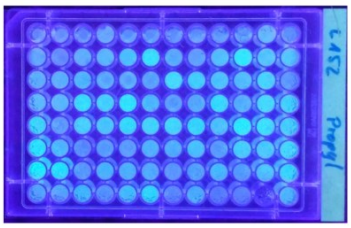

Iso-propyl-substrate **174d**

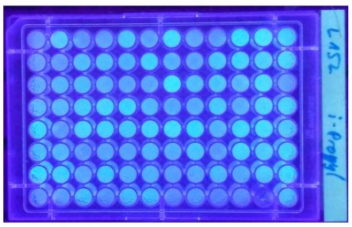

Sec-butyl-substrate **174e**

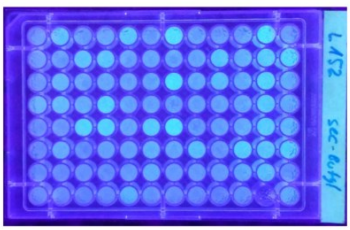

Iso-butyl-substrate **174f**

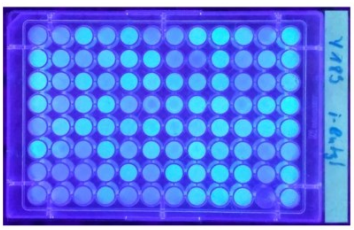

D149X Library

Ethyl-substrate **174b**

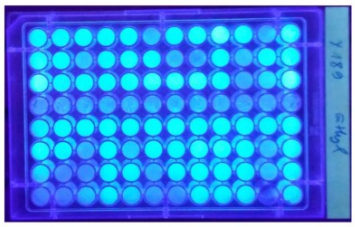

Propyl-substrate **174c**

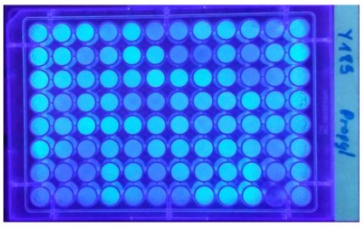

Iso-propyl-substrate **174d**

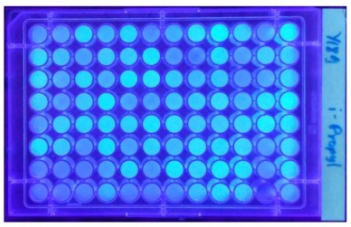

Sec-butyl-substrate **174e**

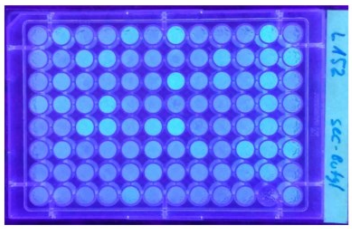

Iso-butyl-substrate **174f**

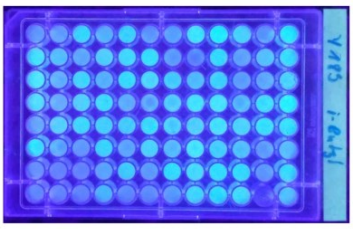

Screening results of 2nd generation library (KREDs)

Methyl substrate

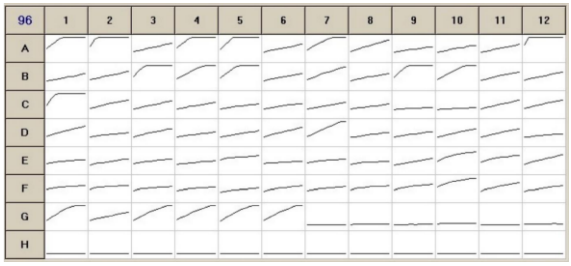

Ethyl substrate

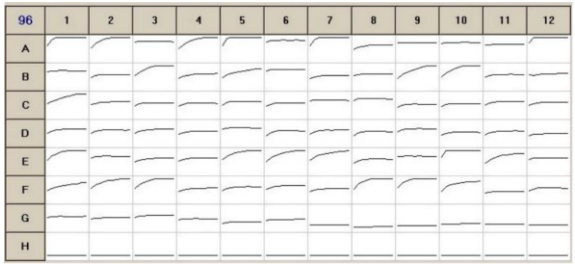

Propyl substrate

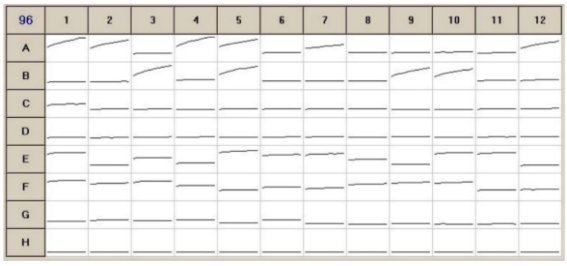

Iso-propyl substrate

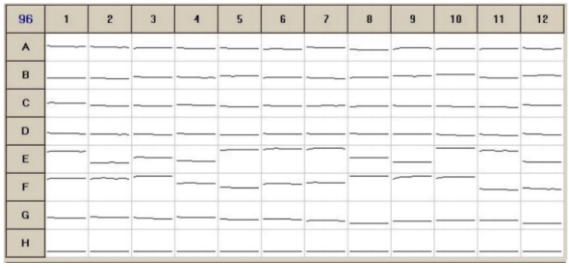

Sec-butyl substrate

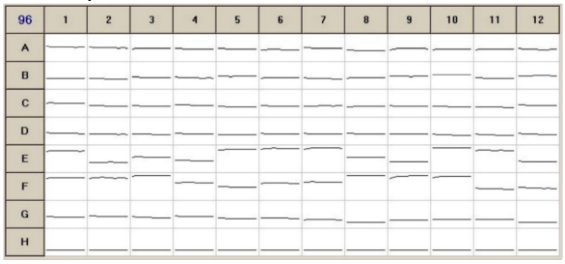

Iso-butyl substrate

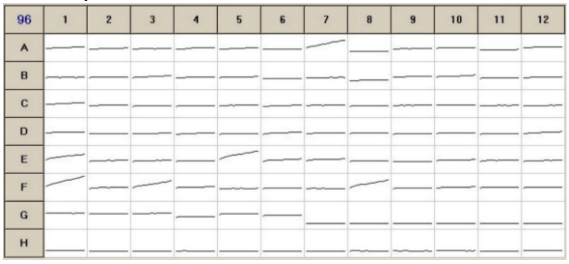

Rescreening of relevant KRED variants towards substrates 174a-f

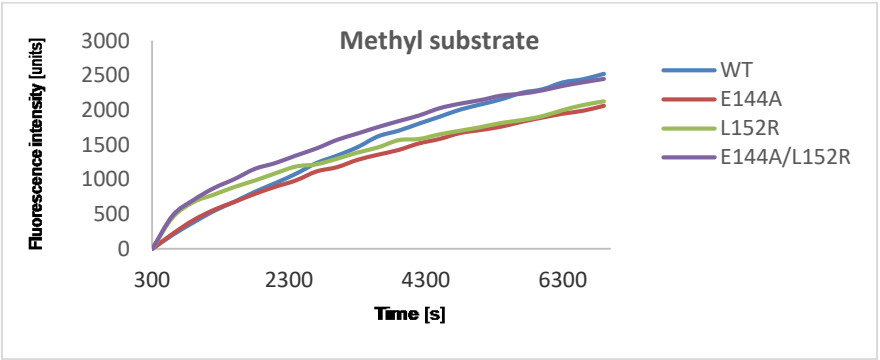

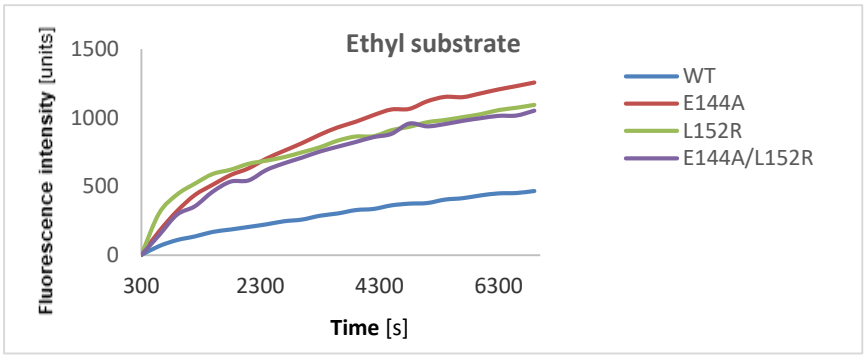
Ethyl substrate
Fluorescence intensity [units]
1500
1000
500
0
300
2300
4300
6300
Time [s]
WT
E144A
L152R
E144A/L152R

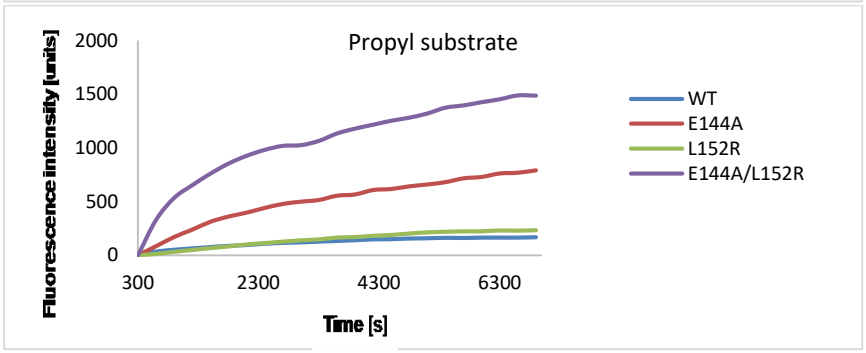
Propyl substrate
Fluorescence intensity [units]
2000
1500
1000
500
0
300
2300
4300
6300
Time [s]
WT
E144A
L152R
E144A/L152R

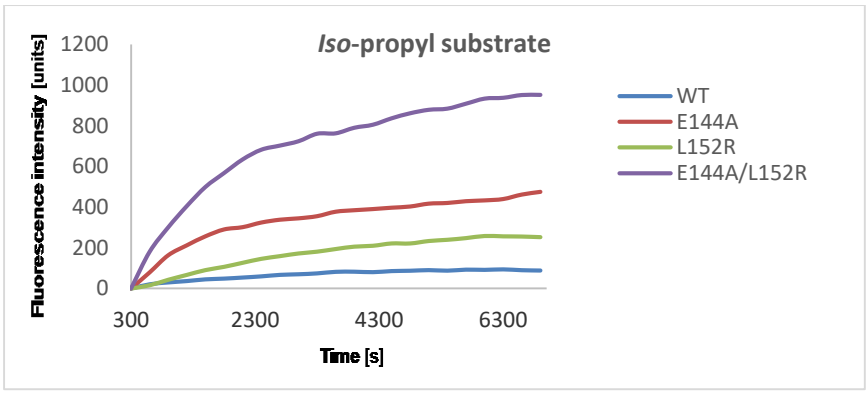
Iso-propyl substrate
Fluorescence intensity [units]
1200
1000
800
600
400
200
0
300
2300
4300
6300
Time [s]
WT
E144A
L152R
E144A/L152R

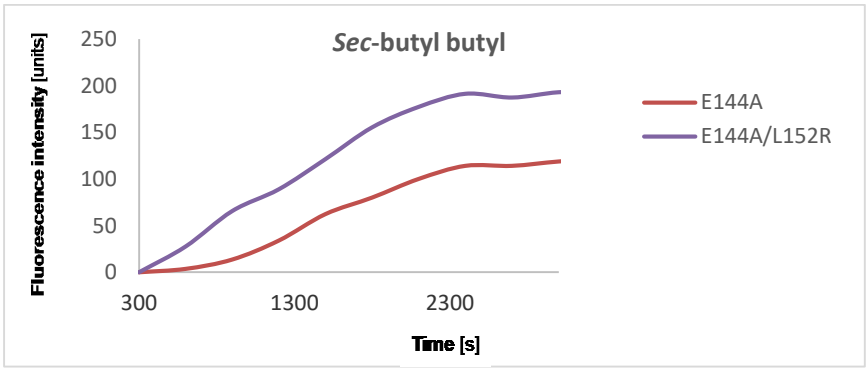
Sec-butyl butyl
Fluorescence intensity [units]
250
200
150
100
50
0
300
1300
2300
Time [s]
E144A
E144A/L152R

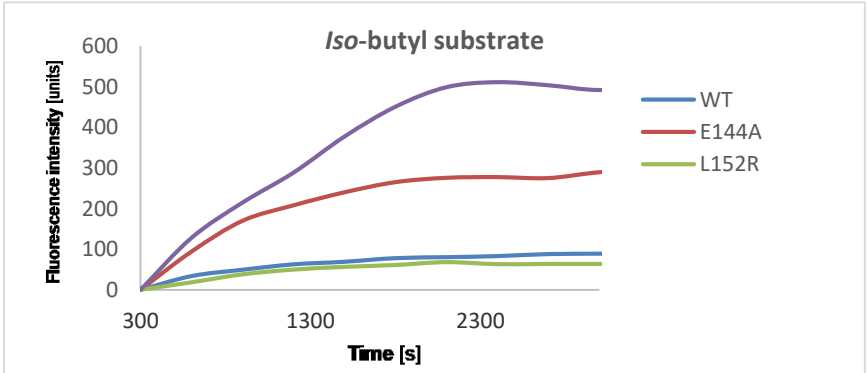
Iso-butyl substrate
Fluorescence intensity [units]
600
500
400
300
200
100
0
300
1300
2300
Time [s]
WT
E144A
L152R

Measurements of KRED enzyme kinetics: Linear standard curves of substrates

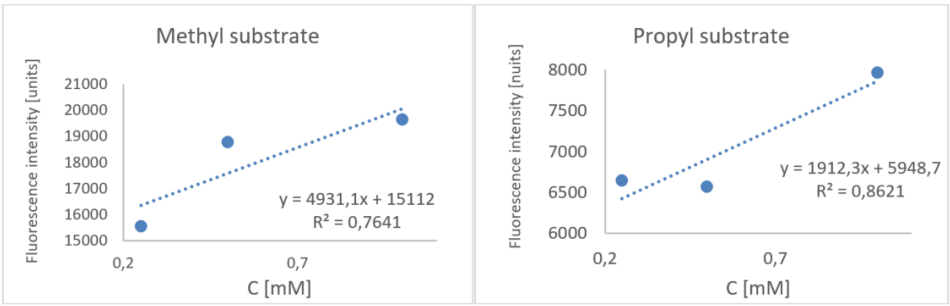

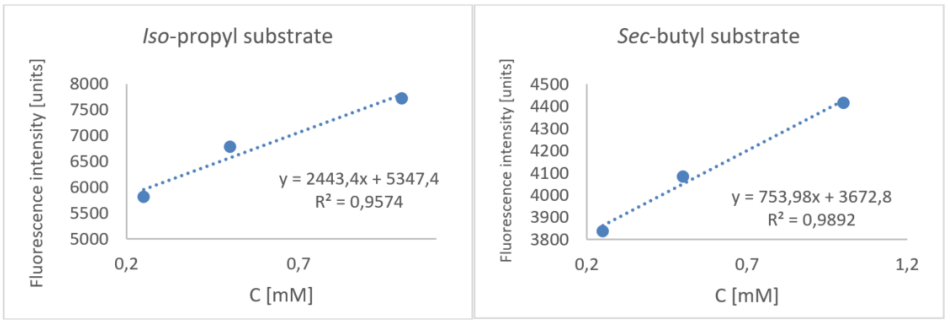

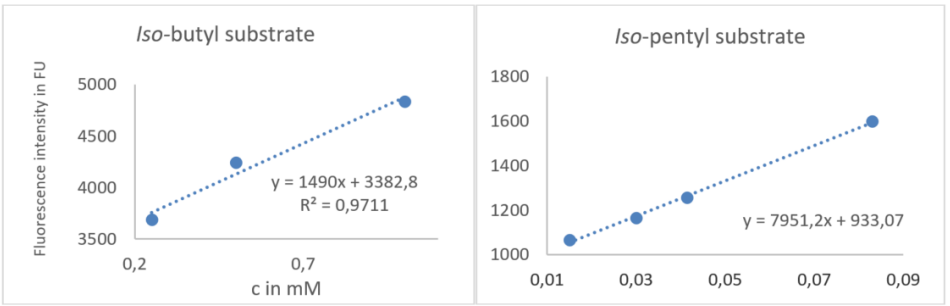

Measurements of enzyme kinetics: MICHAELIS-MENTEN curves

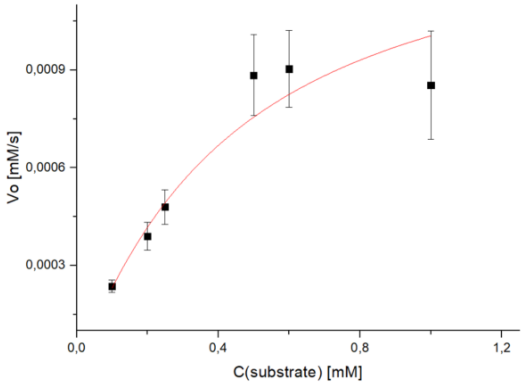

Wildtype

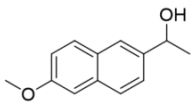

174a

$V_{max} = (1.41 \pm 0.62) \times 10^{-3}$ mM/s

$K_m = 0.44 \pm 0.36$ mM

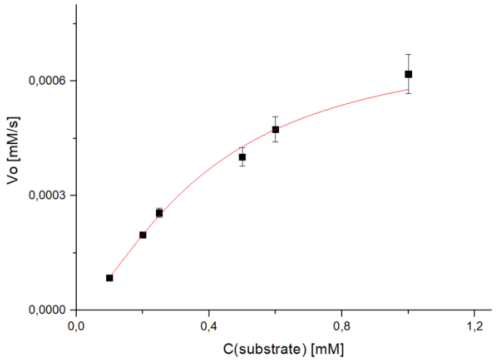

E144A/L152R

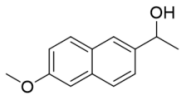

174a

$V_{max} = (\ 5.35\ \pm 0.15\ ) \times 10^{-5}$ mM/s

$K_m = 0.13\ \pm 0.01$ mM

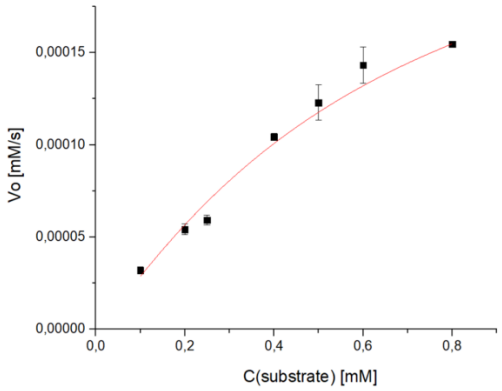

E144A/Y189W

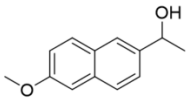

175a

$V_{max} = (\ 2.70\ \pm 0.77\ ) \times 10^{-5}$ mM/s

$K_m = 0.64\ \pm 0.33$ mM

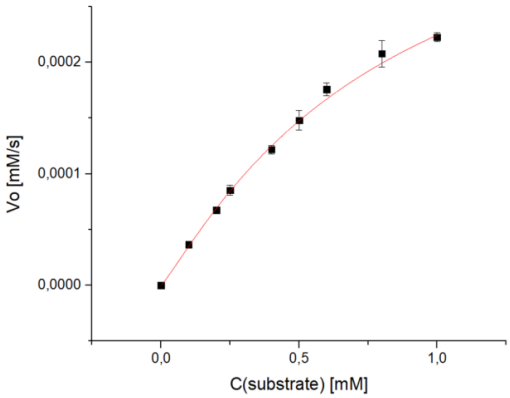

E144A/L152R

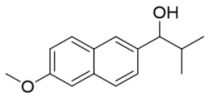

174d

$V_{max} = (\ 4.02\ \pm 5.22\ ) \times 10^{-5}$ mM/s

$K_m = 0.81\ \pm 0.19$ mM

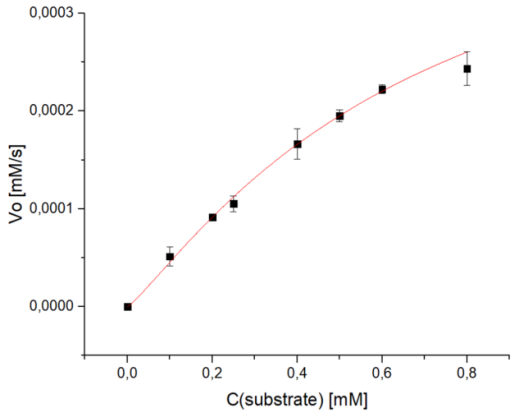

E144A/Y189W

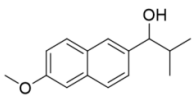

174d

$V_{max} = (\ 4.78\ \pm 1.51\ ) \times 10^{-4}$ mM/s

$K_m = 0.69\ \pm 0.36$ mM

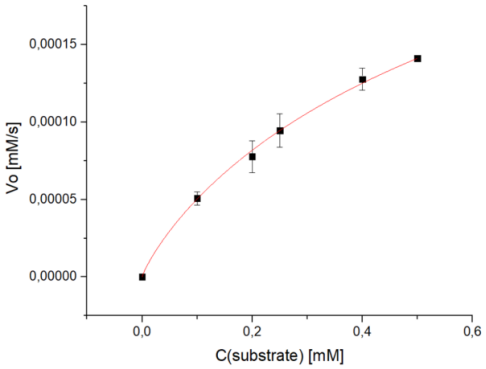

E144A/L152R

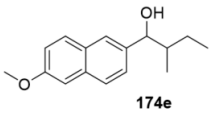

174e

$V_{max} = (3.62 \pm 1.45) \times 10^{-4}$ mM/s

$K_m = 0.85 \pm 0.71$ mM

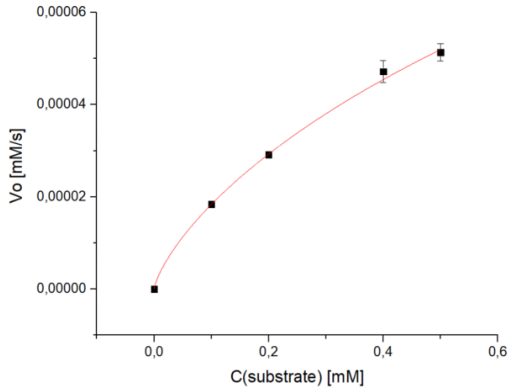

E144A/Y189W

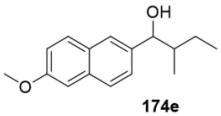

174e

$V_{max} = (2.49 \pm 2.00) \times 10^{-4}$ mM/s

$K_m = 3.00 \pm 4.68$ mM

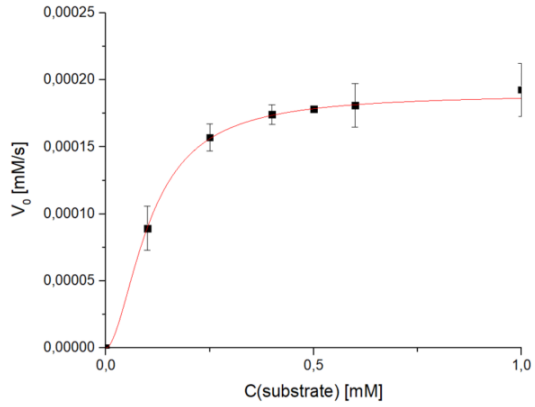

E144A/L152R

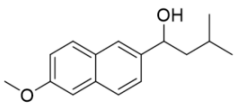

174f

$V_{max} = (1.90 \pm 0.02) \times 10^{-4}$ mM/s

$K_m = 0.11 \pm 0.00$ mM

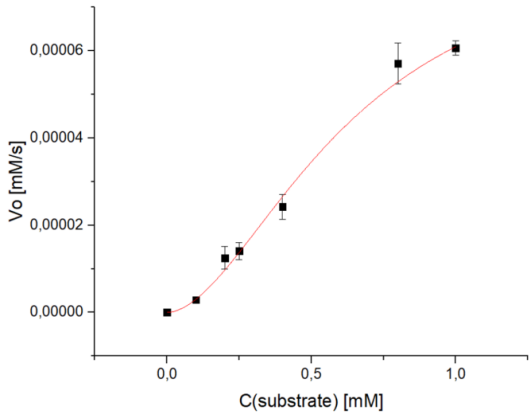

E144A/Y189W

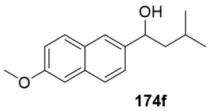

174f

$V_{max} = (8.81 \pm 1.24) \times 10^{-5}$ mM/s

$K_m = 0.64 \pm 0.13$ mM

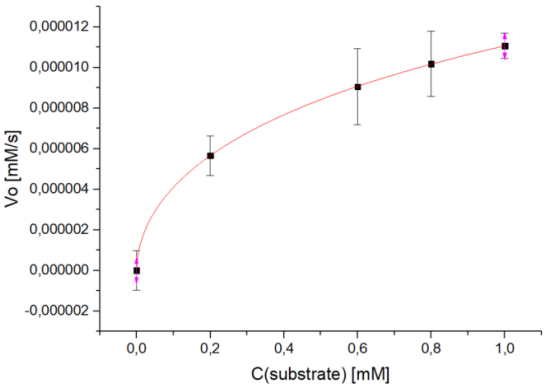

E144A/L152R

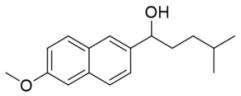

174g

$V_{max} = (\ 1.08\ \pm 3.37\ ) \times 10^{-5}$ mM/s

$K_m = 0.45\ \pm 0.28$ mM

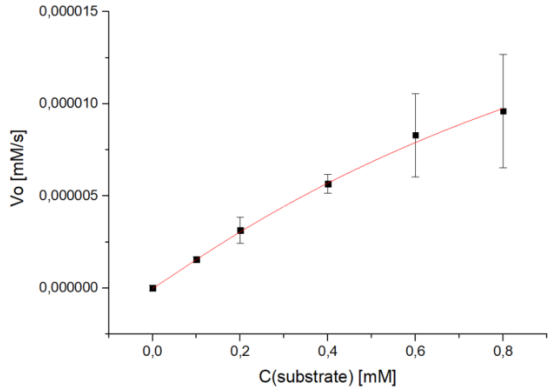

E144A/Y189W

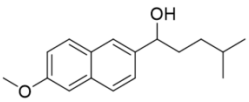

174g

$V_{max} = (\ 2.85\ \pm 9.71\ ) \times 10^{-5}$ mM/s

$K_m = 1.48\ \pm 0.70$ mM

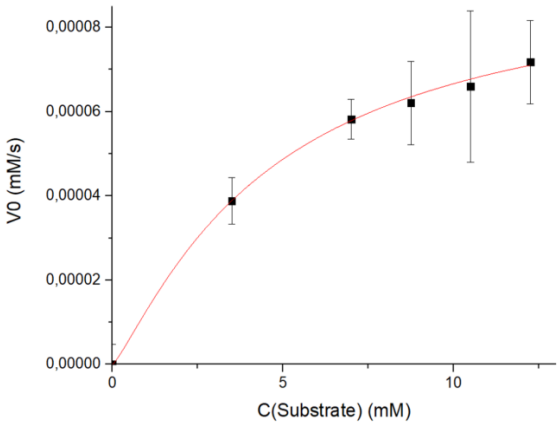

E144A/L152R

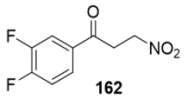

162

$V_{max} = (9.3 \pm 0.96) \times 10^{-5}$ mM/s

$K_m = 4.6 \pm 0.8$ mM